Micro- and Macromixing Studies in Two- and Three-Phase (Gas-Solid-Liquid) Stirred Chemical Reactors

by

Julia Hofinger

A thesis submitted to

The University of Birmingham

for the degree of

DOCTOR OF PHILOSOPHY

School of Chemical Engineering

University of Birmingham

August 2012

ABSTRACT

The iodide/iodate reaction scheme was used to study the effect of gas sparging and/or solid particles on micromixing in a stirred vessel. A literature review illustrated the need for focused work on this matter and gave valuable ideas for the experiments, especially considering the discrepancies reported in previous works. However, the experimental method first had to be validated for the conditions with added gaseous and solid phases air and glass beads, respectively. The experiments covered a range of conditions for micromixing in single-phase, for validation, in gas-liquid, solid-liquid and gas-solid-liquid systems: power inputs up to 1.94 W/kg, gas sparge rates up to 1.5 vvm and up to 11.63 wt.% solids with diameters from 150 to 1125 μm. For comparison, the power inputs from the impeller were kept constant when affected by the added phase(s).

The gas-liquid results clearly showed that micromixing for feeding near the surface was significantly improved by gas sparging. In contrast, no changes were observed near the impeller, when power input was kept constant. Near the surface the contribution from the stirrer towards the local specific energy dissipation rate becomes less dominant compared to the part from gas sparging. In addition, the energy dissipated by the bursting of the air bubbles at the top might be an explanation for the observed improvements.

In the solid-liquid cases low particle concentrations, i.e. up to 2.46 wt.%, showed no significant effect when feeding near the surface, the impeller or ε_{max}. At 11.63 wt.%, cloud formation occurred and micromixing was significantly worse near the impeller, i.e. in the cloud, and near the surface above it, i.e. in the clear liquid layer.

Interestingly, this “dampening” was also found for larger solids which does not indicate turbulence modulation due to the presence of the particles as had been suggested in literature, but might point more towards energy dissipation due to particle-particle interaction.

In addition to the two-phase work, gas-solid-liquid work is reported here which has not been studied before. Due to the above results, low and high solids concentrations were investigated over a range of gas sparge rates for feeding near the surface and near the impeller. In contrast to the two-phase case, even small amounts of particles gave slightly worse micromixing under sparged conditions. Nevertheless, there were still improvements near the surface compared to the single-phase data. For the sparged clouds, the results indicate some improvements compared to the solid-liquid equivalents. However, this picture is more complex and further information on the fluid flow in such systems is needed for detailed discussion.

In order to allow better quantification of the experimental data, variations of the Incorporation model were evaluated for taking recent suggestions for the reaction scheme into consideration. The second dissociation of sulphuric acid was included in the model and different kinetic rate laws from the literature on the Dushman reaction were implemented. It was found that further kinetic data is needed for the particular conditions in the experiments, but that the current variations allow order-of-magnitude estimates and further comparisons of local specific energy dissipation rates.

To my family

ACKNOWLEDGEMENTS

I thank my main supervisors Dr. Waldemar Bujalski and Prof. Alvin Nienow for their outstanding support throughout the project, while giving me plenty of freedom to learn. Especially, Waldek's technical understanding and experience in looking after his many students were of great value. Moreover, working with Alvin was an honour and in particular his knowledge and sense of humour made discussions much more pleasant. In addition, I wish to acknowledge Dr. Serafim Bakalis who helped especially in earlier stages of the project and offered many ideas for CFD work.

I am grateful for the full financial support from Huntsman Polyurethanes, Brussels. In particular, the useful and friendly meetings with Dr. Archie Eaglesham and Dr. Melissa Assirelli, who also gave great technical feedback, were just as helpful as the sponsoring. I also thank them for giving me the opportunity to visit the site in Everberg, Belgium, to work on some aspects of the project.

I want to acknowledge the IChemE Fluid Mixing Processes Subject Group for running the research student competition. The prize for the first place 2011 was used for part of the cost of attending ISMIP in Beijing. The experience was invaluable.

Moreover, a big "thank you" to the staff of the chemical engineering workshop, especially Bob Sharpe: only such high quality technical support allowed me to obtain accurate and consistent experimental results. Moreover, their friendship, the

encouragement served with afternoon teas and the spectacular Christmas parties will be fond memories of this turbulent time at the University of Birmingham.
In addition to the workshop, I also want to thank the rest of the staff, especially Mrs. Lynn Draper, for their great work which helped us focus on our studies.

For some of the CFD simulations, the university's computer cluster, BlueBEAR, was used and I wish to acknowledge the support from Paul Hatton and Aslam Ghurma. I also want to thank Aslam for his help during my time on the postgraduate student trainer team for CFX.

For their undergraduate projects, Yashar Khosrowyar, Yohann Mallet and Thibaut Laurent helped with some of the experiments.

I have had the privilege and pleasure of meeting so many lovely people while being here and it would be impossible to list them all. Therefore, I want to thank everyone from 118 and G2, but also the CFD colleagues, especially Andrea, Dave and Lily, for the great time and their friendship.

Last but not least, I am very grateful for my family's support. Not only have they let me go abroad, helped me financially and done lots of proofreading, but also their encouragement and confidence in me has been fantastic. Thank you.

TABLE OF CONTENTS

LIST OF ILLUSTRATIONS

LIST OF TABLES

NOTATION

Arabic

c	concentration	mol/L
C	impeller clearance	m
Da	Damköhler number	-
Da_M	mixing Damköhler number	-
D	diameter of stirrer	m
d_p	diameter of particle	m
D	diffusivity	m^2/s
E	Engulfment rate	1/s
f	expression for chemical species	-
F	expression for change of species in Incorporation model	-
Fl	dimensionless flow number (or N_Q)	-
Fl_g	gas flow number	-
g(t)	growth function	-
H	fill level of tank	m
k	constant for reaction rate	(depends on reaction)
L or l_c	characteristic length	m
N	rotational speed of stirrer	1/s
P	power	W
Pa	particle momentum number	-
Po	power number	-
$P_{...}$ or $Q_{...}$	factors for Incorporation model	-
Q	discharge flow	
Q_g	gas flow rate	
Q_{VG}	gas flow rate in vvm	volume of air/minute per volume of liquid in the tank

r	radial distance from tank centre	m
R	pipe diameter	m
R_j	reaction term for species j	mol/L s
Re	Reynolds number	-
s	dimensionless factor in Zwietering equation	-
Sc	Schmidt number	-
St	Stokes number	-
T	tank diameter	m
t	time	s
t_c	critical time	s
t_m	micromixing time	s
u or u_i	velocity (instantaneous)	m/s
$\bar{u}$	mean velocity	m/s
u'	fluctuating velocity	m/s
u_R	relative velocity	m/s
u_{TV}	terminal velocity	m/s
V	volume	m
v	velocity	m/s
W	impeller blade width	m
x	axial distance from jet exit	m
X	mass percentage of particles	**%**
X_S	selectivity for side-product	**-**
ΔX_S	deviation of X_S from reference	**%**
Y	yield	-
Y_{ST}	maximum yield at total segregation	**-**
z	axial distance from tank bottom	m

Greek

ε	(local) specific energy dissipation rate	W/kg
$\overline{\varepsilon_T}$	mean specific energy dissipation rate	W/kg
ε_{max}	maximum local specific energy dissipation rate – ensemble-averaged	W/kg
$(\varepsilon_T)_{max}$	maximum local specific energy dissipation rate	W/kg
λ	length scale of turbulent eddy	m
λ_K or η	Kolmogorov length scale	m
μ	dynamic viscosity	kg/m s (or Pa s)
ν	kinematic viscosity	m^2/s
ρ	density	kg/m^3
τ_M	characteristic mixing time	s
τ_R	characteristic reaction time	s
τ_K	Kolmogorov time scale	s
ϕ	ratio of local to mean specific energy dissipation rate	-
ϕ_m	mass fraction	-

Abbreviations

CFD	computational fluid dynamics
DNS	direct numerical simulation
EDD	Engulfment – deformation – diffusion model
GMM	Generalised Mixing Model
IEM	interaction by exchange with the mean model
LDA/LDV	laser Doppler anemometry/velocimetry
LES	large eddy simulation
PIV	particle image velocimetry

PM	perfectly mixed
ST	total segregation
RMS	root mean square
RT	Rushton turbine
VoF	Volume of Fluid

1. INTRODUCTION

1.1. Motivation and objectives

Many industrially relevant fast chemical reactions have fast side-reactions which lead to unwanted products. Such waste products can not only reduce efficiency of a process, but also affect the quality of the actual product. In addition to working on the chemistry of the process, improving micromixing, i.e. contacting of the reactants, can lead to better results.

Examples of processes where micromixing becomes important:

- fast competing parallel or consecutive reactions
- particle size distribution in precipitation
- molecular weight distribution in polymerisation

In single-phase systems, including stirred tanks, micromixing is well studied, see e.g. Assirelli (2004) and valuable progress has been made with the use of reaction schemes employing competing reactions like the Iodide/iodate reaction method. Unfortunately, possible effects of gas bubbles and solid particles on micromixing are still not fully investigated, let alone understood. Other well-established measurements techniques for studying fluid flow and turbulence fields, like PIV or LDA, are laser-based and, therefore, only of use at low concentrations of dispersed phase. There is, however, a small, sometimes contradicting amount of work available in literature on the effect of particles on micromixing and also on turbulence,

but targeted work is needed for gas-liquid, solid-liquid and gas-solid-liquid stirred chemical reactors.

Therefore, the aim of this work is to shed light on micromixing in a two- and three-phase agitated tank at well-defined, not previously studied conditions using the Iodide/iodate reaction scheme. This method has been found to give qualitatively reliable results in single-phase cases which could be verified against results from other methods, but some suggestions have been made recently to move it towards more quantitative use. These ideas will be tested as well.

1.2. Layout of thesis

In order to achieve the above objectives, this thesis is structured as follows: First, the background and the available relevant literature will be discussed in chapter 2. This is necessary to establish which conditions should be studied and which factors might need most attention. Chapter 3 gives details on the method and the experimental set-up with its adaptations for this work. This section also includes single-phase results which are used to validate the approach chosen and to give reference values for the multi-phase results. In chapter 4, recent criticism on and suggestions for the improvement of the Iodide/iodate method are addressed by extending a micromixing model, the Incorporation model, to better describe the employed reaction scheme. These changes to the modelling have not been reported before and could allow more quantitative interpretation of experimental data. In chapter 5, the suitability of using air with the Iodide/iodate reaction scheme is first validated and experimental conditions are chosen. Then the effect of gas sparging on micromixing in stirred tanks is studied in experiments and that data evaluated using the model variations

from chapter 4. In chapters 6 and 7, the same is done for solid-liquid and gas-solid-liquid systems, studying effects in a well defined system over a wider, more industrially relevant range of conditions than in previous work. Finally, chapter 8 gives the conclusions of the work presented in the thesis and suggestions for future work are added as well.

2. BACKGROUND AND LITERATURE

2.1. Turbulent mixing in stirred vessels

In this work, micromixing in agitated tanks will be investigated through experiments and using a model. As micromixing is closely linked to turbulence, relevant aspects of the latter will be summarised first. Then, an overview of necessary background on single- and multi-phase mixing in stirred vessels is given in the following sections.

2.1.1. A brief introduction to turbulence

In literature on mixing, a strong distinction is typically made between laminar and turbulent flows (Harnby *et al.* 1997; Paul *et al.* 2004). Only the latter are relevant in this study and, therefore, turbulence should be discussed here briefly. This might seem fairly straight-forward considering that such phenomena are commonly found in nature, in everyday life and in industry, from rivers, to stirring a cup of tea and many chemical reactors. Still, even though pictures of what turbulent flows can look like might come to mind quite quickly, for instance the images from the well-known methods of observing dye streaks, e.g. Figure 1, characterising this flow behaviour becomes relatively challenging (Tennekes and Lumley 1972; Hinze 1975; Baldyga and Bourne 1999; Davidson 2004).

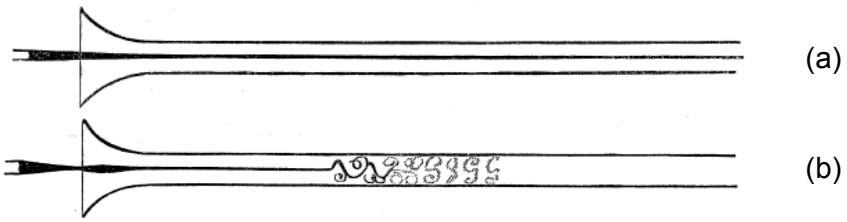

Figure 1: Pictures from early experiments on turbulence by injecting dye into the flow through a pipe (Reynolds 1883) – (a) laminar and (b) turbulent

In early work, Reynolds wrote that pipe flow "assumes one or other of two broadly distinguishable forms-either the elements of the fluid follow one another along lines of motion which lead in the most direct manner to their destination, or they eddy about in sinuous paths the most indirect possible" (Reynolds 1883). Since then, some more insight has been gained and for instance Tennekes and Lumley (1972) listed the following characteristics to describe turbulence: irregularity, diffusivity, large Reynolds numbers, three-dimensional velocity fluctuations, dissipation, continuum (i.e. governed by equations of fluid mechanics); and turbulent flows are flows ("Turbulence is not a feature of the fluids, but of fluid flows"). These ideas are often referred to in literature to illustrate the complexities involved. Still, while turbulence has been studied extensively, it is an open research topic (Clay Mathematics 2011) and there are particular challenges in simulating such problems, although there are useful models available. Plenty of texts (Davies 1972; Hinze 1975; Baldyga and Bourne 1999; Davidson 2004) give excellent introductions to this extensive topic and some variables and ideas are summarised here.

On practical terms, the Reynolds number, Re, which is defined as the ratio of inertial and viscous forces, has been found useful for characterising flows:

$$Re = \frac{inertial\ forces}{viscous\ forces} = \frac{\rho L v}{\mu} \qquad \textbf{(2.1)}$$

With ρ being the fluid density, L a characteristic length (for instance in a pipe the pipe diameter), v the fluid velocity and μ is the dynamic viscosity. Low Re indicate laminar flow, while the turbulent regime is characterised by higher Re. The transitional behaviour between these regions can be complex (Saric *et al.* 2002).

Because of the unsteady, 3-dimensional irregular behaviour of the flow, the instantaneous velocity may be described by mean and fluctuating components:

$$u_i = \bar{u} + u' \qquad \textbf{(2.2)}$$

This turbulent component is usually reported as root mean squared (or RMS) value of the fluctuating velocities (Kresta 1998; Gabriele *et al.* 2009).

Some simplification is possible when the turbulent velocity fluctuations are, on average, equal in all directions in space, i.e. when turbulence is isotropic. Assuming such flow behaviour is of use for instance for computational fluid dynamics (CFD), where a reduction of the number of variables in turbulence modelling allows faster and computationally less expensive calculations. In contrast to isotropy, anisotropic turbulence means that the different components are not equal, which can for instance become relevant for instance near the wall of a pipe (Gore and Crowe 1991).

Turbulence is often described as a cascade of length scales where bigger eddies give rise to smaller ones which again have smaller eddies until, on the smallest scales, viscosity becomes dominant and energy is dissipated into heat (Richardson 1922; Argoul *et al.* 1989). In this approach, turbulence can be seen as a superposition of spectrum of velocity fluctuations and eddy sizes (Nienow 1998). Kolmogorov (1941) suggested that, at high Re, smaller turbulent eddies tend towards isotropic behaviour, becoming independent from turbulence generation. Figure 2 shows such a range of different eddy sizes and their energy in turbulent flow for an agitated vessel. The largest eddies on the left depend on the way they were generated, e.g. in a stirred tank on the flow generated by the impeller; they are

anisotropic and contain the most energetic eddies. The smaller ones are isotropic and independent of the way the turbulent motion had been created. At the smallest scales viscosity becomes dominant and the energy is dissipated into heat. On this scale, which is named after Kolmogorov, where viscous and inertial forces are equal, $Re_k = 1$. From dimensional analysis, the Kolmogorov length scale can then be obtained (Kolmogorov 1941):

$$\lambda_K = \left(\frac{\nu^3}{\varepsilon}\right)^{\frac{1}{4}} \qquad \textbf{(2.3)}$$

This length scale is also indicated in Figure 2 and falls into the universal equilibrium range, i.e. where eddies are do not depend on the way the turbulence has been generated. This range can be divided into inertial sub-range, $\lambda > \lambda_K$, and viscous sub-range, $\lambda < \lambda_K$. On the other side of the range are the larger eddies which contain most of the energy; these most energetic eddies are often characterised by the integral length scale, which is discussed in section 2.3.2. for agitated tanks.

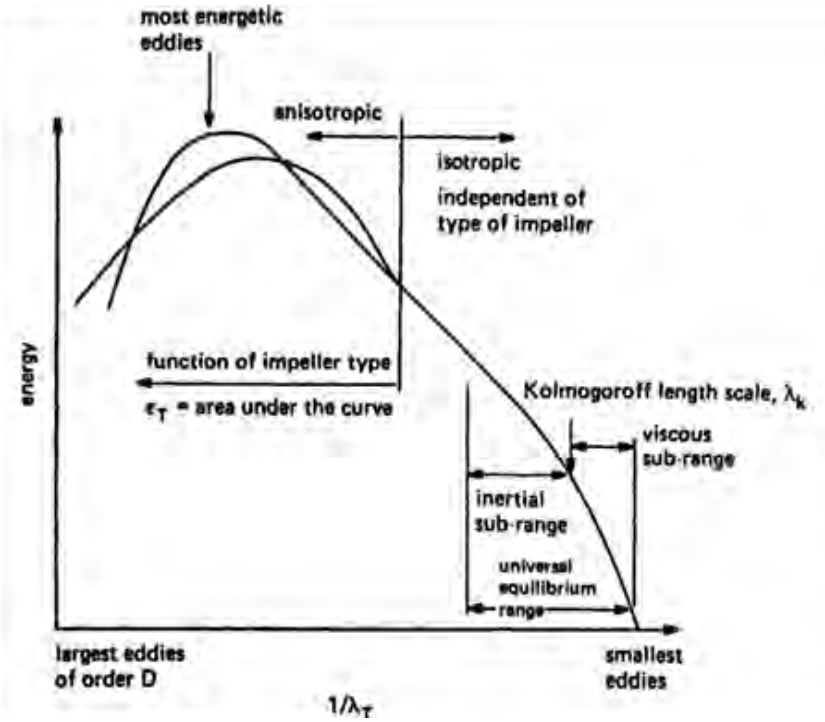

Figure 2: Spectrum of eddies and their energy (Harnby et al. 1997)

2.1.2. Liquid mixing

The Reynolds number, as introduced earlier, can be useful when describing the flow in stirred vessels and is then defined with the impeller speed and diameter as

$$Re = \frac{N\,D^2}{\nu} \qquad \textbf{(2.4)}$$

The flow is laminar at low Reynolds numbers, i.e. less than about 10, and turbulent at Re > $2{\cdot}10^4$ with the transitional regime occurring between these conditions. The fluid motion in the tank strongly depends on the impeller type and for instance with Rushton turbines (RT) is dominated by radial flow, while propellers or pitched blade turbines (PBT) lead to axial or mixed flows, respectively. Such flows are illustrated in Figure 3: for a) radial flow and b) axial flow. These flow patterns and their velocity fields have been studied extensively using a range of experimental methods like photographic techniques, hot-wire anemometry, particle image velocimetry (PIV), laser Doppler anemometry (LDA), positron emission particle tracking (PEPT) and simulations, for instance computational fluid dynamics. Such experimental approaches have been summarised in a review by Mavros (2001). CFD is not generally of direct relevance to this thesis, but was employed for one aspect which is summarised in appendix C.

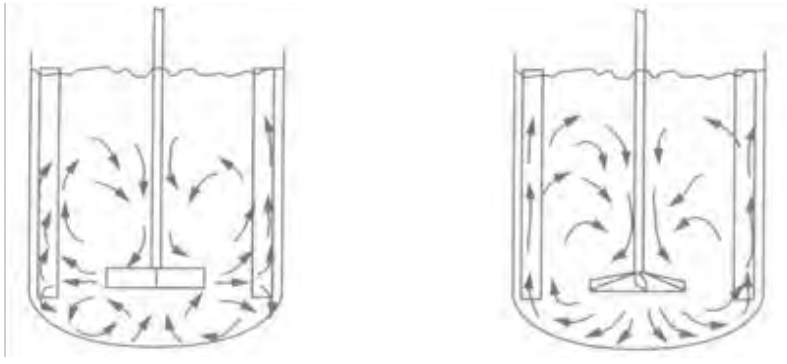

a) radial flow b) axial flow

Figure 3: Possible flow patterns in agitated vessels (Paul et al. 2004)

Such information on fluid velocities can be of use in assessing mixing performance. For instance, the amount of fluid circulated by an impeller may help characterise a mixing system. This internal circulation or discharge flow, Q, can be expressed by the dimensionless flow number, Fl:

$$Fl = \frac{Q}{N\,D^3} \qquad \textbf{(2.5)}$$

Another important parameter is the power put by the impeller into the stirred vessel which can be expressed with the dimensionless Power number, Po:

$$Po = \frac{P}{\rho\,N^3\,D^5} = f\left(\frac{ND^2}{\nu}, \frac{N^2D}{g}, \frac{D}{T}, \frac{H}{T}, etc.\right) \qquad \textbf{(2.6)}$$

The power number is a function of Reynolds number, Froude number [second term in equation (2.6)] and geometric ratios (D = impeller diameter, T = tank diameter, H = fill level etc.). In addition, baffles, which can be installed to reduce gross vortexing, significantly affect the flow field and consequently the power input. The plots of Po vs. Re in Figure 4 show that the power number becomes constant in baffled vessels at turbulent Reynolds numbers and that there are slopes of -1 in the laminar regime, which reflects that viscous effects dominate the flow in the tank.

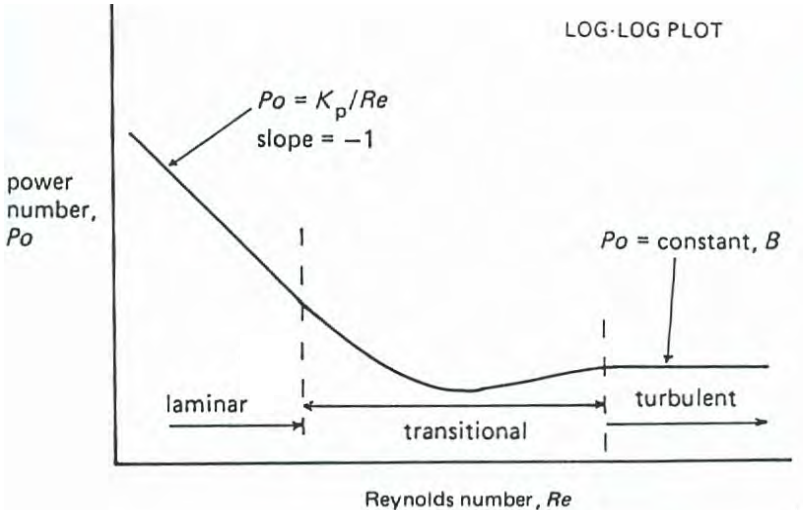

Figure 4: Typical power curves in single phase case for Rushton turbine (Harnby et al. 1997)

In the transitional region, the Power number of the Rushton turbine drops before becoming a constant of about 5 in baffled and about 1 in unbaffled conditions. The exact value of Po can be calculated for standard set-ups using empirical equations which consider various geometric ratios, for instance Bujalski *et al.* (1987).

Experimentally, the power input into mixing devices has been investigated by methods measuring temperature changes due to the energy dissipated in the fluid (Kowalski *et al.* 2011), the power consumed by the motor, while taking potential losses into account (Nagata 1975; Nienow *et al.* 1994), the torque transmitted from the liquid to the vessel or the torque on the shaft (Nienow and Miles 1969; Bujalski *et al.* 1987).

The specific power input or mean specific energy dissipation, $\overline{\varepsilon_T}$, has long been recognised as an important factor for mixing processes. For instance, gas-liquid mass transfer depends, among other factors like for instance viscosity (Cooke *et al.* 1988), on the power input from the impeller (Van't Riet 1979; Nienow 1998):

$$\overline{\varepsilon_T} = \frac{P}{\rho V} \qquad \textbf{(2.7)}$$

Using only this mean value, however, might over-simplify reality as it fails to take into account that the energy is not dissipated evenly throughout the stirred vessel. Earlier measurements of local specific energy dissipation levels were done with photographic technique (Cutter 1966) and hot-film/wire anemometry (Rao and Brodkey 1972), also piezoelectric sensors (Fort *et al.* 1993) have been tried. More recently, mainly laser-based methods have been used, i.e. laser Doppler anemometry (LDA) or laser Doppler velocimetry (LDV) (Wu and Patterson 1989; Ducci and Yianneskis 2005) and particle image velocimetry (PIV) (Baldi and Yianneskis 2004; Gabriele *et al.* 2009).

Such a distribution is shown in Figure 5 for a tank with a Rushton turbine (numbers in figure indicate the feed positions used by the author for related micromixing studies (Schäfer 2001)). The figure clearly illustrates that there are significantly higher energy dissipation levels around the impeller compared to the bulk – in fact there is a difference of orders of magnitude.

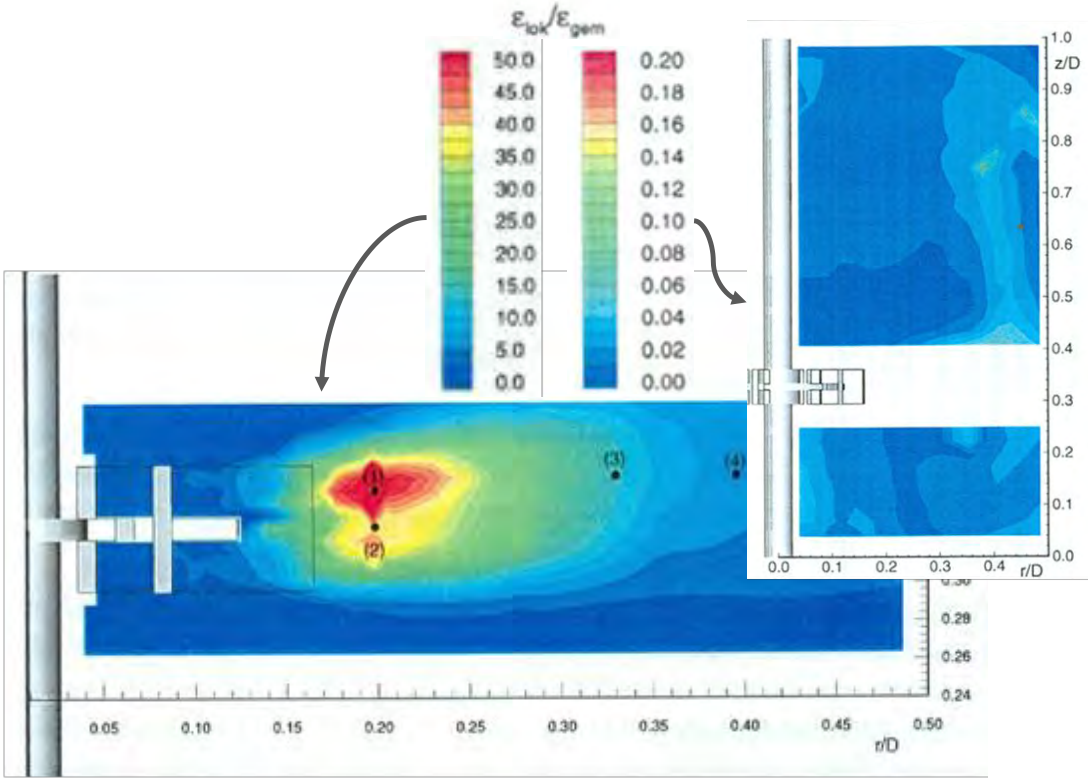

Figure 5: Local energy dissipation rates (normalised with $\overline{\varepsilon_T}$) in stirred tank – for impeller region and bulk (Schäfer 2001)

Literature is in agreement that most of the energy is dissipated near the impeller; nevertheless, absolute values vary considerably. For instance the highest local specific energy dissipation rate, ε_{max}, often expressed as ϕ_{max} (i.e. $\varepsilon_{max}/\overline{\varepsilon_T}$) to allow comparison, has been found to be in the impeller discharge stream but values differ significantly: in literature ϕ_{max} for the Rushton turbine has been reported ranging from as low as around 8 (Bourne and Yu 1994) to moderate values of 52 (Schäfer 2001) or about 70 (Cutter 1966) and up to about 100 (Assirelli 2004; Assirelli *et al.*

2008b). An explanation for these differences may be that the calculation of the local specific energy dissipation rate from the raw LDA or PIV data or from micromixing models is not straightforward – for optical methods (see Baldi and Yianneskis 2004; Gabriele *et al.* 2009) and micromixing approaches (see Assirelli *et al.* 2008b).

Trailing vortices have been observed behind the impeller blades and, in the case of the Rushton turbine, have been studied for a long time (Nienow and Wisdom 1974; Van't Riet and Smith 1975). In this region of the flow, the highest local energy dissipation levels or ϕ_{max} have been measured (Stoots and Calabrese 1995; Schäfer 2001), which is of use for understanding micromixing as discussed later (Assirelli *et al.* 2002).

2.1.3. Liquid-gas mixing

In certain applications, e.g. many bio-reactions, gas is added to the system, often using self-inducing impellers or spargers. Typical sparge rates for fermentations might be around 0.5 to 1.5 vvm (Nienow 1998) and it is quite conceivable that the gas might have a major impact on mixing and the fluid flow in the agitated vessel.

To quantify the amount of sparging, the gassing rate is often expressed as the dimensionless gas flow number, Fl_g, (which is in a similar form as the flow number which is dependent on the flow generated by the impeller, Q, equ. (2.5)) with Q_g being the gas flow rate:

$$Fl_g = \frac{Q_g}{ND^3} \qquad \textbf{(2.8)}$$

When gassing rates are too high for given mixing conditions, “flooding” of the impeller occurs. In this case, the flow in the tank is dominated by the gas flow, while

macromixing and gas dispersion are poor (Nienow 1998; Paul *et al.* 2004) and, therefore, this condition tends to be avoided. With increasing agitator speed, the impeller becomes more significant for the bulk flow, which is referred to a "loaded", and the gas gets dispersed, first throughout the upper part of the tank. The transition from flooding to loading occurs at the impeller speed, N_F. At more intense agitation conditions, above N_{CD}, complete dispersion is achieved, i.e. gas also reaches the lower part of the vessel and circulates back to the impeller. At even higher impeller speeds, recirculation becomes significant and the increased amount of gas which collects in the trailing vortices behind the impeller can lower power input. Figure 6 illustrates the transitions from flooding to loading and to complete dispersion for a Rushton turbine and other radial flow impellers.

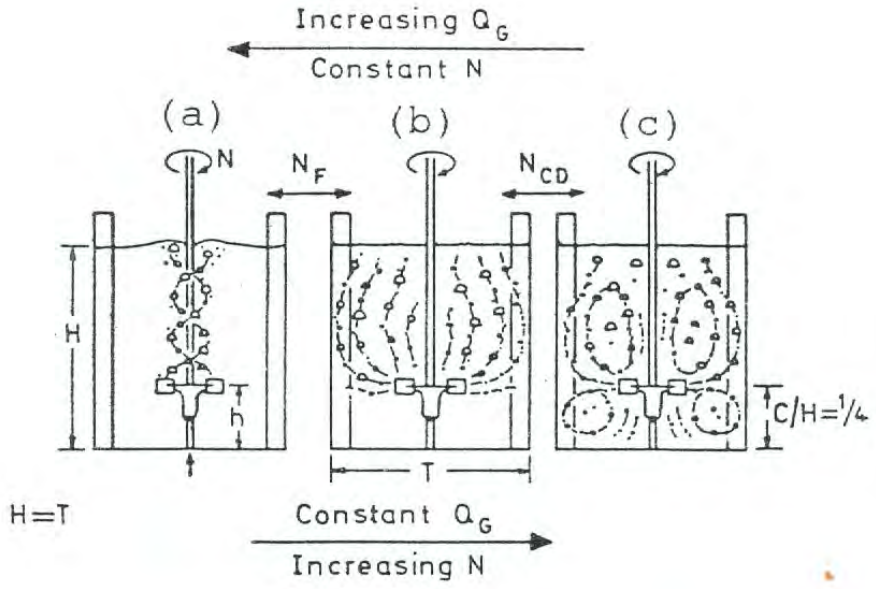

Figure 6: Flow transitions for gassed tanks (Nienow et al. 1985)

These different flow regimes can not only be observed visually, but are also reflected in the power input: It is well-known that the power number of many impellers drops under gassed conditions (Cooper *et al.* 1944; Michel and Miller 1962; Joshi *et al.* 1982; Chapman *et al.* 1983c). For the Rushton turbine this drop can be 50% of the

unsparged value, while some more modern impellers do not show such significant reductions (Nienow 1996). Figure 7 shows the ratio of gassed to ungassed power number for a Rushton turbine as a function of Fl_g. The step at the right occurs at high gas flow number, i.e. relatively high gassing rates with low impeller speed, and shows the transition between flooding and loading. Then a minimum occurs in the curve at N_{CD} from where the relative power input increases again until recirculation becomes relevant at N_R.

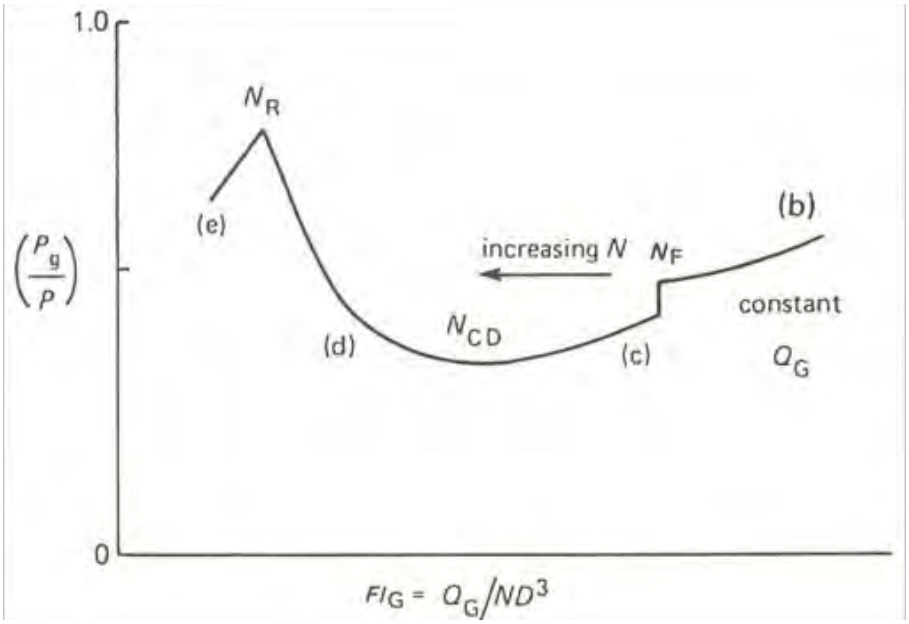

Figure 7: Typical power curve as a function of Fl_g for a Rushton turbine under gassed conditions (Harnby et al. 1997)

A main factor in the drop of power of the Rushton turbine are the low pressure regions behind the impeller blades and its trailing vortices, which were introduced in section 2.1.2.. It has been shown that gas tends to accumulate in different cavity formations behind the blades which reduces the impeller's effect and therefore power.

2.1.4. Liquid-solid mixing

Depending on the application of solid-liquid mixing, different degrees of suspension or distribution of particles may be required. In some cases a homogenous suspension might be the aim of the process, i.e. distributing the solids in the tank, while in others it might only be necessary to get the surface area of all particles into contact with the surrounding fluid, i.e. suspending them. For the latter problem, a frequently used measure is the just suspended criterion where all particles are in motion and no particles rest on the bottom of the tank for more than 1-2 seconds (Zwietering 1958; Baldi *et al.* 1978; Harnby *et al.* 1997). For impeller speeds where the particles are just suspended, N_{JS}, or above, the entire particle surface should be available for the respective process.

Though probably difficult at larger scales, N_{JS} may be obtained experimentally through visual observation of the tank's bottom. In addition, various correlations for the calculation of N_{JS} have been presented in literature. Probably the most well-known one was suggested by Zwietering (1958) – for a particle concentration, ϕ_m, (mass solid/mass liquid x 100) and a particle diameter, d_p:

$$N_{JS} = \frac{s\, d_p^{0.2} \nu^{0.1} (g\, \Delta\rho)^{0.45} \phi_m^{0.13}}{\rho_l^{0.45} D^{0.85}} \qquad \textbf{(2.9)}$$

Impeller speeds higher than N_{JS} might, however, be required to achieve a relatively uniform distribution of solids throughout the tank (Chapman *et al.* 1983b). Consequently, operation conditions will depend on the application. Further studies on solid suspension, have found effects relevant to industry, e.g. Nienow (1968)

showed the importance of impeller clearance in solid-liquid mixing. Still, Zwietering's correlation has been found useful and is widely employed (Paul *et al.* 2004).

At high solid concentrations, i.e. above about 10 wt.%, cloud formation has been observed for certain conditions (Bujalski *et al.* 1999). In these cases, a cloud of solids can be seen in the lower part of the tank near the impeller and a clear, quiescent liquid in the region near the surface develops. This phenomenon has been shown to significantly increase the mixing time for the bulk (macromixing defined in section 2.2.1.), i.e. from a few seconds to minutes, though higher impeller speeds can help improve mixing in such situations (Kraume 1992; Hicks *et al.* 1997; Bujalski *et al.* 1999). The stages of cloud formation are illustrated in Figure 8 for increasing impeller speeds – from most solids sitting on the bottom and the cloud at varying heights to a more uniform distribution of the particles.

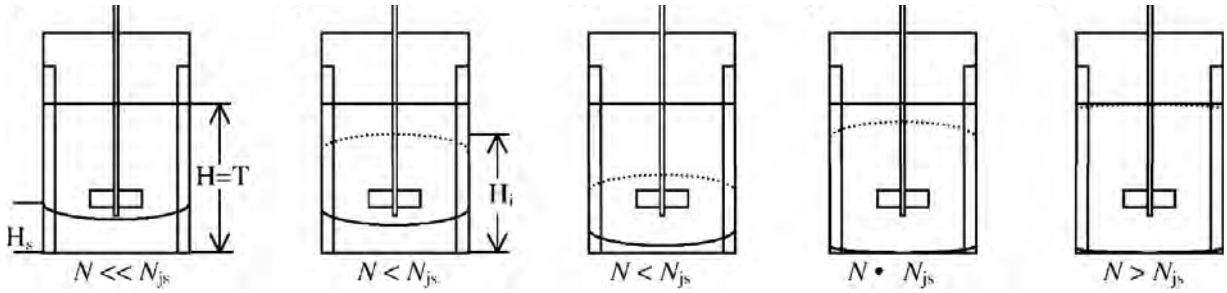

Figure 8: Stages of suspension of particles at high solid concentrations (solid line – static solids; dotted line – interface suspended solids/liquid (Bujalski et al. 1999)

At low impeller speeds, higher amounts of solids can lower the power input compared to the single-phase equivalent (Bujalski *et al.* 1999). An explanation for this is that the particles are not suspended yet and get distributed at the bottom in a "streamlined" shape which affects the flow while reducing the impeller clearance as well (Bujalski *et al.* 1999). Lower amounts of particles, i.e. less than 10 wt.%, have been shown to not significantly affect power input.

2.1.5. Liquid-gas-solid mixing

In a sparged solid suspension a combination of the above effects might occur, i.e. flow and power input might change significantly, but the interaction of particles and bubbles might lead to additional complexity. Unfortunately, there is less information available in the literature on such systems compared to two-phase ones.

Figure 9 gives an idea of how power input in three-phase stirred vessels is affected by gassing rates and solid mass fraction. Overall, the trends resemble sparged systems without added particles: power drops with increasing amounts of gas and lower impeller speeds. Warmoeskerken *et al.* (1984) found that up to 5 wt.% did not affect the gassed power input. However, at higher concentrations, like in Figure 9, it can be seen that power tends to drop for instance with 20 or 30 wt.% when the particles are not well suspended. Chapman et al. (1983a) explained this with the distribution of the particles on the bottom of the tank; the power input is reduced due to this false bottom as in the s-l case.

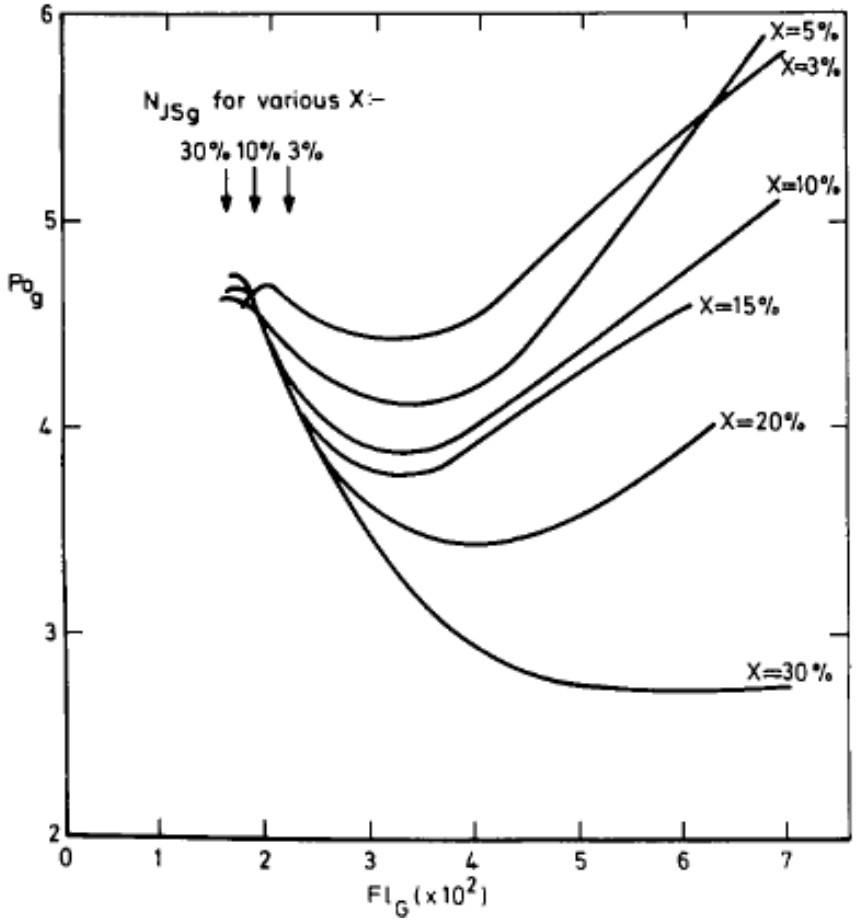

Figure 9: Typical power input curves for three-phase system with Rushton turbine, 0.5 vvm air and various amounts of glass ballotini (Chapman et al. 1983a) (X = mass percentage of particles)

Regarding suspension, N_{js} (for unsparged systems) tends to be lower than N_{js_g} (with gas) (Harnby *et al.* 1997; Kasat and Pandit 2005). For larger Rushton turbines (D=T/2), the following equation has been proposed for estimating N_{js_g} (Chapman *et al.* 1983a; Bujalski 1986):

$$N_{js_g} = N_{js} + 0.94\, Q_{VG} \qquad \textbf{(2.10)}$$

with $\mathrm{Q_{VG}}$ being the gas flow rate in vvm (volume of air/minute per volume of liquid in the tank). The data leading to equation (2.10) was obtained experimentally from 5 tank sizes, but further investigation might be of use.

2.2. Micromixing

2.2.1. Mixing scales and chemical reactions

It can be useful to distinguish between mixing on different scales in the investigated mixing equipment. First of these scales is ***macromixing***. This is mixing on the largest scales of the fluid flow, i.e. in the case of this work, the mixing vessel, and has been studied extensively. It can be described by the macromixing or blend time, which is a measure of how quickly an added substance will be dispersed throughout the vessel. Therefore, it can be determined by adding a "tracer", for instance with a different pH, colour (change) or temperature, and observing when fluctuations in the bulk fall below a specified threshold, e.g. 95% of the final value. This can be done experimentally (Hiby 1979) and has also been attempted using CFD (Bujalski *et al.* 2002). Empirical relationships have been reported to allow calculation of blend times in single-phase cases (Paul *et al.* 2004) and a strong dependence on power input has been found (Nienow 1997; Kresta 1998).

In solid-liquid cases, macromixing time has been shown to be significantly worse when clouds are formed, i.e. mixing time increased by up to more than two orders of magnitude (Bujalski *et al.* 1999) – which means minutes instead of seconds for blending a tank. In gas sparged stirred tanks, blend times have been found to drop with increasing gas rates (Einsele and Finn 1980). Though, when compensating for the reduction in power input, macromixing has been shown to be similar to single-phase equivalents at mean specific energy dissipation rates (Saito *et al.* 1992). The situation becomes more complex in gas-liquid-solid systems, but it has been shown that gas sparging can improve macromixing at higher particle concentrations when cloud formation occurs (Nienow and Bujalski 2002). An example for such conditions

is shown in Figure 10, which gives macromixing times measured experimentally by Rewatkar *et al.* (1991) for 2- and 3-phase systems. Considering that the results are plotted against impeller speed and resemble the behaviour of the respective power curves, further discussion at least of the gas-solid-liquid case might be of use for a comparison at equivalent mean specific power inputs.

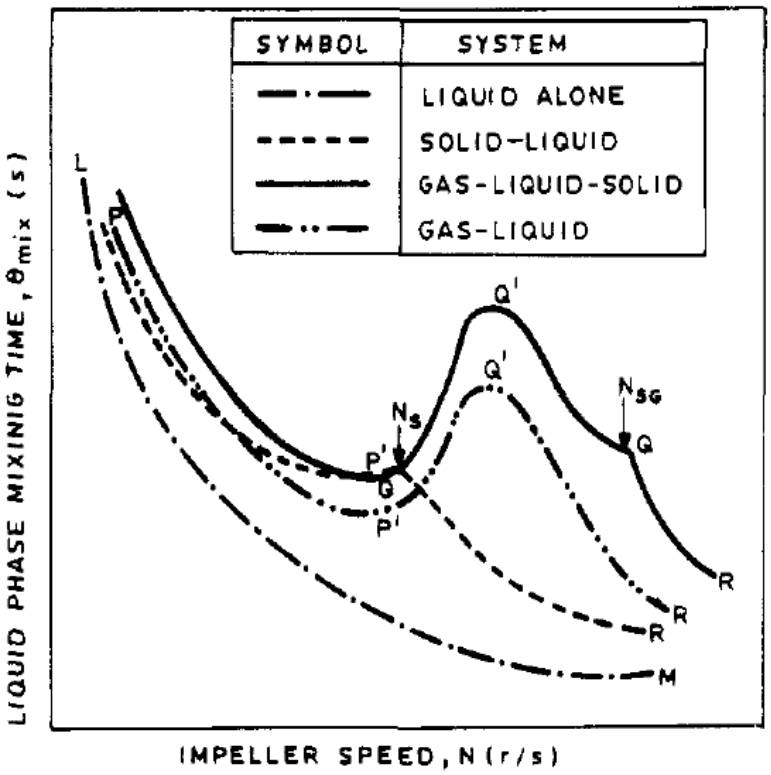

Figure 10: Macromixing time as a function of impeller speed (Rewatkar et al. 1991)

The next scale is ***mesomixing***, which is smaller than the vessel but larger than the smallest mixing scale. It is in the range of a plume of chemical reactant near a feed pipe and relevant for fast reactions and also precipitation and crystallisation (Baldyga *et al.* 1995; Ståhl and Rasmuson 2009). There have been experimental, e.g. Ng and Assirelli (2007), and modelling efforts, e.g. Thoma *et al.* (1991) into such problems, but it is not as well understood as other mixing scales (Paul *et al.* 2004).

Nevertheless, mesomixing is not the focus of this work and further work in this field would be necessary (Baldyga *et al.* 1997; Assirelli *et al.* 2011a).

The last step is ***micromixing*** which includes the smallest scale of fluid flow and also diffusion. This obviously leads to mixing on the molecular level and can consequently affect fast chemical reactions (Baldyga *et al.* 1995; Paul *et al.* 2004) – e.g. when a very fast reaction competes with a fast side-reaction for the same reactant, the product distribution can be affected by poor micromixing leading to local over-concentrations of the added reactant, which might result in more side-product.
The transition between meso- and micromixing can be observed in experiments by varying the feed time as illustrated in Figure 11. At high enough feed times (low feed rates) the amount of side-product is not affected by the feed time, i.e. only determined by micromixing. Below a critical feed time t_c, the product distribution is affected by the feed time which suggests that mixing on larger scales (mesomixing, for example) becomes significant as well (Bourne and Thoma 1991; Baldyga and Bourne 1992; Baldyga and Pohorecki 1995).

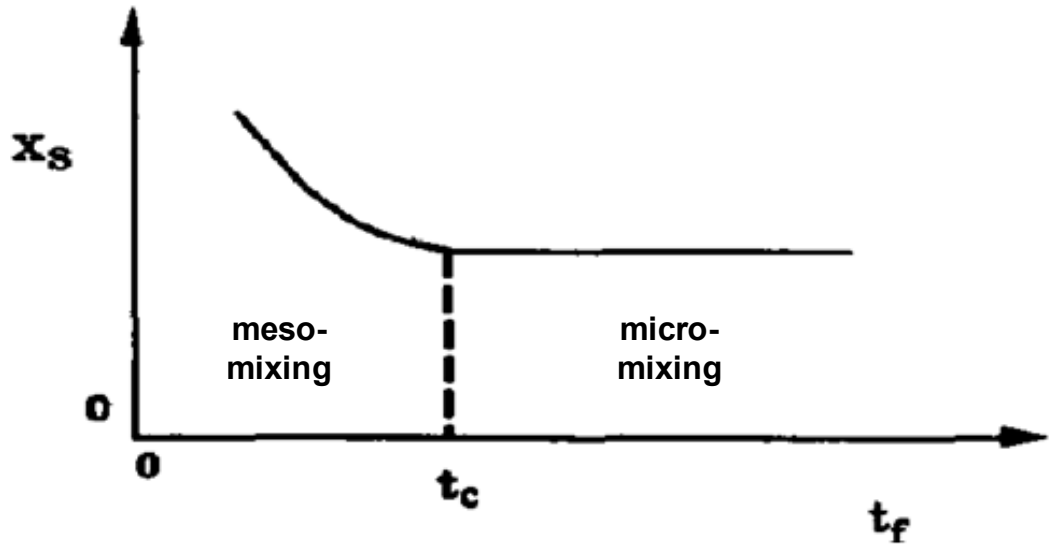

Figure 11: Transition between meso- and micromixing - effect of feed time on product distribution – amended from Baldyga and Bourne (1992)

In addition to these effects on different mixing scales, another aspect might become relevant: under some conditions, i.e. too large feed pipe diameter or low feed rate, fluid from the bulk might flow into the feed pipe which is called backmixing. Some factors that might affect backmixing have been studied, but further work is needed (Baldyga and Bourne 1993; Lee *et al.* 2007; Assirelli *et al.* 2011b).

The possible ***interactions of mixing and chemical reactions***, can be evaluated by comparing the time constants of the relevant processes. That relationship of mixing and reaction is given in the Damköhler number for mixing, Da_M, which is the ratio for characteristic mixing time, τ_M, and reaction time, τ_R, (Paul et al. 2004):

$$Da_M = \frac{\tau_M}{\tau_R} \qquad \textbf{(2.11)}$$

2.2.2. Reaction schemes for experimental micromixing studies

As (micro)mixing can affect fast chemical reactions, such reactions have been widely used to study micromixing (Fournier *et al.* 1996b). These test reactions can be single

reactions (A + B → R) or competing reactions. The latter have the advantage that the information on micromixing efficiency is retained in their product distributions, with R being the primary, desired product and S the secondary (side-) product. They can be divided into consecutive competing reactions (A + B → R; R + B → S) and parallel competing reactions (A + B → R; C + B → S).

Figure 12 shows this dependence of the selectivity towards the side-product, X_S, on the Damköhler number. The amount of waste product increases with higher reaction rate and with slower micromixing time. Therefore, it can be used to assess micromixing efficiency qualitatively for the same reaction conditions and quantitatively if the reaction kinetics are sufficiently well understood.

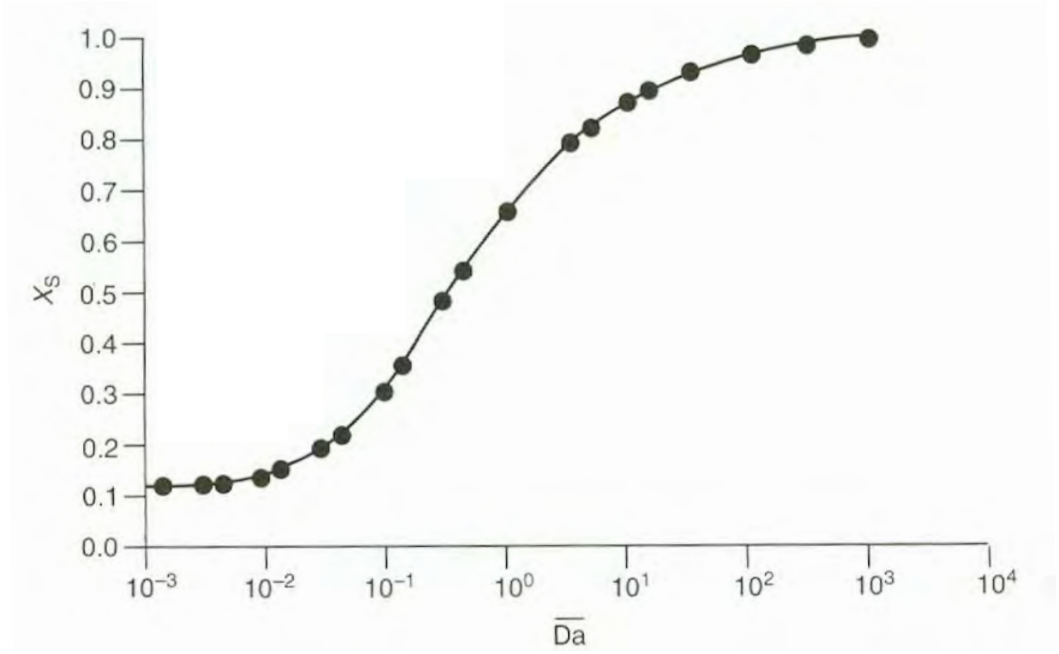

Figure 12: Selectivity towards side product, X_S , as a function of Damköhler number (Bourne 1997)

Many test reactions have been proposed over the years and the most important ones can be found in several summarising tables by Fournier *et al.* (1996b).

The most frequently used reaction schemes are the iodide/iodate method and the "Bourne reactions", several methods developed by J.R. Bourne and co-workers. To the latter would belong, for instance, the azo-coupling of 1-naphthol with diazotized sulphanilic acid (Bourne *et al.* 1981b). The iodide/iodate method was proposed by Villermaux and co-workers to avoid problems found with other reactions like difficult handling or toxic reactants (Fournier *et al.* 1996b). The reactions of the iodide/iodate method are a neutralisation and a redox-reaction which compete for H^+:

$$H_2BO_3^- + H^+ \rightleftharpoons H_3BO_3 \qquad \textbf{(2.12)}$$

$$5I^- + IO_3^- + 6H^+ \rightleftharpoons 3I_2 + 3H_2O \qquad \textbf{(2.13)}$$

Unfortunately, also this reaction scheme has got at least one weakness: though it is easy to use and gives qualitatively useful results, quantitative interpretation is difficult due to unknowns regarding one of the reactions involved (Bourne 2008; Aubin *et al.* 2010). This will be discussed in section 2.2.3. and then an approach addressing this issue will be tested in Chapter 4.

Taking all advantages and disadvantages of the range of available reaction schemes into account, the iodide/iodate method was chosen for this study for the following reasons:

- safety
- environmental and
- economic considerations
- option of performing successive injections, i.e. using a batch for more than one injection (saves time and money, reduces waste)

- (expected) suitability for the planned multi-phase work, which was tested and is reported at the beginning of the respective experiments
- it also enabled a detailed comparison with extensive earlier similar work by Assirelli (2004) but in single-phase systems.

The experimental setup and the method are described in Chapter 3.

2.2.3. Micromixing modelling

Motivation for micromixing modelling

The results from experimental studies can be used, when combined with micromixing models, to give an indication of local specific energy dissipation rates (Bourne and Yu 1994; Schaer *et al.* 1999); for instance Assirelli *et al.* (2008b) estimated local specific energy dissipation rates at various feed positions in a stirred vessel. The authors found that the ratio of the maximum local energy dissipation rate, $(\varepsilon_T)_{max}$ to the maximum ensemble-averaged energy dissipation rate was in reasonable agreement with literature (Ducci and Yianneskis 2005), but that the absolute values of $(\varepsilon_T)_{max}$ were relatively high compared to results from LDA and PIV results. It was suggested that a weakness in the model or in the kinetics might be the cause. Recent literature (Bourne 2008; Kölbl and Schmidt-Lehr 2010) also points in this direction and further work with modelling has been suggested as a solution. The particular need for micromixing modelling with the iodide/iodate method will be discussed further in the next section.

In addition to giving an estimate of local ε_T, micromixing models might be useful for comparing experimental results: for example, the reactant concentrations employed in the iodide/iodate reaction scheme may be altered for specific experimental

conditions to enhance sensitivity to micromixing (Guichardon and Falk 2000). This option also allowed the wide use of the method in various systems for instance to study micromixers. Such changes, however, affect the reaction kinetics and make comparisons between different concentrations more difficult (Assirelli *et al.* 2002). Nevertheless, this has been done using segregation indices (Li *et al.* 2012), though probably only to illustrate orders of magnitude. Therefore, micromixing modelling could allow comparing results from different experiments and make the method more versatile and quantitative.

Specific need for micromixing modelling with I/I method

As mentioned by Assirelli *et al.* (2008b), the reliability of the micromixing time, t_m, critically depends on appropriate modelling and realistic kinetics. Issues in this respect might explain some qualitatively reasonable, but quantitatively unexpected results reported by the authors. In fact, more doubts in this context have recently been expressed in literature on the current approach: so far, the limiting specie, H^+, has been provided by sulphuric acid in experiments and it has been assumed that it is already initially fully dissociated (Guichardon and Falk 2000; Marchisio and Barresi 2003; Assirelli *et al.* 2008b). However, Bourne (2008) commented that the second dissociation of sulphuric acid is not complete at the employed concentrations and should consequently be considered in modelling the iodide/iodate reaction scheme. Recently, Kölbl and Schmidt-Lehr (2010) have shown experimentally that sulphuric acid and a stronger acid, i.e. perchloric acid, indeed do not give the same result, also concluding that the dissociation needs to be included or suggesting the use of a stronger acid. Interestingly, this might also explain the poor agreement between the results from experiments and CFD simulations reported by Marchisio and Barresi

(2003). A comparison of experiments and Comsol simulations of a hollow fibre membrane device also only showed qualitative agreement (Baccar *et al.* 2009). Moreover, discrepancies between results of very similar experiments (Schäfer 2001; Assirelli *et al.* 2002) using different reactant concentrations might be – in part – explained by this issue.

Therefore, in addition to the general motivation for micromixing modelling to obtain information on local energy dissipation rates and to allow comparison between different reactant concentrations, including the dissociation of sulphuric acid in a model might aid quantitative use of the method.

On micromixing models

As with the chemical reaction schemes, a number of micromixing models have been developed. There are also further options for CFD calculations (Fox 1998; Vicum 2005; Vicum and Mazzotti 2007), but only micromixing models are relevant to this thesis.

Among several earlier models, ideas for the Interaction by exchange with the mean (IEM) model were developed by several researchers independently (Harada *et al.* 1962; Costa and Trevissoi 1972b; Costa and Trevissoi 1972a; Villermaux and Devillon 1972) as confirmed by (Villermaux and Falk 1994; Baldyga and Bourne 1999). It follows the concentration of a reactant at a point and, in addition to chemical reaction, there is exchange with the mean surrounding environment. This early model has been criticised (Baldyga and Bourne 1990) but still was found useful for some applications (Fox and Villermaux 1990).

A more complex model is the Engulfment, Deformation and Diffusion (EDD) model, developed by Baldyga and Bourne (1984) and well-documented since then (Baldyga and Pohorecki 1995; Baldyga and Bourne 1999). It describes the micromixing process in 3 stages:

- Engulfment: of reactant solutions into a vortex – see Figure 13 (a)
- Deformation: of layers in lamellar structures – see Figure 13 (b)
- Diffusion: of reactants in and between layers

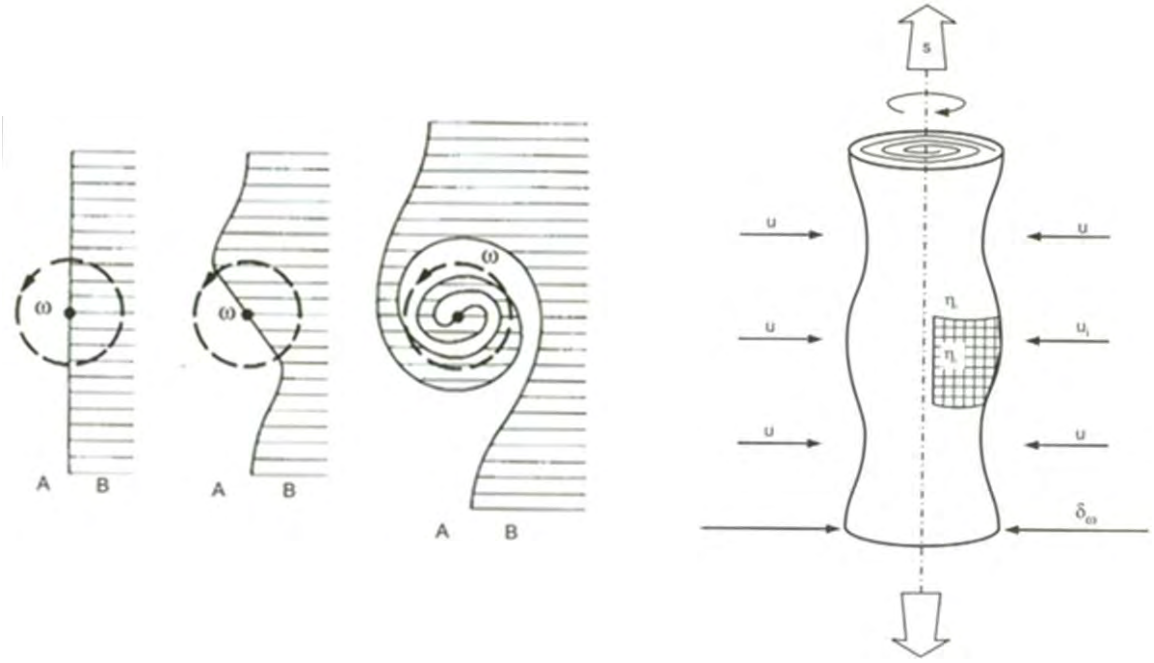

(a) (b)

Figure 13: Schematic of formation of laminated structure due to vorticity (a) and vortex stretching (b) (Baldyga and Bourne 1999)

For $Sc \ll 4000$ (with Schmidt number $Sc = \nu/D =$ kin. viscosity/diffusion coefficient) and small amounts of feed compared to the bulk, engulfment has been shown to become the limiting step and, consequently, the EDD model can be simplified to the Engulfment model (Baldyga and Bourne 1989a). This simpler approach follows the reactions and engulfment for a small volume of feed solution in to the bulk fluid. The

growth of this volume is described by the Engulfment rate, E, and the change of concentration of a substance α in this reaction region is (Baldyga and Bourne 1999):

$$\frac{\mathrm{d}(c_\alpha)}{\mathrm{d}t} = E(c_{\alpha 0} - c_\alpha) + r_\alpha \qquad \textbf{(2.14)}$$

with the first term describing the effect of engulfment, $c_{\alpha 0}$ being the concentration of α in the bulk and c_α in the reaction zone, and the second term accounting for the reaction(s).

The engulfment behaviour was found to depend on local energy dissipation and viscosity. The authors analysed turbulence spectra and found that the energetically most active eddies, i.e. with the highest vorticity, are at a size around ~12η. From this, a characteristic time scale could be obtained – for exponential growth of the behaviour of the reacting zone was found to follow (Baldyga and Pohorecki 1995; Baldyga *et al.* 1997):

$$E = 0.058\left(\frac{\varepsilon}{\nu}\right)^{\frac{1}{2}} \; or \; \tau_E = \frac{1}{E} = 17.24\left(\frac{\nu}{\varepsilon}\right)^{\frac{1}{2}} \qquad \textbf{(2.15)}$$

The reciprocal value of E then gives a characteristic engulfment and, therefore, when it is limiting, micromixing time.

The above form of the Engulfment model is only valid for low volume fractions of added solution. Otherwise, interaction between the eddies of feed fluid, self-engulfment, might need to be considered (Baldyga and Bourne 1999).

The E model requires less computation time, i.e. it is 1-2 orders of magnitude faster to solve, than the EDD model (Baldyga and Bourne 1989a). Moreover, it has been applied to stirred tanks successfully which is supported by experimental results (Baldyga and Bourne 1990; Bourne and Yu 1994).

Another, similar approach is the Incorporation model as developed and described by Villermaux and his co-workers (Villermaux 1990; Villermaux *et al.* 1992). This was found to be on an equivalent basis as the Engulfment model (Villermaux and Falk 1994). The Incorporation model was adapted for the Iodide/iodate method by Fournier *et al.* (1996a) and has been employed in further studies (Fang and Lee 2001; Assirelli *et al.* 2008b). In these cases the product distribution could be calculated for a range of micromixing times, τ_m, and the corresponding values then used for interpretation of experimental data – for instance by employing equation (2.15) for estimating energy dissipation rates from the obtained micromixing time.

A more universal model, the Generalised Mixing Model (GMM), was described by Villermaux and Falk (1994), included the following mixing steps:

- erosion of fresh fluid
- dilution of the smaller eddies into the reacting zone
- incorporation of bulk fluid into the reacting cloud
- exchange or diffusion between small eroded and incorporated eddies in the reacting cloud

The authors showed that the GMM includes other models like the IEM, the Incorporation and Engulfment models as special cases.

Of the above models, the incorporation model was chosen for this work, because it and the equivalent engulfment model have been shown to be suitable for such applications, while being computationally less demanding than other options. In addition, this approach had already previously been used with this reaction scheme

(Fournier *et al.* 1996a; Assirelli *et al.* 2008b). Therefore, it is described in more detail in the following section.

Incorporation model

As can be expected from its equivalence to the engulfment model, the incorporation model is based on similar ideas and equations: Figure 14 shows a blob or aggregate of fresh feed, fluid 2, as it slowly grows due to incorporation of surrounding fluid 1.

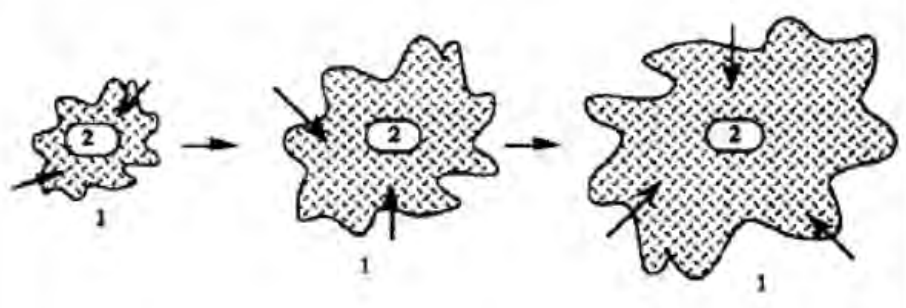

Figure 14: Incorporation between an aggregate of feed fluid 2 and bulk fluid 1 (Fournier et al. 1996a)

The characteristic incorporation time and the micromixing time, τ_m, are expected to be the same. The growth behaviour of the aggregate is described by

$$V_2 = V_{20} g(t) \qquad \textbf{(2.16)}$$

In contrast to the engulfment model, this can but does not necessarily have to be exponential growth, but can follow different functions g(t). Two suggested options (Fournier *et al.* 1996a) would be linear with $g(t) = 1 + t/t_m$ or exponential:

$$g(t) = e^{t/t_m} \qquad \textbf{(2.17)}$$

The concentrations of the different species can be described by considering the effects of the incorporation and the chemical reaction(s):

$$\frac{\mathrm{d}C_j}{\mathrm{d}t} = \left(C_{j10} - C_j\right)\frac{1}{g}\frac{\mathrm{d}g}{\mathrm{d}t} + R_j \qquad \textbf{(2.18)}$$

The above repeatedly suggested similarity to the E model becomes apparent when comparing equations (2.18) and (2.14). The details of the iodide/iodate reaction scheme will be discussed in section 3.1. and further details on the implementation of the model including the equations for all chemical species follow in section 4.2.1.

Calculating an independent value, like a micromixing time, e.g. the reciprocal value of the Engulfment rate (Baldyga and Bourne 1999) or the incorporation time (Villermaux and Falk 1994), should allow comparing results obtained from different reactant concentrations. In addition, for quantitative or even just comparative use of the Iodide/iodate method, the criticism and suggestions by Bourne (2008) and Kölbl and Schmidt-Lehr (2010) have to be considered. Therefore, model variations following these ideas will be evaluated in chapter 4.

2.3. Relevant studies in literature - What do we know already about the impact of additional phases on turbulence and its impact on reactions?

The effect of a dispersed phase, i.e. bubbles, drops or particles, on specific energy dissipation rates in a turbulently flowing carrier fluid is of interest for various (chemical) engineering applications, like multi-phase stirred tanks, bubble columns, jet flows, pneumatic conveying and combustion, but also in other fields, for instance higher in the atmosphere for studying cloud physics (Vaillancourt and Yau 2000) but

also under water for sediment transport and sand beds (Best *et al.* 1997). (In this part of the text, “particles” will be used to include bubbles and drops.)

In spite of the subject’s wide relevance and considerable research efforts, it is still not fully understood (Balachandar and Eaton 2010). Simulating the problem is particularly challenging, as calculations of such flows, i.e. direct numerical simulations (DNS) to resolve all turbulence scales, are computationally demanding, especially at higher Reynolds numbers. Moreover, turbulent flows are still poorly understood (Davidson 2004; Clay Mathematics 2011) and turbulence models, even in single-phase turbulence, can be of limited use (Elghobashi 1994; Versteeg and Malalasekera 2007). Sommerfeld and Decker (2004) mentioned in a review that commercial CFD codes like Ansys CFX and Fluent do not offer options to include, among other relevant effects, turbulence modulation due to the presence of particles in multi-phase flow simulations. Nevertheless, calculations using such commercial codes have been shown on occasions to give good agreement with experimental results (Micale *et al.* 2000; Montante *et al.* 2001). Of course, better understanding of these phenomena is needed for implementing them in mainstream software.

The purpose of the following section is to review relevant literature on the effect of added second or third phases on turbulent flows, especially on turbulence modulation and also micromixing in stirred vessels, will be discussed. Firstly, single-phase operation, including open questions relating to unbaffled vessels, will be briefly discussed to give a baseline and some background. Then phenomena involving interaction of turbulence and a second, dispersed phase, especially turbulence modulation will be introduced starting with literature on general fluid flow, though with a specific focus on possible consequences for stirred tanks. Finally, modelling and

results from experiments on turbulence (modulation) and micromixing in gas-liquid, solid-liquid and gas-solid-liquid stirred tanks will be reviewed.

2.3.1. Single phase

The distribution of turbulence parameters in stirred vessels has been measured for many years, starting with Cutter (1966) who used a photographic technique. In particular, he was the first person to show experimentally that the local specific energy dissipation rate, ε_T, close to the impeller was much higher than the average; whilst well away from the impeller near the extremities of the tank, ε_T was much less than the average. The early work of Bourne and co-workers, e.g., Bourne *et al.* (1981a), on micromixing in turbulent systems showed that it was the local ε_T value that controlled the selectivity in fast chemical reactions, hence the importance of this parameter.

Recently, turbulence has mainly been studied using LDA or PIV, which are much more accurate techniques. However, the raw data still require significant data treatment and a number of modelling assumptions to give information on the local specific energy dissipation rates, ε_T (Kresta 1998; Unadkat *et al.* 2009b). That treatment and model choices are not straightforward and can have a major impact on the local values of ε_T estimated, as has been illustrated by Gabriele *et al.* (2009). In addition to modern laser based measurements, micromixing experiments, in combination with micromixing modelling, also allow estimations of local ε_T levels (Bourne and Tovstiga 1988; Assirelli *et al.* 2002). Though both approaches, of course, should essentially give the same value of ε_T at any location for each particular flow system, they generally do not and each has some advantages and some disadvantages. Optical methods actually try to measure the local ε_T and the

PIV technique can give more information, e.g. local data for a plane, than micromixing experiments. The latter, on the other hand, assume that the reactions that occur depend on the local ε_T, which is then obtained from a model, and therefore the estimated value depends on a realistic model. In addition, it only measures ε_T at the location of the reactant feed position. On the other hand, optical methods are more likely to become problematic or even to fail in multi-phase and especially opaque systems. Data treatment needs attention in both cases.

Figure 5 illustrated the well-established concept that the local specific energy dissipation levels near an impeller are significantly higher than in the bulk of a liquid-only, baffled, stirred vessel. Micromixing experiments using competing reactions confirm this, as less side-product is formed when feeding close to the impeller compared to feeding closer to or onto the liquid surface (Bourne and Yu 1994; Villermaux *et al.* 1994; Schäfer 2001; Assirelli *et al.* 2002). Assirelli *et al.* (2005) showed that continually feeding into the trailing vortices of a Rushton turbine using rotating feed pipes gives even better micromixing.

2.3.2. Possible effects of an added phase

Suggested effects in the presence of particles

It is well-known that even small amounts of polymer additives can significantly decrease drag, which is of use for instance in pipelines (Patterson *et al.* 1969; White and Mungal 2008). In these cases, the pressure drop in pipes is lowered as well. Similarly, such additives lower power input in stirred tanks too (Quraishi *et al.* 1976). Also, solid particles have been observed, depending on the particle and flow properties, like characteristic response times, enhancing or delaying the transition

from laminar to turbulent flow (Saffman 1962; Brennen 2005). These are examples of possible effects of dispersed phases in (turbulent) fluid flows. In the following section, further literature on turbulence - particle interaction effects which have been shown to be relevant for stirred tanks will be discussed.

Preferential concentration – also called inertial clustering – is another well-recognised aspect of particle - turbulence interaction which has been reported extensively (Maxey 1987; Squires and Eaton 1991; Crowe *et al.* 1996; Balkovsky *et al.* 2001): it has been shown that particles which are heavier than the fluid may accumulate in regions of low vorticity, i.e. move away from eddies, while bubbles and lighter particles tend to move towards intense vorticity, as can also be observed with bubbles collecting in the trailing vortices of rotating impellers. Heavier particles will be moved out of eddies due to their inertia and resulting centrifugal forces, while lighter particles can follow such flows, as has been illustrated for instance by Sundaram and Collins (1997) who used DNS – Figure 15 shows how particles may be distributed due to inertial clustering: the circles and arcs represent the turbulent eddies and the dots are particles; with the bigger ones getting centrifuged out of the turbulent region.

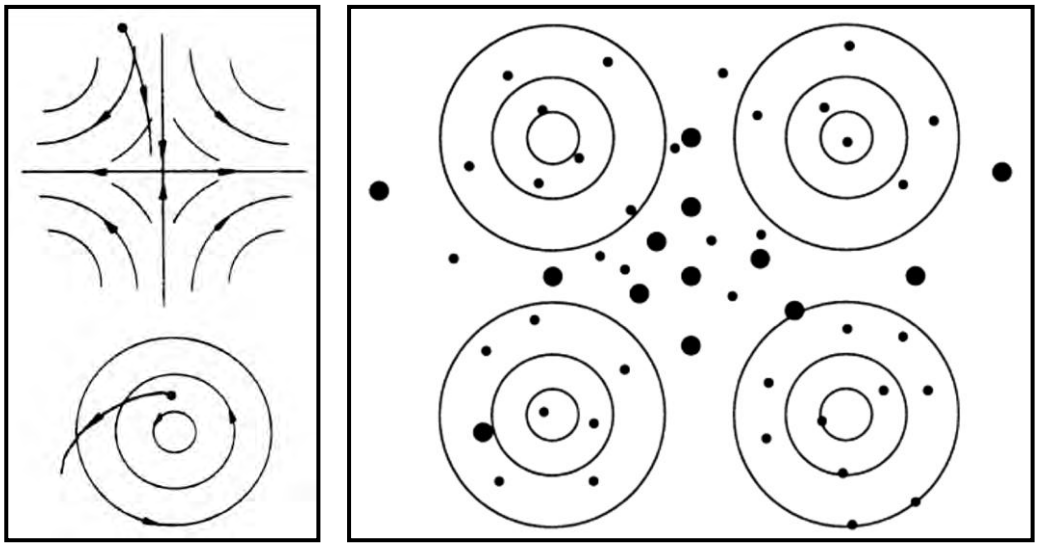

Figure 15: Schematics showing particle distribution due to inertial clustering – left: Eaton and Fessler (1994) – right: Sundaram and Collins (1997)

This phenomenon has been observed in experiments, in addition to, as mentioned, fluid flow simulations (Salazar *et al.* 2008). They investigated the behaviour of hollow glass spheres in nearly isotropic turbulence at three (very low) Reynolds numbers between 110 and 149. This is one of few studies where experimental and computational data have been compared. The authors employed digital holographic particle imaging and DNS and found good agreement between their results. Still, the authors mentioned issues with the experiments and information from such low Reynolds numbers is probably not directly relevant to turbulent stirred suspensions. This should illustrate the wide gap between what can be measured and simulated today and industrially relevant conditions like those encountered during solid-liquid mixing in a turbulent stirred tank.

The locally increased particle concentration might be expected to affect particle collision rates and this has therefore been studied, mainly in simulations, e.g. by

Sundaram and Collins (1997) and Wang and Wexler (2000) who employed DNS. In spite of recent advances, further work needs to be done in this field (Wang and Wexler 2000).

The most relevant part of the existing body of published knowledge was reviewed by Eaton and Fessler (1994) and more recently by Balachandar and Eaton (2010).

Interestingly, such locally increased particle concentrations, as described above for simpler systems, were also reported for stirred solid-liquid systems, e.g. by Derksen (2003) who performed LES of suspensions in an agitated vessel and Micheletti and Yianneskis (2004) who employed LDA with a refractive index matching technique. This phenomenon has nevertheless not been extensively studied for stirred tanks and further research would be warranted.

In addition to being affected by the turbulent fluid flow, particles can also have effects on the carrier fluid. Elghobashi (1994) gave an overview of these possibilities in a graph which maps them with respect to particle volume fraction and relative particle size, expressed as the ratio of characteristic times of fluid and solid (called Stokes number which is discussed later). This graph is reproduced in Figure 16; it shows that particles will not affect turbulence at very low concentrations, but that turbulence can affect the dispersed phase. This is often referred to as one-way coupling and inertial clustering, as discussed above, might be an example of such effects. At higher concentrations, two-way coupling can be observed, i.e. particles may also alter the fluid flow and its turbulence, in addition to being affected by it. When

particle concentrations increase even further, four-way coupling can be seen and particle-particle interactions like particle-particle collisions become relevant.

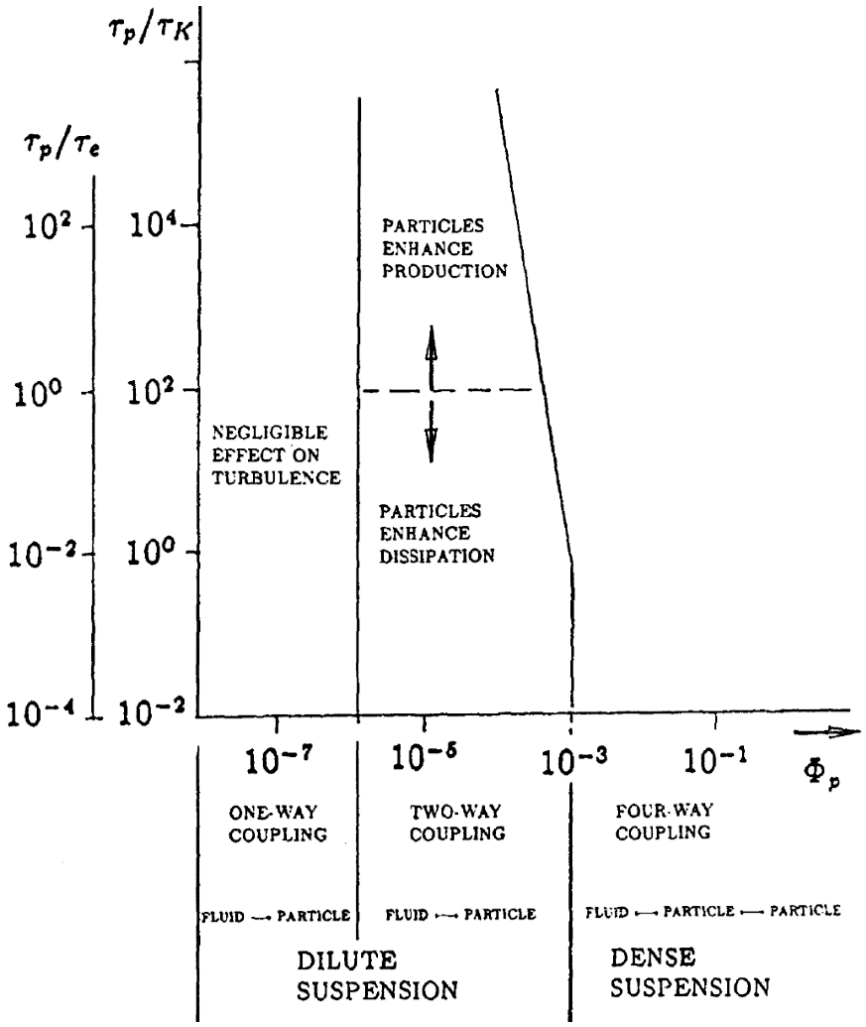

Figure 16: Map of regimes of interaction between particles and turbulence (Elghobashi 1994)

Moreover, Figure 16 shows that in two-way coupling particles may enhance turbulence production or dissipation. This effect of dispersed solid phases on turbulence in fluids has been studied extensively. Reviews of data from LDA and some hot-wire anemometry experiments in pipe and jet flows suggest that “small” particles suppress turbulence while “large” particles enhance turbulence (Gore and Crowe 1989; Hetsroni 1989; Gore and Crowe 1991). Several parameters have been

proposed for determining the significant characteristics of “small” and “large” particles, i.e. at which conditions the transition between attenuation and augmentation occurs. Some of these suggested criteria are discussed below, though it is worth mentioning that in most experimental work, relatively simple flow fields have been studied and often air has been used as the continuous (often in such studies called, carrier) phase, which might make comparisons to stirred tanks difficult. Unfortunately, these phenomena are not fully understood yet, but a number of mechanisms have been given in literature to explain the observed effects of particles on turbulence (Brennen 2005; Balachandar and Eaton 2010).

In the book “Particles, bubbles & drops: their motion, heat and mass transfer”, Michaelides (2006) suggested that the following mechanisms may contribute to turbulence modulation in two phase mixtures:

a) Vortex breaking and dissipation of turbulence kinetic energy on the surface of the immersed objects
b) Modification of the effective viscosity of the fluid
c) Eddy energy dissipated on the acceleration and deceleration of the elements of the dispersed phase
d) Wakes and shedding of vortices behind the immersed objects
e) Fluid moving with the immersed objects or being displaced by them
f) Enhancement of the fluid velocity gradients between two neighbouring immersed objects
g) Deformation and vibrations of the surface of the immersed objects

Of these points g) is not applicable for solid particles and f) and g) can usually be neglected for low solid concentrations as well (Michaelides 2006).

Adding to these options, Ferrante and Elghobashi (2003) suggested explanations for their unexpected results from simulations without gravity and with particles which were smaller than Kolmogorov length scale. The calculations showed that small particles might also produce the opposite of the usually observed effect: The authors found increases in turbulent kinetic energy and energy dissipation levels. They suggested that the particles might stay in the vortices which adds inertia and consequently allows the vortices to stay stable for longer. In contrast, larger particles would leave the eddies and enter new ones, creating counter-torques, which would then reduce turbulence.

In a recent review (Balachandar and Eaton 2010), possible turbulence modulation mechanisms were summarised as:

- for suppression:
  a) the enhanced inertia of the particle-laden flow
  b) increased dissipation arising from particle drag
  c) the enhanced effective viscosity of the particle-laden fluid
- for enhancement:
  d) enhanced velocity fluctuation due to wake dynamics and vortex-shedding
  e) buoyancy-induced instabilities due to density variation arising from preferential particle concentration

The authors (Balachandar and Eaton 2010) stated that sometimes several mechanisms might, over a range of different scales, become relevant simultaneously. They also added that current understanding still needs to be extended and that contradictory results can be found in literature.

The last sentence also applies to such effects in stirred tanks, as will be discussed in the following sections, 2.3.3. and 2.3.4.. These will cover experimental data from stirred tanks and a distinction between added gaseous and solid phases is made, not only because of the different density ratios compared to typical liquids, but also due to different behaviour of particles compared to bubbles, which can deform and break up and may coalesce. First, however, several suggested ways for determining the transition between augmentation and suppression due to turbulence modulation are discussed.

Transition criteria for turbulence modulation proposed in literature

A few parameters have been proposed for determining the transition of turbulence modulation between suppression and enhancement. These will be introduced in the following paragraphs with particular emphasis on possible application to flows in stirred tanks. Such estimates might be useful for the interpretation of experimental and modelling results.

Ratio of length scales – Gore and Crowe criterion

Gore and Crowe (1989) showed, based on an extensive literature review of experimental data, that a ratio of characteristic lengths may be used for estimating which turbulence modulating effect the added dispersed phase might have.

Specifically, the particle diameter, d_p, and a characteristic turbulent length scale, l_c, i,e, fluid integral length scale, L, or the characteristic length of the most energetic eddy when only one phase is present, were given:

$$\frac{d_p}{l_c} \cong 0.1 \qquad \textbf{(2.19)}$$

For pipes, Gore and Crowe (1989) estimated the characteristic fluid length scale from $l_c/R = 0.2$ (with R = pipe diameter) as suggested by Hutchinson *et al.* (1971) which is only valid near the centreline of a pipe. For jets, another ratio was used: $l_c/x = 0.039$ (with x = axial distance from jet exit) again with some limitations in applicability (Wygnanski and Fiedler 1969). The authors (Gore and Crowe 1991) later published more data also adding results from pipes and jets, but in contrast to the previous work also from other radial positions than the centreline. In these cases the trends were still in agreement with the suggested ratio. The correlation, however, becomes weaker in pipes near the wall. Gore and Crowe argued that this might be because the flow becomes more anisotropic towards the wall which leads to less well-defined length-scales. In stirred tanks, this spatial variation needs to be considered (Kresta 1998). Gore and Crowe emphasised that the criterion does not aid estimating by how much turbulence is altered. For this purpose more factors would have to be considered. Further the authors argue that this criterion, nevertheless, is useful to determine which effect is expected. In addition, they state that the characteristic length of the most energetic eddy is usually known (though they do not elaborate on this point) and that this might be an advantage compared to other, less readily available parameters.

Unfortunately, that length scale is probably often not known for more complex and many industrially relevant flows: it may, for instance, be argued that the integral

length scale for instance in stirred tanks is not well-defined. As an approximation, a value of 0.1 D or W/2 has been suggested, though higher values might be expected for regions further away from the impeller discharge stream (Kresta and Wood 1993). Also later, Kresta (1998) emphasised that the integral scale of turbulence changes from the impeller to the bulk of the tank.

Various authors have reported values for the integral length scale and a few examples will be given here to illustrate the general trend of the available data: Lee and Yianneskis (1998) found 0.1 to 0.3 W in the impeller stream using LDA. They added that the above mentioned estimate of the integral length scale being around 0.1 D could give an overestimation of L by a factor of 2 near the blade tip. Moreover, Ducci and Yianneskis (2005) reported that the average integral length scale in the vicinity of ε_{max} was around 0.05 D, i.e. about 50% of what would usually be expected from the above estimates. Similarly, Gabriele *et al.* (2009), who normalised their results against 0.1 D, found values from ~0.2 near a pitched-blade turbine to ~0.8 towards the wall, i.e. 20 to 80% of the estimate. In contrast, higher values have been found in the bulk of the tank, e.g a range of 0.25 W near the impeller to 1-3 W in the bulk (Costes and Couderc 1988). In a particularly careful study, Schäfer (2001) also found significant differences between the region near the impeller and the bulk. He suggested using different length scale values for these two parts of the vessel – 0.221 W for the impeller region and 0.333 T for the bulk, which is far away from justifying the use of a constant value for the entire tank.

The examples given should illustrate that the integral length scale of turbulence may vary throughout a stirred tank, i.e. an approximation with e.g. 0.1 D or W/2 could lead to overestimation of L near the impeller and underestimation in the bulk. Therefore,

local information for particular cases might be necessary. Otherwise, correlations that work reasonably well in geometries like pipes or jets might not be as useful in agitated vessels. Another aspect of this is that a variation of L could, according to (2.19), lead to more complexity, e.g. turbulence augmentation in one part of the vessel and suppression in another region.

Table 1 gives an impression of how this criterion could be applied to agitated vessels. For this, the examples given above were used to estimate whether turbulence augmentation or suppression would have to be expected in the tank used in this work (for details see 3.2) when $500\ \mu m$ particles are added to the flow. The given criterion would suggest both effects and the range of values for $\frac{d_p}{l_c}$ is significant.

Table 1: Gore and Crowe criterion applied to a stirred tank (geometry, as used in this work) with $d_p = 500\ \mu m$

reference	options for l_c	location in tank	$\frac{d_p}{l_c}$ (for given example)	comments (↑/↓ = augment./suppr.)
Kresta and Wood (1993)	$L = 0.1D\ or\ W/2$	general ("rule of thumb")	0.052	↓
Lee and Yianneskis (1998)	$L = 0.1\ to\ 0.3\ W$	impeller stream	0.260 to 0.0868	↑ and ↓ (factor of 3)
Ducci and Yianneskis (2005)	$L = 0.05D$	near ε_{max}	0.104	↑
Costes and Couderc (1988)	$L = 0.25\ W$ $L = 1\ to\ 3\ W$	near impeller in the bulk	0.104 0.026 to 0.009	↑ and ↓ (factor of 12!)
Schäfer (2001)	$L = 0.221$ W $L = 0.333T$	impeller region for the bulk	0.118 0.005	↑ and ↓ (factor of 23!)

Particle Reynolds number in stirred vessels

Hetsroni (1989) argued after reviewing literature, similar to Gore and Crowe's approach (1989), that the interaction between the particles and the fluid is based on their size, relative velocity and density difference, which can consequently be correlated using a particle Reynolds number, which the author suggested to define as:

$$Re_p{}^* = \frac{(u_f - u_p)d_p(\rho_p - \rho_f)}{\mu_f} = \frac{u_R d_p(\rho_p - \rho_f)}{\mu_f} \qquad \textbf{(2.20)}$$

This definition of the Reynolds number deviates from that usually employed, as the density and velocity differences between the phases and not the liquid density and velocity are used. The author justified this definition because of the significant effects of inertia and buoyancy on particle movements. In the actual argumentation, Hetsroni (1989) did use the Reynolds number which only contains the fluid density and based the review and interpretation of experimental data on that variable:

$$Re_p = \frac{u_R d_p}{\nu_f} \qquad \textbf{(2.21)}$$

The author concluded that particles with a low particle Reynolds number tend to suppress turbulence of the carrier fluid while particles with high particle Reynolds number, Re_p, i.e. larger than about 400, tend to enhance the turbulence, which Hetsroni (1989) suggested was probably due to vortex shedding. More recent work suggests that the onset of vortex shedding depends on surrounding turbulence to some extent (Balachandar and Eaton 2010). Hetsroni (1989) also added that further experimental data was needed to quantify these effects.

Data on the velocity difference might not be available in some cases and other formulations of the particle Reynolds number might need to be considered.

Fessler and Eaton (1999) studied turbulence modification by particles in a backward-facing step flow and gave three options for the slip velocity in Re_p:

- particle-fluid mean velocity difference
- terminal velocity of the particles
- fluctuating particle or fluid velocities

The authors concluded that all three options are suitable in their case, as all of them are in the same order of magnitude. For other applications, this might not be true. Moreover, velocity data is often not available to estimate values for the first and third option. Therefore, the second suggestion, the terminal velocity, might be worth considering and it indeed has been suggested: in their review, Poelma and Ooms (2006) defined the particle Reynolds number as

$$Re_p = \frac{d_p u_{TV}}{\nu_f} \qquad \textbf{(2.22)}$$

with u_{TV} being the terminal velocity, i.e. the velocity a particle reaches when falling in a quiescent fluid. The authors stated that Re_p can otherwise be defined using, e.g., the root-mean-square value of the free-stream turbulence as well.

It might be possible that such definitions using a different velocity could lead to deviations from the original suggestion by Hetsroni (1989) and obtaining data like RMS values might not be an option in many cases. In fact, the terminal velocity, i.e. from a fluid at rest, could be determined quite easily. However, its use might not be appropriate in the case of turbulent flows like in a stirred vessel, as it has been shown that actual settling velocities tend to be much lower than expected. For instance, Schwartzberg and Treybal (1968) reported settling velocities in an agitated tank which were about 30-50% of the terminal velocity in a quiescent fluid. Also other early experimental investigations (Levins and Glastonbury 1972; Nienow and Bartlett

1974) in stirred tanks also showed lower values and Brucato *et al.* (1998) even observed a drop down to 15% in a study of a Taylor-Couette-flow. In addition to reports of such measurements, correlations based on experimental data have been proposed and relatively successfully employed in CFD simulations (Lane *et al.* 2004; Doroodchi *et al.* 2008). Indeed, earlier simulations had shown the necessity of considering the effects of turbulence on particle drag coefficients in such simulations (Micale *et al.* 2000). Unfortunately, this significantly complicates the otherwise quite simple approach for finding the transition between turbulence augmentation and suppression by using the settling or terminal velocity to calculate the particle Reynolds number.

In stirred tanks, as with the Gore and Crowe criterion, such calculations tend to become less straightforward to implement compared to simple geometries like pipes or jets. The relative velocity, as suggested by Hetsroni (1989), might be difficult to use for many engineering problems where even detailed information on local single-phase velocities might not be available, let alone multi-phase data. In some cases lab-scale data might be available, but scale-up would still need to be considered. For some problems, it might seem more feasible to obtain such information computationally, for instance Ochieng and Onyango (2008) tested drag models in CFD and could therefore get values for the relative velocities from their simulations. Actually, apart from flow simulations, obtaining relative velocities for a given set-up would require experimental investigation of the two-phase flow and consequently would not help with reducing the need for such measurements.

Stokes number in stirred vessels

Another dimensionless expression, the Stokes number, has also been suggested for characterising turbulence modulation (Owen 1969; Poelma and Ooms 2006).

The Stokes number is a measure of how faithfully a particle follows a flow or, in other words, if it will follow a fluid flow around an obstacle or if it will hit the object. In many cases and usually also in the context of turbulence modulation, it is defined as the ratio of particle response time to fluid response time (Schetz and Fuhs 1996; Post 2010; Yeoh and Tu 2010):

$$St = \frac{\tau_p}{\tau_{flow}} \qquad \textbf{(2.23)}$$

This variable is in general relevant for investigating flows like those in stirred tanks, as smaller numbers suggest that the particle will be strongly affected by the surrounding fluid flow and that it may be used as a flow tracer, for instance in PEPT (Fangary *et al.* 2000; Chiti *et al.* 2011) and PIV (Melling 1997; Unadkat 2009).

As it gives an idea of how strongly a particle will follow a flow, it is also frequently used for describing preferential particle concentration due to inertial clustering which is introduced above (see: Suggested effects in the presence of particles). It is quite well-established that inertial clustering is strongest around $St = 1$ (Squires and Eaton 1991; Balachandar and Eaton 2010). In this case, the particles will not follow the flow perfectly, but will still be affected by it.

As suggested above, the Stokes number has also been employed in the context of turbulence modulation, in addition to characterising inertial clustering. Therefore, a closer look especially in the context of stirred tanks is warranted. For this variable

there are two aspects to consider: a) the critical value and b) the calculation of the number. These are linked, of course, but will be discussed separately for clarity.

a) Critical value:

Owen (1969) argued that large particles with much higher relaxation times than energy containing eddies would act more as fixed locations of resistance, while much smaller ones would follow the turbulent motion. Therefore, the critical value would be $St = 1$. Elghobashi (1994) (see Figure 16) followed this idea, but gave two Stokes numbers, one for the integral scale and one using the Kolmogorov scale. The latter had a critical value of 100 for a flow Reynolds number of 10^4. In recent studies (Ferrante and Elghobashi 2003; Poelma and Ooms 2006) this definition of using the Kolmogorov scale was followed too, but in these cases a value around 1 was found critical, in contrast to the higher one of 100 indicated by Elghobashi (1994). In work on stirred tanks, this definition has also been used with assuming the transition of suppression and augmentation around unity (Gabriele *et al.* 2011). A recent review (Balachandar and Eaton 2010) gives an overview of relevant studies, but the authors do not find a clear critical value for turbulence modulation when using the Stokes number.

b) Calculation of the Stokes number:

Owen (1969) was (one of) the first to propose the Stokes number for evaluating the interaction between particles and a turbulent fluid flow, suggesting to calculate the particle relaxation time, τ_p, according to Stokes' law:

$$\tau_p = \frac{1}{18}\frac{\rho_p}{\rho}\frac{d_p^2}{\nu} \qquad \textbf{(2.24)}$$

In Owen's (1969) study, pneumatic phenomena were discussed, i.e. air was the carrier phase – in stirred tanks it might make sense to use the density difference instead of ρ_p to take the more significant effect of buoyancy into account. Clearly, this seems less relevant for the original case of air and heavier particles.

The author stated that Stokes' law was sufficient in this case for simplicity and, because he was concerned with orders of magnitude only. This needs consideration, especially when taking the before mentioned settling behaviour into account. Unfortunately, using Stokes' law to characterise the particle behaviour might be debatable, as it is – strictly speaking – only applicable for low Re_p around 0.1 (Rhodes 2008) or 1 (Micheletti and Yianneskis 2004) and, therefore, clearly does not cover the range of interest in turbulence augmentation, for instance when vortex shedding occurs at $Re_p > 400$ (Hetsroni 1989). Nevertheless, in some cases, finding a suitable characteristic fluid time for complex flows like in stirred tanks could be a bigger issue than the one for particles. Owen suggested using the characteristic time of an energy-containing eddy for describing the fluid flow. Such large eddy time scales, for instance the integral time scale, were employed by several authors (Fessler and Eaton 1999; Sommerfeld 2001). In contrast, other authors calculated the Stokes number considering the smallest turbulent eddies using the Kolmogorov time scale as the characteristic fluid time (Ferrante and Elghobashi 2003; Poelma and Ooms 2006), as mentioned for the critical value. This might, however, be interpreted as a contradiction to Gore and Crowe (1989) who employed a characteristic length scale of turbulence which usually is the integral length scale, i.e. on the other extreme of the spectrum. If it can be shown that one of both length

scales works for predicting turbulence modulation in specific situations and another criterion is useful in other cases, this might suggest different mechanisms, as listed above, becoming relevant in those cases.

In stirred tanks, the Stokes number has been used as well and, while the calculation of the particle response time has usually followed equation (2.24) (Fangary *et al.* 2000; Derksen 2003; Gabriele *et al.* 2011), there are several options for the fluid time scale: Nouri and Whitelaw (1992), for instance, defined the single-phase flow response time, based on blade width and impeller tip speed. Other workers (Fangary *et al.* 2000; Chiti *et al.* 2011) used a fluid relaxation time based on impeller diameter and, again, impeller tip velocity:

$$\tau_{f_{Chiti}} = \frac{1}{\pi N} \qquad \textbf{(2.25)}$$

Derksen (2003) gave the Stokes number for particles in a stirred vessel as the ratio of the Stokesian particle relaxation time, and the time of one impeller revolution:

$$\tau_{f_{Derksen}} = \frac{1}{N} \qquad \textbf{(2.26)}$$

Obviously, a comparison between these Stokes numbers would give different results for the transition between turbulence suppression and augmentation in the same system. Also, the integral time scale as proposed in literature on other flows (Owen 1969; Sommerfeld 2001) might be useful in stirred systems. Unfortunately, this could be problematic due to the issues already discussed for the integral length scale. It seems that choosing the flow response time is not straightforward in this case where a wide range of time and length scales might be relevant – and affected.

However, the Stokes number has also been defined as the ratio of the particle time scale and the Kolmogorov time scale by several authors (Elghobashi 1994; Poelma and Ooms 2006) on particle-turbulence interaction. And, this definition has been applied to particle-turbulence interaction in stirred tanks as well (Gabriele *et al.* 2011):

$$St = \frac{\tau_p}{\tau_k} \qquad \textbf{(2.27)}$$

Sundaram and Collins (1997) chose this option too, but admitted that the choice of the normalising scale is not obvious. Even though this might indeed be a reasonable definition considering the importance of the smallest scale of turbulence for energy dissipation and also for micromixing problems, good estimates of power input, let alone local energy dissipation levels and consequently the Kolmogorov scales might not be available in some systems. In addition, energy dissipation levels vary by orders of magnitude in stirred tanks and, therefore, a Stokes number employing ***local*** turbulence values might show different effects in different parts of the flow, as mentioned for the ratio of length scales as well. Turbulence augmentation and suppression occurring in the same vessel might be a possible scenario, but has so far not been reported in literature (and would further complicate the issue).

The above gives an idea of the discrepancies in literature on defining the Stokes number – from the time of rotation of the impeller, including π or not, to integral time scales or smallest turbulence time scales – and on the critical value. In such complex flows, these options could lead to significantly different interpretation of experimental or modelling data, as illustrated in Table 2. This example is a stirred tank (geometry as used in this work, but with H=T) with N = 10 rps, Po = 5, water as

fluid and glass beads ($d_p = 500\ \mu m$) and estimating values for τ_k from literature data. A critical value of $St = 1$ was assumed, as other options would lead to more confusion.

Table 2: Stokes number criterion applied to a stirred tank example

reference	options for τ_f	St (using ρ_p)	St (using $\rho_p - \rho_f$)	comments (↑/↓=aug./sup.)
Fangary *et al.*(2000) Chiti *et al.* (2011)	$\frac{1}{\pi N}$	1.09	0.66	↑ and ↓
Derksen (2003)	$\frac{1}{N}$	0.35	0.21	↑
Gabriele *et al.* (2011) (conservative estimates: ϕ_{max}=50 (Schäfer 2001) ϕ_{bulk}=0.2 (Geisler and Mersmann 1988))	τ_k	363.02 (ε_{max}) 22.96 (ε_{bulk}) 51.34 ($\overline{\varepsilon_t}$)	218.25 (ε_{max}) 13.80 (ε_{bulk}) 30.86 ($\overline{\varepsilon_t}$)	↓ (note variation between values)

Regardless of the above points, critical value and calculation of Stokes number, the range of scales in stirred tanks, as shown for τ_k in Table 2, can complicate the use of the suggested transition criterion.

Apart from the difficulties with the Stokes number discussed so far, another issue was suggested by Gore and Crowe (1991) and later by Tanaka and Eaton (2008). Gore and Crowe (1991) showed in a diagram the change of turbulence modulation as a function of Stokes number and did not find good correlation. Tanaka and Eaton (2008) plotted experimental results in a Re-St graph which did not give a clear picture either and therefore, they argued that the Stokes number is (even) less useful for determining the transition than the ratio of length scales proposed by Gore and

Crowe (1989). For this reason, Tanaka and Eaton (2008) introduced another dimensionless number, the particle momentum number.

Particle momentum number – Pa

Recently, Tanaka and Eaton (2008) suggested a new expression, the particle momentum number, Pa, as a criterion for determining the transition between turbulence modulation effects. The dimensionless number was obtained from the normalised Navier-Stokes in the presence of particles and can be expressed as a function of Stokes and Reynolds number:

$$Pa_{St} = St\, Re_L^2 \left(\frac{\eta}{L}\right)^3 \qquad \textbf{(2.28)}$$

with Re_L being the large scale Reynolds number, η the Kolmogorov length scale and L a (large scale) length scale. When plotting data from experiments in pipe and channel flows, suppression was found for at $3 \cdot 10^3 \leq Pa_{St} \leq 10^5$ and enhancement occurring at higher and lower values (Tanaka and Eaton 2008; Balachandar and Eaton 2010). Aside from Pa_{St}, the authors gave a second particle momentum number, Pa_{Re}, as an alternative:

$$Pa_{Re} = \frac{1}{18}\frac{Re_L^2}{Re_p}\frac{\rho_p}{\rho_f}\left(\frac{d_p}{L}\right)^3 \qquad \textbf{(2.29)}$$

which also contains Re_p and d_p, the particle Reynolds number and diameter, respectively, and the densities of the particle (ρ_p) and the fluid (ρ_f).

Tanaka and Eaton (2008) state that mass loading is relevant for the extent of turbulence modification, but not a factor for the transition itself, as there are no experiments where augmentation and suppression were observed depending on the amount of particles. Interestingly, Unadkat *et al.* (2009a) did find changes over a range of particle concentrations, though it may reasonably be argued that their

results at higher concentrations were already affected by particle-particle interaction and not just two-way coupling anymore.

As the particle momentum number has only been introduced recently, further work evaluating its limitations is needed. In addition, it might be difficult to use in poorly characterised or complex flows as it requires values like the Stokes number or the particle Reynolds number. Therefore, the issues mentioned above are also relevant for the particle momentum number and its use for applications like stirred tanks might be limited. Nevertheless, it is based on fundamental principles i.e. the Navier-Stokes equations and an interesting, new approach which could and should be studied further (Lohse 2008).

Conclusion for transition criteria

The above dimensionless numbers – ratio of length scales, particle Reynolds number, Stokes number and particle momentum number – have been suggested in consideration of the available data for turbulence modulation. In spite of the research efforts in this direction, none of these options has actually been agreed on, let alone become a well-established standard (yet). Moreover, a reasonable definition and consequently calculation of such numbers for more complex flows than in pipes or jets, as for instance in stirred tanks, might be problematic due to the wide range of scales and turbulence intensities involved.

Once qualitative trends of turbulence modulation have been shown to consistently agree with one criterion, quantitative estimates of the extent to which modification occurs would be of interest for modelling tasks, especially for CFD. Further factors like the effect of particle concentration or density differences will need to be investigated as well.

One might, however, argue that it will be difficult to find one number which describes the conditions in all parts of a stirred tank. Ratios containing local information, like the particle Reynolds number, would at least allow a more flexible approach, but would then require data which are very difficult to obtain.

In addition to determining the transition between enhancement and suppression in general, there are also disagreements between experimental data for stirred tanks; a brief review of available literature is given in the following sections.

2.3.3. With gas bubbles

As shown in part 2.1.3, sparging a stirred vessel with gas can strongly affect the power input from an impeller and therefore the mean specific energy dissipation rate (Chapman *et al.* 1983c; Harnby *et al.* 1997; Paul *et al.* 2004) – Figure 7. There is less information on the effect of the presence of gas bubbles on local energy dissipation levels and consequently micromixing in stirred vessels: Morud and Hjertager (1996) reported velocity and RMS data for the gas phase using LDA/PDA and used it to verify CFD results. Information on the distribution turbulence levels in the liquid phase, however, was not given by the authors. PIV measurements from a similar study of the liquid phase (Deen and Hjertager 2002) again are of limited use in terms of micromixing for this study, as they are not at constant power input. However, the authors did report effects of the gas on the fluctuating velocities which could allow more detailed discussion of micromixing results. Also other studies using various methods (Lu and Ju 1987; Khopkar *et al.* 2003; Khopkar *et al.* 2005; Montante *et al.* 2008) do not aid understanding in this specific context, as they either were focused on the general flow field or had relatively low gas sparge rates.

Measurements with a mechanical-piezoelectric sensor by Fort *et al.* (1993) suggested that the gas flow significantly suppressed the local energy dissipation rate in the impeller discharge flow and enhanced it in the rest of the vessel. Unfortunately, such sensors probably have insufficient frequency response to make accurate measurements of this parameter.

Bourne (1994), based on concepts of micromixing and results from diazo-coupling experiments set out in the PhD thesis of Hilber (1987), reported that $(\varepsilon_T)_g$ (subscript g for "with gas") near the impeller was not affected by gassing rates of up to 1.5 vvm at constant power input, i. e., if $(\overline{\varepsilon_T})_g = \overline{\varepsilon_T}$. In that thesis (Hilber 1987), it was also shown that micromixing near the surface was improved by sparging. On the other hand, a similar study (Brilman *et al.* 1999) in a 0.7 L vessel also using diazo-coupling found a negligible effect of sparging from ~ 0.5 to 10 vvm on micromixing, both near the impeller and half way between it and the liquid surface at constant impeller speed. This result is somewhat surprising as, at constant speed, $(\overline{\varepsilon_T})_g < \overline{\varepsilon_T}$ and so are the equivalent local values. Lin and Lee (1997) used the iodide/iodate reaction scheme again in a small 1 L stirred vessel sparged at ~ 1.5, 10 and 20 vvm with nitrogen and compared the results with those without sparging. They used various impeller speeds (without power measurement) with three feed positions, two at the height of the impeller and one close to the bottom of the vessel. They generally reported improved micromixing but most of the experiments were conducted under flooded conditions where, especially at the higher rates, the specific energy dissipation rate from the sparged gas would have been greater than that from the impeller. The latter condition may also have applied to the work of Brilman *et al.* (1999) at the higher sparge rate. For the non-flooded conditions, Lin and Lee (1997)

found that when feeding the closest to the impeller, the X_S values were generally greater than the unsparged especially at the lower flow rate with little impact at the higher rates. Data for the unsparged case were not reported for feeding near the base so a comparison cannot be made for that location.

Two other relevant studies are those of Langheinrich and Nienow (1999) and Boulton-Stone and Blake (1993). The former found that under flooded conditions, sparging improved macromixing of material added to the top of a vessel when $\overline{\varepsilon_T}$ was very low; whilst the latter showed that $(\varepsilon_T)_{bub}$ associated with bursting bubble but very localised to them is many orders of magnitude greater than that from stirring.

Clearly, the impact of sparging on micromixing is unclear. Therefore, it was decided to use the iodide/iodate method to study it, especially measuring the power input so that agitator speeds giving $(\overline{\varepsilon_T})_g = \overline{\varepsilon_T}$ could be selected, at a position near the impeller where ε_T is high giving efficient micromixing in single-phase systems (Assirelli *et al.* 2002), and near the surface, which is convenient for industry but not effective for micromixing with Rushton turbines under unsparged conditions (though the use of up-pumping impellers leads to a significant improvement as verified in Bhattacharya and Kresta (2004)).

2.3.4. With solid particles

Direct measurements in stirred suspensions

In stirred solid suspensions, flow fields have been investigated experimentally at sufficiently low concentrations, some with refractive index matching, that laser-based techniques could be used. Mostly these studies have concentrated on the impeller region. The first to measure the local specific energy dissipation rate, $(\varepsilon_T)_{max}$ were

Geisler and Mersmann (1988). They used laser Doppler anemometry (LDA) with refractive index matching and found that with 715 μm particles at 5 vol.% agitated by a Rushton turbine, $(\varepsilon_T)_{max}$ increased (but without any effect near the top surface). More recently, Unadkat *et al.* (2009a; 2009b) using PIV have made similar measurements for a pitched blade turbine with up to 0.5% by wt glass beads of 300, 750 and 1000 μm. They found a reduction in $(\varepsilon_T)_{max}$ very close to the impeller with the 300 and 1000 μm particles, the former giving the highest fall of ~ 25 %; and no effect at 750 μm. In spite of the problems with the Gore and Crowe criterion as discussed above, they suggested that the suppression found with the 300 μm particles agreed with their criterion but on the other hand, the augmentation expected for the larger sizes was, however, not found. Montante *et al.* (2010) using PIV measured $(\varepsilon_T)_{max}$ for 115 and 774 μm particles in the same region at up to 0.1 and 0.2% by volume, respectively. While the deviations of the mean flow field from the single-phase results were negligible, $(\varepsilon_T)_{max}$ was suppressed with the smaller particles and enhanced by the larger ones. They concluded that their results agreed with the Gore and Crowe criterion when estimating it from 0.1 (near the impeller) to 0.3 (towards the wall) D/4.

Other work has not measured $(\varepsilon_T)_{max}$ directly but assessed turbulence in terms of RMS velocities. For example, Guiraud *et al.* (1997) found that the axial and radial rms velocities of the continuous phase from a down-pumping propeller were unaffected by the presence of 253 μm particles at 0.5 vol%. However, they observed higher values in the axial RMS velocities for the particles. Later, Virdung and Rasmuson (2007; Virdung and Rasmuson 2008) found that with a pitched-blade turbine, rms enhancement occurred for 1, 1.5 and 2 mm particles again at 0.5%

volume, but also at 1 and 1.5%. In contrast to this, Micheletti and Yianneskis (2004) using two sizes of Rushton turbines reported rms suppression in the impeller region of the tank (which extended out to the equivalent feed point used here) by up to 70% when dispersing 186 μm particles, again at 0.5 vol%. Of these studies, only the latter two were in agreement with the Gore and Crowe criterion as perceived by the workers themselves. Complementary to such experimental work, CFD modelling using large eddy simulation (LES) for liquid-solid suspensions with up to 3.6 vol.% particle concentration of 300 and 470 μm stirred by a Rushton turbine was published by Derksen (2003). The turbulence levels were suppressed by the particles, more strongly in the impeller stream than in other regions of the vessel. Interestingly, locally increased solid concentrations near the impeller and especially in front of its blades were observed in the simulations and have also been indicated experimentally (Micheletti and Yianneskis 2004), which might be an explanation for the large effects seen at such low solid concentrations. Clearly, though quite a lot of work directly measuring turbulence in the presence of solids has been undertaken, there is little agreement between the different studies; nor is there with the interpretation of the Gore and Crowe criterion as perceived by each worker.

Over the last few years, new techniques have been developed which allow studies in opaque systems and consequently at up to high particle concentrations, e.g. up to 19 wt.% using computer automated radioactive particle tracking (Guha et al. 2007) or up to 40 wt.% using positron emission particle tracking (Guida et al. 2010). Such techniques are not able to measure true turbulence parameters but do indicate very little difference between the velocity of the fluid with and without particles present when the concentrations are low, i.e. around 0.5 to 5 wt.% (Pianko-Oprych *et al.* 2009).

Micromixing in stirred suspensions

In addition to turbulence measurements, macro- and micromixing studies have also been undertaken. As discussed in section 2.1.4., macromixing time is strongly affected by the presence of more than about 10% granular solid particles, which leads to 'solid cloud formation' in the lower part of the vessel above which a clear layer of liquid appears (Bujalski *et al.* 1999). Under these conditions, the fluid above the 'cloud' is very quiescent and the macromixing time, which is especially linked to that region, maybe up to two orders of magnitude longer than without solids present.

The iodide/iodate method was first used to investigate micromixing in the presence of glass particles (Villermaux *et al.* 1994; Guichardon *et al.* 1995). Initially, enhanced micromixing was reported, but after correcting for loss of iodine during filtration (Guichardon *et al.* 1995), the effect on micromixing for up to 6 wt.% for a range of particle sizes from 20 to 1300 μm was found to be negligible. Barresi (1997) investigated the effect of glass spheres of ~ 175 and 450 μm and also of 3mm diameter cylindrical PET beads of low density up to 13 vol.% using a Rushton turbine in a closed vessel to avoid any air ingestion and feeding above the impeller approximately ¼ of the way to the top surface. They employed a reaction scheme developed by Bourne and Yu (1994). At the lower concentrations with the beads at 2 and 7 vol% and with the PET particles at all concentrations, the selectivity was not affected. At the higher concentration, 'cloud' formation was observed and feeding into the 'cloud' led to a marked increase in selectivity, i.e. poorer micromixing. Later Barresi (2000) used the same equipment with the same feed position but with a lower level in the tank with both a down-pumping pitched blade turbine and a Rushton turbine. They also used similar sized glass beads plus barite sand the size of the

smaller glass beads but of higher density (4280 compared to 2450 kg/m^3) at 12 and 18 vol %. They also measured the power input and adjusted the impeller speeds to give the same value with and without solids. With the Rushton turbine, cloud formation was found in the earlier study and selectivity increased (Barresi 1997); in the later study with the lower liquid level, it did not occur and selectivity was generally unaltered. With the pitched blade turbine, cloud formation was found in every case and the selectivity was increased by about 20 to 50%. Brilman *et al.* (1999) used azo-coupling for investigating several feed positions but some very close to the impeller but none near the top surface where clear liquid would be found if 'cloud' formation occurred. They used various sizes of glass beads from 30 to 700 μm and solid concentrations from about 2.5 up to 40 wt.% agitated by a Rushton turbine. They found when feeding at approximately the mid-point between the impeller and the upper surface that selectivity increased with increasing solid concentration except with beads of ~ 300 μm which did not have any effect. At a concentration of about 23 wt. %, the increase depended on particle size, with a minimum at ~ 300 μm where the effect was very small. Though they made no comment about it, it is likely that at the higher concentrations, cloud formation would have occurred (Bujalski *et al.* 1999). The only micromixing study done at the low solids concentration where direct turbulence measurements showed a significant suppression or augmentation of turbulence in $(\varepsilon_T)_{max}$ close to the impeller was that of Unadkat *et al.* (2009a). Their micromixing experiments with the iodide/iodate method were largely in good agreement with their PIV measurements. With 300 μm glass particles, they found that selectivity compared to that without particles was increased (turbulence suppression) by up to 5% at < 1% vol solids and reduced (turbulence augmentation)

by up to 10% at between 1 and ~ 1.3% vol solids; with 750 μm, there was no detectable effect; and at 1000 μm, selectivity was increased up to ~ 10% (turbulence suppression). Thus, as with the PIV measurements, their results do not agree with the Gore and Crowe criterion.

Clearly, the direct measurement of turbulence parameters in the presence of particles does not give a coherent picture and hence is not able to greatly help understand their impact on micromixing phenomena. On the other hand, the apparent disparity found in the direct micromixing studies does not necessarily mean that they contradict each other. In general, different size and density particles have been used at a wide range of concentrations with different impellers and various reactants at a variety of feed positions. At high solids concentrations, the possibility of cloud formation is a complicating factor and it is not clear how important its formation is on the impact of solids on micromixing (though cloud formation clearly has a major impact on macromixing). Nevertheless, there are certain direct contradictions. For example, even when the same reaction scheme was used, Guichardon *et al.* (1995) did not find any effect on micromixing of particles of 200 μm (or with the other sizes investigated) from 1 to 5 wt.%, while Unadkat *et al.* (2009a) using similar sized (300 μm) particles found significant augmentation at concentrations for 1 to 1.3% but none at 750 μm. Brilman *et al.* (1999), on the other hand, found essentially no effect with particles of 300 μm up to 15 %wt.

On the basis of this analysis of the literature, it was decided to study a range of low concentrations (up to 1 vol.% or ~2.5 wt.%) where fluid dynamic measurements have been used to quantify their effect on turbulence; and higher concentrations where cloud formation would occur.

3. EXPERIMENTAL METHOD AND ITS VALIDATION

3.1. The iodide/iodate method

3.1.1. Reaction scheme

The iodide/iodate reaction scheme was developed by Villermaux and co-workers and full details were given by Fournier *et al.* (1996b), Guichardon and Falk (2000). In this method, two reactions compete for the limiting reactant, H^+, in parallel:

$$H_2BO_3^- + H^+ \rightleftharpoons H_3BO_3 \qquad \textbf{(3.1)}$$

$$5I^- + IO_3^- + 6H^+ \rightleftharpoons 3I_2 + 3H_2O \qquad \textbf{(3.2)}$$

The acid-base neutralisation (3.1) is instantaneous compared to the rate of micromixing and gives the desired product. On the other hand, the redox-reaction (3.2), often called Dushman reaction, is very fast but slower than neutralisation (3.1) and in the range affected by micromixing. It gives the undesired side-product, iodine, which reacts to give the triiodide via the quasi-instantaneous equilibrium (3.3)

$$I_2 + I^- \rightleftharpoons I_3^- \qquad \textbf{(3.3)}$$

The concentration of triiodide can then be measured using a spectrophotometer.

The Dushman reaction has been studied extensively, but shown to be complex and dependent on factors like ionic strength (Dushman 1904; Barton and Wright 1968; Palmer and Lyons 1988; Schmitz 1999; Xie *et al.* 1999; Agreda B. *et al.* 2000; Guichardon *et al.* 2000; Schmitz 2000). Consequently, Guichardon *et al.* (2000) measured possibly relevant kinetic data for the conditions of the iodide/iodate

method. These results have so far been used by authors employing this reaction scheme (Assirelli *et al.* 2008b; Baccar *et al.* 2009; Falk and Commenge 2010). This kinetic data has been suggested as a possible factor explaining problems when the method is used for quantitative studies (Assirelli *et al.* 2008b; Bourne 2008; Kölbl and Schmidt-Lehr 2010). This issue will be addressed in chapter 4.

3.1.2. Experimental procedure

The experimental procedure employed in this work has been described by Guichardon and Falk (2000) and was followed closely. It consisted of feeding a small amount (0.5 or 1 mol/L) of sulphuric acid to a solution of borate, iodide and iodate in a basic buffer formed by boric acid and sodium hydroxide.

The employed chemical concentrations were the same as those that have been found useful before (Fournier *et al.* 1996b; Assirelli *et al.* 2002) and are given in Table 3. When solids were added, the tank fill level was kept the same as in the liquid-only cases and, therefore, the amount of chemicals was adjusted accordingly to still give the same reactant concentrations in the liquid.

Table 3: Concentration of reactants (mol/L)

$[NaOH]$	$[H_3BO_3]$	$[KI]$	$[KIO_3]$	$[H_2SO_4]$
0.0909	0.1818	0.0117	0.00233	0.5 or 1.0

As suggested by Guichardon and Falk (2000), the concentration of triiodide was determined two minutes after the injection and for higher particle concentrations where cloud formation occurred, the speed was raised to ensure that macromixing was completed before sample-taking. With the data from this measurement, the

segregation index or selectivity for side-product, X_S, can be calculated which is used to quantify micromixing efficiency:

$$X_S = \frac{Y}{Y_{ST}} \tag{3.4}$$

It is defined as the ratio of actual yield of unwanted product, Y, to the maximum yield at total segregation, $Y_{ST.}$ Therefore, the segregation index can range from 0 to 1 with $X_S = 0$ in the case of perfect micromixing and $X_S = 1$ for total segregation.

For these reactions, the yield is calculated as:

$$Y = \frac{2(n_{I_2} + n_{I_3^-})}{n_{H^+0}} = \frac{2V_{Tank}[(I_2) + (I_3^-)]}{V_{Injection}(H^+)_0} \tag{3.5}$$

In the case of total segregation, both reactions are quasi-instantaneous compared to micromixing time and consequently stochiometry determines the amount of side-product:

$$Y_{ST} = \frac{6[IO_3^-]}{6[IO_3^-] + [H_2BO_3^-]} \tag{3.6}$$

Another way of quantifying micromixing, as described by Villermaux and David (1983), is the micromixedness ratio, α. The idea is that the flow consists of regions which are either perfectly mixed or fully segregated. From this concept, α has been defined as the ratio of the volumes of perfectly mixed (PM) to totally segregated (ST) fluid. It can be easily calculated from the segregation index which is well-defined for these cases (PM: $X_S = 0$; ST: $X_S = 1$) (Fournier *et al.* 1996b; Guichardon and Falk 2000):

$$\alpha = \frac{V_{PM}}{V_{ST}} = \frac{1 - X_S}{X_S} \qquad \textbf{(3.7)}$$

The values of the micromixedness ratio might be more intuitive to use for some, as micromixing effectiveness improves with increasing α.

An advantage of the iodide/iodate technique, compared to other reaction-based methods, is that more than one injection can be done per experiment, which reduces waste, time and cost. The segregation index is then calculated taking the previous injections and samplings into account as described in literature (Guichardon and Falk 2000; Assirelli 2004).

For the two-and three-phase results, in addition to the "normal", i.e. single-phase, definition of the segregation index itself, it was found in this work useful to plot data as the deviation of X_S, in %, from the corresponding reference, e.g. single-phase, results:

$$\Delta X_S = \frac{X_{S\,reference} - X_{S\,value}}{X_{S\,reference}} \qquad \textbf{(3.8)}$$

This way of expressing changes in the segregation index has also been employed in this context by other authors (Unadkat 2009).

3.2. Experimental set-up

3.2.1. The rig

For the experimental part of this work, a cylindrical Perspex vessel with a flat bottom and a diameter of 288 mm was employed. It was surrounded by a square water jacket which allowed distortion-free viewing and helped keeping the temperature in the tank constant. In addition, the vessel contained four equally-spaced baffles

(B = T/10) and could be equipped with a ring sparger for gassed experiments. The rig is shown in Figure 17.

Figure 17: Image of the rig

The set-up in this study was similar to that of Assirelli *et al.* (2002) to allow comparisons and especially to validate initial results. The stirrer, a Rushton turbine, was made specifically for this project. Again, it was similar to the one used by Assirelli (2004) to allow comparisons. It had a material thickness of 3 mm.

The geometric ratios of the tank and the impeller are given in Table 4 – with impeller diameter (D), filling level (H), impeller clearance (C), blade width (W), blade length (L) and material thickness (x).

Table 4: Geometric ratios of the stirrer and the vessel (T = 288 mm)

D	H	C	W	L	x = 3 mm
T/3	1.3 T	T/4	0.2 D	0.25 D	0.03125 D

The fill level and the impeller clearance were chosen to avoid air entrainment from the liquid surface (Assirelli 2004).

The power input from the impeller could be measured with a strain gauge on the shaft combined with telemetry. Such measurements are well-established and have been described in literature (Bujalski *et al.* 1987; Ascanio *et al.* 2004). Initial liquid-only tests were performed to check the power number of the Rushton turbine used. Table 5 shows these results compared against literature and good agreement was found; the match is especially close with Assirelli *et al.* (2002), who used a very similar system.

Table 5: Power number in liquid-only system – compared to literature

Water height	**this work**	**reference**	
H=T	4.20	4.61	Bujalski *et al.* (1987)
H=1.3H	4.35	4.33	Assirelli *et al.* (2002)

3.2.2. Adaptions for the reaction system

The reactant, in these experiments, sulphuric acid, could be fed with glass pipes which had inner diameters of 0.8 to 1 mm at the tip. The glass pipes were stabilised by steel pipes and fixed from the sides and top of the vessel. This allowed accurate positioning and re-positioning – even when the pipes had to be taken out of the system, for instance for cleaning or repairs. A steady flow was ensured by employing a peristaltic pump with two pump heads which were out of phase. Such a set-up was chosen because Assirelli (2004) reported pulsation from a pump with less rollers than the one employed in the actual study.

Figure 18 shows the employed locations for feeding sulphuric acid and Table 6 gives the coordinates. The choice of the feed positions was based on current knowledge from single-phase experiments: considering that significant differences in micromixing quality between feeding near the surface and closer to the impeller are now well-established, a position in the impeller discharge stream and another one close to the surface were chosen, similar to Assirelli *et al.* (2002). It must be emphasised that these locations are similar, but not exactly equivalent due to technical differences in the rigs employed. Moreover, studies on turbulence modulation in stirred tanks have indicated that turbulence might be most significantly spatially affected near ε_{max}. Therefore, position 4 in this study is equivalent to position 4 in Assirelli *et al.* (2002), though the difficulty of accurate positioning of feed pipes still needs to be remembered – especially, in the light of the significant changes of energy dissipation near the impeller. In addition, feed position 3, at a height halfway between vessel bottom and impeller, was employed for some single-phase

and further sparged experiments to give a better picture of the effect of bubbles on micromixing.

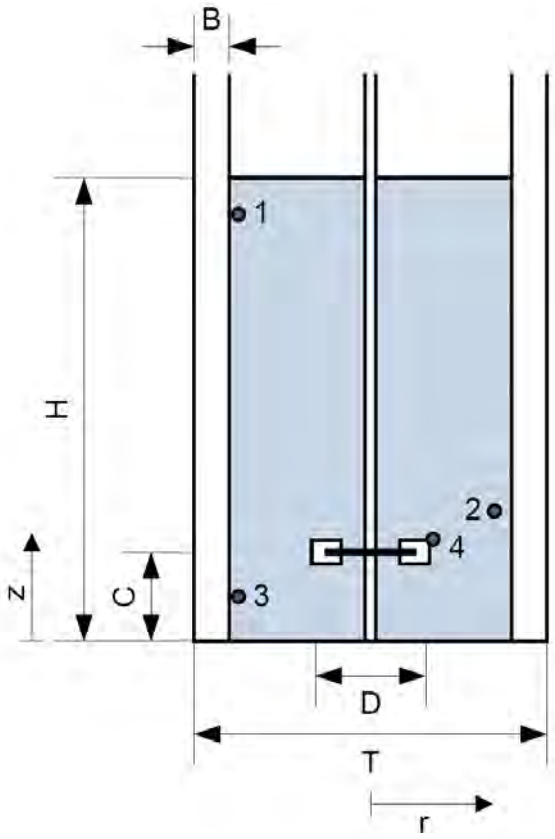

Figure 18: Schematic of mixing tank and feed positions

Table 6: Coordinates of the feed positions

	2r/D	z/H
position 1	2.24	0.92
position 2	2.19	0.27
position 3	2.24	0.096
position 4	1.06	0.22

3.2.3. Sample taking and measurement of triiodide

Samples could be taken from a pipe with a tap at the side of the vessel. This pipe and tap were repositioned to check independence of sampling position. As expected for a well (macro-)mixed tank, the location of sample taking did not have any

influence on the micromixing results. Obviously, the dead volume in the pipe was always removed before actual samples were taken.

Each measured value actually consists of the average of the reading from three samples in separate cuvettes, to avoid errors.

The concentration of triiodide was determined using a single-beam spectrophotometer (Cecil CE 1020) at 353 nm, which is one of the two peaks in the spectrum of triiodide and iodine (Awtrey and Connick 1951). Guichardon and Falk (2000) illustrated that the extinction factor of triiodide varies for different spectrophotometers. Therefore, a calibration curve was obtained, following the procedure described by Assirelli (2004), for the employed apparatus. This gave an extinction coefficient of 2560.8 m^2/mol at 353 nm which is in very good agreement with literature (Guichardon and Falk 2000; Assirelli 2004). Details of the calibration and a comparison to values from literature can be found in Appendix A.

3.3. Validation of method - single-phase results

The method is validated in this section by repeating similar experiments those in literature. In addition, this data will give a baseline for comparison of the results of the 2- and 3-phase studies.

3.3.1. Meso-/micromixing transition

Initial experiments had the purpose of finding feed rates suitable for micromixing studies, i.e. lower than mesomixing dominated while still avoiding backmixing. Assirelli (2004) found a range of 1-3 ml/min useful in a similar stirred vessel. Figure 19 gives a similar result and a feed rate of 2 ml/min was chosen for all experiments

apart from those close to ε_{max}which had to be checked separately to ensure that backmixing was avoided.

Note: In the literature, feed time tends to be varied whilst using a constant feed volume, i.e. the axis is labelled in s or min. However, to compare with a different feed position, which was measured for different injection volumes due to the different local micromixing conditions, the reciprocal feed rate in min/ml was used. It has been shown previously that the injection volume does not affect the result (Assirelli 2004) and initial tests in this study confirmed these findings (data not shown).

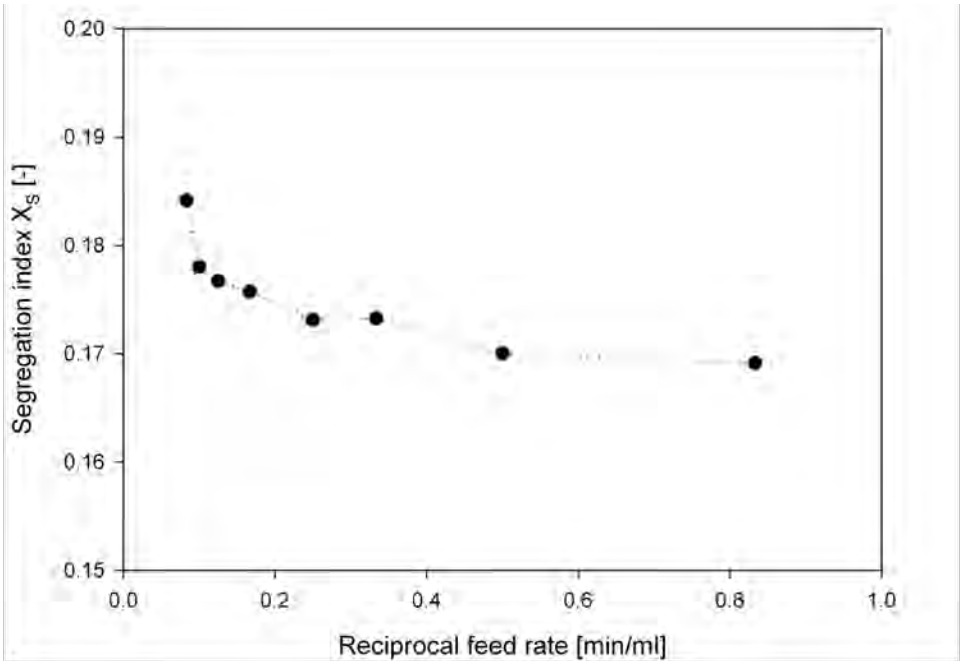

Figure 19: Effect of feed rate on segregation index – transition between meso- and micromixing – feed position 2 (near impeller)

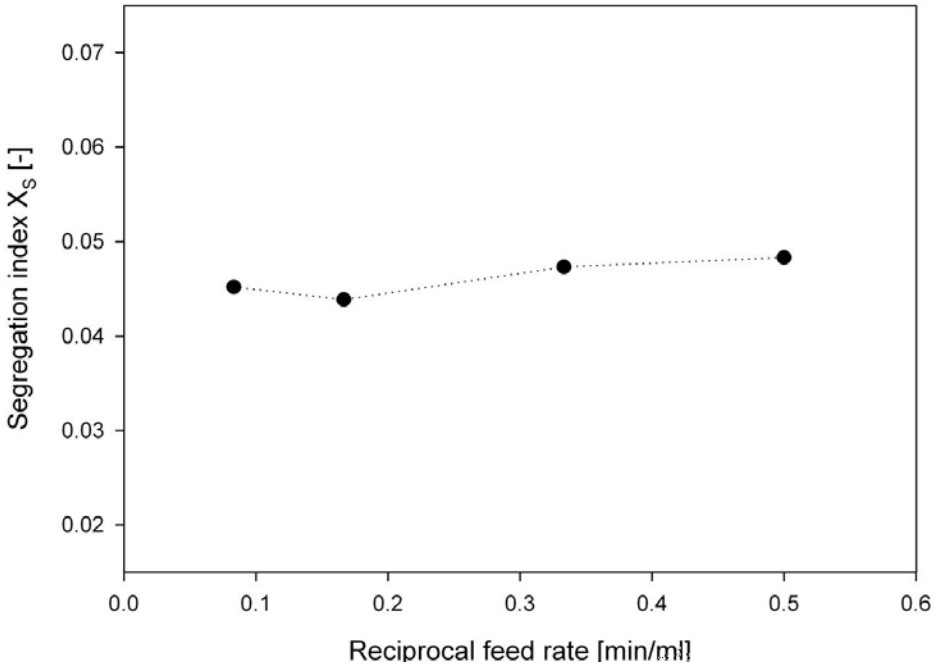

Figure 20: Effect of feed rate on segregation index – transition between meso- and micromixing – feed position 4 (near ε_{max})

Figure 20 illustrates that the effect of the tested feed rates near ε_{max} is relatively small compared to Figure 19, but, in order to avoid backmixing, a higher rate of 3 ml/min was chosen. Moreover, higher amounts of sulphuric acid were fed per injection at this position due to good micromixing which led to low iodine yields. Consequently, the increased feed rate also helped keeping the duration of the experiments within a reasonable range.

3.3.2. Single-phase – comparison to literature

Figure 21 presents micromixing results as a function of mean specific power input obtained for three feed positions and these are compared to literature (Assirelli 2004). In the current work, the range of impeller speeds was also extended to higher values mainly, to allow possibly complete particle suspension in corresponding solid-liquid experiments.

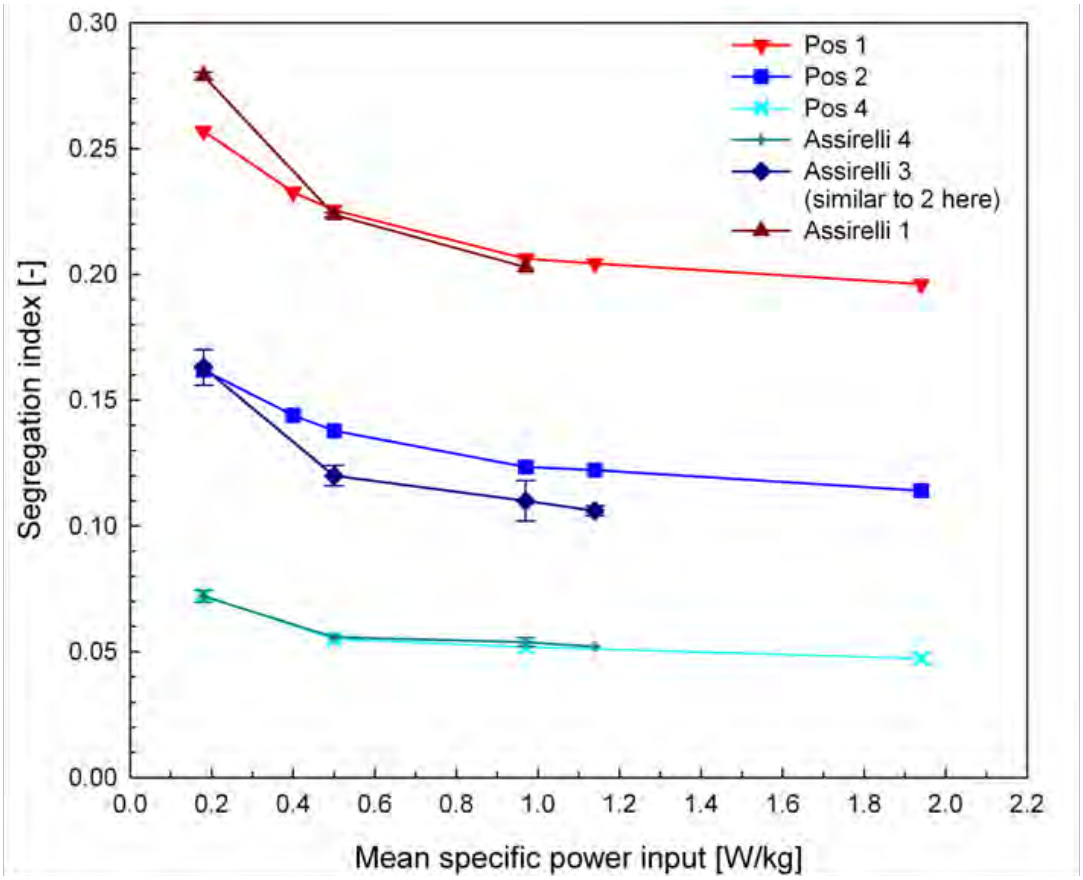

Figure 21: Segregation indices at 3 feed positions as a function of mean power input – compared to results from similar experiments (Assirelli 2004)

In spite of the slightly different feed points (they deviated by about 0.5 and 1 cm radially for position 1 near the surface and 2 near the impeller respectively from the equivalent position in the earlier work), the data (Figure 21) agrees very well with the results of Assirelli (2004). In two tanks and impellers designed to be identical with exactly the same feed rates and compositions and the same range of specific power inputs, Assirelli (2004) observed differences in X_s of between 8% and 14% and the current results were all within 14% of the previous ones.

The excellent agreement at position 4, near ε_{max}, is especially remarkable as this region could be expected to show particular sensitivity to positioning due to the strong gradients of local energy dissipation rates (Assirelli *et al.* 2002).

It can be concluded that the single-phase experiments are in good agreement with earlier ones, which gives confidence in the method and the set-up. Therefore, the results are suitable as a baseline for comparing with the data obtained in the presence of the second phase and also for testing the micromixing modelling.

4. INCORPORATION MODEL: ADAPTATION AND ITS USE TO INTERPRET EXPERIMENTAL DATA

4.1. Introduction

Though the iodide/iodate method has been widely used, recently, its usefulness as a means of obtaining quantitative data about the local turbulence has been questioned (Bourne 2008; Kölbl and Schmidt-Lehr 2010) because the reaction kinetics are not sufficiently well understood, as discussed in further detail in section 2.2.3. Especially, the dissociation of sulphuric acid, which supplies the limiting reactant, H^+, needs attention. Nevertheless, this method has been found to give qualitatively reliable results (Bourne 2008), while being easier to use than other reaction schemes (Aubin *et al.* 2010) and versatile, especially, as this method allows adapting the reactant concentrations to give maximum sensitivity for micromixing in a specific case (Guichardon and Falk 2000). In order to address the issues found in recent literature, micromixing modelling might be of use, as calculating an independent value, like a micromixing time, e.g. the reciprocal value of the Engulfment rate (Baldyga and Bourne 1999) or the incorporation time (Villermaux and Falk 1994), might allow comparing results obtained from different reactant concentrations. Taking into account that such models have been found useful in various systems (Baldyga and Bourne 1989a; Baldyga and Bourne 1989b), such an approach is worth further evaluation. Before the mentioned criticism was published and could have been considered, such work had already been done with the Iodide/iodate method to estimate energy dissipation levels in a stirred tank using the incorporation model

(Assirelli *et al.* 2008b). Unfortunately, the results were only in reasonable agreement with comparable data from other methods.

The incorporation model will also be employed here, as it has been attacked less and taking into account that a similar model, the Engulfment model, has given realistic results for stirred tanks when validated against experimental data (Bourne and Yu 1994). Therefore, further work on such an approach seems warranted. In addition, its advantages are that it is relatively simple (Fournier *et al.* 1996a) and computationally not too expensive, especially when solved with efficient algorithms as suggested by Assirelli *et al.* (2008b).

The incorporation model follows the changes of the species' concentrations in a small volume of feed solution while it grows due to incorporation, as described in section 2.2.3. For a given characteristic time, micromixing time, t_m, this model then allows calculating the product distribution of chemical test reactions which are sensitive to micromixing, in this case the iodide/iodate method. Therefore, a connection between an experimentally obtained segregation index and t_m is given. This micromixing time then allows estimating the local specific energy dissipation rate "experienced" by the chemical reactants via 1/E (Baldyga and Bourne 1990) or t_m (Fournier *et al.* 1996a):

$$t_m = 17.24 \sqrt{\frac{\nu}{\varepsilon_T}} \qquad \textbf{(4.1)}$$

Unfortunately, the existing approach for the Iodide/iodate reaction scheme does not reflect too well what is actually expected to occur during such studies. New variations are presented here: the model is extended to include the partial

dissociation of sulphuric acid and different kinetic rate laws are tested. These modelling results are then applied by interpreting experimental data from a single-phase stirred tank, for instance to estimate local specific energy dissipation rates. Comparisons of these results to literature might help selecting the (currently) most suitable approach and could give ideas for further studies.

4.2. Materials and method

4.2.1. Adapted model for the iodide/iodate method

As discussed in section 2.2.3., Kölbl and Schmidt-Lehr (2010) demonstrated that H_2SO_4 is not fully dissociated when being fed into a stirred tank and, therefore, not all protons are immediately available for the reaction, which had been assumed in most previous work. As a solution, the authors proposed using a stronger acid, e.g. perchloric acid, or considering the second dissociation of sulphuric acid when using a micromixing model. The latter option has also been suggested by Bourne (2008) in a critical discussion of the iodide/iodate method. Therefore, the current approach (Fournier *et al.* 1996a) is first briefly explained and then extended to include the dissociation of the sulphuric acid.

In the incorporation model, the changes of the reactant concentrations in an aggregate or blob of feed solution are observed: as described in section 2.2.3., the concentrations of the species j in the reaction zone are given by considering the balance of incorporation and chemical reaction (with subscript 10 indicating the concentration in the surrounding liquid):

$$\frac{\mathrm{d}C_j}{\mathrm{d}t} = \left(C_{j10} - C_j\right)\frac{1}{g}\frac{\mathrm{d}g}{\mathrm{d}t} + R_j \qquad \textbf{(4.2)}$$

The reaction volume grows over time due to incorporation of surrounding fluid, i.e. $V_2(t) = V_2(0)\, g(t)$. This behaviour has been tested for instance for linear and exponential growth rates (Assirelli *et al.* 2008b), with the latter being the better established one (Zwietering 1984; Baldyga and Bourne 1999; Assirelli *et al.* 2008b):

$$g(t) = e^{t/t_m} \qquad \textbf{(4.3)}$$

A mole balance following equation (4.2) can then be formulated for each of the species as described by Fournier *et al.* (1996a). This was given in a dimensionless form using Damköhler numbers and by normalising against $n_{\mathrm{H}_0^+}$, the initial concentration of protons in the injection volume, assuming full dissociation, and t_m, for the reactants and for time, respectively. The species were then represented by f:

$$f_j = \frac{n_j}{n_{\mathrm{H}_0^+}} \quad \left(j = \mathrm{H}^+, \mathrm{I}^-, \mathrm{IO}_3^-, \mathrm{I}_2, \mathrm{I}_3^-\right) \qquad \textbf{(4.4)}$$

With the initial conditions:

$$\theta = 0,\ f_{\mathrm{I}^-} = f_{\mathrm{IO}_3^-} = f_{\mathrm{I}_2} = f_{\mathrm{I}_3^-} = 0$$

The balances for the species can then be summarised (Fournier *et al.* 1996a; Assirelli *et al.* 2008b) as:

$$\frac{\mathrm{d}f_{\mathrm{H}^+}}{\mathrm{d}\theta} = -6F_2 - P\frac{\mathrm{d}g}{\mathrm{d}\theta} \qquad \textbf{(4.5)}$$

$$\frac{\mathrm{d}f_{\mathrm{I}^-}}{\mathrm{d}\theta} = -5F_2 - F_3 + F_3' + Q_1\frac{\mathrm{d}g}{\mathrm{d}\theta} \qquad \textbf{(4.6)}$$

$$\frac{\mathrm{d}f_{\mathrm{IO}_3^-}}{\mathrm{d}\theta} = -F_2 + Q_2\frac{\mathrm{d}g}{\mathrm{d}\theta} \qquad \textbf{(4.7)}$$

$$\frac{\mathrm{d}f_{\mathrm{I}_2}}{\mathrm{d}\theta} = 3F_2 - F_3 + F_3' \qquad \textbf{(4.8)}$$

$$\frac{\mathrm{d}f_{\mathrm{I}_3^-}}{\mathrm{d}\theta} = F_3 + F_3' \qquad \textbf{(4.9)}$$

with (c' refers to concentration before mixing):

$$\theta = \frac{t}{t_m},\ P = \frac{C'_{\mathrm{H_2BO_{3,0}^-}}}{C'_{\mathrm{H_0^+}}},\ Q_1 = \frac{C'_{\mathrm{I_0^-}}}{C'_{\mathrm{H_0^+}}},\ \ Q_2 = \frac{C'_{\mathrm{IO_{3,0}^-}}}{C'_{\mathrm{H_0^+}}}$$

and:

$$\boldsymbol{F_2 = Da_2 \frac{f_I^2 - f_{IO_3^-} f_{H^+}^2}{g^4},\ F_3 = Da_3 \frac{f_{I^-} - f_{I_2}}{g},\ F_3' = Da_3' f_{I_3^-}}$$

where:

$$\boldsymbol{Da_2 = t_m k_2 C_{H_0^+}'^4,\ Da_3 = t_m k_3 C'_{H_0^+},\ Da_3' = t_m k_3'}$$

This approach was presented by Fournier *et al.* (1996a). For this work, some changes to the mole balances and additional values are needed for $\mathrm{HSO_4^-}$ and $\mathrm{SO_4^{2-}}$ to calculate their change during the dilution. Of course, the initial values for $\mathrm{H^+}$, $\mathrm{HSO_4^-}$ and $\mathrm{SO_4^{2-}}$ depend on the concentration of sulphuric acid before the injection and would be the respective concentration at equilibrium divided by the initial proton concentration. However, as the assumption of a known, well-defined $C'_{\mathrm{H_0^+}}$is not valid, the dimensionless expressions were changed in the approach used here from the original $n_{\mathrm{H_0^+}}$ to $n_{\mathrm{IO_3^-}\,0}$, the initial amount of iodate in the bulk:

$$f_j = \frac{n_j}{n_{\mathrm{IO_3^-}\,0}} \quad (j = \mathrm{H^+, I^-, IO_3^-, I_2, I_3^-, HSO_4^-, SO_4^{2-}}) \qquad \textbf{(4.10)}$$

Consequently, the Damköhler numbers Da_2 and Da_3 become:

$$Da_2 = t_m k_2 C_{\mathrm{IO_{3,0}^-}}'^4 \qquad \textbf{(4.11)}$$

$$Da_3 = t_m k_3 C'_{\mathrm{IO_{3,0}^-}} \qquad \textbf{(4.12)}$$

And in the incorporation terms in the dimensionless form for the species are:

$$P = \frac{c'_{H_2BO_{3,0}^-}}{c'_{IO_{3,0}^-}},\ Q_1 = \frac{c'_{I_0^-}}{c'_{IO_{3,0}^-}},\ Q_2 = \frac{c'_{IO_{3,0}^-}}{c'_{IO_{3,0}^-}}$$

These alterations from normalising against initial H^+-concentration to initial iodate concentration in the bulk should not affect the final results of the incorporation model as long as it is being done consistently. The results are validated in section 4.3.

The main adaptation here, compared to Fournier *et al.* (1996a), is to include the second dissociation of sulphuric acid. This was fairly straight-forward: the relevant dimensionless concentrations were converted back to absolute concentrations, the change in the equilibrium due to the dilution calculated and then the respective slope returned to the solver algorithm, here Runge-Kutta. This allows calculation of the dissociation at each time step.

Technical note: The equilibrium changes due to dilution are, however, always calculated ahead for the next time step as the change in concentrations will only effectively be “available” to the reactions in that next step. This formulation was chosen, as it might be argued that the effect of dilution and dissociation is instantaneous compared to the other reactions. Therefore, this effect should immediately become relevant in the current time step. In spite of being, if neglected, only a small delay, it was considered accordingly.

Regardless of such details, the calculation of the dilution requires a constant (or, at least, known) time step size which reduces the options of accelerating the code, for instance with adaptive time steps.

4.2.2. Kinetics

Kinetics for the current approach

So far, the approach presented by Fournier *et al.* (1996a), which employs kinetic data for the Dushman reaction, equation (3.2), measured by the same research group (Guichardon *et al.* 2000), has been used for modelling the Iodide/iodate reaction scheme. They gave the reaction rate as a function of ionic strength:

$$\mu < 0.166M\text{: } \log_{10}(k_2) = 9.28105 - 3.664\sqrt{\mu}$$

$$\mu > 0.166M\text{: } \log_{10}(k_2) = 8.383 - 1.5112\sqrt{\mu} + 0.23689\mu$$

for the classic 5th order behaviour which has been found by many workers before (see the papers by Guichardon *et al.* 2000; Bourne 2008):

$$r_{5th\ order} = k_2[IO_3^-][H^+]^2[I^-]^2$$

In the kinetic study by Guichardon *et al.* (2000), sulphuric acid was used and the authors assumed that it was fully dissociated. This might not, like in the actual experimental procedure, be valid at the employed concentrations, especially considering the use of K_2SO_4 to adjust the ionic strength, which has also been found problematic in recent measurements (Kölbl and Hecht 2012). Consequently, the concentration of H^+ in the original model seems to be in doubt.

For this extended incorporation model, the question of using appropriate kinetic data needs to be addressed again because the dissociation of the acid will be added and this might be an (even) less than ideal combination with the original approach. Other options can at least be considered, particularly, as it has been suggested that the incorporation model is very sensitive to kinetics (Villermaux and Falk 1994) and as such data is available and has not been tested in such an approach before.

Options for employing alternative kinetics

To discuss the kinetics in more detail, the reactions are summarised again:

$$H_2BO_3^- + H^+ \rightleftharpoons H_3BO_3 \qquad \textbf{(4.13)}$$

$$5I^- + IO_3^- + 6H^+ \rightleftharpoons 3I_2 + 3H_2O \qquad \textbf{(4.14)}$$

$$I_2 + I^- \rightleftharpoons I_3^- \qquad \textbf{(4.15)}$$

While reactions (4.13) and (4.15) are kinetically well defined and have not been criticized in this context, reaction (4.14) is more problematic, in spite of significant research efforts. More than a century ago, Dushman (1904) was the first author who suggested a rate law for this reaction which is now known as the Dushman reaction. Nevertheless, its kinetics are still being discussed in literature (Schmitz 1999; Xie *et al.* 1999; Agreda B. *et al.* 2000; Schmitz 2000; Bourne 2008; Kölbl 2008; Kölbl *et al.* 2011). Thus, this section gives a brief review of the most appropriate data and also mentions some problems with the measurements in the kinetic studies.

Some of the difficulties encountered in earlier work may be explained by the results of Barton and Wright (1968): They found in their experiments that species present in buffers can have an effect on the Dushman reaction by causing catalysis by carboxylate and phosphate ions. The authors proposed a reaction rate of

$$r_{BW} = k_0[IO_3^-][H^+]^2[I^-]^2 + k_b[B^-][IO_3^-][H^+]^2[I^-]^2/(1 + k'[I^-]) \qquad \textbf{(4.16)}$$

where B^- is for the investigated buffer species. The authors found, for five bases studied, that the catalytic rate constant k_b follows Brönsted law with

$$\log(k_b) = 8.89 + 0.17pK_a$$

even though Bamford and Tipper (1972) showed changes of up to 30% of the observed rate due to catalysis. This illustrates that it could be necessary to consider

also the effect of additional species which are present in the solution during the experiments. For instance, in the case of the iodide/iodate reaction scheme, the effect of the borate ions has not been investigated.

Liebhafsky and Roe (1979) concluded a paper on this reaction emphasising the computer's value when ***a*** mechanism, not ***the*** mechanism, is the only realistic goal. This might not sound exceedingly encouraging for solving the difficulties with this reaction, but some of the authors' suggestions were considered in later work by Palmer and Lyons (1988). In that case, stopped-flow spectrophotometry was used to study the Dushman reaction at three ionic strengths, with variation of iodide and perchloric acid concentrations, at several temperatures. Palmer and Lyons (1988) found, as have many other authors (Guichardon *et al.* 2000; Bourne 2008), 5th order kinetics and dependence on ionic strength. Table 7 gives their rate constants, which the authors also found to be in good agreement with previous work.

Table 7 : Rate constants of Dushman reaction for three ionic strengths by Palmer and Lyons (1988)

I [M]	k [$M^{-4}s^{-1}$]
0.015	$6.72 \cdot 10^8$
0.10	$4.27 \cdot 10^8$
1.00	$2.62 \cdot 10^8$

Schmitz (1999) reviewed issues found in literature, like the effect of the buffer and changes in the order of iodide, i.e. from 1 to 2 and then less than 2, with increasing concentrations of that reactant. Starting from this point, the author described a kinetic mechanism which accounts for the effects mentioned above, like the buffer's

influence. Unfortunately, there is still significant uncertainty regarding the coefficients of the resulting kinetic model, as also admitted by the author. For this reason, the model suggested by Schmitz (1999) is not employed in this work.

Xie *et al.* (1999) measured kinetics in a special device, which is suitable for fast reactions, at relatively high iodide but low iodate concentrations and also showed saturation effects at higher reactant concentrations. Therefore, the following expression, which leads to lower orders for H^+ and I^- than with the established classic 5th order law, was given:

$$r_{Xie} = \frac{2.8 \cdot 10^8 [H^+]^2 [I^-]^2 [IO_3]}{(1 + 2.53[H^+])(1 + 2.3[I^-])} \qquad \textbf{(4.17)}$$

Without such saturation, the rate constant would be $2.8 \cdot 10^8\ M^{-4}s^{-1}$ at an ionic strength of 0.5 M (Xie *et al.* 1999). A similar study (Agreda B. *et al.* 2000) using a stopped-flow apparatus found such saturation effects at higher concentrations too. The authors suggested that the ratio $[IO_3^-]/[I^-]$ has been found relevant, but in their study $[IO_3^-] \gg [I^-]$, which is not comparable to conditions found when using the Iodide/iodate method.

Schmitz (2000) soon afterwards showed new data and argued that the above two publications (Xie *et al.* 1999; Agreda B. *et al.* 2000) support previously presented ideas (Schmitz 1999). Schmitz's measurements (2000) covered, both, the first and the second order behaviour of iodide. Unfortunately, the conditions, especially the low iodide concentrations and the ratio $[IO_3^-]/[I^-]$, were far from being comparable to those for the iodide/iodate reaction scheme, which might not be ideal for application to the conditions typically used in micromixing studies. A rate law was proposed in this study for an ionic strength of 0.2 M:

$$r_{Schm} = [IO_3^-][H^+]^2\,(1200[I^-] + 4.2 \cdot 10^8[I^-]^2) \qquad \textbf{(4.18)}$$

All the experiments leading to the above kinetic information were performed at much lower concentrations than would be present in the iodide/iodate measurements during micromixing studies, in particular in stirred tanks. Considering that changes in reaction order have been observed over a range of reactant concentrations, applying these rate laws could be problematic. It might be argued that the rate-determining step changes for such different conditions (Bourne 2008). In addition, buffers and various ions have been shown to affect the reaction. Therefore, a more targeted investigation should be considered for this case.

In addition to the above full kinetic rate laws, Kölbl *et al.* (2011) recently presented new reaction orders for the Dushman reaction which were measured at higher concentrations and with borate, which should give more useful data for using the Iodide/iodate method in stirred tanks than previous studies. Unfortunately, to date the authors have not found a full expression which would include a kinetic constant. Nevertheless, this new interest in the reaction gives hope for moving the reaction scheme towards a more quantitatively reliable method. Kölbl *et al.* (2011) proposed the following orders at conditions relevant to micromixing studies in stirred tanks:

$$r_{Kölbl} = k * [I^-]^{1.4}[IO_3^-]^{0.6}[H^+]^{0.6} \qquad \textbf{(4.19)}$$

As no other or more suitable data is available at this point, several of the above rate laws are tested.

Possible indications from studies on reverse reactions

As mentioned earlier in this section, the effect of borate on the Dushman reaction is not known. However, results from studies on related processes might give some indication: other phenomena in this context like the reverse reaction and reaction steps for instance the disproportionation of iodine in basic media or related species like hypoiodous acid, respectively, have been investigated in several studies, too. Motivation behind such work was for instance in the context of nuclear plant accidents, clock reactions or regarding drinking and sea water (Bichsel and von Gunten 2000; Sebodblack-Nagy and Körtvélyesi 2004; Buxton and Mulazzani 2007; Schmitz 2008).

It has been shown that the disproportionation of hypoiodous acid may be catalysed by buffers containing phosphate, borate, or acetate, but inhibited by ammonia (by 50-80%) (Bichsel and von Gunten 2000). In fact, the behaviour with added species has been found to be complex and might not be easily described for a wide range of conditions (Truesdale *et al.* 2003). As mentioned above, catalysis of the Dushman reaction due to carboxylate and phosphate ions has also been reported (Barton and Wright 1968), but the effect of borates is not known and there is not as much information on buffer species as in the reverse cases. Therefore, a brief look at such literature might give some indication of appropriate directions for future work or even help with improving the modelling in the current work.

In addition to changes in rate-limiting reaction steps due to the different reactant concentrations or “an” interaction of borate and/or boric acid and the reacting species being an option in general, specific effects might be hypothesised. Such effects may

be suggested from literature, for instance between borate and HIO, which has been repeatedly mentioned as an intermediate in the Dushman reaction (Schmitz 1999; Xie *et al.* 1999). It was even suggested as part of the potentially rate-determining step (Barton and Wright 1968). In addition, as would be expected, also other intermediates which have been proposed for the mechanisms can be found for both reactions (Urbansky *et al.* 1997). Considering that borate has already been shown to catalyse the disproportionation of hypoiodous acid for some time (Buxton and Sellers 1985; Truesdale 1995), it might be conceivable that such phenomena could slow down the Dushman reaction under the conditions of the Iodide/iodate reactions scheme – i.e. the intermediate product, HIO, would not only react to iodine but to an increased extent follow the catalysed disproportionation back to iodide and iodate due to the presence of borate. Clearly, these are just ideas and need experimental investigation.

Interestingly, also unusual behaviour has been shown: among the few studies into buffer effects, it has been found that acetate can both catalyse and suppress the disproportionation of hypoiodous acid (Urbansky *et al.* 1997). This is remarkable for the iodide/iodate method as such opposing phenomena might precipitate unexpected additional complexities into an already challenging reaction system. Though, taking the consistent qualitative data from micromixing experiments into account, there is hope that the overall effect of borate might be less difficult to handle here.

Again, it has to be emphasised that the above is only speculative as also other steps of the reaction might be affected and the overall effect cannot be adequately estimated, let alone calculated, without suitable data from a targeted experimental study – which, unfortunately, is not within the scope of this work. Therefore,

regardless of the conclusions here, a study investigating the Dushman reaction under conditions similar to those in the Iodide/iodate reaction scheme is needed. Nevertheless, also trends in the modelling results from employing the kinetics discussed above might give some indication of what kinetics would have to be expected when taking evidence from the extensive amount of data on mixing experiments into account.

From the literature above, an “informed guess” of the effect of borate might be a reduction in reaction rate. From the changes reported and considering the concentrations in the reacting volume in micromixing experiments in stirred tanks, it might be estimated that the reaction could be slowed down to half or a quarter of the unaffected kinetics. Therefore, a third of k (from possibly suitable and reliable uncatalysed kinetic data) might be tested as an additional option, if the rate laws above fail to give more realistic results than the current model. It can be argued that such effects could depend on the concentration of borate, which changes throughout the micromixing process and consequently would have to be considered, if this is indeed the critical species. However, Truesdale *et al.* (2003) found that such buffer interactions also depend on the iodide concentration, which, again, changes throughout the process. Consequently, the above variation seems to be the most reasonable estimate possible at this point, i.e. as long as there is no further information on the specific conditions.

4.2.3. Numerical method

Guichardon (1996) used the fourth-order Runge-Kutta method to solve the incorporation model for the iodide/iodate reaction scheme, while Assirelli *et al*. (2008b) employed Bader and Deuflhard's semi-implicit discretisation in the Bulirsch-

Stoer method. The latter approach is more complex, but is computationally more efficient and especially suitable for stiff equations. Assirelli *et al.* (2008b) neglected the effect of the reactions on the ionic strength in the Jacobian matrix, which was justified because it changes slowly and only has a small effect compared to other parameters. Both methods give, as expected, very similar results (Assirelli 2004), further justifying both ways of solving the model.

In this study, the fourth-order Runge-Kutta method was chosen because of its simplicity which allows quick adaptation of the code to different kinetic models, in spite of being less efficient compared to the second option. Moreover, calculating the dissociation of sulphuric acid ahead of the next time step, as discussed above (see section 4.2.1), was less problematic to implement with this method with defined time steps.

The code was written in C and is based on the information given in literature (Fournier *et al.* 1996a; Assirelli 2004).

4.2.4. Polynomial regression for quantitative comparison

Micromixing experiments, as described in section 3.1.2., give results as segregation index, X_S, or micromixing ratio, $\propto$, for specific experiments, i.e. particular fluid dynamic conditions and reactant concentrations. Micromixing models calculate the final reactant concentrations – and consequently give X_S or $\propto$ – from given values of micromixing time. The results from the models are then usually plotted in graphical form with $\propto$ (or X_S) as a function of micromixing time. In order to make use of these results, functions tend to be fitted to the modelling data which then allows micromixing times to be obtained for each experimental condition.

In this work, polynomial regression was chosen for this quantitative comparison as suggested by Assirelli *et al.* (2008b). The equation used is: $f = y0 + ax + bx^2 + cx^3$ with y = ln(t_m) and x = ln(α).

Other authors (Camps Rota 1998; Rousseaux *et al.* 1999) reported fitting different functions to separate parts of the data, which would be an option if polynomial regression does not work sufficiently well. The validity and accuracy of employing this function was checked for all results with R^2.

4.3. Results and discussion

4.3.1. Validation of the implemented model

There are two options for testing the code: firstly, the results of the model without the dilution routine should still give the same results as those found in the literature. Figure 22 shows the result from the approach in this work, as outlined in section 4.1., and compares the predictions to those of Guichardon (1996) and Assirelli (2004). As can be seen, excellent agreement is obtained. Any small differences between the predictions are probably due to different numerical approaches (Assirelli 2004).

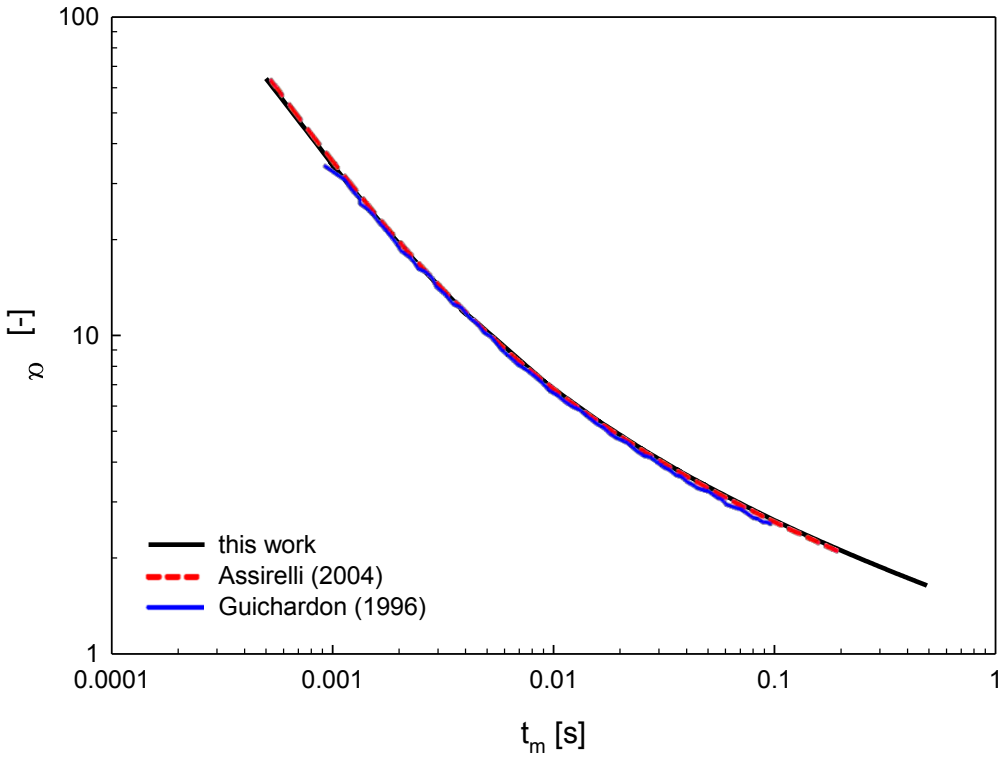

Figure 22: Comparison of the implemented routine to equivalent results from the literature (Assirelli 2004)

Due to the close agreement between the three predictions shown in Figure 22, the earlier values for three different sulphuric acid concentrations taken from Assirelli *et al.* (2008b) were used for further validation of the code. Again, Figure 23 shows excellent agreement. Still, as these graphs are plotted over a wide range of values for α and t_m on logarithmic axes, smaller differences might not be apparent. Therefore, also polynomial regression was employed and a comparison of 3 points for each group of curves confirms that the method is working, as only deviations of less than 0.5% were found (data not shown).

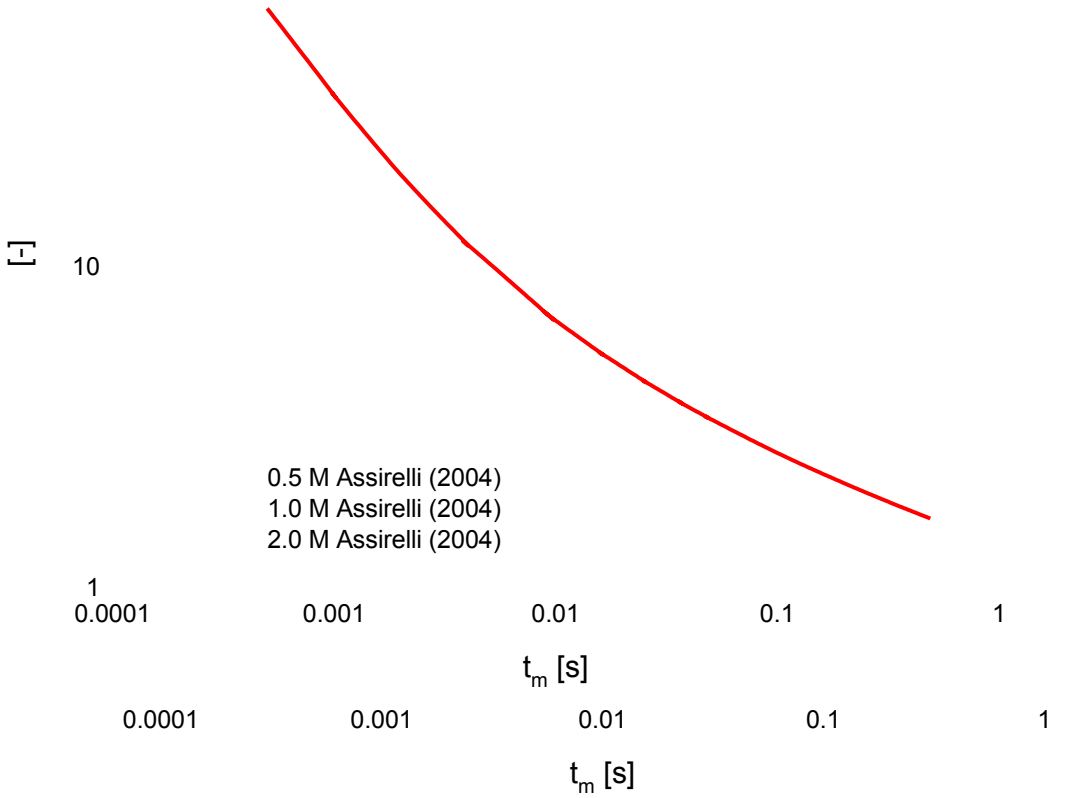

Figure 23 : Comparison of results from the present model with those of Assirelli et al. (2008b) at 3 acid concentrations

In addition to validating the results of the model with fully dissociated sulphuric acid, the dilution of the latter can be checked separately as well, i.e. without the other reactions occurring. The data presented in Figure 24 is obtained from simple equilibrium calculations using Excel spreadsheet for several concentrations and equivalent cases when using the model. The results clearly agree well. Moreover, there is an overlap of the concentrations of HSO_4^- and SO_4^{2-} at the dilution of 2 M by 250; this is exactly at the concentration suggested by Leenson (2004).

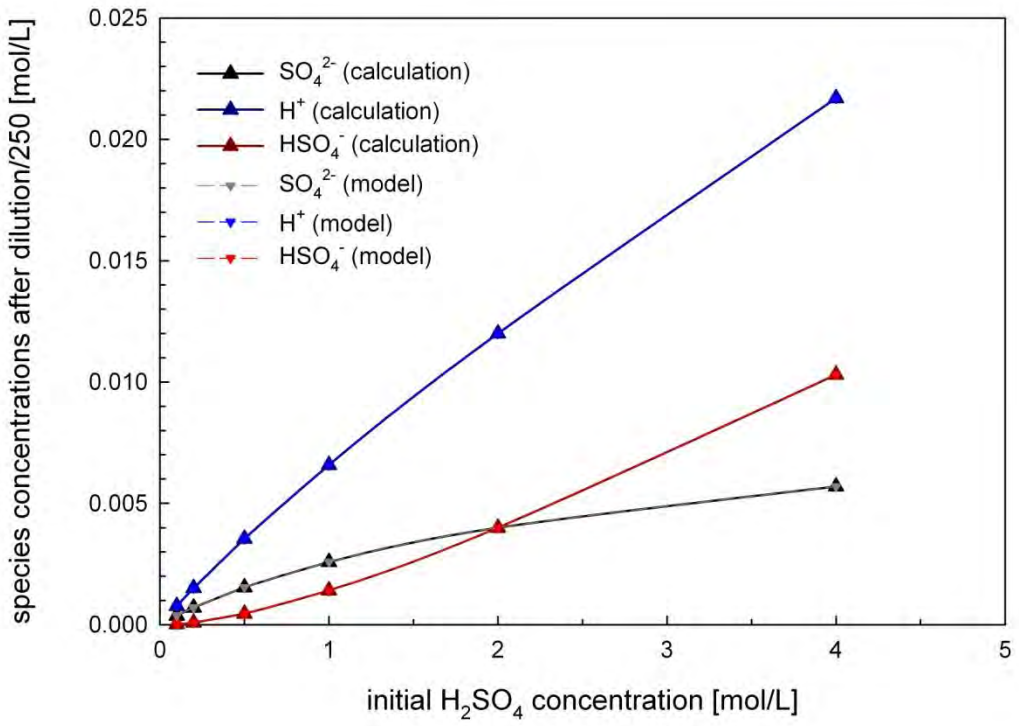

Figure 24: Species concentrations after dilution without reactions occurring

A comparison of all data points to the manually calculated values showed excellent agreement with the worst deviation being -0.012%, which is to be expected due to rounding errors.

4.3.2. Modelling results and use for interpreting experimental data

Established model and implemented dissociation

After testing the code, the combination of the original kinetics with implemented dilution and dissociation of the sulphuric acid was evaluated. This first combination might be considered to be mainly for demonstration purposes as this kinetic data was obtained assuming that all protons are already initially available.

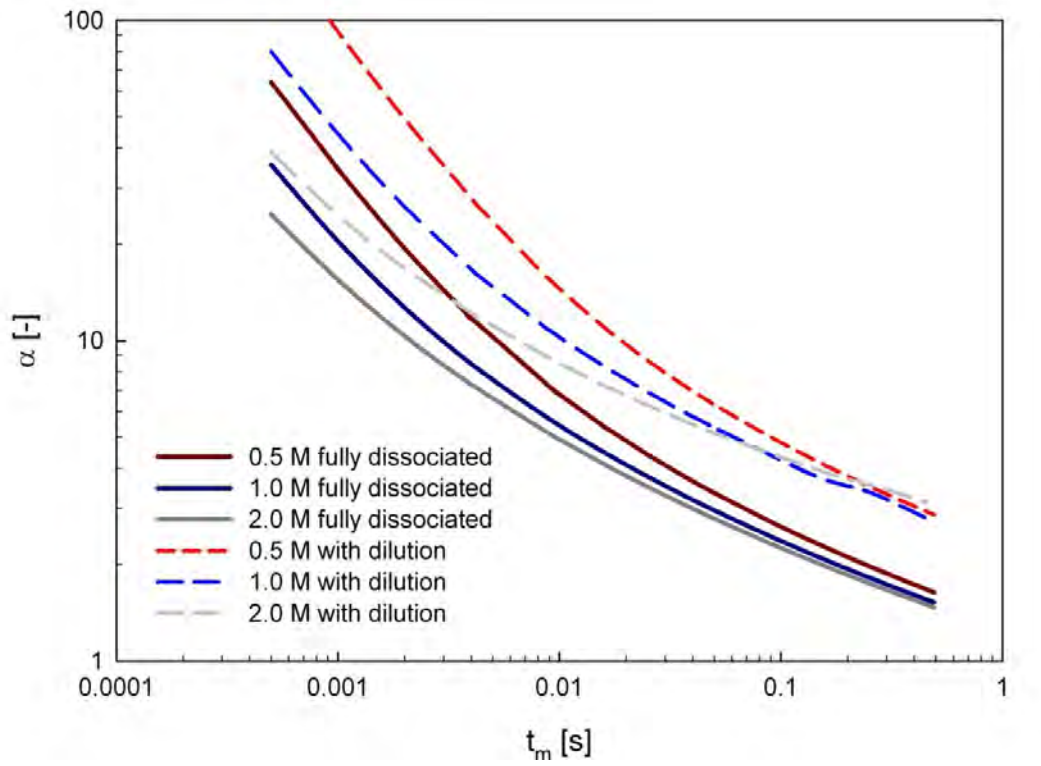

Figure 25: Incorporation model with initially fully dissociated sulphuric acid and with dilution implemented – kinetic data: Guichardon et al. (2000)

Figure 25 shows the results for the model with implemented dilution of the acid compared to the original data. There is a significant shift of the curves on the log-log-graph when dilution of the acid is implemented. Considering Assirelli *et al.* (2008b) found that the original model allowed at least reasonably realistic interpretation of experimental data, this large change may indicate that the original kinetic data might not be suitable in this case with dilution. This can be tested by comparing the variations for actual experimental data. Therefore, the micromixing times for the segregation indices are calculated from regression of the model results, as discussed above. These t_m values are then put into equation (4.1) to estimate ε_T and ϕ. The results at different power inputs for feeding near ε_{max}, the impeller and the surface are summarised in Table 8, Table 9 and Table 10, respectively.

Table 8: Comparison of assuming full dissociation or including dissociation in model for position 4 (near ε_{max}) – using kinetics from Guichardon et al. (2000)

	fully dissociated acid		partial dissociation of acid	
$\overline{\varepsilon_T}$ [W/kg]	ε_T [W/kg]	ϕ [-]	ε_T [W/kg]	ϕ [-]
0.18	24.143	134.129	2.008	11.158
0.50	53.958	107.915	5.118	10.235
0.97	63.406	65.367	6.148	6.338
1.94	81.481	42.000	8.145	4.199

Table 9: Comparison of assuming full dissociation or including dissociation in model for pos. 2 (near impeller) – using kinetics from Guichardon et al. (2000)

	fully dissociated acid		partial dissociation of acid	
$\overline{\varepsilon_T}$ [W/kg]	ε_T [W/kg]	ϕ [-]	ε_T [W/kg]	ϕ [-]
0.18	0.978	5.434	0.043	0.239
0.40	1.752	4.379	0.087	0.216
0.50	2.147	4.294	0.110	0.221
0.97	3.492	3.600	0.198	0.204
1.14	3.649	3.201	0.209	0.183

Table 10: Comparison of assuming full dissociation or including dissociation in model for pos. 1 (near surface) – using kinetics from Guichardon et al. (2000)

	fully dissociated acid		partial dissociation of acid	
$\overline{\varepsilon_T}$ [W/kg]	ε_T [W/kg]	ϕ [-]	ε_T [W/kg]	ϕ [-]
0.18	0.053	0.293	0.001	0.008
0.40	0.110	0.275	0.003	0.008
0.50	0.136	0.273	0.004	0.008
0.97	0.246	0.253	0.008	0.009
1.14	0.261	0.229	0.009	0.008

Of course, ε_T increases with increasing power input, which is correctly reflected in the above tables. On the other hand, the obtained ϕ decreased with impeller speed, especially closer to the impeller, which is found with both versions of the model. Literature indicates that this value should be relatively independent of impeller speed in each location, for instance: LDV data for a Rushton turbine reported by Zhou and Kresta (1996) fluctuated by less than 2.5 % over the range from 225 to 510 rpm when expressed as $\varepsilon_{max}/\bar{\varepsilon}$. Effects of the impeller speed, however, have already been found previously in micromixing experiments (Baldyga and Bourne 1999; Assirelli *et al.* 2008b). It can be argued that either the path of the reaction becomes shorter due to better (micro)mixing at higher impeller speeds, giving more localised information, or that the reactants might be swept away more quickly into regions of different energy dissipation rate, which could lead to the observed effect. The above trends point more towards the latter explanation because there are reductions of X_S which are stronger near the impeller, i.e. there is a substantial drop to 49% of ϕ from 0.18 to 0.97 W/kg near ε_{max}, but only a drop to 87% near the surface. For this reason, most of the following considerations will discuss lower impeller speed – assuming that having a possibly localised reaction zone allows sensible comparisons to local energy dissipation rates reported in literature. It should be noted, though, that such significant changes might be explained partially by a less than suitable micromixing model.

Measurements of local specific energy dissipation rates have been done with a range of methods: values from ~20 (Sharp and Adrian 2001)(PIV) or 25 (Wu and Patterson 1989), 35 (Laufhütte and Mersmann 1987)(LDA) to ~70 (Cutter 1966), using a photographic technique, have been found for ϕ_{max}, which is close to the impeller. In

the bulk and in particular towards the surface, much lower values have been observed for ϕ, i.e. around and well below 1. Such wide ranges of potentially realistic ϕ for different locations in the tank are clearly far from ideal for the validation of a model and the difficulties of the various laser-based methods for obtaining such values have also been illustrated (Micheletti *et al.* 2004; Gabriele *et al.* 2009). Still, there is enough data from detailed and careful studies using modern techniques which can aid verifying that the results are in a realistic order of magnitude. For this purpose, the most reasonable estimates seem to be around 50 near ϕ_{max} (Zhou and Kresta 1996; Schäfer 2001), around or slightly less than 1 for the feed position in the impeller discharge stream but away from the impeller and well below 1 near the surface.

A comparison of this literature to the results in Table 8, Table 9 and Table 10 shows that the original model consistently gives higher values than expected while including the dissociation of sulphuric acid leads to rather low ones. Clearly, both versions are not giving the expected results, but are still within a reasonable range. Further testing of variations of the model seems warranted.

Considering dissociation – combined with other kinetics from literature

Using the implemented dissociation with other kinetic data might give more realistic results and some of the investigated options are summarised here.

One interesting kinetic rate law, as proposed by Schmitz (2000), shows first and second order behaviour of iodide and could be relevant because it might cover a wide range of conditions. Unfortunately, the concentrations of iodide were still very low in that study and this might render the data less useful in this context considering recent criticism (Bourne 2008). Nevertheless, it seemed interesting to test.

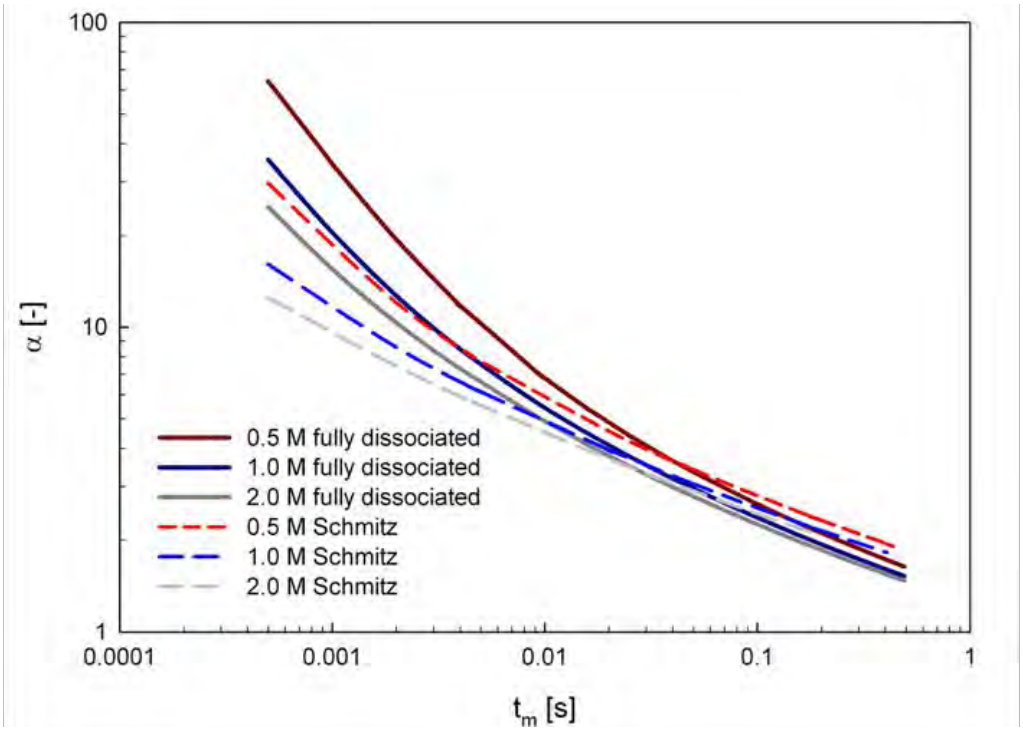

Figure 26: Results for original model (fully dissociated) – compared to: with dilution implemented using kinetic data by Schmitz (2000)

Figure 26 shows that the curves are closer to the original model than the same version with dilution. Nevertheless, there are deviations especially towards very high and lower micromixing times because the new curves are less steep than the original ones. The resulting values of ε_T and ϕ do not give more realistic results than the original approach. Especially, ϕ near $\boldsymbol{\varepsilon_{max}}$ is significantly higher instead of giving a lower value as would be expected:

Table 11: Results for model considering dissociation of acid using kinetics from Schmitz (2000) – at different feed positions at 0.18 W/kg

feed position	ε_T [W/kg]	ϕ [-]
1 – near surface	0.038	0.213
2 – near impeller	1.505	8.360
4 – near ε_{max}	97.668	542.598

Another option would be the kinetic data reported by Palmer and Lyons (1988). As they gave rates for three different ionic strengths, the one for I = 1M was first tested. Figure 27 shows that the graphs are, again, less steep than the previously reported ones and, overall, in spite of the different measurement approaches, resemble the result for the kinetics reported by Schmitz (2000) - see Figure 26.

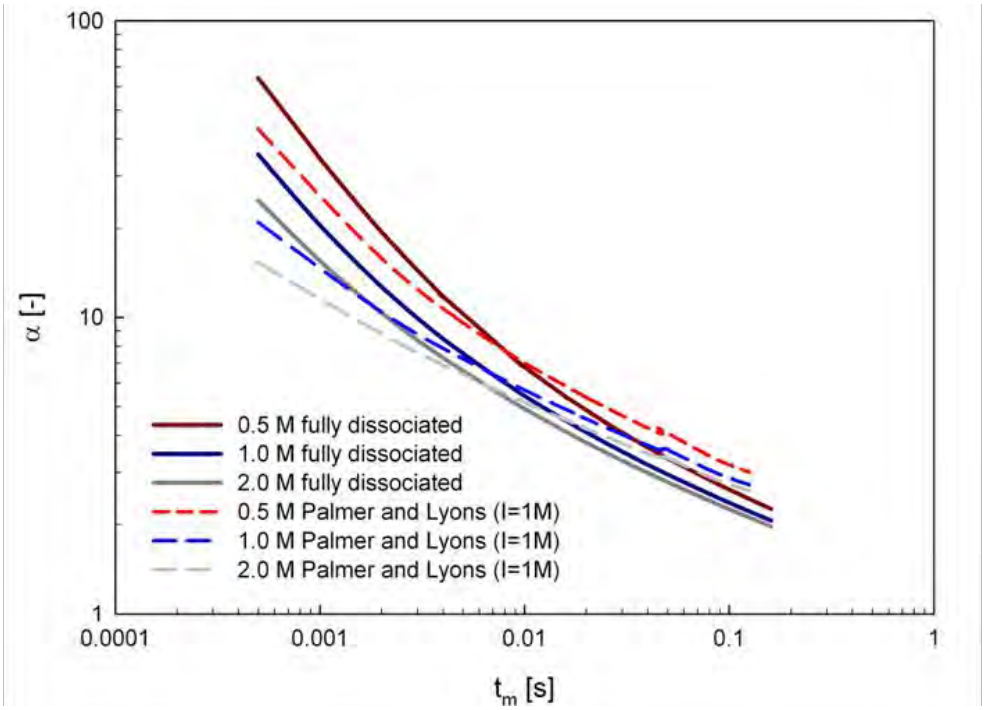

Figure 27: Results for original model (fully dissociated) – compared to: with dilution implemented using kinetic data by Palmer and Lyons (1988) for I = 1M

Table 12: Results for model considering dissociation of acid using kinetics from Palmer and Lyons (1988) for I = 1M – at different feed positions at 0.18 W/kg

feed position	ε_T [W/kg]	ϕ [-]
1 – near surface	0.047	0.260
2 – near impeller	1.79	9.93
4 – near ε_{max}	103	573

Table 12 shows that the values of ϕ are surprisingly close to the ones in Table 11 and they are still worse, i.e. further away from expected for these values, than the

currently established approach. However, it might be argued that the reaction rate constant employed was for I = 1M and therefore neglected the changes of ionic strength in the reaction zone. In order to make better use of the data from Palmer and Lyons (1988), a simple power law was used to fit a function to the results:

$$k = 259807884.1962\, x^{-0.2239} \qquad \textbf{(4.20)}$$

(Equation (4.20) gives the factors as used in the code, though such numbers clearly have more significant numbers than can be justified experimentally. The full figures are nevertheless given to allow reproduction of the employed method.)

This is plotted in Figure 26 to show the validity of the fit. By better accounting for the sensitivity to ionic strength, the model might improve. Fortunately, the given range of I from 0.015 to 1 M is relatively close to what would be expected in the reaction zone from less than ~1.5 M to more than ~0.05 (Assirelli 2004). As higher ionic strengths seem to affect the reaction rate less, a range up to 2 M was accepted in the code before cutting off (though not necessary, as such values were not reached).

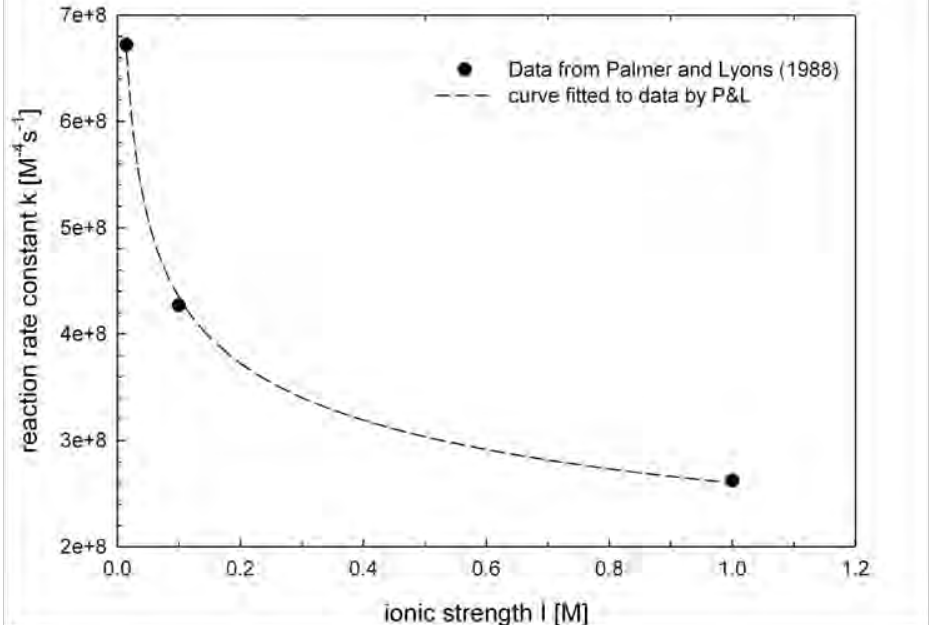

Figure 28 : Kinetic rate constants obtained by Palmer and Lyons (1988) for three ionic strengths and power law function fitted to data

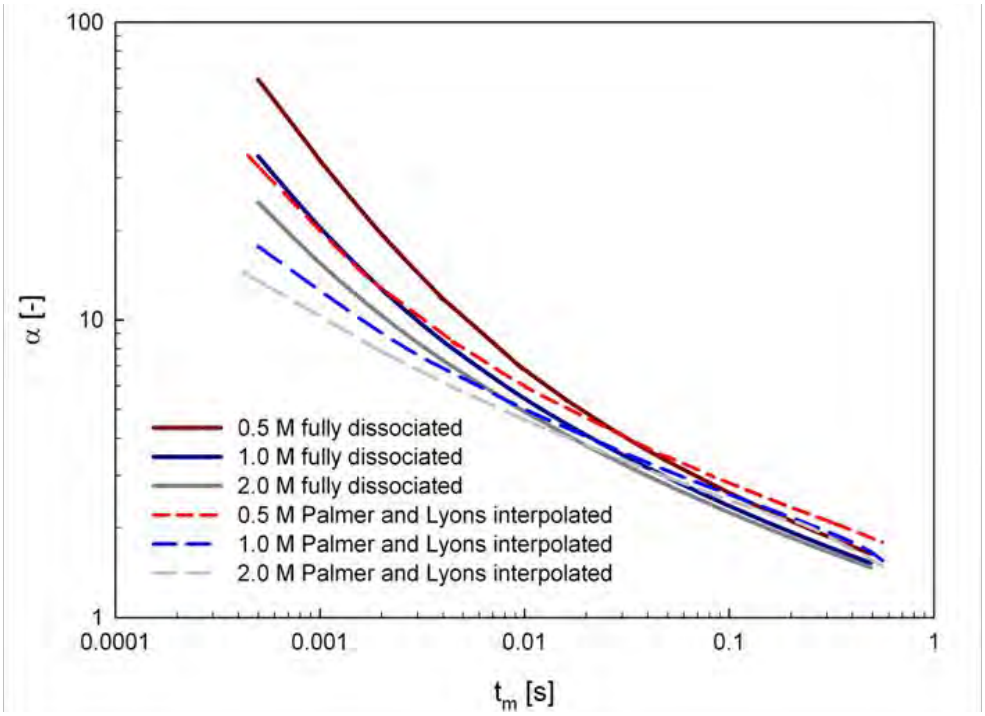

Figure 29: Results for original model (fully dissociated) – compared to: with dilution implemented using interpolated function of kinetic data by Palmer and Lyons (1988)

This interpolation does indeed move the results slightly closer towards what would be expected for ϕ, as illustrated in Table 13. Nevertheless, this still does not give more realistic values than the original, heavily criticised method.

Table 13: Results for model considering dissociation of acid using data from Palmer and Lyons (1988) interpolated function for l – at different feed positions at 0.18 W/kg

feed position	ε_T [W/kg]	ϕ [-]
1 – near surface	0.035	0.197
2 – near impeller	1.32	7.34
4 – near ε_{max}	76.7	426.4

Another study with relevant kinetic data was presented by Xie *et al.*(1999) who used a special method which is particularly suitable for studying such fast reactions. The

kinetics may be employed, as described above, in full with dependence on saturation or as a constant. Both options were tested and gave very similar results. Therefore, the constant value (for I=0.5 M) was used for detailed evaluation and Figure 30 shows that this also resembles the above trends.

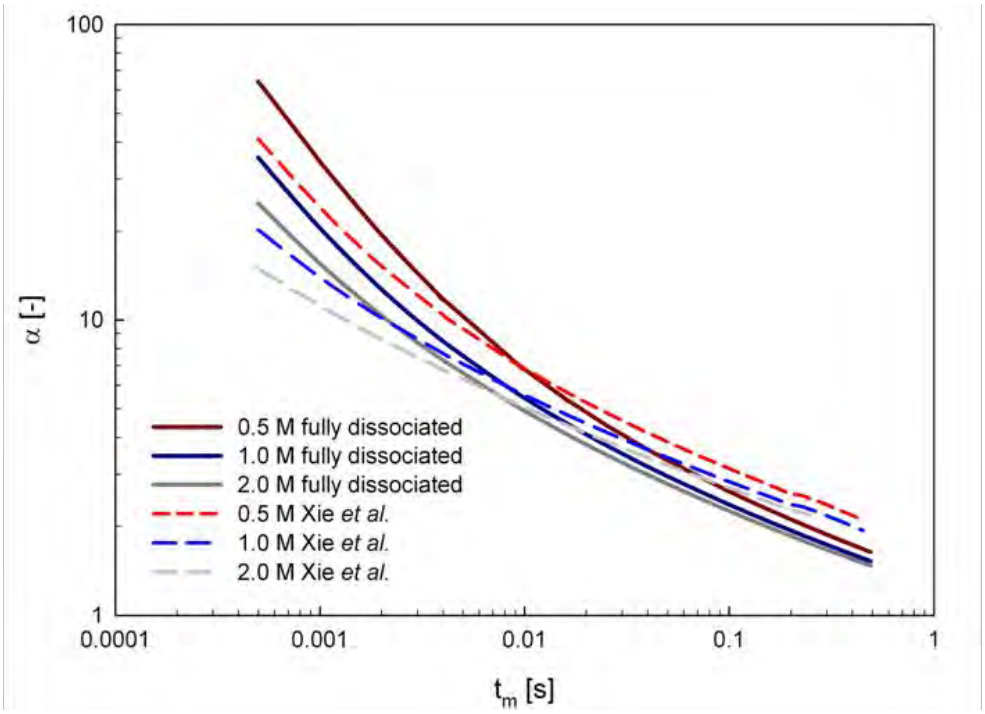

Figure 30: Results for original model (fully dissociated) – compared to: with dilution implemented using kinetic data by Xie et al. (1999)

Table 14: Results for model considering dissociation of acid using data from Xie et al. (1999) – at different feed positions at 0.18 W/kg

feed position	ε_T [W/kg]	ϕ [-]
1 – near surface	0.017	0.093
2 – near impeller	0.685	3.803
4 – near ε_{max}	41.399	229.995

In this case, the values for ϕ lie between the original and the other adaptations' but also do not move much closer to improving the method for interpreting experimental

data obtained by the Iodide/iodate method. However, all of these results are surprisingly consistent which is remarkable when taking the different measurement methods into account and that even the relatively unrelated data by Schmitz (2000) points towards a similar direction. This would not have been expected, considering the many, but valid, points of criticism (Bourne 2008).

To further emphasise the agreement of these kinetics: it was even possible to combine the data by Palmer and Lyons (1988) and Xie *et al.* (1999) in one interpolated function. This equation (4.21) is very similar to (4.20) and should not affect the results reported above too much, but was still tested for completeness:

$$k = 250789676.2644x^{-0.2323} \qquad \textbf{(4.21)}$$

(Again, level of detail only to allow exact reproduction of data!)

The agreement of the (little) available (relatively) suitable data is illustrated in Figure 31 which also shows the functions fitted to the kinetic constants.

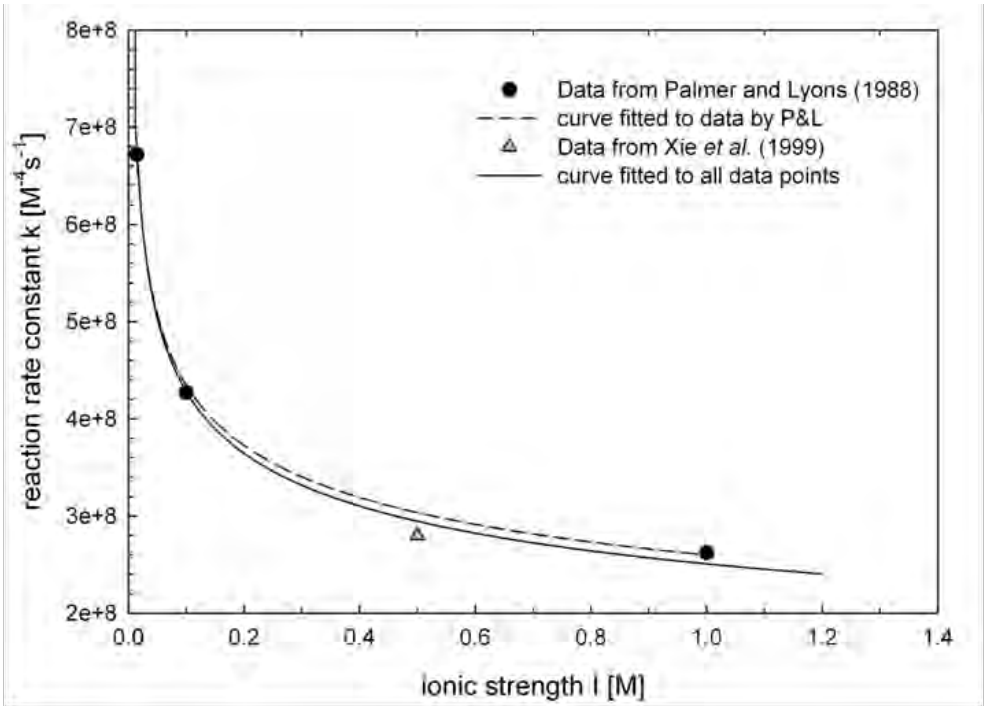

Figure 31: Kinetic rate constants obtained by Palmer and Lyons (1988) and Xie et al. (1999) for different ionic strengths and power law function fitted to data

As expected, the results summarised in Table 15 are comparable to the other variations'.

Table 15: Results for model considering dissociation of acid using data from Palmer and Lyons (1988) and Xie et al. (1999) – at different feed positions at 0.18 W/kg

feed position	ε_T [W/kg]	ϕ [-]
1 – near surface	0.035	0.194
2 – near impeller	1.22	6.79
4 – near ε_{max}	79.6	442.0

The above evaluation of various modelling options, unfortunately, did not lead to values of ϕ that would be expected from literature but the trends found are still consistent which is surprising (Bourne 2008). This consistency could suggest that there are significant differences between the conditions of the available kinetic data and the conditions during experiments employing the iodide/iodate method, i.e. that a relevant factor is not appropriately reflected here. Therefore, more effects might need to be considered for reasonable quantitative use of such micromixing data. Of course, including the dissociation of the sulphuric acid should be more realistic than assuming full ionisation from the beginning of the injection. However, there are no full kinetic studies at relevant concentrations reported in literature, apart from the new reaction orders proposed by Kölbl *et al.* (2011), even less any reliable indication whether the other species present, for instance borate, might affect the reaction. Therefore, more targeted work on these reactions is indicated – especially considering possible interactions with the buffer, as this is the most obvious difference, apart from the concentrations, to the conditions of the available data.

4.3.3. Including dissociation and adapted kinetic model

Due to the effects of borate on the reverse reaction and reaction steps discussed in section 4.2.2., it could be argued that the reaction might be slowed down significantly in the presence of the buffer. The above modelling results also suggest a slower side-reaction and therefore, that option had to be considered too. This is especially true due to the excellent agreement of the data from uncatalysed and not inhibiting systems. The data from the most sophisticated methods (Palmer and Lyons 1988; Xie *et al.* 1999) agreed well and, consequently, the interpolated function (4.21) was used for this purpose. The initial estimate, for order of magnitude, was a reduction, as explained in section 4.2.2., to a third of the unaffected reaction rate and, therefore: $k_{adapted}=k_{(4.19)}/3$.

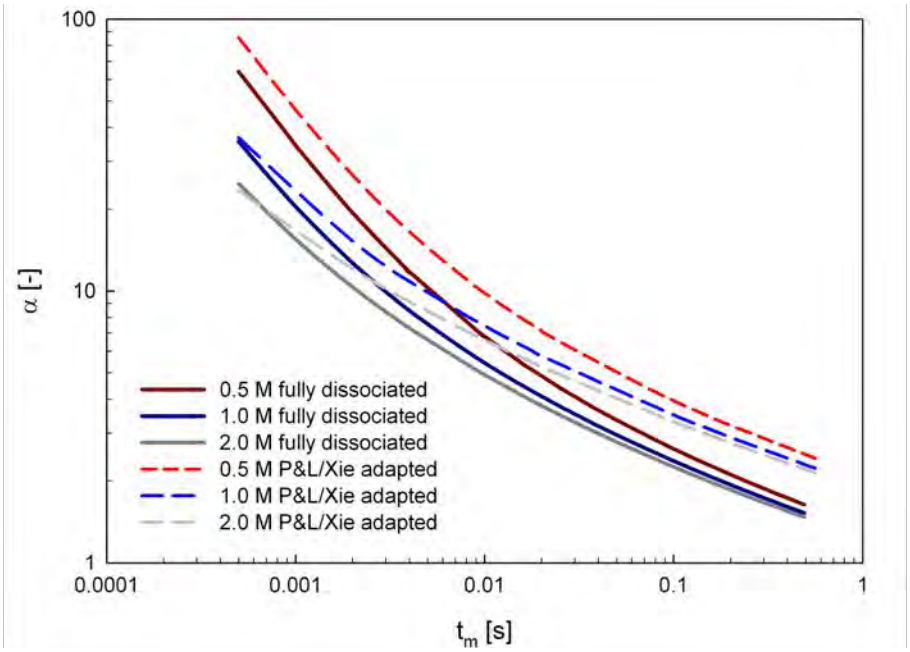

Figure 32: Results for original model (fully dissociated) – compared to: included dissociation and adapted kinetic behaviour

The trend of the curves in Figure 32 looks different from the previous ones, as they are above the original ones, while again being less steep. Of course, application to experimental data is necessary for quantification. Therefore, a range of power inputs for three feed positions are evaluated and summarised here:

Table 16: Comparison of original model and new approach including dissociation and using adapted kinetics - for position 4 (near ε_{max})

	fully dissociated acid		partial dissociation of acid	
$\overline{\varepsilon_T}$ [W/kg]	ε_T [W/kg]	ϕ [-]	ε_T [W/kg]	ϕ [-]
0.18	24.14	134.13	8.04	44.69
0.50	53.96	107.92	21.10	42.21
0.97	63.41	65.37	25.50	26.29
1.94	81.48	42.00	34.11	17.58

Table 17: Comparison of original model and new approach including dissociation and using adapted kinetics - for position 2 (near impeller)

	fully dissociated acid		partial dissociation of acid	
$\overline{\varepsilon_T}$ [W/kg]	ε_T [W/kg]	ϕ [-]	ε_T [W/kg]	ϕ [-]
0.18	0.978	5.434	0.146	0.809
0.40	1.752	4.379	0.304	0.761
0.50	2.147	4.294	0.394	0.787
0.97	3.492	3.600	0.727	0.749
1.14	3.649	3.201	0.768	0.674

Table 18: Comparison of original model and new approach including dissociation and using adapted kinetics - for position 1 (near surface)

	fully dissociated acid		partial dissociation of acid	
$\overline{\varepsilon_T}$ [W/kg]	ε_T [W/kg]	ϕ [-]	ε_T [W/kg]	ϕ [-]
0.18	0.053	0.293	0.004	0.020
0.40	0.110	0.275	0.009	0.023
0.50	0.136	0.273	0.012	0.024
0.97	0.246	0.253	0.025	0.026
1.14	0.261	0.229	0.027	0.024

The results of ϕ for the adapted version are, for the conditions in a stirred tank, much closer to what would be expected, even though the effect of the buffer is assumed to be constant, i.e. 1/3 of k. There could, however, be a concentration dependence which would be difficult to estimate due to the complex behaviour reported for other species (Truesdale 1997). Consequently, this is mainly for illustration purposes, but can be easily changed once suitable experimental data is available.

In addition it could be noted, that the original kinetics by Guichardon *et al.* (2000) give reasonable results and show strong dependence on ionic strength. Their observation of dropping reaction rate with increasing ionic strength might be explained by their use of $K_2SO_4$to adapt ionic strength, which then reduced the amount of available H^+. In fact, their rate constant changes by orders of magnitude with ionic strength: from ~10^9 to ~10^7 $\mathrm{M^{-4}s^{-1}}$ from 0 to 1.4 M, respectively. Such dramatic effects were not observed by Palmer and Lyons (1988). Considering that the buffer significantly contributes to the ionic strength, an inhibiting effect of borate might have been "accidentally included" and, therefore, explain the reasonable results when interpreting stirred tank experiments. In addition, iodide concentration, which has been shown to shift such effects (Truesdale *et al.* 2003), also depends on incorporation to which ionic strength is correlated. Therefore, the kinetics reported by Guichardon *et al.* (2000) might also indirectly account for such phenomena.

This also supports the assumption of an inhibited reaction, but further data is needed.

4.3.4. Use of such models to compare data

At same reactant concentrations – with varied flow conditions

Such modelling results might not only be of use for giving absolute information on local turbulence. Also, comparisons of results for different flow conditions would be useful. Therefore, the single-phase data presented above (section 3.2.3.) is expressed here once as Φ in Table 19, which shows the strong variations of the data. However, when given as percent of reference values at different feed positions, as illustrated in Table 20, the data becomes much more consistent – even for the wide range of values tested, i.e. from the highest to the lowest local specific energy dissipation rates in the stirred tank. This suggests that, although the kinetics and the effect of the buffer need further consideration, comparisons of experimental results are possible at least with same reactant concentrations in the stirred tank.

Table 19: Summary of Φ at various locations at 0.18 W/kg – shows significant differences, but consistent pattern in data

model	near ε_{max}	near impeller	near surface
original	134	5.43	0.293
original + diss.	11	0.24	0.008
Schmitz	543	8.36	0.213
Palmer and Lyons (1M)	573	9.93	0.260
P&L (interpolated)	426	7.34	0.197
Xie et al.	230	3.80	0.093
P&L+Xie (interpolated)	442	6.79	0.194
adapted	45	0.80	0.020

Table 20: Relative comparisons of Φ in % of various locations at 0.18 W/kg – data becomes more consistent than in Table 19

model	impeller to ε_{max}	surface to ε_{max}	surface to impeller
original	4.05%	0.218%	5.39%
original + diss.	2.14%	0.068%	3.17%
Schmitz	1.54%	0.039%	2.55%
Palmer and Lyons (1M)	1.73%	0.045%	2.62%
P&L (interpolated)	1.72%	0.046%	2.68%
Xie et al.	1.65%	0.040%	2.44%
P&L+Xie (interpolated)	1.54%	0.044%	2.86%
adapted	1.78%	0.045%	2.51%

This agreement of the data in Table 20 suggests that these model variations can be used for comparisons, though the absolute values (Table 19) vary significantly.

At same flow conditions– with varied reactant concentrations

Besides testing the models at different feed positions, different acid concentrations might be used as well. In this case, the segregation indices are not the same at equal conditions, as the reactions are affected by the reactant concentrations. Therefore, the micromixing model should then give comparable micromixing times and local specific energy dissipation rates, i.e. the results should then overlap within experimental error.

Such tests have already been done before (Assirelli 2004; Assirelli *et al.* 2008b). In that work, the original modelling approach was used and good agreement of the data for different acid concentrations was found once the results were presented as micromixing times or local specific energy dissipation rates, instead of X_S or α. The

model variations tested above will, therefore, be applied to the experimental data by Assirelli (2004). This might help evaluate the suitability of the employed kinetics.

For feed position 3, Assirelli (2004) reported micromixedness ratios for two acid concentrations ($[H^+]$ = 1 and 2 M) at four impeller speeds. With the original micromixing model a standard deviation around 20% for ϕ is found between the data for the two acid concentrations for the four power inputs. The adapted versions give slightly worse agreement with standard deviations around 27% for ϕ. However, experimental errors are also magnified in such calculations and can reach over 30% for ϕ in the given data set, even when only the reported experimental error is considered. In addition to this, there might also be differences in micromixing itself, as changes in acid concentrations might lead to differently long trajectories before the last H^+ has reacted and therefore different local conditions experienced – similarly to the deviations with changing impeller speeds. Assirelli (2004) used $[H^+]$= 1 and 4 M to study micromixing near the impeller and found backmixing effects for the higher acid concentration at higher impeller speed. This finding also supports the above argument about inherent differences with varied acid concentrations, which can (and should) not be compensated for by the model, as they indeed are real effects in the flow. Therefore, a comparison of the data near ε_{max} – where such phenomena might be especially likely – is not of use for evaluating the model variations.

Unfortunately, no further data is available for such comparisons, but the above does not suggest significant differences in the suitability of the different adaptations and the more established original version.

4.4. Conclusions

The current approach of the iodide/iodate method, which assumes fully dissociated sulphuric acid, has been criticised in literature and, consequently, the incorporation model, which has been used for this reaction scheme before, was extended accordingly. In addition, different kinetics were implemented to find a variation that gives more realistic values of ϕ than the existing modelling – with a focus on stirred tanks.

The results from employing different rate laws for the Dushman reaction were surprisingly consistent, but gave higher ϕ than would be expected from mixing literature. As the effect of the buffer is not well understood in this case, information on the possible interaction of borate with the reverse reaction of the Dushman reaction and related reactions was discussed. From these considerations, the effect of borate on the reaction scheme was estimated. This lead to more realistic results, but further work in this direction is needed. Recently, the potential difficulties encountered with such measurements, even in modern apparatuses, were discussed (Kölbl 2008). Nevertheless such data is urgently needed to develop the iodide/iodate method from a qualitatively reliable to a quantitatively sound technique to study micromixing processes in a variety of geometries.

Until such data becomes available, the previously reported model and above approach should be suitable, at least, for comparing experimental results relative to each other and for order of magnitude estimates of local energy dissipation rates or ϕ in stirred tanks. Therefore, in this thesis, data will be interpreted using the original model and some variations, as presented in this chapter.

5. MICROMIXING IN GAS-LIQUID SYSTEMS

5.1. Introduction

A dispersed, gaseous phase, i.e. bubbles, is present in many mixing applications using stirred tanks, including those where micromixing is important, for instance fluorination or hydrogenation. The effect of gas bubbles on micromixing in agitated vessels is not very well characterised, see section 2.3.3., and this chapter is aimed at giving a clearer picture of whether and, if so, how significantly gas sparging affects micromixing in them. For this purpose, three feed positions were investigated under gassed conditions: near the surface (pos 1), near the impeller (pos 2) and below the impeller (pos 3) – see Figure 18.

In this chapter, first the method is validated for gas-liquid studies, then experimental conditions defined and results from these experiments reported. In addition, these will be discussed using the modelling described in the previous section.

5.2. Validation of the experimental method for sparged conditions

To use the iodide/iodate technique in gassed systems, the chemicals and their reactions should only be affected by the sparging of the gas due to changes in micromixing, not by any undesired reactions, either physical or chemical. Therefore, it was necessary to check that the method would not fail in these conditions.

5.2.1. Loss due to gas stripping

One question was whether the gassing process might strip any reactants from the liquid which would cause misleading results. Especially iodine, which is produced

during the experiments, needs to be considered because of the substance's high volatility.

Several solutions containing all reactants including iodine and triiodide at various concentrations and different pH-values which would be present in typical experiments were sparged with air and samples taken over time. The triiodide concentration from these experiments was compared to samples of the solution taken from the vessel before sparging.

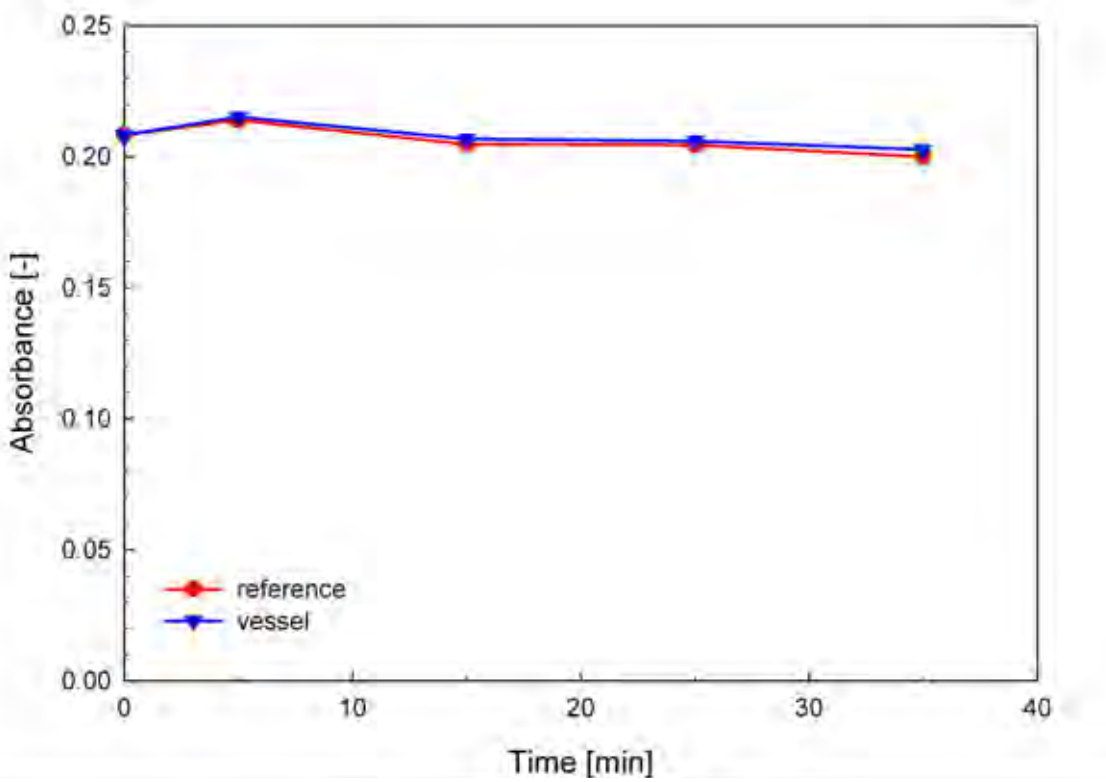

Figure 33: An example of the effect, with time, of air sparging at 1.0 vvm on the absorbance, i.e. triiodide concentration, of a typical solution of reactants

A typical set of data from these tests is plotted in Figure 33 and allows observation of any stripping effects for the duration of the planned experiments. Even after 35 minutes of aeration, deviations of less than ±1.5% between the triiodide concentration in the sparged vessel and the unsparged reference solution were

observed. This is in agreement with Lin and Lee (1997) who did not find any losses either, even at their higher sparge rates of up to 10 vvm.

5.2.2. Oxidation of iodide

Another concern which has been mentioned previously by some authors (Lin and Lee 1997; Schäfer 2001) is the oxidation of iodide:

$$O_2 + 4H^+ + 6I^- \rightleftharpoons 2I_3^- + H_2O \qquad \textbf{(5.1)}$$

Due to this Lin and Lee (1997) used nitrogen instead of air and also prepared the solutions with continuous N_2 stripping in order to avoid any oxidation of reactants. Considering that this oxidation can only take place when H^+ is available and is relatively slow (Harris 1995), it can be expected that it would not be relevant in the bulk of the stirred liquid which has to have a higher pH for these studies anyway.

Sparging iodide/iodine solutions in a pH-range from the expected basic conditions to neutral with nitrogen or air did not show any deviations in behaviour in triiodide concentration, which was expected for the above reasons.

Consequently, the gassed experiments could be performed using air.

5.3. Power input in sparged cases

5.3.1. Power measurement results in gas-liquid cases

As discussed in section 2.1.3., the power input of Rushton turbines can be significantly affected by the sparging of gas. In order to investigate the effect of the added phase on micromixing, the impeller speed had to be adapted to give constant impeller power input. For this, power measurements of the gassed system were performed. Considering the well-established fact that some salts can affect

coalescence (Lessard and Zieminski 1971; Craig *et al.* 1993), all experiments were conducted using the actual solutions and the resulting power curves are plotted in Figure 34 – as relative power demand against gas flow number.

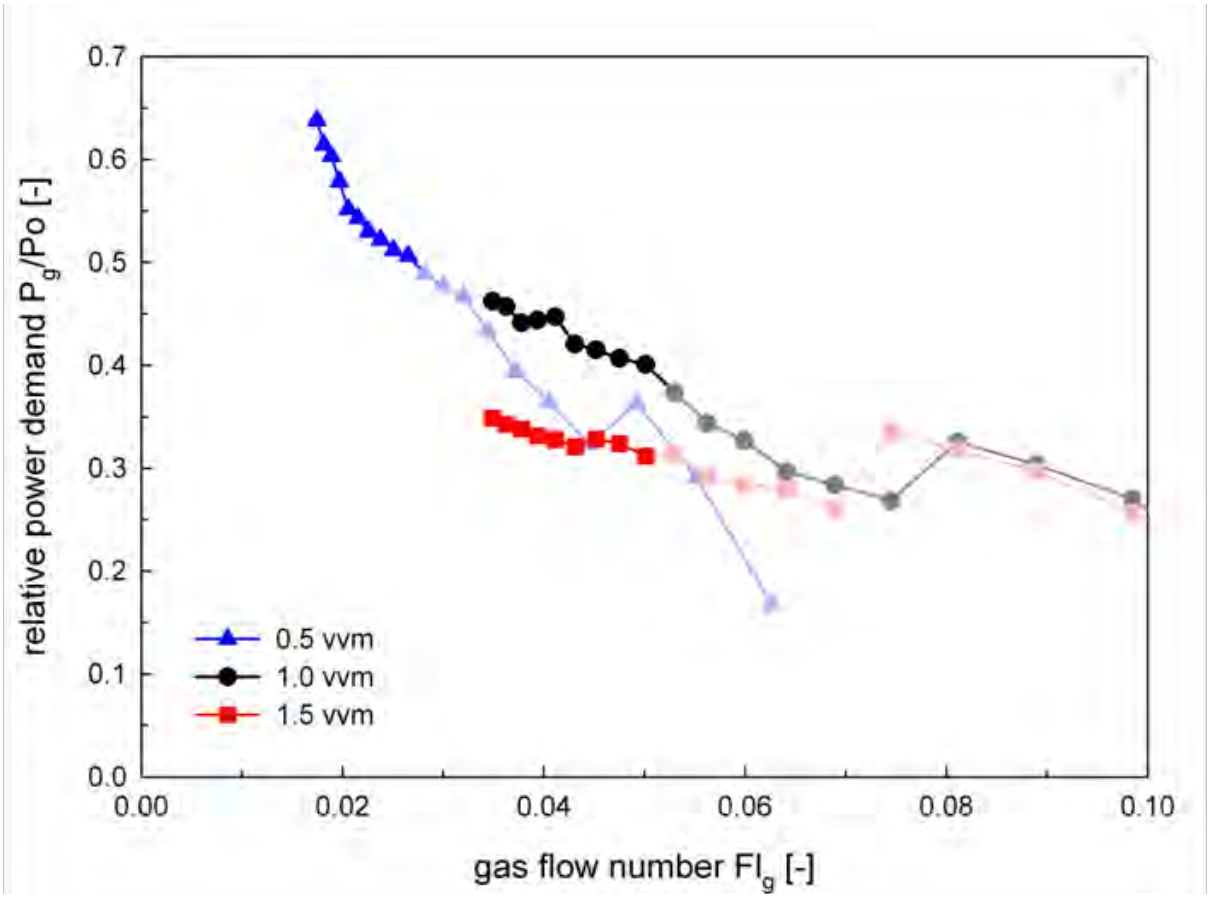

Figure 34: Relative power demand as function of gas flow number – gassed

Figure 34 generally shows the typical power behaviour of Rushton turbines in sparged systems, i.e. dropping with increasing gassing rates. However, the minimum at N_{CD} cannot be seen because these parts of the power inputs were outside of the measurement range of the torque meter. Still, for all three gassing rates, the points of flooding were captured, which could also be observed visually during the experiments, though the absolute values of power input in this lower range will be different. The lower values of the measured power were, unfortunately, out of range for technical reasons (these parts of the graphs are in a faint colour) and

consequently could not be used for determining constant mean specific power input in the micromixing experiments. For all results below 0.4 W/kg, the measurement was considered to not be accurate enough for the intended purpose and only values above that level have been used. Nevertheless, the overall trends look as expected compared to literature (Harnby *et al.* 1997). In addition, also the power measurements in the single-phase case agree well with literature which shows that the data in the range above 0.4 W/kg should be reliable.

5.3.2. Conditions for micromixing experiments with gas

For the above reasons, the following impeller speeds were employed to keep the power input from the impeller constant:

Table 21: Impeller speeds at several gassing rates for matching mean specific energy dissipation rates

$\overline{\varepsilon_T}$ [W/kg]	0.0 vvm [rpm]	0.5 vvm [rpm]	1.0 vvm [rpm]	1.5 vvm [rpm]
0.18	300			
0.40	395	495	535	569
0.50	420	527	567	607
0.97	522	638	682	745
1.14	552	670	721	781

5.3.3. Flow at the chosen conditions

At all of these conditions for the micromixing experiments, even at the lowest power input and highest gassing rate, the impeller was not flooded, which could be observed visually and from the power data which is summarised in section 5.3.1. At

such, conditions, when the gas is dispersed in the tank, it would usually not be possible to see the feed pipe during the experiments. However, Assirelli (2004) recommended leaving a small gas bubble at the tip of the feed pipe before starting the injection to keep the fluids from interacting too early which was found useful in this work as well. The start of the injection would then start when that little bubble has left the pipe which can be seen clearly in single-phase experiments with glass pipes. For many multi-phase cases shown here this was not possible, but the "dead time" was checked during test runs and could therefore easily be considered in the actual experiments.

Sometimes the amount of gas sparged is expressed as superficial gas velocities. For completeness, these are given in Table 22 – note that in this case the aspect ratio of the tank is 1.3.

Table 22: Superficial gas velocities

gas rate [vvm]	superficial gas velocity [m/s]
0.5	0.00312
1	0.00624
1.5	0.00936

5.4. Micromixing near impeller under gassed conditions

Figure 35 shows the segregation index as a function of impeller power input for two gassing rates, 0.5 and 1.0 vvm, and corresponding single-phase data for comparison. Only broad conclusions can be drawn from this graph, as the segregation index is slightly higher in some of the gassed cases, but these deviations

might be negligible, considering the error bars. In addition, one might expect stronger effects with increasing gassing rates, which is not the case in these results. Figure 35 does indicate, however, that any possible effects on micromixing due to the presence of gas bubbles can be expected to be small or negligible near the impeller at constant energy input.

Although it has been shown in the previous section that power data below 0.4 W/kg is not reliable enough for being used in the main part of this study, some tests were done at the lowest power input, 0.18 W/kg, and 0.5 vvm. Interestingly, the segregation index is lower than under “comparable” single-phase conditions. This might be due to the underestimated power number of the gassed impeller which leads to higher impeller speeds than actually needed, i.e. higher power input into the system and therefore improved micromixing.

Another explanation might be the ratio of power put into the system due to gassing compared to stirring: it may be argued that the power input from the impeller is low enough in this case to actually have a noticeable effect of the power put into the system from the gas sparging, which would be relatively small at the higher power inputs. The power input from the gas is discussed in part 5.8.

Obtaining more reliable power data would be necessary to allow comparisons in that range, but technical limitations did not permit this at lower power inputs. Consequently, only conditions with accurately measured power inputs, as described above, are considered in the further investigation – which still leaves a useful range of power inputs which are relevant to industry.

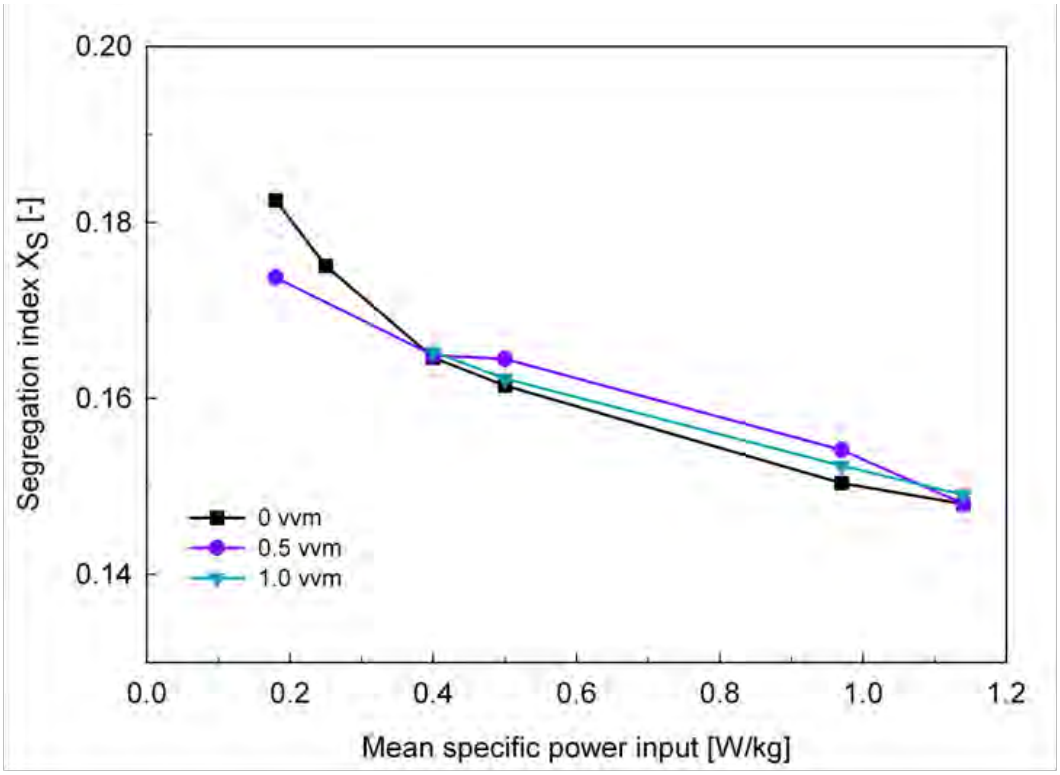

Figure 35: X_S as a function of mean specific energy dissipation rate at various gassing rates – impeller feed with 1 mol/L H_2SO_4

As the set of results from the experiments with 1 mol/L sulphuric acid is rather limited in number of data points and does not show any systematic trends due to sparging, further runs were done with 0.5 mol/L which is expected to give higher sensitivity to micromixing. This improvement is due to the different relative changes in reaction rates with varying acid concentration and has already before been used for adapting the method to specific measurement problems (Guichardon and Falk 2000; Assirelli 2004; Kölbl *et al.* 2008).

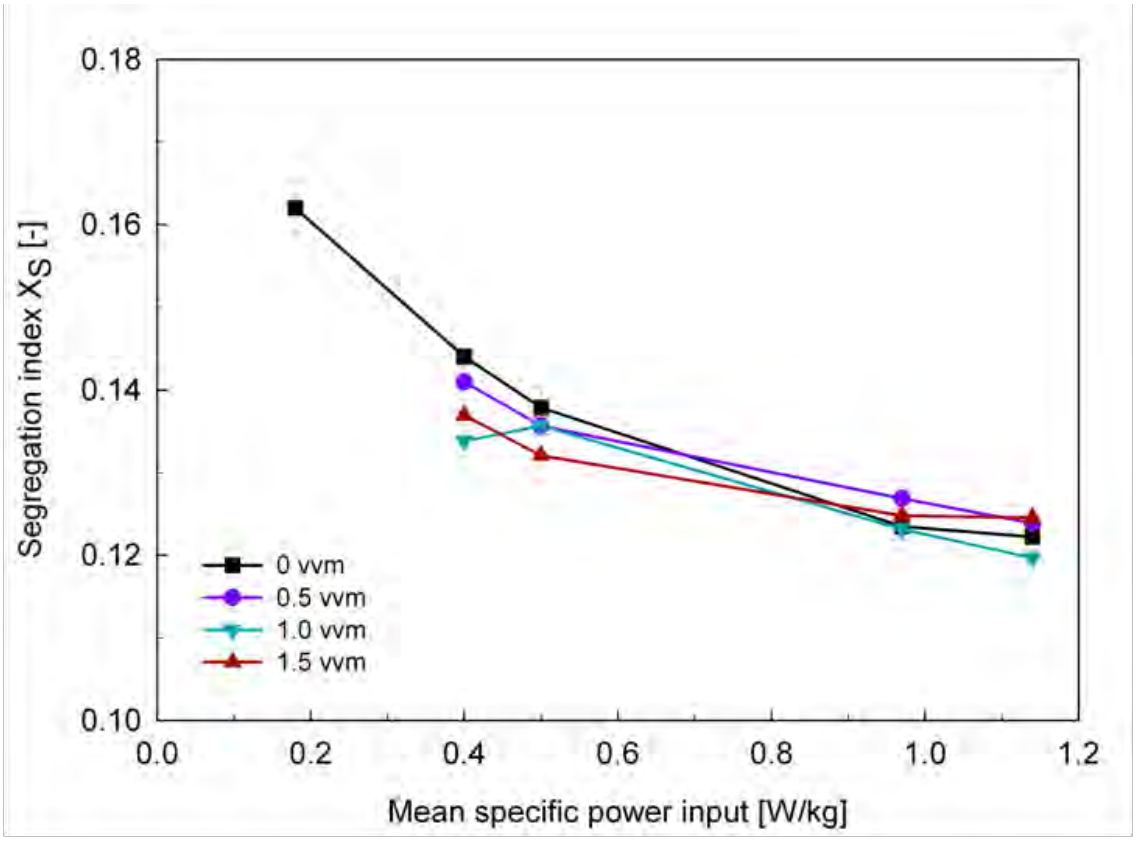

Figure 36: X_S as a function of mean specific energy dissipation at varied gassing rates – impeller feed with 0.5 mol/L H_2SO_4

Figure 36 illustrates the effect of gassing on the segregation index dependent on the impeller power input – as shown in Figure 35, but here for a different acid concentration (0.5 mol/L) and up to 1.5 vvm gassing rate. As in the previous figure, there is no significant deviation or systematic trend due to gassing: the values are relatively close to the single-phase results, i.e. with overlapping error bars, and there is no consistent pattern with increasing gassing rate. At the lowest investigated power input, i.e. 0.4 W/kg, a small improvement of micromixing efficiency could be suspected due to the consistent, though small, deviation from the unsparged value. This might be explained, as mentioned above, by the higher relative impact of the power input from the gas compared to the impeller.

Overall, Figure 36 nevertheless shows that micromixing near the impeller under gassed conditions is mainly affected by the impeller power input, at least for the conditions investigated. The deviations from the single-phase result can be explained with experimental error of the micromixing experiments themselves and also with errors from the power measurements.

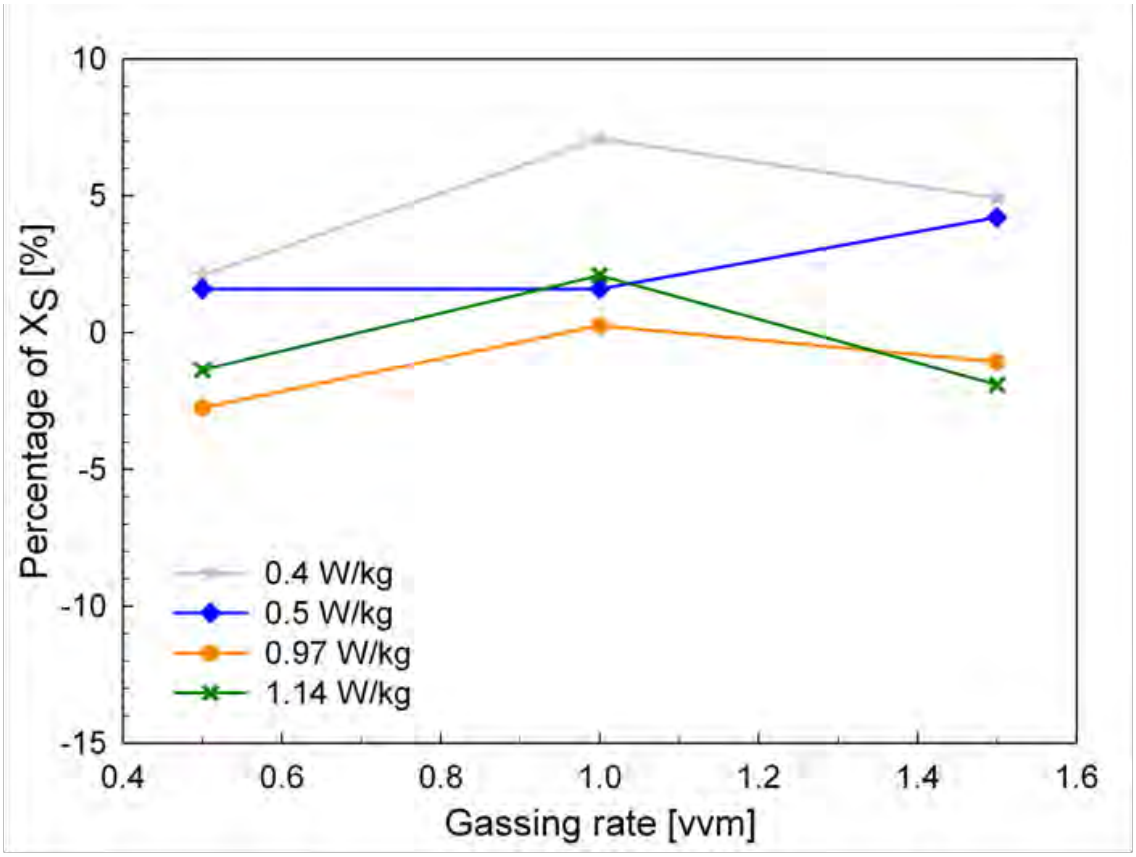

Figure 37: Influence of aeration rate on segregation index at several levels of mean specific energy dissipation rate as percentage of single-phase results – impeller feed with 0.5 mol/L H_2SO_4

Figure 37 compares the data to the single-phase reference as ΔX_S, which magnifies any effects from Figure 36. The graph confirms that the deviations of the gassed experiments from the liquid-only cases at equivalent power inputs from the impeller are small, i.e. not more than 7% and usually less than ±5% of the segregation index deviation, which is within the expected and observed ranges of error.

An alternative criterion to mean specific power input might be impeller tip speed or impeller speed. Figure 38 gives an impression of the data's correlation with impeller speed. Clearly, the data does not correlate as well as with $\overline{\varepsilon_T}$ and $\overline{(\varepsilon_T)_g}$.

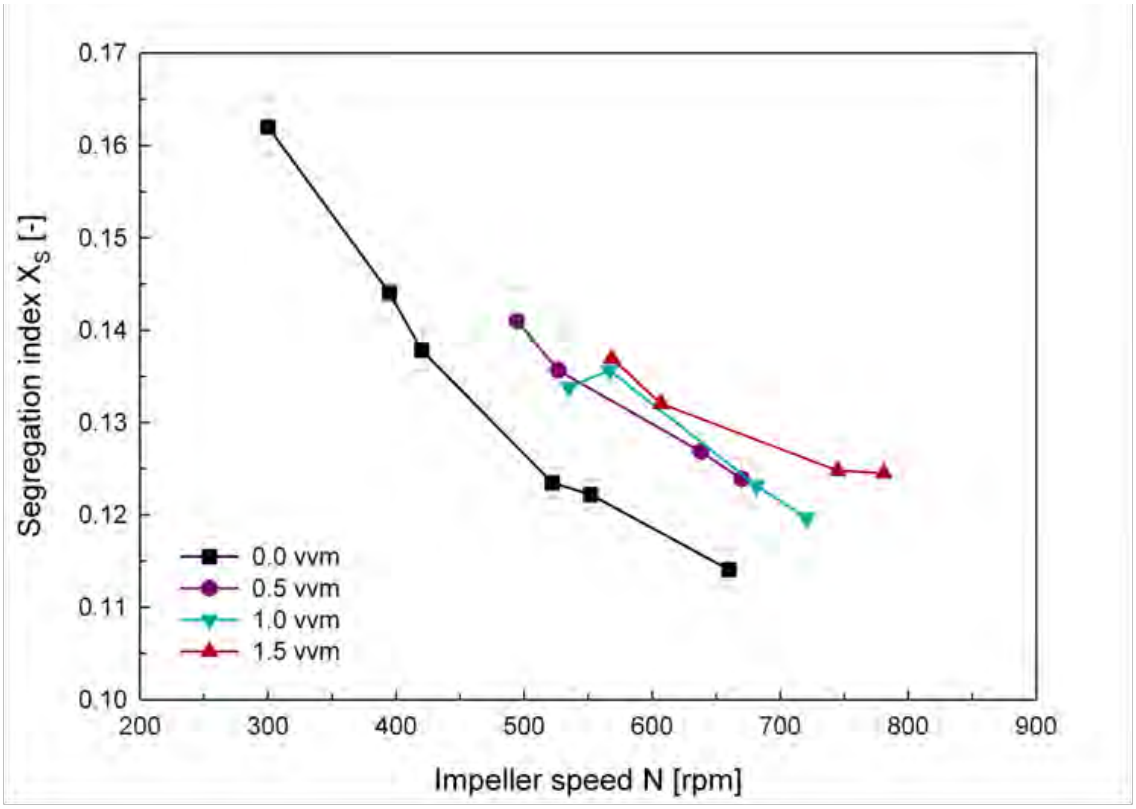

Figure 38: X_S as a function of impeller speed at varied gassing rates – impeller feed with 0.5 mol/L H_2SO_4

From the above results, it can be suggested that the impeller is the dominating factor for specific energy dissipation rates and, linked to it, micromixing in this region of the agitated vessel. Consequently, any contribution to or effect on micromixing due to the gas is negligible at the conditions investigated. A similar conclusion was drawn by Bourne (1994) referring to data from a PhD thesis (Hilber 1987) employing a Bourne reaction. Interestingly, Brilman *et al.* (1999) used diazo-coupling and only reported very little effect of gassing when feeding near the impeller or about halfway

between impeller and surface. This would, of course, still be in agreement with this work, but the authors kept the impeller speed constant in their work. Therefore, it is expected that the mean energy dissipation due to agitation was not constant, especially as a six-bladed "Rushton-like" (Brilman *et al.* 1999) turbine was used. At least for the lower gassing rates in their work, i.e. about 0.5 and 1.0 vvm, this cannot be explained. At their highest gassing rate, the system might have been flooded, which may lead to different results.

In addition to directly contributing to the energy dissipated, the bubbles might also lead to turbulence modulation. Considering the wide range of bubble sizes found in stirred tanks (Barigou and Greaves 1992), it would be difficult, if at all possible, to estimate an overall effect. The results for the feed position in the impeller discharge stream, however, do not indicate turbulence modulation.

In order to get a better impression of micromixing in a sparged stirred vessel, further feed positions were studied.

5.5. Micromixing near free surface under gassed conditions

The results for the same experimental conditions when feeding near the free surface are shown in Figure 39. In contrast to the results for the impeller region, the segregation index significantly drops with increasing aeration rate. Moreover, while at 0.5 vvm some dependence on mean specific power input from the impeller might still be seen, micromixing seems to become dominated and, in fact, determined by gas sparging.

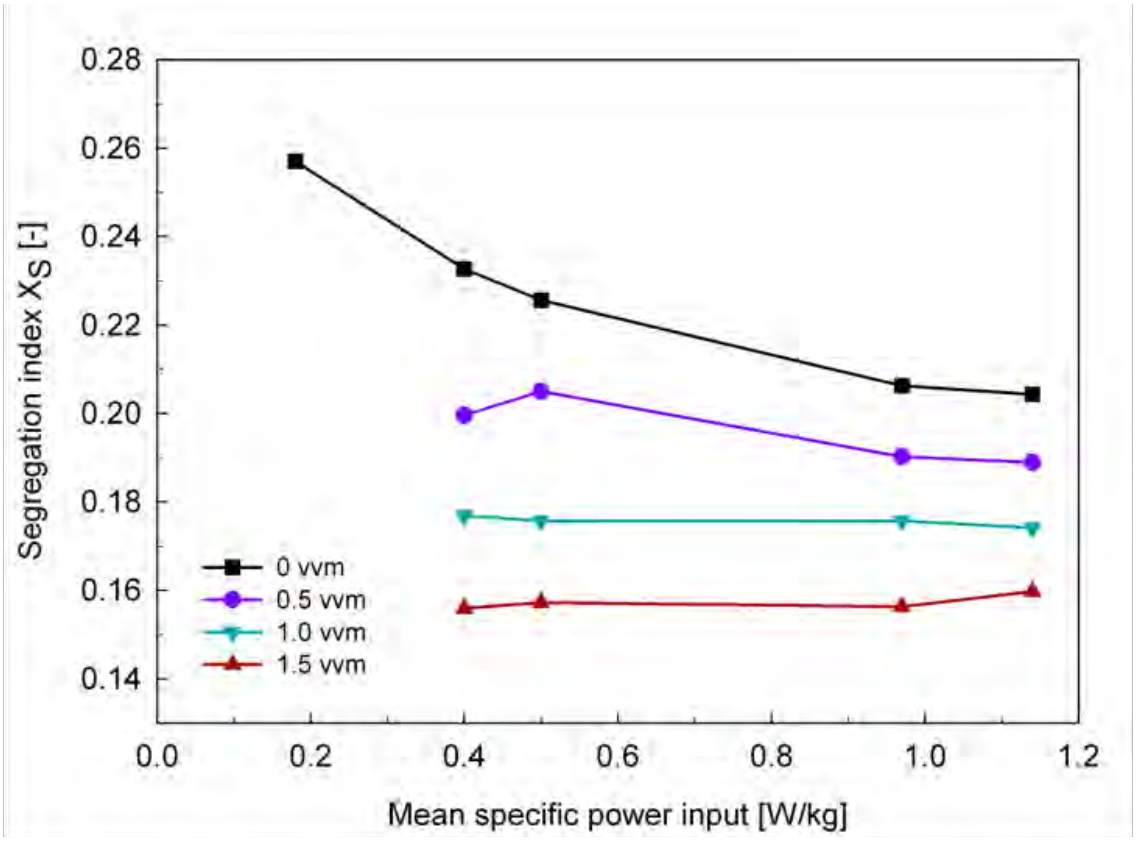

Figure 39: X_S as a function of mean impeller specific energy dissipation rate at different gassing rates – surface feed with 0.5 mol/L H_2SO_4

The improvements of X_S for feeding near the surface as seen in Figure 39 are dramatic: the segregation index drops at 0.5 W/kg from 0.23 without gas to 0.16 with 1.5 vvm. This is comparable to X_s values measured in the impeller discharge stream, e.g. 0.14 at 0.5 W/kg.

In order to quantify that improved micromixing, the deviation of the gassed segregation indices from the single-phase data is plotted in percent against the gassing rate in Figure 40. This graph shows improvements of up to 30% in terms of segregation index. Furthermore, the similar improvements, regardless of power input, clearly illustrate the significant effect of the gassing rate on micromixing efficiency.

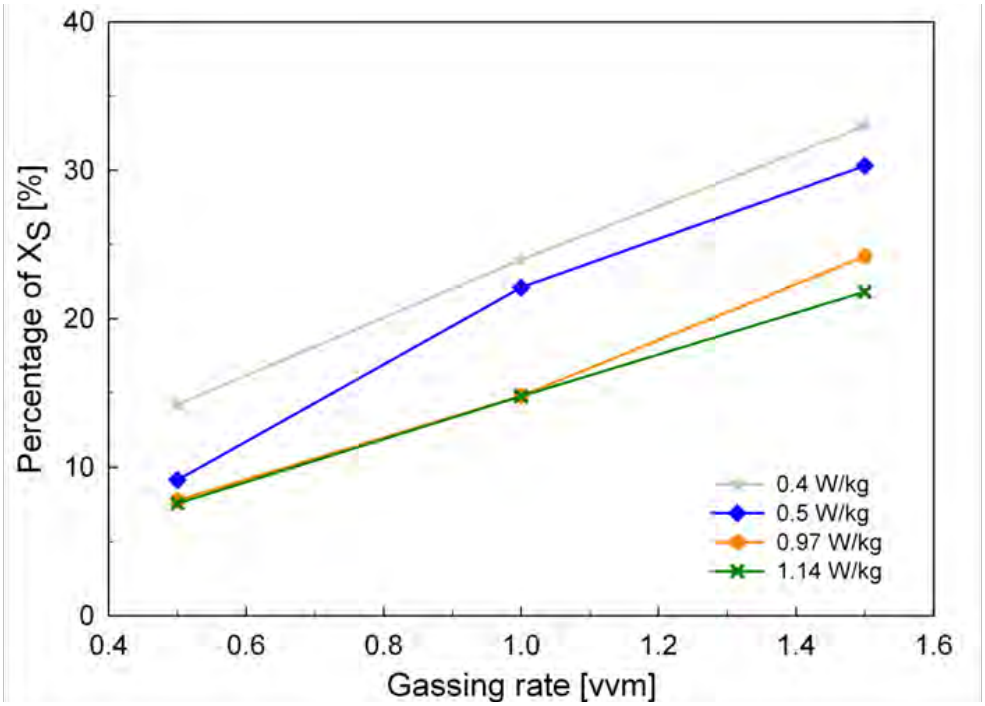

Figure 40: Reduction of segregation index compared to the unsparged value at several mean specific energy dissipation rates – surface feed with 0.5 mol/L H_2SO_4

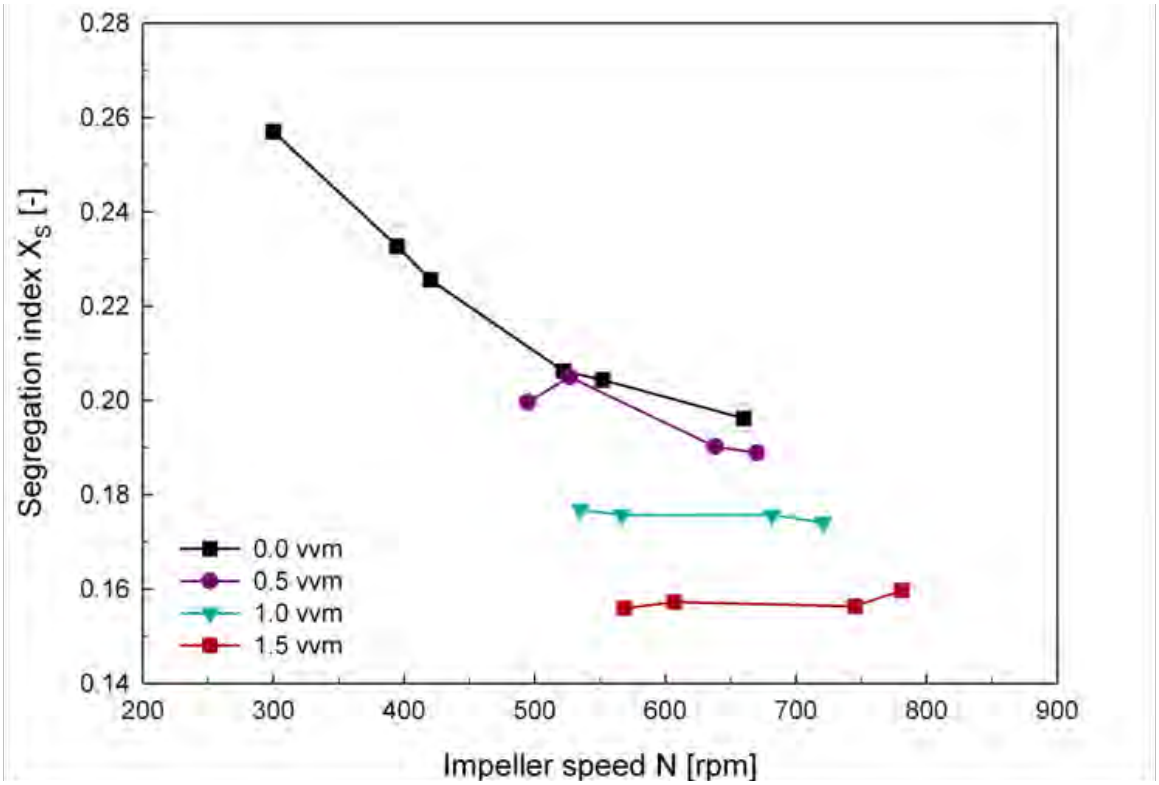

Figure 41: X_S as a function of impeller speed at different gassing rates – surface feed with 0.5 mol/L H_2SO_4

Figure 39 and Figure 40 indicate that the power input from the impeller becomes less relevant with increasing gassing rates. This is emphasised in Figure 41 which shows that the segregation index does not correlate any better with impeller speed than with mean specific energy dissipation rate. Sparging seems to be the critical factor.

5.6. Micromixing below impeller under gassed conditions

As gas sparging dramatically improves micromixing near the surface, but shows no significant effects near the impeller for the investigated conditions, an additional feed position (3) below the stirrer was studied. Figure 42 gives an overview of the results for feeding below the impeller. As expected, the segregation indices of the unsparged reference data are slightly higher – about 10% in X_S – than the ones from feeding into the impeller discharge stream (previous section, 5.5.). In addition, the errors are slightly larger below the impeller, i.e. from 1-2% at position 2 to 3-4% at position 3.

These gassed results do not show a clear trend with increasing sparge rate and fluctuate near the single phase values. At most conditions, the error bars overlap and a consistent effect is not obvious from Figure 42, though the data for most gassed cases, especially 1 vvm, is slightly lower than the single-phase equivalents. This might indicate that there is a small contribution from the gas power input towards the local specific energy dissipation rates, which might be more relevant in this region of the tank where the absolute value of ε is expected to be lower than in position 2, but higher than in position 1 – which is confirmed by the single-phase micromixing data. Another explanation for the fluctuations could be that the flow below the impeller might change slightly between the various conditions even though

the impeller was always loaded. Errors in the measurements of the impeller's power input do not seem responsible for the deviations in Figure 42 as the same impeller speeds were set for the experiments at position 2 which, however, do not lead to comparable trends.

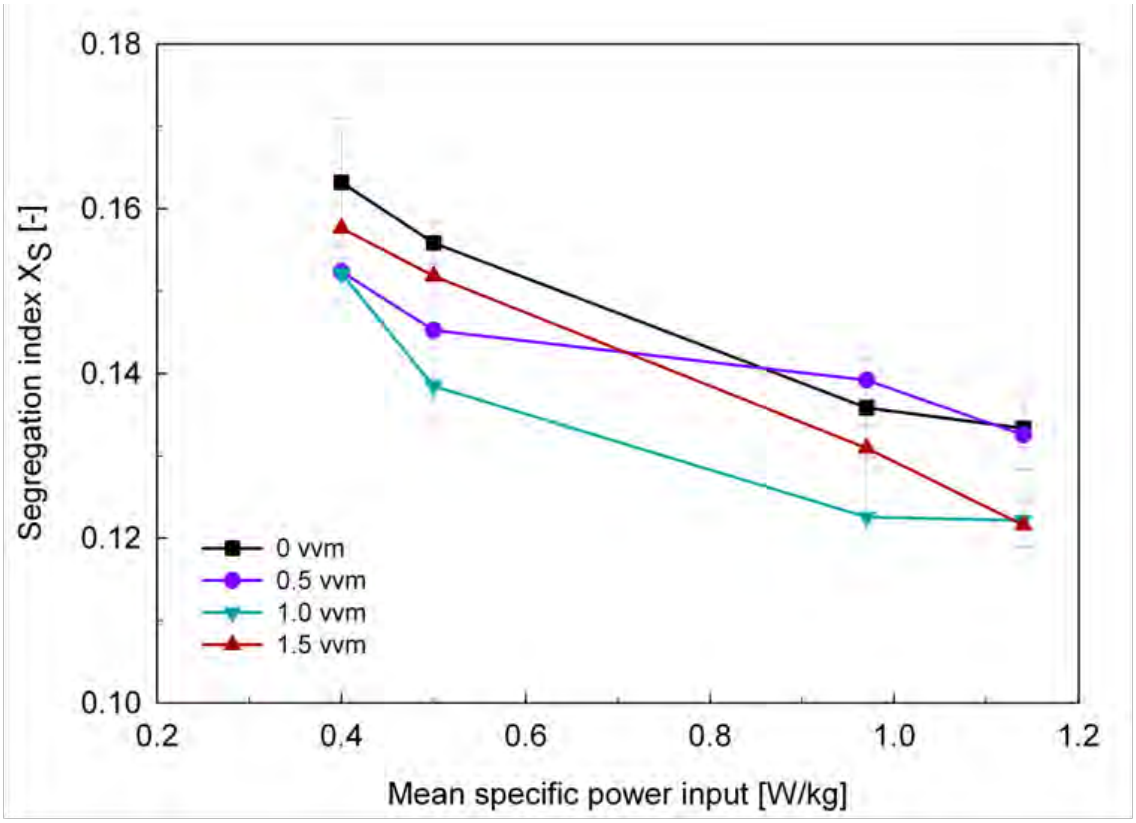

Figure 42: X_S as a function of mean specific energy dissipation at varied gassing rates – feed below impeller with 0.5 mol/L H_2SO_4

In order to emphasise and clarify any effects in the sparged experiments, the results are plotted in Figure 43 as deviation from the reference single-phase data. Again, the slight improvements of up to 5-10% of the segregation index, in particular at 1 vvm, can be seen. It may be argued that, at least at the lowest power input, an effect of the gassing rate is indicated, but, overall, it is not possible to draw clear conclusions from the available data.

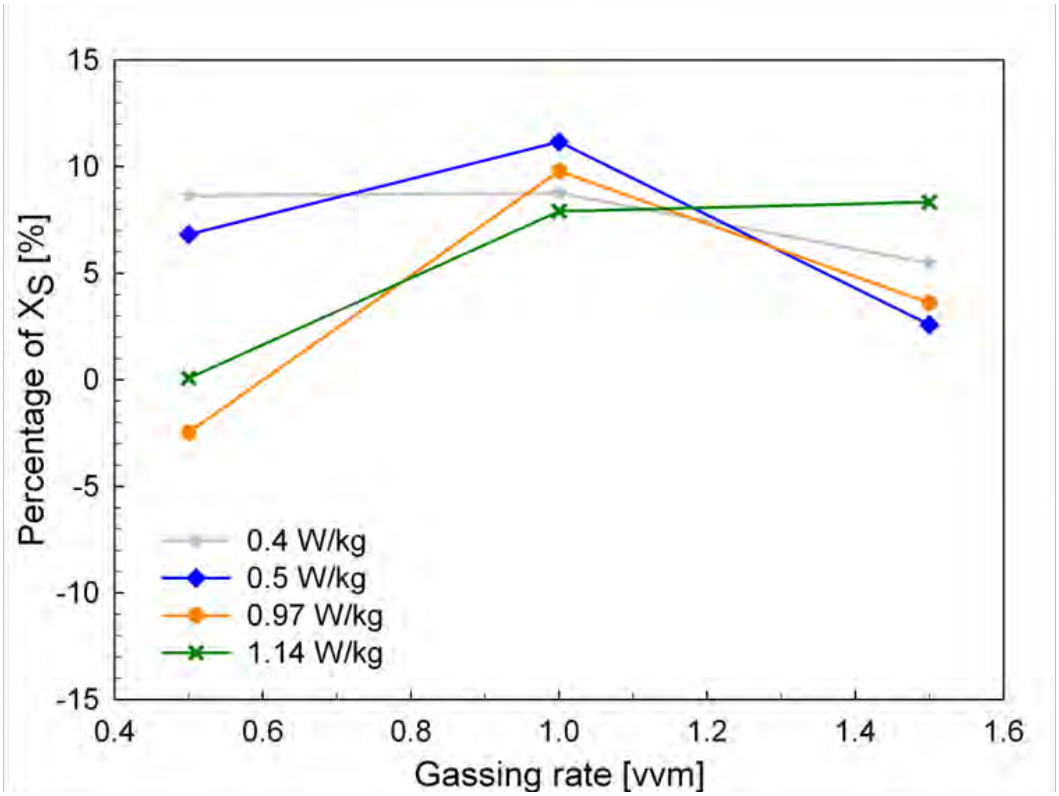

Figure 43: Influence of aeration rate on segregation index at several levels of mean specific energy dissipation rate as percentage of single-phase results – feed below impeller with 0.5 mol/L H_2SO_4

Considering the proximity to the stirrer, an effect of the impeller speed or impeller tip speed (in contrast to mean specific power input) might be another option. Therefore, the results are plotted against N in Figure 44. Although the experiments were not laid out for comparable impeller speeds, they are within a similar range and allow a reasonable plot. Unfortunately, the graph does not indicate any better correlation with N than with $\overline{(\varepsilon_T)_g}$.

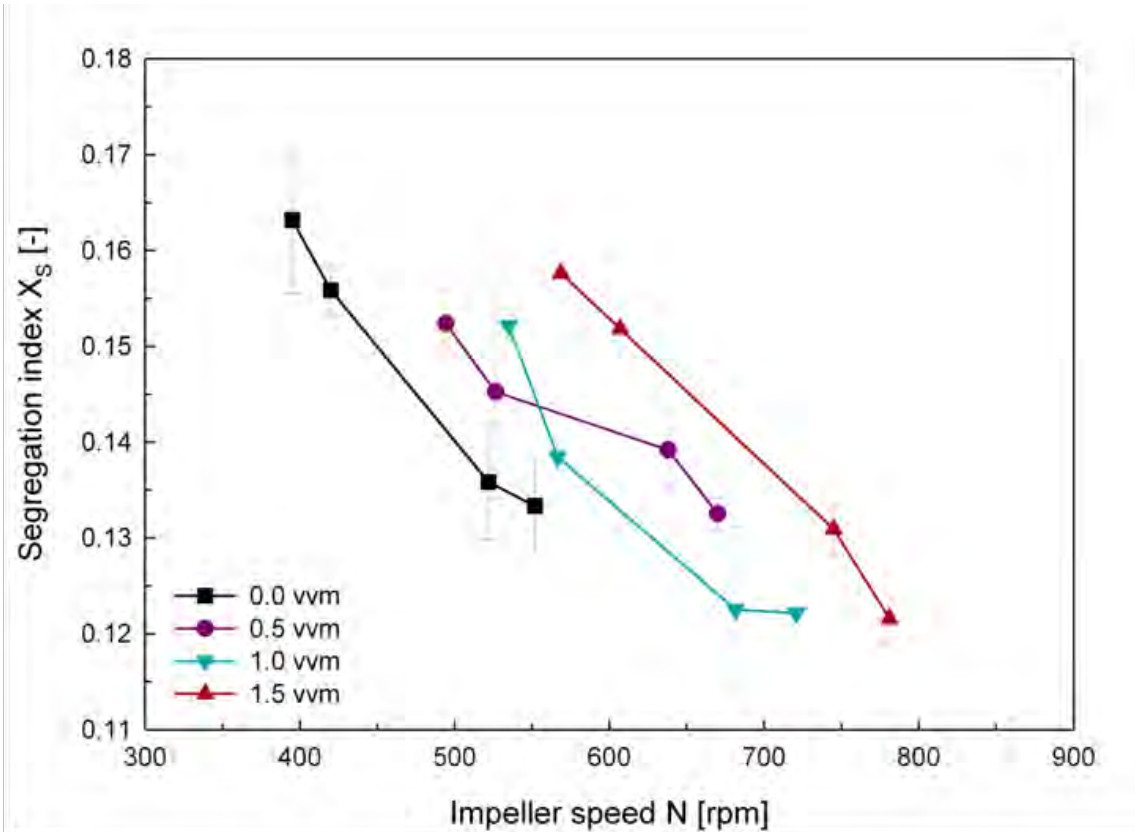

Figure 44: X_S as a function of impeller speed at varied gassing rates – feed below impeller with 0.5 mol/L H_2SO_4

5.7. Micromixing under gassed conditions without power input from impeller

Some micromixing experiments were done with the impeller not being switched on to investigate the effect of the gas bubbles without any further power inputs. Figure 45 shows the segregation indices as a function of sparge rate for feeding near the surface and near the impeller with N = 0 rpm.

The result for the feed position near the impeller is almost constant and, consequently, found to not be affected by the passing bubbles. In fact, the segregation indices around 0.3 indicate very poor micromixing and though visual observations showed that the rising bubbles generate some fluid flow near the feed

pipe, this clearly does not lead to significant changes with increasing gassing rate in this location. On the other hand, micromixing near the free surface does improve significantly from 0.5 to 1.5 vvm, as was already observed in the experiments when the impeller had been switched on.

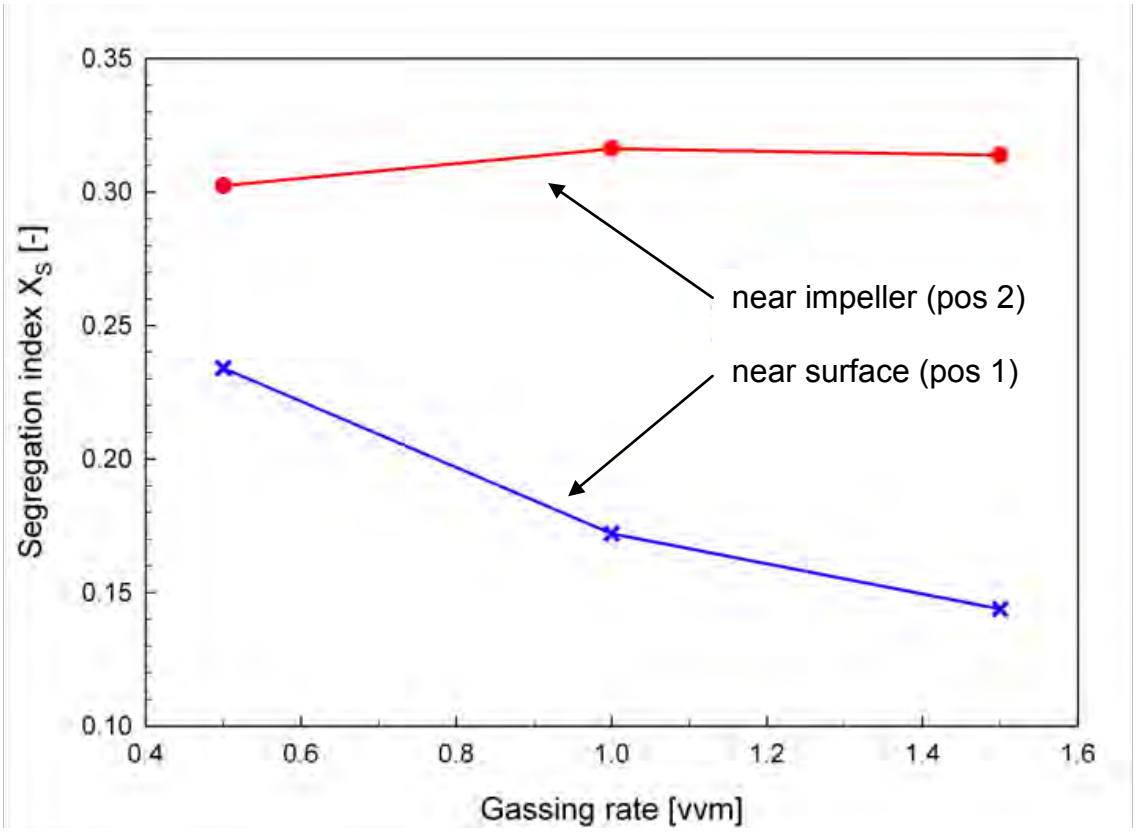

Figure 45 : Effect of gassing – without power input from the impeller – on segregation index in feed positions 1 (near surface) and 2 (near impeller)

Near the surface at 1.5 vvm, X_S = 0.14 which is in the range of when feeding into the impeller discharge stream (where $\phi \sim 1$) at 0.4-0.5 W/kg. This indicates relatively high local energy dissipation rates and, as such results have only been found near the surface, it might be suggested that the bursting of the bubbles is significant here. The energy dissipation from the rising gas bubbles might be less dominant, considering the (constantly) poor micromixing in the tank (position 2) when the impeller is not contributing power.

5.8. Power input from gas

To aid interpretation of the above data, the power input from the gas was calculated for incompressible gas:

$$P_{gas,incompr} = Q\ \rho\ g\ h \qquad \textbf{(5.2)}$$

where Q is the gas sparge rate, ρ the liquid density and h the "tank height" or liquid fill level.

The expansion of the gas with rising in a tall tank can be taken into account for a compressible gas with p being the ambient pressure:

$$P_{gas,compr} = Q\ (p + \ \rho\ g\ h) \ln\left(\frac{p + \rho\ g\ h}{p}\right) \qquad \textbf{(5.3)}$$

Table 23 summarises the results of equations (5.2) and (5.3) for the investigated conditions. As can be expected for a relatively small vessel, there is little difference, i.e. in the last 3 or 4 significant figures, between the incompressible and compressible results. Moreover, these values clearly are lower - by about an order of magnitude - than the impeller power inputs.

Table 23: Power input from gas

	ε_{gas} [W/kg] incompressible	ε_{gas} [W/kg] compressible
0.5 vvm	0.03(0607)	0.03(1155)
1.0 vvm	0.06(1214)	0.06(2311)
1.5 vvm	0.09(1822)	0.09(3466)

To allow better comparison, the results are also expressed as percent of mean specific energy dissipation rates from mechanical agitation (i.e. impeller power input, as measured in section 5.3.):

Table 24: Power input from compressible gas in percent of power from impeller

from impeller	0.5 vvm	1.0 vvm	1.5 vvm
0.4 [W/kg]	7.8%	15.6%	23.4%
0.5 [W/kg]	6.2%	12.5%	18.7%
0.97 [W/kg]	3.2%	6.4%	9.6%
1.14 [W/kg]	2.7%	5.5%	8.2%

Table 24 shows that at higher impeller speeds and low sparge rates the gas contributes less than 10% of the power input, compared to that from the stirrer. At 1.5 vvm and 0.4 W/kg from the impeller, the gas does however add almost a quarter of the stirrer's power input to the system. Due to lack of other information, it will be assumed that the power from the gas is dissipated evenly throughout the tank and, considering that (much) higher local specific energy dissipation rates can be found near the impeller, the overall effect of the bubbles would be relatively small in that region – which agrees with the results shown above. Towards the surface, however, much lower local specific energy dissipation rates would be expected in the single-phase tank and, therefore, the contribution from the gas is not negligible anymore. Still, the low side-product formation observed when feeding near the surface might indicate even higher local energy dissipation levels which, as discussed above, would point towards the bursting bubbles in that region.

5.9. Interpretation with micromixing model

The above considerations could become more quantitative by estimating energy dissipation rates from the measured segregation indices by employing the model

discussed in chapter 4. The data is presented as $\boldsymbol{\varepsilon_T}$ and compared relatively (in percentages) to investigate the bubbles' and the impeller's effects.

5.9.1. General comparison

The original model, as suggested in literature (Fournier *et al.* 1996a; Assirelli *et al.* 2008b) shows the significant improvement near the surface, by more than an order of magnitude, as summarised in Table 25. In contrast, the fluctuations near the impeller are less remarkable, though the actual $\boldsymbol{\varepsilon_T}$ are still higher than near the surface. The data in Table 26 is usually at least 2-3 times higher than that in Table 25.

Table 25: Estimates for ε_T at pos. 1 (near surface) – using original model

$\overline{\varepsilon_T}$ [W/kg]	0.0 vvm ε_T [W/kg]	0.5 vvm ε_T [W/kg]	1.0 vvm ε_T [W/kg]	1.5 vvm ε_T [W/kg]
0.40	0.110	0.302	0.610	1.189
0.50	0.136	0.255	0.634	1.141
0.97	0.246	0.403	0.634	1.174
1.14	0.261	0.420	0.666	1.053

Table 26: Estimates for ε_T at pos. 2 (near impeller) – using original model

$\overline{\varepsilon_T}$ [W/kg]	0.0 vvm ε_T [W/kg]	0.5 vvm ε_T [W/kg]	1.0 vvm ε_T [W/kg]	1.5 vvm ε_T [W/kg]
0.40	1.752	1.934	2.458	2.216
0.50	2.144	2.307	2.307	2.612
0.97	3.488	3.105	3.525	3.336
1.14	3.648	3.441	3.992	3.371

The model using the adapted interpolation of the most suitable kinetic data, i.e. estimating an inhibiting effect at the conditions in the stirred tank, shows very similar trends; though in about an order of magnitude lower absolute values:

Table 27: Estimates for ε_T at pos. 1 (near surface) – using adapted model

$\overline{\varepsilon_T}$ [W/kg]	0.0 vvm ε_T [W/kg]	0.5 vvm ε_T [W/kg]	1.0 vvm ε_T [W/kg]	1.5 vvm ε_T [W/kg]
0.40	0.009	0.033	0.080	0.185
0.50	0.012	0.026	0.083	0.176
0.97	0.025	0.047	0.083	0.182
1.14	0.027	0.050	0.089	0.159

Table 28: Estimates for ε_T at pos. 2 (near impeller) – using adapted model

$\overline{\varepsilon_T}$ [W/kg]	0.0 vvm ε_T [W/kg]	0.5 vvm ε_T [W/kg]	1.0 vvm ε_T [W/kg]	1.5 vvm ε_T [W/kg]
0.40	0.303	0.343	0.465	0.408
0.50	0.391	0.429	0.429	0.502
0.97	0.724	0.625	0.734	0.685
1.14	0.767	0.712	0.859	0.694

Interestingly, the values for position 1 are about an order of magnitude higher than the calculated power input from the gas. Assuming that the latter is dissipated evenly throughout the tank, this points at an additional, though still gas-related, factor contributing towards the significant improvements near the surface. Again, this suggests bubble bursting as suspected earlier and also discussed in literature (Boulton-Stone and Blake 1993).

5.9.2. Comparisons near surface

Expressing these results in relative terms, i.e. in percent of a reference value, will allow stronger distinctions between sparging and impeller effects. Moreover, the modelling section showed that this could be more reliable for quantification than employing the absolute values.

Therefore, the data for feeding near the surface is given in Table 29 in percent of the equivalent single-phase condition, i.e. at same impeller power input. This emphasises the dramatic improvements near the surface and the above conclusions:

Table 29: Estimates for ε_T as % of equivalent single-phase value at pos. 1 (near surface) – to highlight effect of sparging – using adapted model

$\overline{\varepsilon_T}$ [W/kg]	0.5 vvm ε_T [W/kg]	1.0 vvm ε_T [W/kg]	1.5 vvm ε_T [W/kg]
0.40	357%	872%	2031%
0.50	221%	697%	1468%
0.97	187%	332%	725%
1.14	182%	327%	584%

These tables refer to data from the adapted model. Other results, including those for the original approach are very similar and are not shown for brevity.

In order to reflect the influence of the impeller, a comparison to the results at the lowest power input is given in Table 30. This shows some effect for lower sparge rates, while the results become relatively independent from the impeller speed towards 1.5 vvm.

Table 30: Estimates for ε_T as % of lowest power input for sparged case at pos. 1 (near surface) – to highlight effect of impeller – using adapted model

$\overline{\varepsilon_T}$ [W/kg]	0.5 vvm ε_T [W/kg]	1.0 vvm ε_T [W/kg]	1.5 vvm ε_T [W/kg]
0.40	100%	100%	100%
0.50	81%	105%	95%
0.97	144%	105%	98%
1.14	152%	112%	86%

5.9.3. Comparisons near impeller

Such considerations are also of interest for position 2 in order to amplify the observed fluctuations and to separate between impeller and gas effects more clearly. Table 31 shows that the deviations at the lower power inputs might indeed be relevant. Remarkably, the order of magnitude of these changes is roughly in agreement with the calculated power input from the gas (see Table 24), though here the experimental error clearly becomes almost equally relevant too. Overall, the effect of the impeller is dominant, as emphasised in Table 32.

Table 31: Estimates for ε_T as % of equivalent single-phase value at pos. 2 (near impeller) – to highlight effect of sparging – using adapted model

$\overline{\varepsilon_T}$ [W/kg]	0.5 vvm ε_T [W/kg]	1.0 vvm ε_T [W/kg]	1.5 vvm ε_T [W/kg]
0.40	113%	154%	135%
0.50	110%	91%	128%
0.97	86%	101%	95%
1.14	93%	112%	90%

Table 32: Estimates for ε_T as % of lowest power input for sparged case at pos. 2 (near impeller) – to highlight effect of impeller – using adapted model

$\overline{\varepsilon_T}$ [W/kg]	0.5 vvm ε_T [W/kg]	1.0 vvm ε_T [W/kg]	1.5 vvm ε_T [W/kg]
0.40	100%	100%	100%
0.50	125%	92%	123%
0.97	182%	158%	168%
1.14	207%	185%	170%

5.10. Conclusions

The effect of gas sparging on micromixing was studied experimentally using the Iodide/iodate method and a model was applied to that data. The reaction scheme was found suitable for such measurements, even using air, which confirms earlier work (Lin and Lee 1997) who, however, used N_2.

At constant power input from the impeller, the segregation index near the impeller and below it was not significantly affected by gas rates up to 1.5 vvm. Applying the incorporation model to the data confirmed relatively small fluctuations. Near the surface, however, micromixing was improved significantly with increasing sparge rates and became relatively independent from impeller power input. This was confirmed in experiments without power contribution from the impeller, i.e. N = 0 rpm. Overall, the interpretation of the experimental data using the incorporation model revealed increases in local specific energy dissipation rate by about an order of magnitude near the surface. Considering all available information, the significant improvements near the surface, the results without impeller contribution and simple calculations of the power input from the gas itself, suggests that the bursting bubbles might be a relevant factor for the effects found.

6. MICROMIXING IN SOLID-LIQUID SYSTEMS

6.1. Introduction

In addition to chemical reactors with solid catalysts, precipitation and crystallisation are obvious examples for cases where micromixing might become relevant when solid particles are present. Even though such systems have been studied before, conflicting results have been reported especially for stirred tanks, see section 2.3.4.

In this chapter, the effects of a range of different particle sizes and concentrations were investigated at three feed positions: near the surface, near the impeller and near ε_{max}. As in the previous chapter, but here for solids, the method is validated, experimental conditions defined and results from these experiments reported and interpreted, also using the modelling described in the previous sections. The experimental results are also discussed in the context of available literature.

6.2. Validation of the experimental method in a liquid-solid system

As for the gas-liquid studies, the Iodide-Iodate method had to be validated for experiments with added solid particles, In fact, the technique has already been applied in stirred tanks with glass particles by Villermaux *et al.* (1994). Unfortunately, their (unexpected) results had to be corrected later (Guichardon *et al.* 1995): the authors explained that there had been losses of iodine during the experimental procedure. Mass balances showed that adsorption to the glass had not occurred, but that evaporation during a filtration step had affected the findings.

In studies employing reaction systems different from the Iodide-Iodate method, issues with adding solid phases have been reported, e.g. Bennington and co-workers applied diazo-coupling reactions in suspensions of fibres and had to take disturbing effects due to adsorption of reactants into account (Bennington and Bourne 1990; Bennington and Thangavel 1993; Mmbaga and Bennington 1998).

For these reasons, tests similar to those for the gas sparged cases in section 5.2. were undertaken. Again, iodine/triiodide containing solutions with the added second phase, here glass beads in various amounts, were stirred and observed over time. No losses due to the presence of glass beads were found, which agrees with other authors (Guichardon *et al.* 1995; Unadkat 2009).
In order to avoid losses during filtration, a fine mesh was installed inside the tank in front of the sampling pipe. Thanks to this set-up, the glass beads remained in the vessel and no further treatment of the samples was necessary.

6.3. Power input in the presence of particles

6.3.1. Power measurement results in solid-liquid cases

Figure 46 shows the power number as a function of Reynolds number for single-phase and with 2.46 wt.% and 11.63 wt.% 500 µm glass beads. As stated in 5.3. Power input in sparged cases, only higher power inputs will be considered valid here due to technical limitations (rest is plotted in faint colour). Nevertheless, the trends in Figure 46 agree with what would be expected (see section 2.1.4.): the lower particle concentration and the single-phase curve are very similar. In contrast, the power number for the higher concentration is at first lower than the other two curves

due to the formation of a “false bottom” and then, once sufficient amounts of particles have become suspended, higher which can be explained with the higher density around the impeller. A similar result was obtained for 1125 µm particles (data not shown).

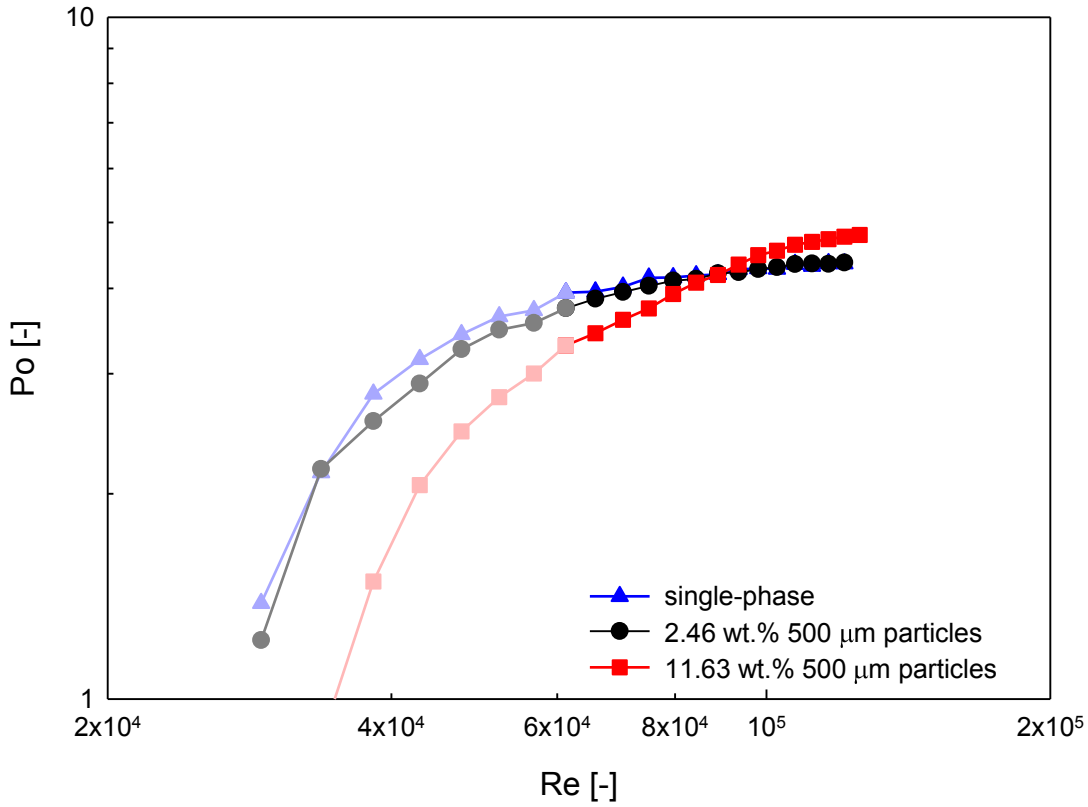

Figure 46: Power number as a function of Reynolds number – with and without 500 µm particles

6.3.2. Conditions for micromixing experiments with particles

From Figure 46 it can be concluded that lower particle concentrations, i.e. up to 2.46 wt.%, do not significantly affect power input and consequently single-phase impeller speeds can be used for such conditions as well. These are summarised in Table 33.

In addition to the 500 µm glass beads, also other sizes, i.e. 150, 250, 625 and 1125 µm particles, were used at such low concentrations. For this range of sizes, only one power input was employed. In order to suspend the particles as well as possible, while avoiding surface aeration, an impeller speed of 660 rpm was chosen for these cases (including single-phase experiments for reference).

Table 33: Impeller speeds for experiments with solid particles $(d_p = 500\ \mu m)$ ***for matching mean specific energy dissipation rates,*** $(\overline{\varepsilon_T})_{sus}$

$(\overline{\varepsilon_T})_{sus}$ [W/kg]	up to 2.46 wt.% [rpm]	11.63 wt.% [rpm]
0.18	300	
0.40	395	433
0.50	420	456
0.97	522	548
1.14	552	570

In addition to the experiments with 11.63 wt.% of 500 µm, also a second particle size was tested for comparison at a higher power input in the range – a discussion on how the mean specific energy dissipation rate was defined is given on the next page:

→ for 1.14 W/kg: 1125 µm particles – also at ***570 rpm***

At this power input, the results of the measurements were very similar for both glass bead sizes, i.e. 570 and 569.5 rpm for 500 and 1125 µm, respectively.

As demonstrated in part 2.3., particle size is critical for turbulence modulation and, therefore, the effect of several sizes of glass particles at low particle concentrations, i.e. up to 2.46 wt.%, was studied at one power input:

→ for 1.94 W/kg: 150, 250, 500, 625 and 1125 µm particles – at ***660 rpm***

It has to be emphasised that it is not obvious how the mean specific energy dissipation rate should be maintained at the same level as in the single phase case: it might be based on power per mass of liquid or per total mass, i.e. solid and liquid. Considering that a model for higher concentrations of suspended particles in earlier work (Nienow and Conti 1978) assumed power input going into particle abrasion, elastic deformation and into fluid motion, the second option, power per mass of solid and liquid, was chosen.

6.3.3. Flow at the chosen conditions

The above conditions are a result of taking several factors into account, e.g. trying to maintain good particle suspension while avoiding surface aeration. Similar issues have also been reported by other authors (Barresi 2000; Unadkat 2009). Due to the range of particle sizes and concentrations investigated here, fully suspending the particles might be an issue, especially with increasing size and concentration. Therefore, N_{js} was calculated according to Zwietering (1958), see equation (2.9), and the chosen impeller speeds compared to it.

Table 34 gives the impeller speeds for the investigated power inputs as percent of N_{js}. The lower power inputs are not expected to be sufficient for fully suspending all particles and the calculated values show that these stirred speeds indeed are as low as half N_{js}. However, Brucato and Brucato (1998) showed that at 80% of N_{js} almost all particles are suspended and that the final 20% of N_{js} are only necessary for getting the last few particles into suspension. Also, considering that concentration

gradients have to be expected even above N_{js}, the values given for particle concentration will still only be a general indication of the amount of particles suspended in the vessel and probably not accurately reflect the actual concentration experienced by the turbulence and chemical reactants near the feed pipe.

Table 34: Suspension state of 500 µm particles over range of power inputs - expressed as percent of N_{js}

wt.%	300 rpm	420 rpm	522 rpm	552 rpm
0.25%	59.1%	82.8%	102.9%	108.8%
0.75%	51.3%	71.8%	89.2%	94.3%
1.24%	48.0%	67.2%	83.5%	88.3%
2.46%	43.9%	61.5%	76.4%	80.8%

At the highest investigated particle concentration, 11.63 wt.%, fully suspending all particles was not expected, as equivalent power inputs in the single-phase case would have led to surface aeration. However, it was not necessary to reach a state of complete suspension, as the aim was to investigate cloud formation. Consequently, the criterion was to compare the clouds of 500 and 1125 µm particles at the same power input. At 570 rpm, 68.2% and 58.0% of N_{js} was achieved for the smaller and larger glass beads, respectively.

A photograph of such a cloud of 500 µm particles is shown in Figure 47. The quiescent liquid which is almost free of particles can be seen at the top, while the lower parts of the vessel is opaque due to the large amount of glass beads.

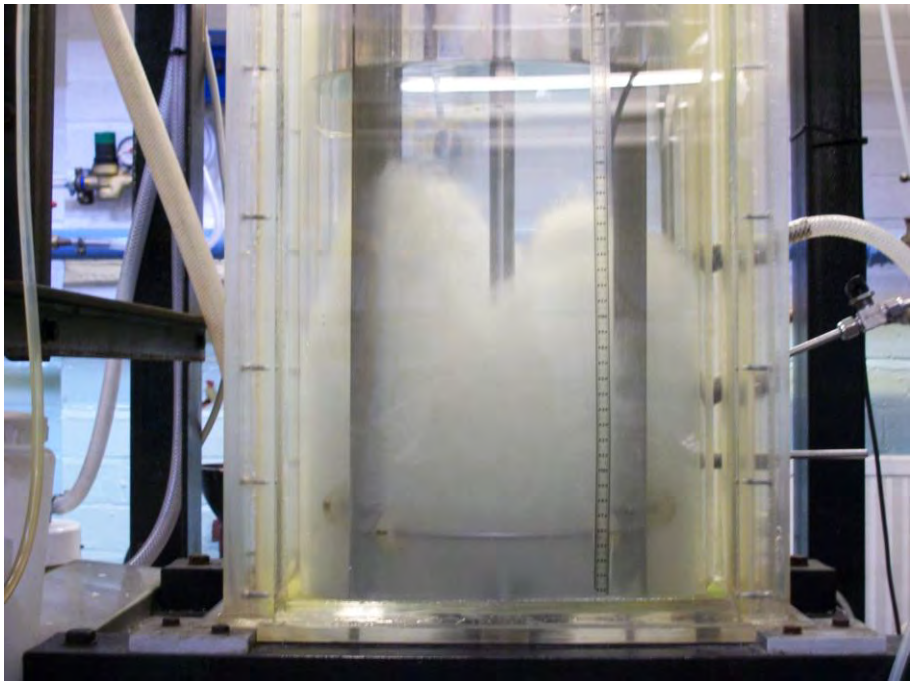

Figure 47: Example of cloud (d_p = 500 µm; 11.63 vol.%)

In Table 35, the impeller speed, 660 rpm, is expressed as percent of N_{js} for the different particle sizes is shown. With these conditions only the biggest glass beads (1125 µm) at the highest concentration (7.2 vol.%) fall below the 80% of N_{js} suggested by Brucato and Brucato (1998). This is in agreement with the visual observation of the vessel's bottom which showed most particles being suspended during the experiments.

Table 35: Suspension state at 660 rpm - expressed as percent of N_{js}

wt.%	150 µm	250 µm	500 µm	625 µm	1125 µm
0.25%	165.5%	149.4%	130.1%	124.4%	110.6%
0.75%	143.5%	129.6%	112.8%	107.9%	95.9%
1.24%	134.3%	121.3%	105.6%	101.0%	89.8%
2.46%	122.9%	110.9%	96.6%	92.4%	82.1%
7.2%	106.9%	96.5%	84.0%	80.4%	71.5%

Nevertheless, the distribution of the glass beads is clearly not uniform even throughout the cloud, as discussed above and in section 2.1.4. For this reason, the concentrations of particles for the various experiments must be seen as the amount present in the tank but they will not represent the actual value in the proximity of the feed pipe positions.

6.4. Effect of particle size on micromixing in dilute suspensions

As discussed extensively in part 2.3.2, adding a dispersed phase has been shown to affect turbulence in a range of fluid flows and it has been suggested that particle size is a critical parameter. In stirred tanks, solid particles might also affect energy dissipation, but literature is conflicting. These aspects are presented in section 2.3.4. and in literature (Micheletti and Yianneskis 2004; Unadkat 2009; Hofinger *et al.* 2011). In spite of the uncertainties, particle size has repeatedly been suggested as the determining factor whether turbulence augmentation or suppression occurs.

For this reason, this parameter was studied for three feed position: in the impeller discharge stream, near the surface and in the region of ε_{max}.

6.4.1. Near impeller

Figure 48 shows the results of these experiments for 5 particle sizes over a range of concentrations at constant impeller speed (and, at these concentrations, constant power input) for feeding into the impeller discharge stream. Interestingly, no systematic difference in behaviour according to glass bead size can be seen in this case, which is unexpected, considering the range of effects presented in literature. For lower concentrations, the results are actually so close to the liquid-only value that

they fall within the error bars. At the highest concentration, all points indicate slightly worse micromixing, which might be explained by four-way coupling, i.e. some energy being dissipated by particle-particle interaction. Still, this graph does show the significance of these deviations.

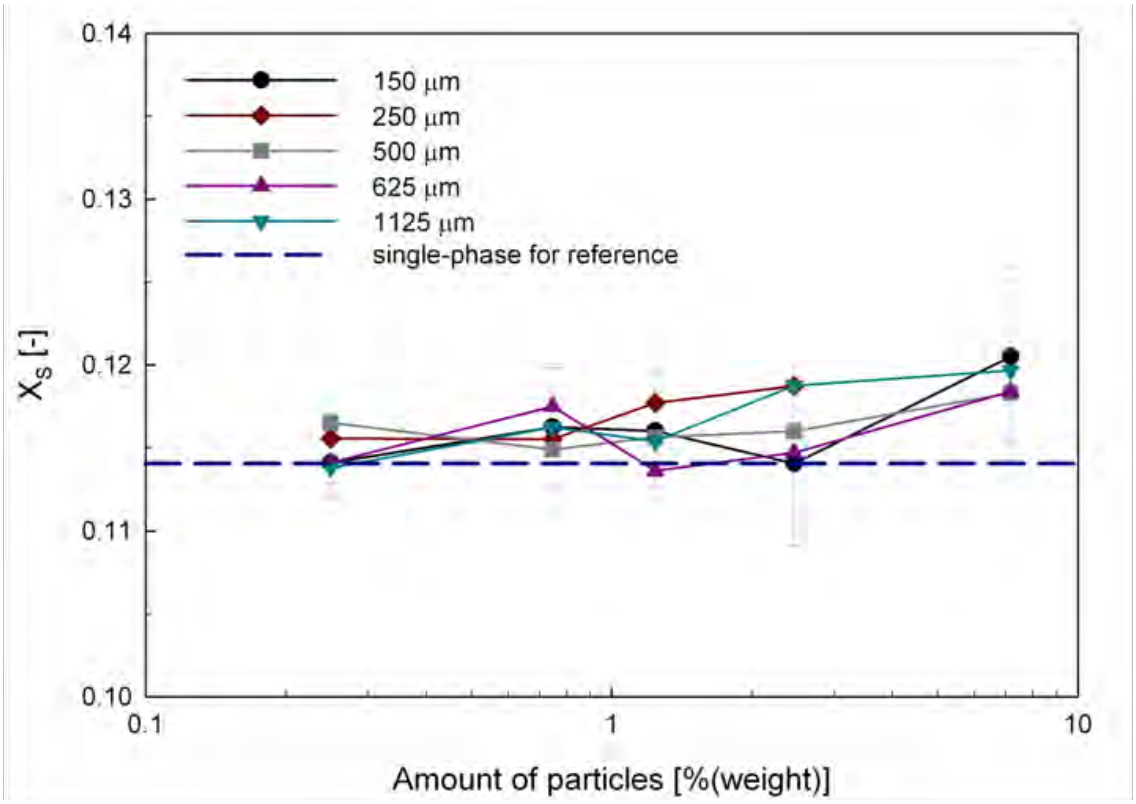

Figure 48: Effect of particle size in dilute suspensions on the segregation index as a function of particle concentration – near impeller at 660 rpm

Figure 49 gives the data presented in Figure 48 as percent of the single-phase equivalent. This might give a clearer view of the magnitude of any deviations observed and magnifies any effects. Lower amounts of particles, i.e. from about 0.2 to 2 wt.%, the glass beads did not affect micromixing significantly, as any deviations are usually less than 2% of X_S and always less than 4% which is within the expected experimental error. This agrees with some literature (Guichardon *et al.* 1995), but

might be in conflict with more recent results (Unadkat 2009) which indicate significant suppression by more than 20 % of X_S by 100 µm glass beads around 0.5 to 1 vol.%. In the latter work, the feed was in the region of ε_{max} which may help explain the differences, in spite of results showing that particles should also affect the region here studied (Micheletti and Yianneskis 2004).

At concentrations over 2 wt.%, the results drop slightly to about -5 % of X_S, i.e. a small increase in side-product formation. This drop might be interpreted as still falling within the experimental error. Taking into account that all particle sizes investigated follow the same trend, this may, however, be a genuine, though small trend towards turbulence suppression at these higher particle concentrations.

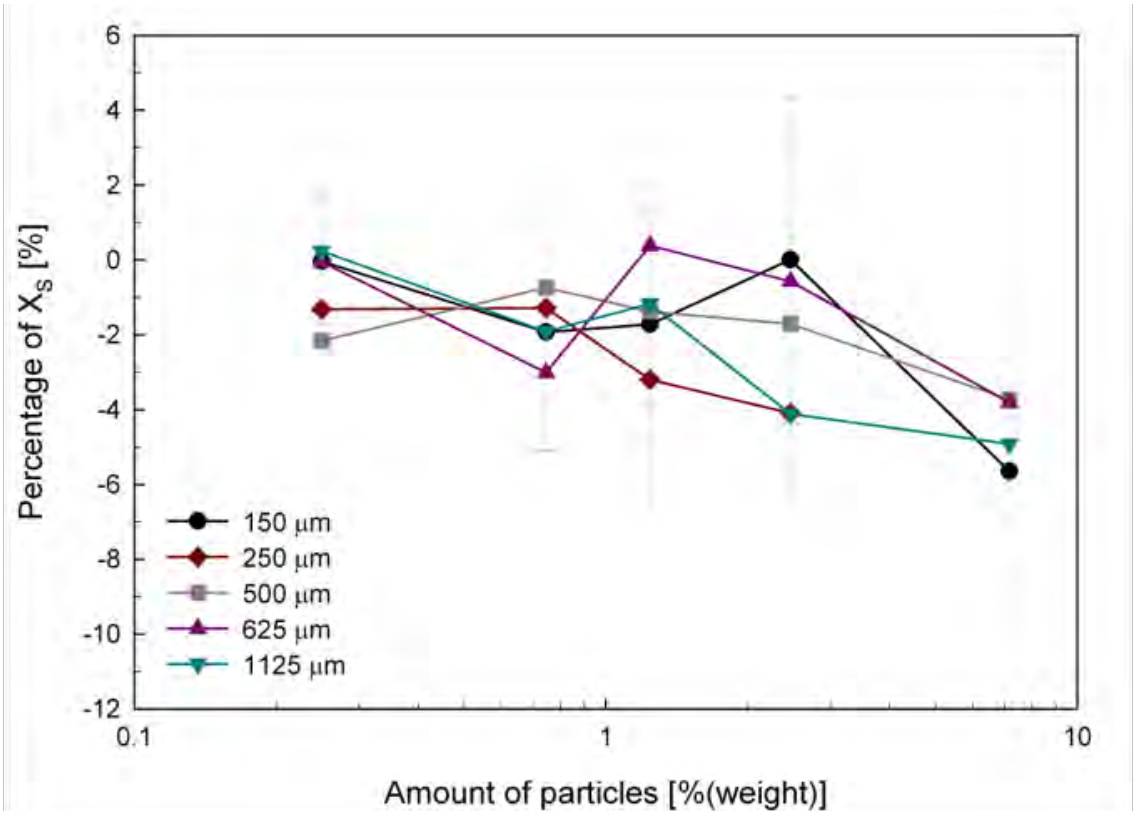

Figure 49: Effect of particle size in dilute suspensions at several particle concentrations – in percent of single-phase segregation index – near impeller

6.4.2. Near surface

Literature has focused on turbulence modulation in the impeller region, but not near the surface – even though, in industry, this may be the preferred position for feeding. Therefore, some experiments were undertaken in this location and the results are plotted in Figure 50. The segregation indices fluctuate around the single-phase value and increase slightly at the highest concentration. As suggested above, the higher particle concentrations might already fall into a region where particle interaction becomes relevant. The overall effect looks very similar to the result for feeding closer to the impeller, but the magnitude of the deviation needs to be compared as well.

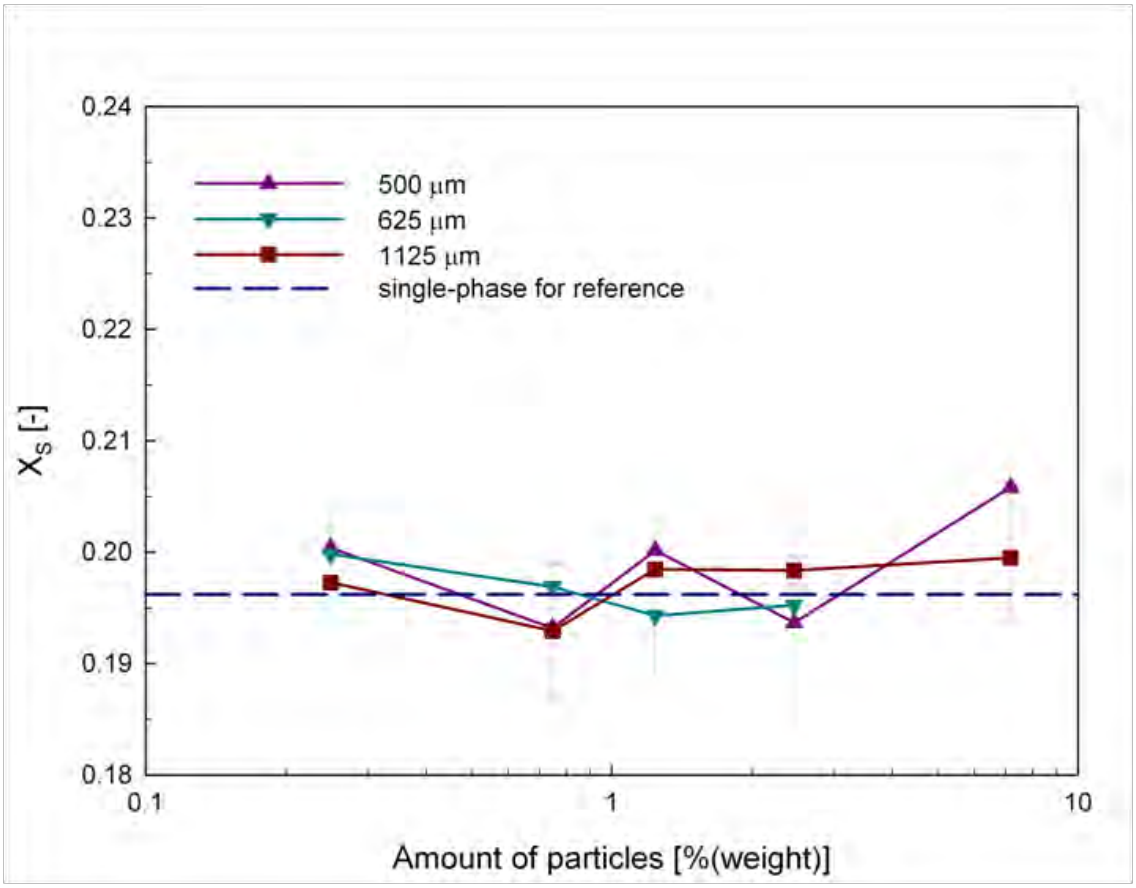

Figure 50: Effect of particle size in dilute suspensions on the segregation index as a function of particle concentration – near surface

Figure 51 shows the deviations of the segregation indices from the single-phase reference with all data being within ±2.5% at concentrations up to 2 wt.% of glass beads. At around 7.2 wt.%, in contrast to the previous results, there only seems to be an effect with the smallest investigated particles, which is as before, around -5%. However, the larger particles probably did not get dispersed well enough to reach the surface at representative concentrations and, therefore, the smaller deviation is probably less a turbulence modulation effect and more a suspension and dispersion issue. Unfortunately, this could not be avoided, as reference data was needed and higher impeller speeds would have caused surface aeration (at least in the single-phase case and probably also with these low particle amounts). Other setups, like using different impellers or a differently shaped vessel bottom, might be useful in future studies. However, the overall effect is small and, in fact, might even still be considered as within experimental error. Taking the consistent trend of the behaviour near the impeller and near the surface into account, minor reduction in micromixing efficiency and energy dissipation rates might be a more reasonable explanation than arguments regarding measurement errors. A relatively simple explanation would be that, at higher concentration, the particles interact and dissipate some of the energy, for instance in not fully elastic collisions. At 7.2 wt.% or 3 vol.%, significant particle interaction might be expected, since for instance Elghobashi (1994) indicated turbulence modulation for lower volume fractions. That work would suggest that four-way coupling becomes a significant factor for the higher particle concentrations. Consequently, the small deviations found here are attributed to particle interaction, not turbulence suppression.

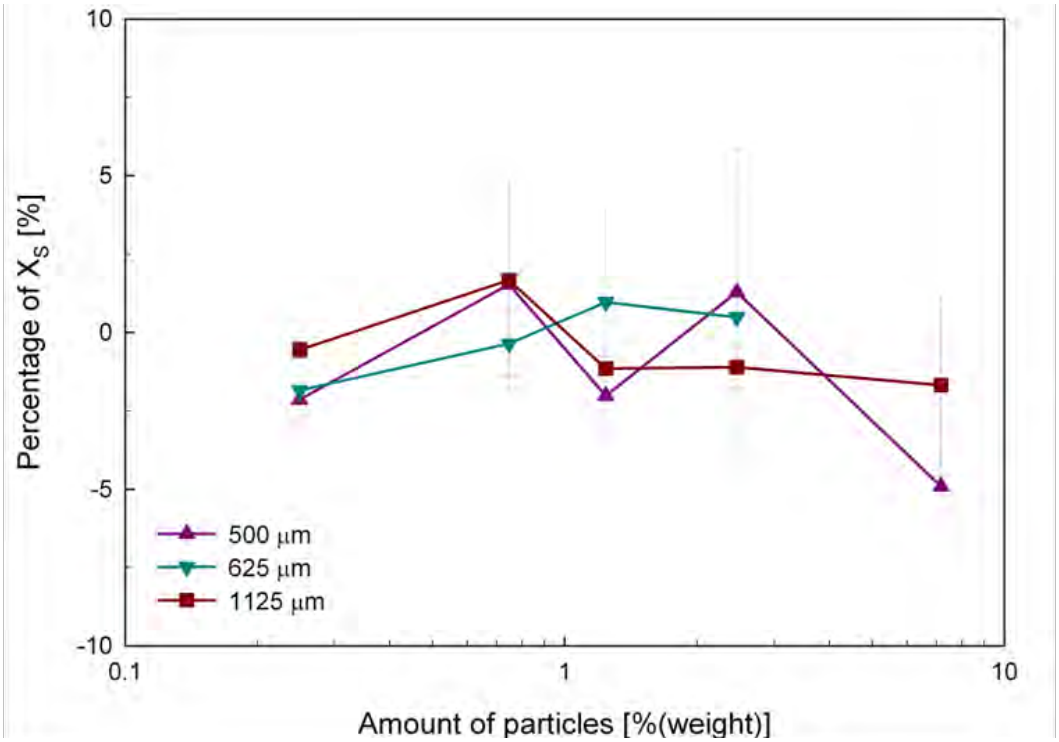

Figure 51: Effect of particle size in dilute suspensions at several particle concentrations – in percent of single-phase segregation index – near surface

6.4.3. Near location of highest energy dissipation rates, ε_{max}

As no significant turbulence modulation has been observed near the surface and in the impeller discharge stream, measurements when feeding into the region of highest energy dissipation rates are necessary. Unfortunately, as discussed in section 2.3., there are already a number of conflicting publications and a range of suggested mechanisms to explain some aspects of these findings. This section is intended to contribute to giving a picture of such phenomena especially by also comparing these results to those from other feed positions in a stirred tank.

Possible effects of particle size and concentration were investigated and Figure 52 gives the results for five sizes as segregation index against amount of particles. Again, the single-phase value is plotted as a dashed line and, interestingly, behaviour

similar to the previous results can be found: at the lowest concentrations the data is close to the liquid-only case and at the highest concentration some deviation from that value is seen. This is surprising, considering the reports of turbulence augmentation and suppression near ε_{max}, which would lead to expectations of more significant effects – at least more than the size of the error bars.

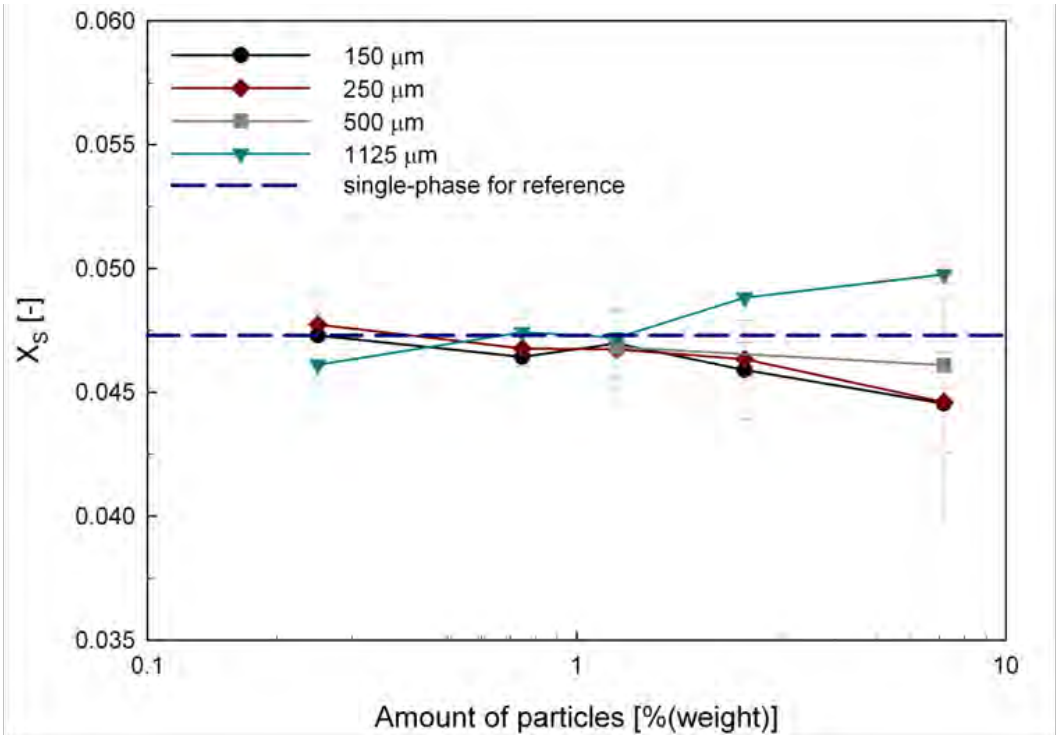

Figure 52: Effect of particle size in dilute suspensions on the segregation index as a function of particle concentration – near ε_{max}

Figure 53 gives the deviations as percent of the single-phase value. The graph shows that all the values are within ±5% which is what might be tolerated as error. In contrast, Unadkat (2009) found deviations of around 10 to 15% and for one particle size even around 20% when feeding into ε_{max} of a pitched blade turbine. It is worth remembering how low X_S is near ε_{max} compared to the other locations – i.e., in this work, less than 0.05 here instead of almost 0.2 near the surface. This explains the slightly larger error bars in this feed location compared to others, because small

deviations are proportionately more stronger reflected in such small values, i.e. due to the scale errors become amplified. Nevertheless, the deviations do not follow the previous trends, as not all values indicate slight turbulence suppression at higher concentration – assuming that such small changes do actually indicate effects of the particles on micromixing. Near this feed point, the values seem to diverge, though not in the way predicted by literature: here the values for small particles point towards turbulence enhancement and the bigger ones towards suppression. However, it has to be emphasised again that these deviations are small.

Overall, it is difficult to draw more conclusions from these results than that, ***if*** there are effects, they are relatively small. Interpretation of the data might show more useful details when energy dissipation rates are discussed instead of segregation indices. This would also aid connecting these results with those from other methods like PIV and LDA.

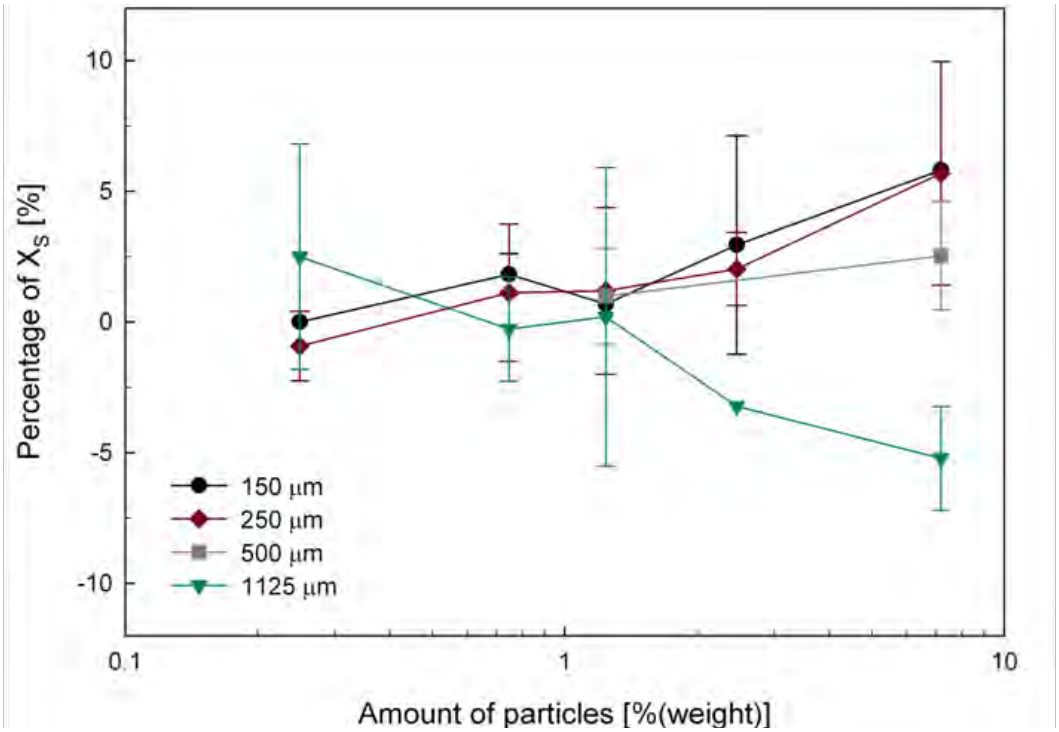

Figure 53: Effect of particle size in dilute suspensions at several particle concentrations – in percent of single-phase segregation index – near ε_{max}

6.5. Effect of solid concentration on micromixing

In the previous section, it was found, for a range of particle sizes, that low concentrations of glass beads do not affect micromixing in a stirred tank or at least do so less significantly than would have been expected from reports in literature. Another aspect is the amount of particles in the system. Therefore, two extremes are tested: low concentrations, i.e. dilute suspensions, and a higher concentration, i.e. a dense suspension, in which cloud formation occurs.

6.5.1. Near impeller

Several concentrations of 500 µm particles were tested for a range of power inputs and the results are summarised in Figure 54. The data points for up to 2.46 wt.% fluctuate around the single-phase value and do not show any significant patterns. Therefore, the previous conclusion for small amounts of glass beads is confirmed for different power inputs – and therefore particle distribution and fluid dynamic conditions. The higher particle concentration gave a cloud at the impeller speeds employed during the experiments. In these conditions, micromixing clearly becomes worse – even at constant power per total mass. If the second option for keeping mean specific energy dissipation constant, power per liquid mass, had been chosen, this effect would be even more significant, as the impeller speed would have been reduced further instead of the increase due to the increase in total mass in this work.

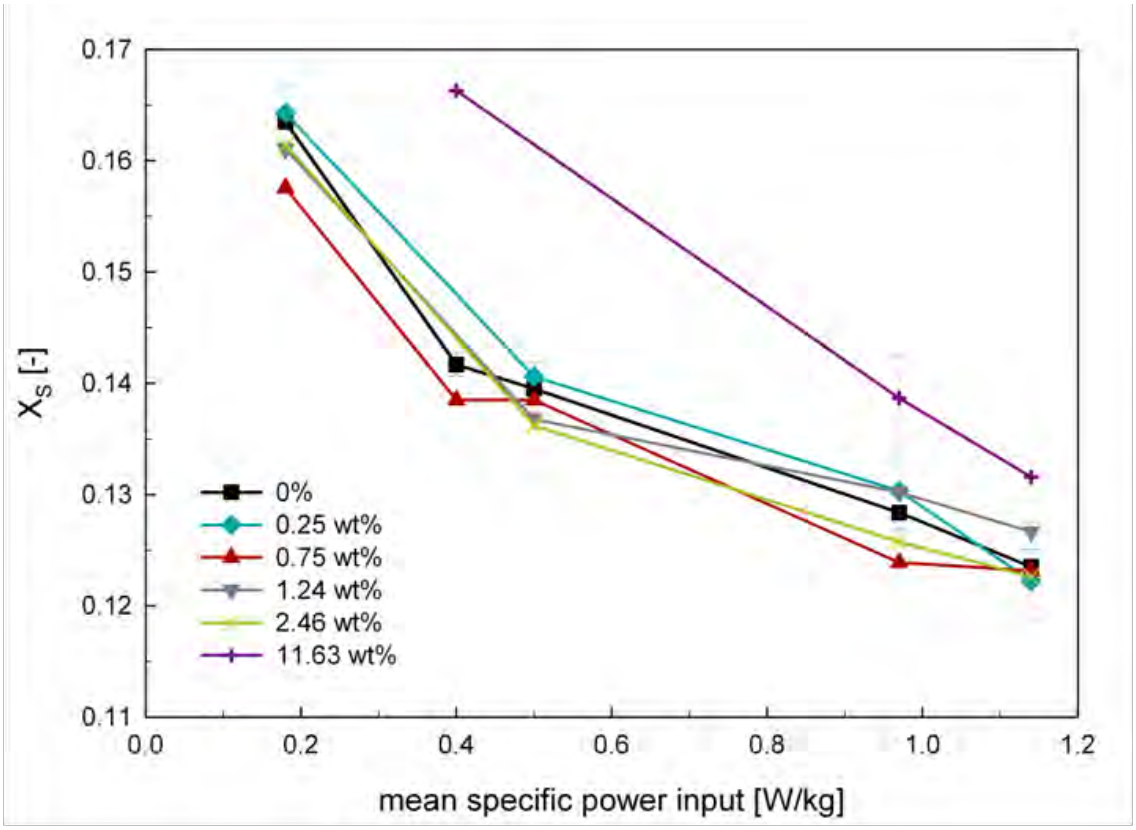

Figure 54: Effect of particle concentration ($d_p = 500\mu m$) on segregation index – feed position 2 (near impeller)

Figure 55 emphasises that there also is no effect of the particles at different power inputs – the fluctuations around the liquid-only value are less than ±4% and there is no trend in these deviations. In contrast, Figure 56 shows the significant reduction of micromixing efficiency in the cloud: the results drop by almost -20% of the single-phase value. Interestingly, the effect becomes less pronounced at higher power inputs which is easily explained as the cloud is more strongly developed around the lower values. At even higher impeller speeds than investigated here, the cloud disappeared and the particles were mixed throughout the entire vessel. Unfortunately, such conditions could not be measured and compared to single-phase data, as reference values could not be obtained without air entrainment at relevant power inputs.

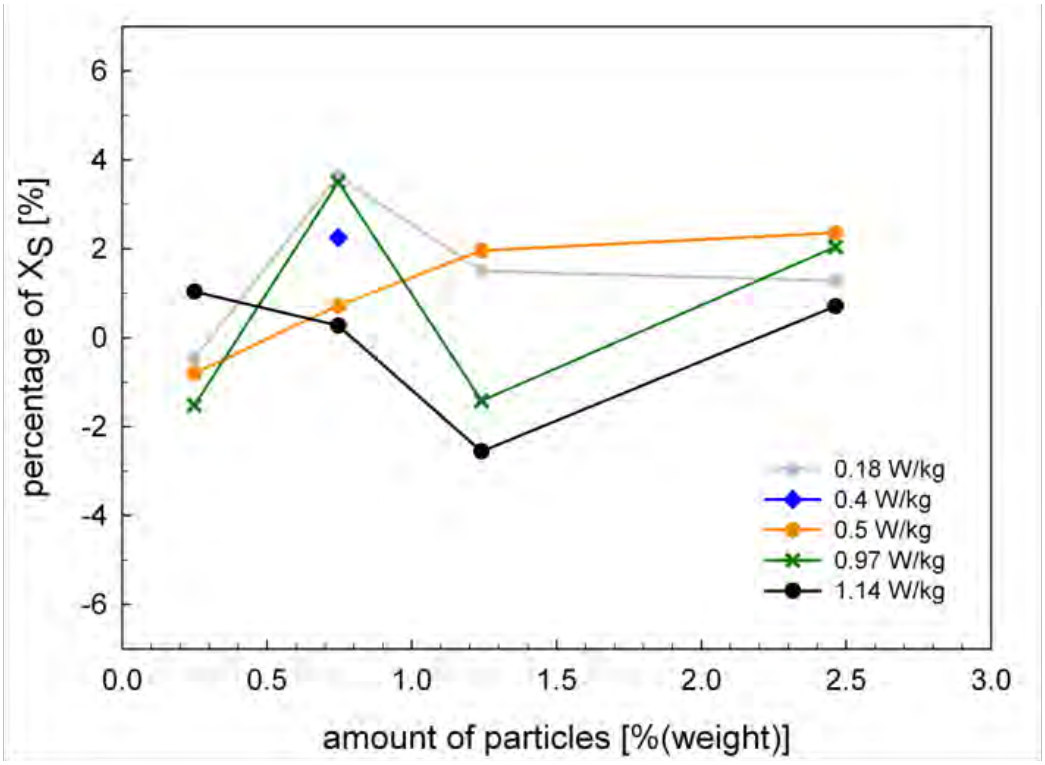

Figure 55: Effect of particle concentration ($d_p = 500\mu m$) at low particle concentrations as percent of single-phase segregation index – feed position 2

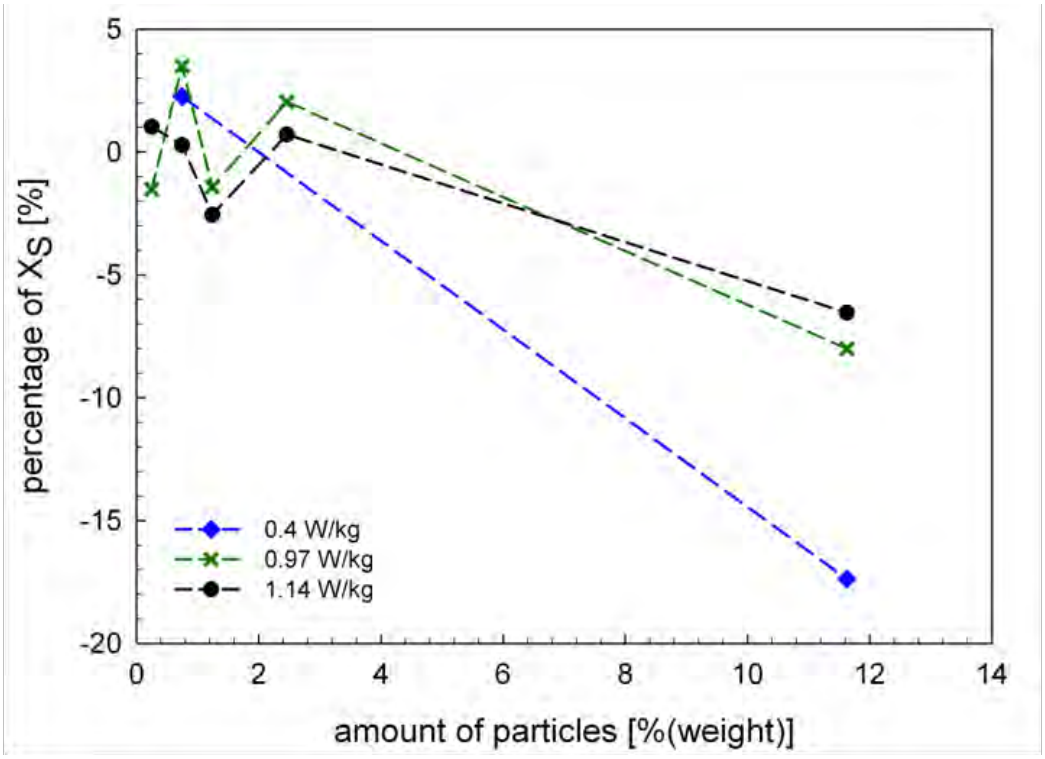

Figure 56: Effect of particle concentration ($d_p = 500\mu m$) at particle conc. with and without cloud as percent of single-phase segregation index – feed position 2

As 500 µm glass beads have resulted in suppression of micromixing and literature would indicate augmentation due the presence of big(ger) particles, another larger size was tested. Considering that studying different power inputs has not shown any significant additional effects or changes in behaviour of the solid-liquid mixtures, one power input was found sufficient for these purposes. Therefore, Table 36 summarises the data for micromixing when feeding into a cloud at 1.14 W/kg:

Table 36: Effect of cloud on micromixing near impeller

particle size	percentage of X_S
500 µm	-7.7%
1125 µm	-14.2%

Interestingly, the bigger particles lead to an even more significant reduction of micromixing efficiency. This directly contradicts expected behaviour from turbulence modulation literature and, therefore, indicates that two-way coupling alone will not aid interpretation of such cases. As measurable turbulence enhancement is not found in this case, particle interaction could have become relevant – which is quite reasonable at such particle concentrations. This is in agreement with the PIV results presented by Gabriele *et al.* (2011). However, their argumentation employing turbulence modulation theories seems less appropriate than considerations of four-way coupling.

6.5.2. Near surface

Visual observation and literature indicate that fluid circulation and macromixing are very poor in the clear liquid layer above the cloud. As previous studies did not clearly state whether feeding occurred in or above the cloud, this section is dedicated to

feeding above, while the previous one (section 6.5.1.) was on feeding near the impeller, i.e. into the cloud.

Figure 57 shows that different power inputs do not change the conclusion for low particle concentrations: there is no significant effect. For the 11.63 wt.% case, however, the results for feeding above the cloud do show significantly higher formation of side-product. This result is not surprising, considering that the fluid in this region is rather quiescent. Nevertheless, it is relevant, as surface feeds are popular in industry and data for such a well-defined feed position has not been shown before.

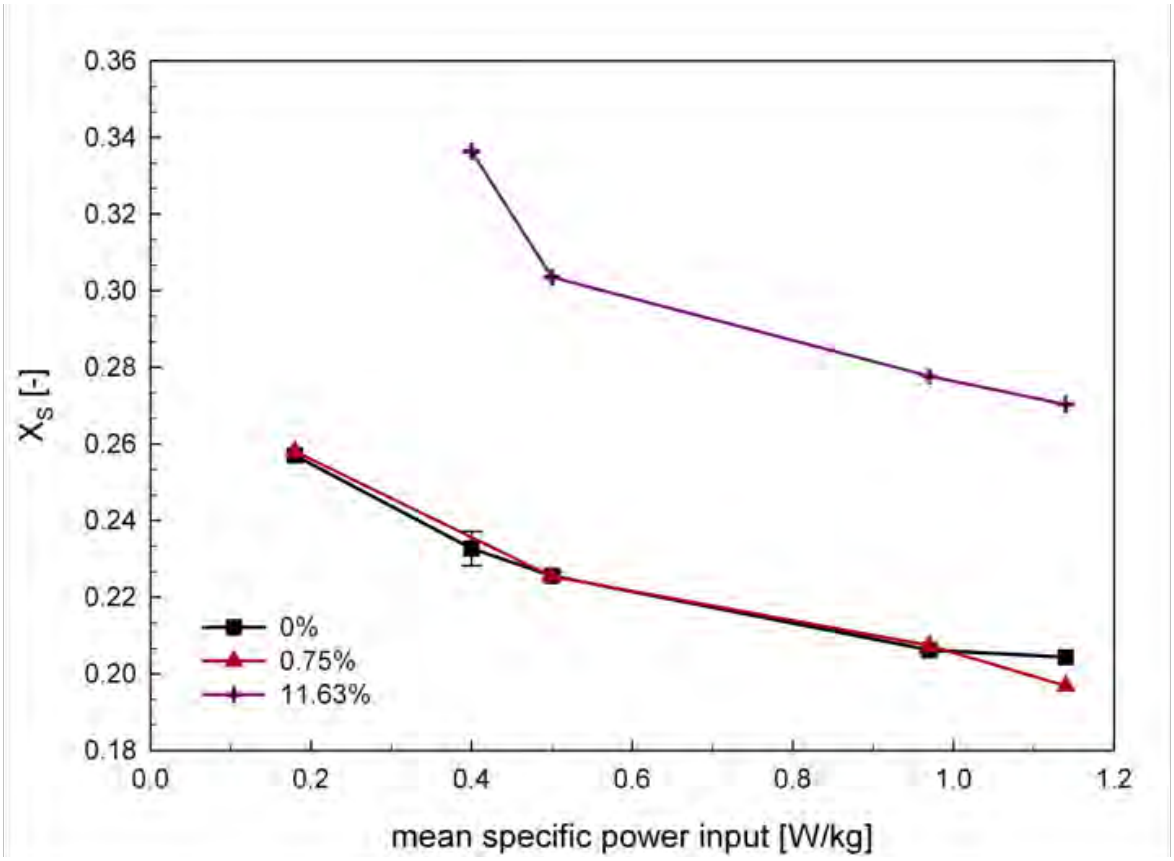

Figure 57: Effect of particle concentration ($d_p = 500\mu m$) on segregation index – feed position 1 (near surface)

As before, a second particle size was tested at 1.14 W/kg and the data is summarised in Table 37. In this case, the bigger particles lead to better micromixing than the smaller ones. Hypothetically, this might conform to turbulence modulation theory, but: there are no particles in the relevant region near the feed pipe. A more sensible explanation might come from simply looking at the clouds: the bigger particles lead to a much less well-defined cloud than the smaller ones. Therefore, the layer above the cloud is less quiescent and micromixing consequently better.

Table 37: Effect of cloud on micromixing near surface

particle size	percentage of X_S
500 µm	-32.3%
1125 µm	-16.9%

6.6. Interpretation with micromixing model

6.6.1. Effect of particle size at low particle concentrations

As lower amounts of particles only had relatively little effect on X_S, the most "extreme" case will be discussed here: though it might not even fall into a region where only turbulence modulation is relevant, the changes with 3 vol.% (7.2 wt.%) glass beads are discussed here. Regarding the feed position, there is most indication from literature for effects when feeding near ε_{max}. Therefore, the deviations discussed in 6.4.3. are summarised in Table 38 by giving them for different model solutions as the changes in ε_T compared to the single-phase value. Considering that the deviations of X_S were within experimental error and that such models amplify such differences, these fluctuations of 20% or less cannot be considered significant. However, other

reports in literature showed much larger effects on the segregation index and would, therefore, indicate much larger changes on local specific energy dissipation rates. This would support the data presented by Unadkat (2009) which suggested strong turbulences modulation in PIV and micromixing measurements. As the concentrations used in that work are different from this work, a more extensive comparison or even application of the model would not be reasonable.

Table 38: Effect of particle size on ε_T – pos. 4 (near ε_{max}) - 3 vol.% - deviation of ε_T compared to single-phase result

	original model	diluted + kinetics: Xie et al.	adapted interpolated kinetics
150 µm	17%	20%	20%
250 µm	17%	20%	19%
500 µm	7%	8%	8%
1125 µm	-13%	-15%	-14%

As the changes in the “worst” case are already relatively modest, using the model is futile for further investigation of other conditions in dilute suspension which show even less effects in segregation index.

6.6.2. Effect of particle concentration (cloud formation)

While the above gave effects within the range of expected error and less than or around 20% of estimated specific local energy dissipation rates, clouds did lead to significant changes in segregation index, which can be expected to translate into effects on ε_T as well. The deviations are again expressed in percent of the equivalent single-phase values for different models – near the surface and near the impeller in Table 39 and Table 40, respectively. Table 39 illustrates how much worse

micromixing becomes near the surface when clouds are formed: these deviations suggest drops in ε_T by almost or around an order of magnitude, which is especially remarkable taking into account that the micromixing conditions in this region have already been found less than ideal in liquid-only measurements. This result fit surprisingly well with results from LDV measurements in the clear liquid over clouds by Bittorf and Kresta (2003). They found a drop by 75% for the turbulent RMS velocity, which is in good agreement with the present results, considering the differences in the experimental stet-ups and conditions.

Table 39: Effect of clouds on ε_T – pos. 1 (near surface)

	original model	**diluted + kinetics: Xie *et al.***	**adapted interpolated kinetics**
500 µm	-86%	-92%	-92%
1125 µm	-65%	-74%	-73%

In comparison to the clear liquid layer, the effects in the clouds are not as substantial but still significant as shown in Table 40. This region is not accessible for laser-based methods because of the high concentration of solids. This new data gives insight into such systems, which is especially relevant because such dense suspensions can be found in industrial processes.

Table 40: Effect of clouds on ε_T – pos. 2 (near impeller)

	original model	**diluted + kinetics: Xie *et al.***	**adapted interpolated kinetics**
500 µm	-27%	-34%	-33%
1125 µm	-39%	-48%	-47%

6.7. Conclusions

The effect of solid particles on micromixing in a stirred tank was investigated using the iodide/iodate reaction scheme. The method was found suitable for the use with glass beads and three feed positions were employed for this work: near the surface, near the impeller and near ε_{max}.

At low concentrations, up to 2.5 wt.%, five sizes of glass beads did not affect the segregation indices for the feed locations studied, but slightly more side-product was formed at 7.2 wt.% for feeding near the surface and the impeller. Therefore, it is concluded that no turbulence modulation, as would have been expected from corresponding literature, was observed at lower concentrations. In contrast, for both feed positions, all sizes slightly, but consistently dampen turbulence and micromixing at the highest concentration which can be attributed to particle-particle interaction. This might also be expected from the general, well-established literature on particle-fluid and particle-particle interaction (Elghobashi 1994), though there are investigations discussing only turbulence modulation for such conditions (see review in section 2.3.). Near ε_{max}, there, again, was no effect at low concentrations which is in agreement with some of the literature, e.g. Guichardon *et al.* (1995), although such effects have been shown in some previous work on turbulence modulation in stirred tanks, e.g. Unadkat (2009) and Montante *et al.* (2010). At 7.2 wt.%, when particle-particle interaction might already become relevant, the data is more scattered and the experimental errors become larger than in the other experiments. Nevertheless, the deviations found here indicate only small effects, even when expressed as changes in local specific energy dissipation rates calculated from the micromixing

model variations, and, overall, correspond well to the trend reported here for the other two feed positions.

At higher concentrations, when clouds were formed, micromixing was consistently worse than in the equivalent single-phase case – interestingly, in the clear liquid layer and also in the cloud. This, again, does not point towards the expected effects due to turbulence modulation but more towards four-way coupling. The high segregation indices when feeding into the clear liquid above the cloud emphasise the importance of feed pipe positioning.

7. MICROMIXING IN LIQUID-GAS-SOLID SYSTEMS

7.1. Introduction

Three-phase systems consisting of sparged gas bubbles and solid particles in liquids can be found in industrial processes like oxidation, hydrogenation and polymerisation. In spite of the relevance to real applications, such conditions are still poorly understood and especially micromixing data has not been reported. Considering the effects found in the previous chapters on gas-liquid and solid-liquid cases, micromixing will be investigated near the surface and near the impeller, for dilute and dense suspensions over a range of sparge rates while keeping power input from the impeller constant. As the validation of the method has already been covered before (chapters 5.2. and 6.2.), power measurement data will be presented first and then micromixing results will be shown and discussed. Again, the micromixing model from chapter 4 will be applied for further interpretation of the data.

7.2. Power input in 3-phase (l-g-s) system

7.2.1. Power measurement results in liquid-gas-solid cases

As in the previous parts, power data was necessary because the experiments are set out to run at equivalent power inputs. At low particle concentrations of 1.24 wt.%, the measured power was very similar, i.e. deviations were within experimental error, to the corresponding gas-only results for the three sparge rates investigated. This is in agreement with literature, e.g. Warmoeskerken *et al.* (1984) who found that up to 5 wt.% did not affect sparged power inputs.

When sparging the cloud, i.e. at the higher particle concentration, power had to be measured. This was done for both sizes of glass beads employed. The results are plotted in Figure 58 for the 500 µm particles and in Figure 59 for the 1125 µm ones. The general trends of both graphs agree with literature (Chapman *et al.* 1983a; Frijlink *et al.* 1990; Roman and Tudose 1997).

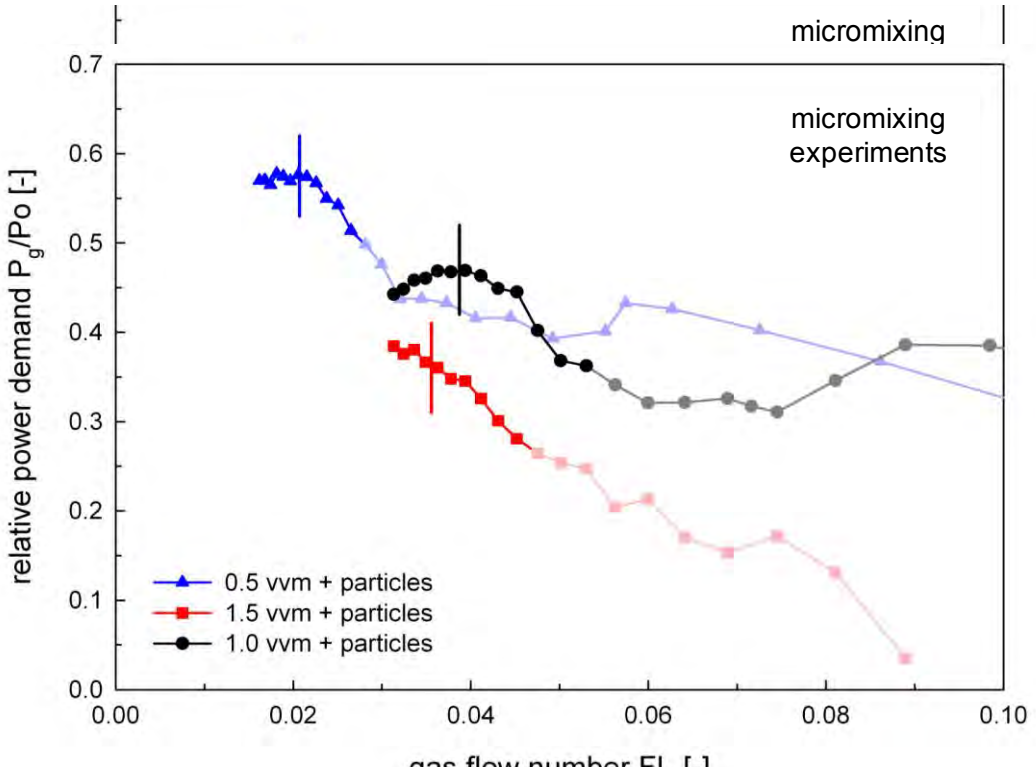

Figure 58: Relative power input as a function of gas flow number – gassed with particles – 500 µm and 11.63 wt.%

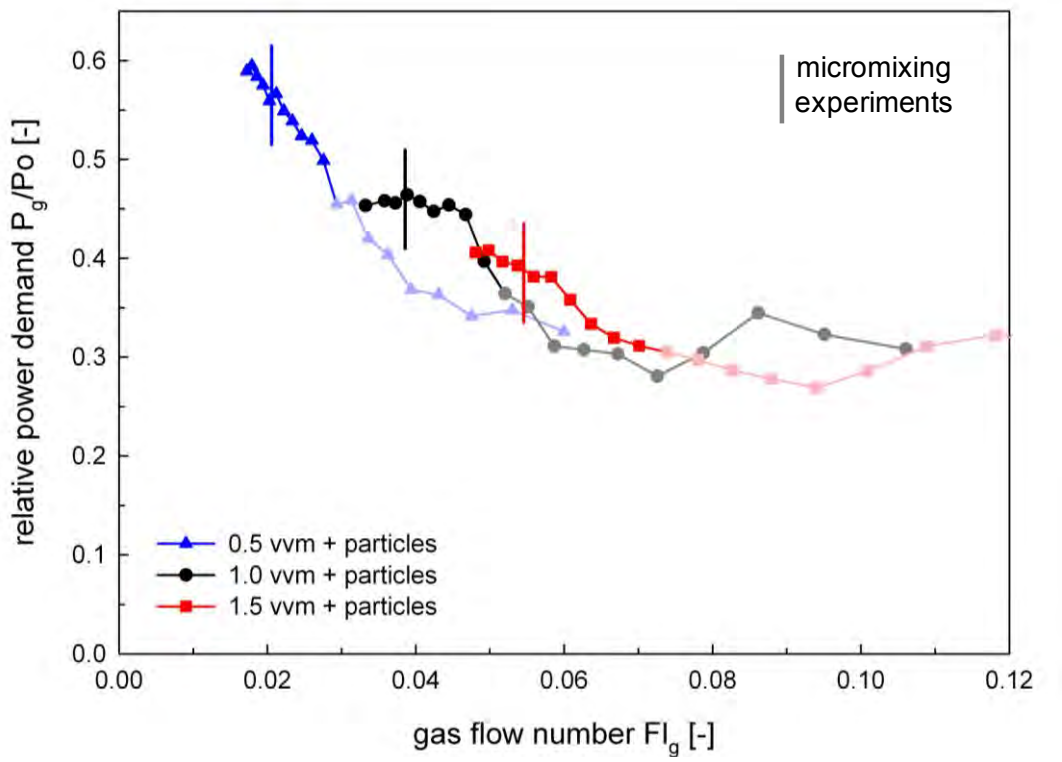

Figure 59: Relative power input as a function of gas flow number – gassed with particles – 1125 µm and 11.63 wt.%

Maxima of P_g/P where gross recirculation starts to lead to drops in gassed power can be seen on both graphs and also some of the minima at N_{CD} are captured even though the measurements are not expected to be accurate at such low power inputs.

7.2.2. Conditions for micromixing experiments with gas and particles

As low amounts of particles did not affect the gassed power input, the impeller speeds for the gas-liquid conditions, see Table 21, were used for the three-phase experiments with 1.24 wt.% Ballotini. In the case of 11.63 wt.%, the impeller speeds were adapted for both particle sizes as summarised in Table 41 to match the power input to 1.14 W/kg.

As in the solid-liquid considerations, the question of keeping power constant per total mass or per liquid mass was not straightforward. The same considerations as in section 6.3.2. led to the choice of constant power per total mass.

Table 41: Impeller speeds for three-phase experiments with 11.63 wt.% for matching mean specific energy dissipation rate, $(\overline{\varepsilon_T})_{3-ph} = 1.14\ W/kg$

	for 500 µm [rpm]	for 1125 µm [rpm]
0.5 vvm	665	670
1.0 vvm	712	715
1.5 vvm	775	758

7.2.3. Flow at the chosen conditions

For the lower particle concentration, the flow appeared similar to the gas-liquid equivalents. Due to the presence of the gas bubbles, the degree of suspension and distribution of the particles in the tank could not be observed as accurately as at solid-liquid conditions. Nevertheless, suspension of 1.24 wt.% glass beads at the chosen sparge rates appeared complete when observing the tank through the bottom.

The conditions for the micromixing experiments with the sparged cloud are indicated in Figure 58 and Figure 59. It can be seen that they are all near the maximum of P_g/P between complete gas dispersion and gross gas recirculation. Visual observation confirmed that the impeller was clearly not flooded and that significant interaction of gas, liquid and impeller was taking place. Regarding solid suspension, the aim for the higher concentration was not necessarily to reach N_{js} or N_{js_g} - instead

any effects of gas bubbles on the poor micromixing in the presence of a cloud was of interest. To get an impression of how well the particles may be expected to get suspended, equation (2.9) was employed, although this is will only give general estimates as the correlation was obtained for larger Rushton turbines. The results are summarised in Table 42 – expressed as percentage of calculated N_{js_g} for the respective actually used impeller speeds (see previous section):

Table 42: Suspension state for dilute and dense suspensions over range of sparge rates - expressed as percent of N_{js_g}

	1.24 wt.%			11.63 wt.%	
	250 µm	500 µm	1125 µm	500 µm	1125 µm
0.5 vvm	117.06%	102.56%	87.78%	76.94%	66.24%
1.0 vvm	120.06%	105.80%	91.09%	79.78%	68.77%
1.5 vvm	124.22%	110.05%	95.28%	84.18%	70.98%

Unfortunately, visual observation is only possible to a limited extent at such high fractions of added phases (therefore, no image is given). With the lower amounts of glass beads, visual observation through the bottom of the tank confirmed that all particles were fully suspended as suggested in Table 42.

7.3. Dilute, sparged suspension

In chapter 5, it was shown that gas bubbles do not significantly affect micromixing in the impeller discharge stream when the power input from the impeller is kept constant. Small amounts of solid particles did not lead to considerable effects either, as presented in chapter 6. Here, the combination of gas and small amounts of solid particles is investigated.

7.3.1. Near impeller

Figure 60 shows the segregation indices in sparged dilute suspensions for 3 particle sizes as a function of gas flow rate. For reference, the equivalent data from single-phase and gas-liquid experiments is plotted in this graph as well. Overall, these three-phase results are close to the liquid and g-l data – especially considering the size of the error bars, the deviations appear relatively small. However, there seems to be a slight drop in segregation index of the g-s-l cases with increasing amounts of gas. Though this trend is only small and within the error bars, it is consistent for all three particle sizes.

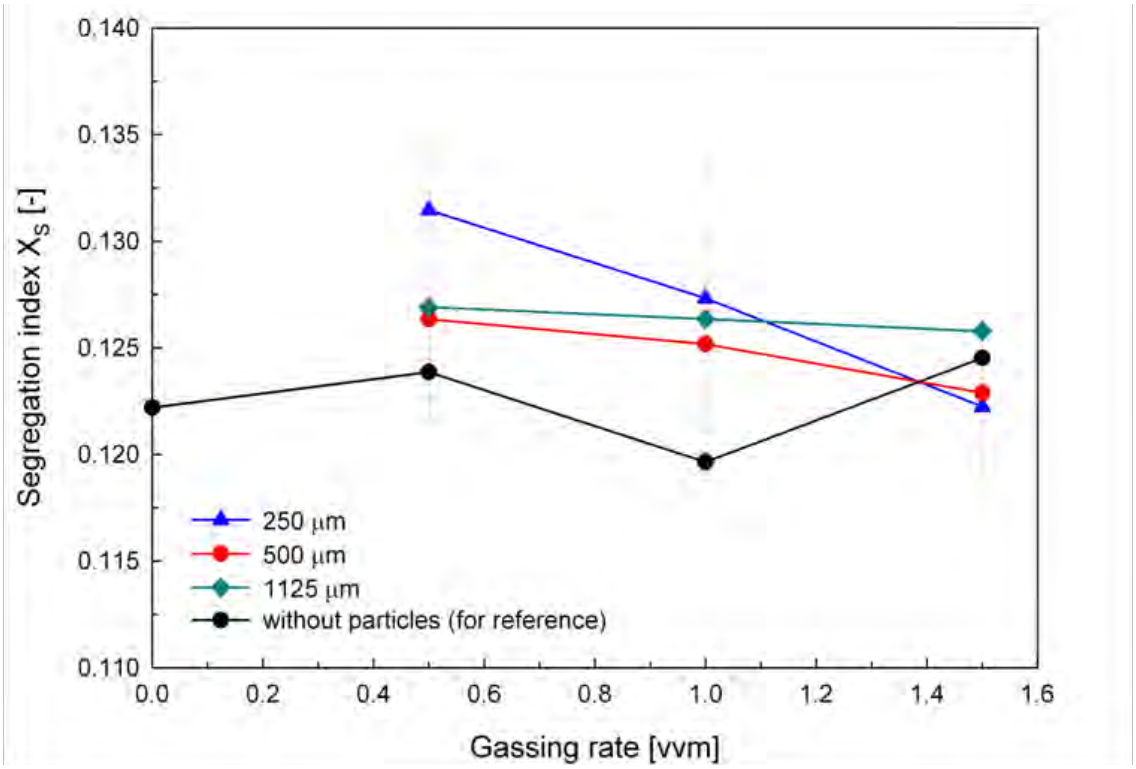

Figure 60: Segregation index as a function of gassing rate in dilute suspension (1.24 wt.%) - feed near impeller

As in previous chapters, the results are also given as the deviation from reference data. There are three options: compared to single-phase, gas-liquid or solid-liquid which will be discussed in the following paragraphs. Figure 61 emphasises that there

might be a small effect of the bubbles and particles at 0.5 vvm, but that the results stay close to the single-phase results. Three-phase micromixing in the impeller discharge stream seems to be, within experimental error, relatively unaffected by the added phases. In order to minimise errors due to the power measurements which might skew the comparison with single-phase data, the results are compared to the g-l equivalents in Figure 62. This might highlight effects of the combination of particles and bubbles on micromixing. Figure 62, however, does not show any significant trends and the deviations of usually less than 5% could be considered within the expected error. Still, the consistency of the deviations is surprisingly good and, if effects are found in other feed positions, these results might be seen in a different light.

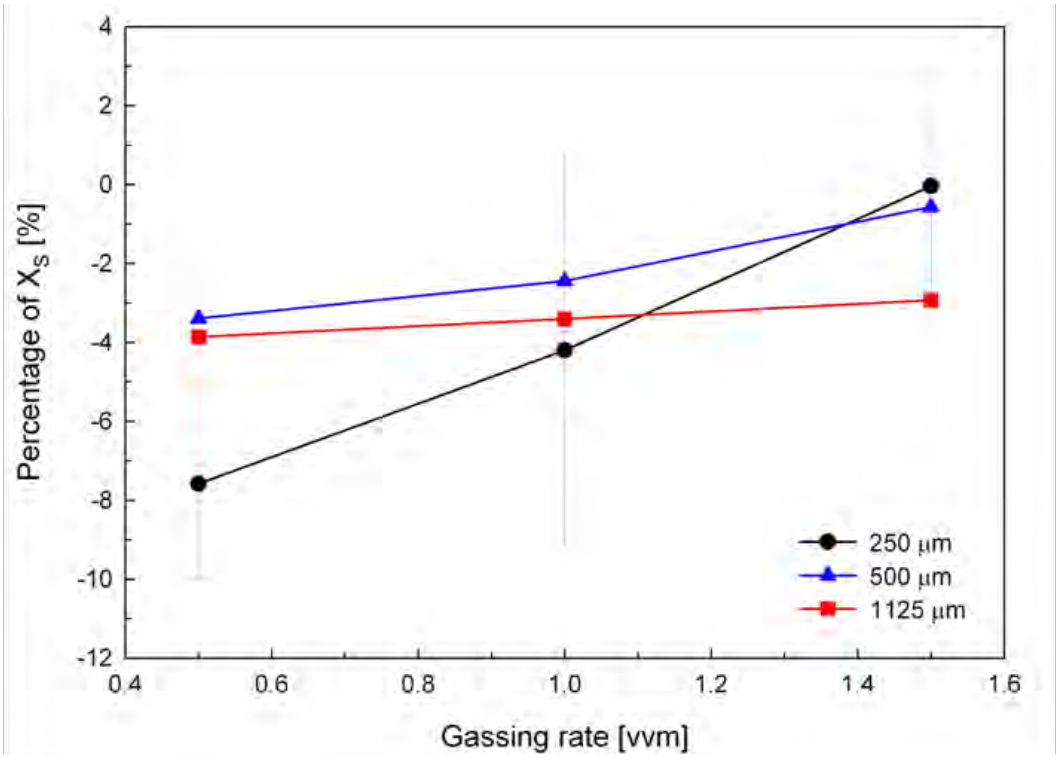

Figure 61 : Effect of particle size and sparge rate on micromixing – in percent of single-phase segregation index – near impeller

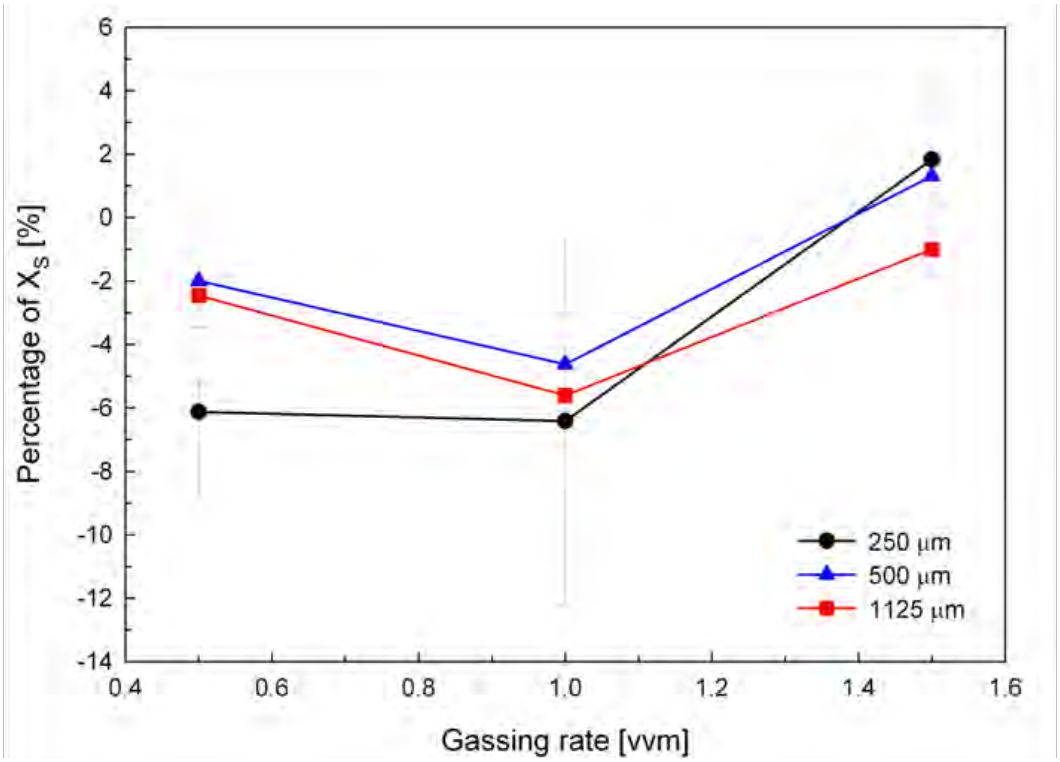

Figure 62 : Effect of particle size and sparge rate on micromixing – in percent of gas-liquid segregation index – near impeller

7.3.2. Near surface

As with the above data for feeding near the impeller, Figure 63 shows liquid-only, gas-liquid and three-phase segregation indices as a function of sparge rate. The reference data follows a consistent trend with increasing gas flow: micromixing is significantly improved. The same tendency is found for the dilute, sparged suspension. The absolute values, however, are higher than in the gas-liquid case, i.e. micromixing becomes worse near the surface when solid particles are added to a gas-liquid stirred tank.

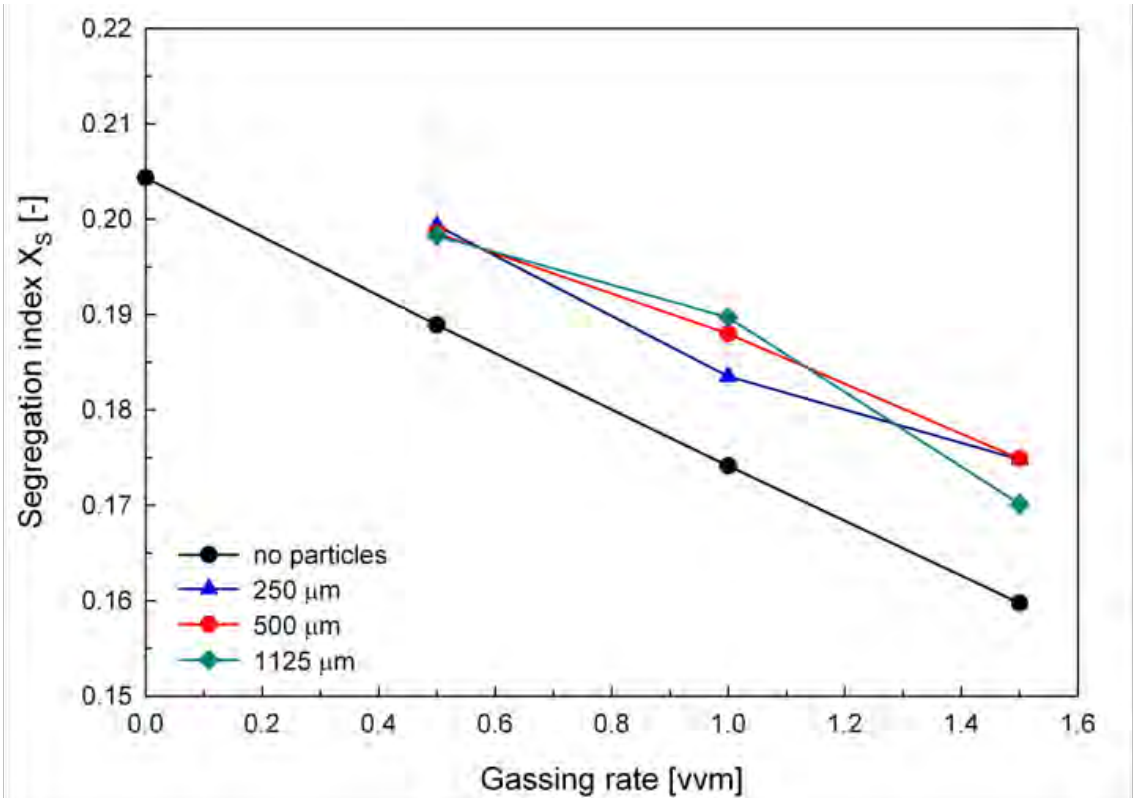

Figure 63: Segregation index as a function of gassing rate in dilute suspension (1.24 wt.%) - feed near surface

To quantify these deviations, they are expressed as percent of the reference segregation index again. The comparison to the liquid-only equivalent in Figure 64, as expected from the absolute values, shows significant improvement of up to about 15% at 1.5 vvm, though this is lower than the improvement of up to ~30% in the g-l case without any solid particles. Interestingly, there seems to be very little, if any, difference between the 3 tested particle sizes. In order to magnify the effect of the particles, a comparison to the gas-liquid data is drawn in Figure 65. This graph clearly illustrates that particles consistently reduce the improvements in micromixing that had been observed under gassed conditions near the surface. It might be worth noting that there is a slight downward trend in this plot, i.e. the effect of the particles might become more significant – though, taking the error bars into account, this might

only be a small effect. It could be explained by a different solids distribution in the tank with increasing gas rate at constant power input. The trend in Table 42 for instance indicates improvements in suspending the particles which might contribute to the observed trend, as one might expect more glass beads to become relevant to the flow once they are suspended. The slight increase for the largest solids at 1.5 vvm might be also attributed to experimental error or to these particles settling more easily and therefore not reaching relevant regions in as significant numbers as the smaller ones. Unfortunately, no relevant information could be found in literature on particle distribution in three-phase stirred tanks and further work is needed. Another option could be a possible interaction of bubbles and particles, for instance stronger or reduced coalescence of the bubbles (Nienow *et al.* 1986).

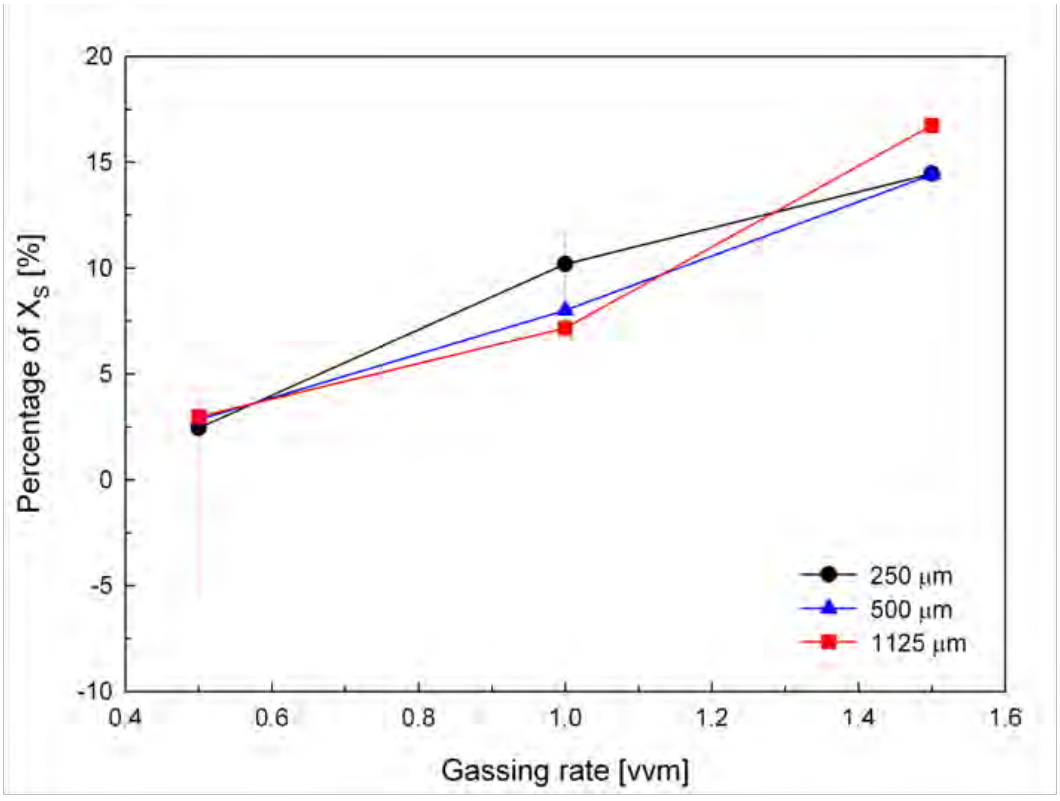

Figure 64 : Effect of particle size and sparge rate on micromixing – in percent of single-phase segregation index – near surface

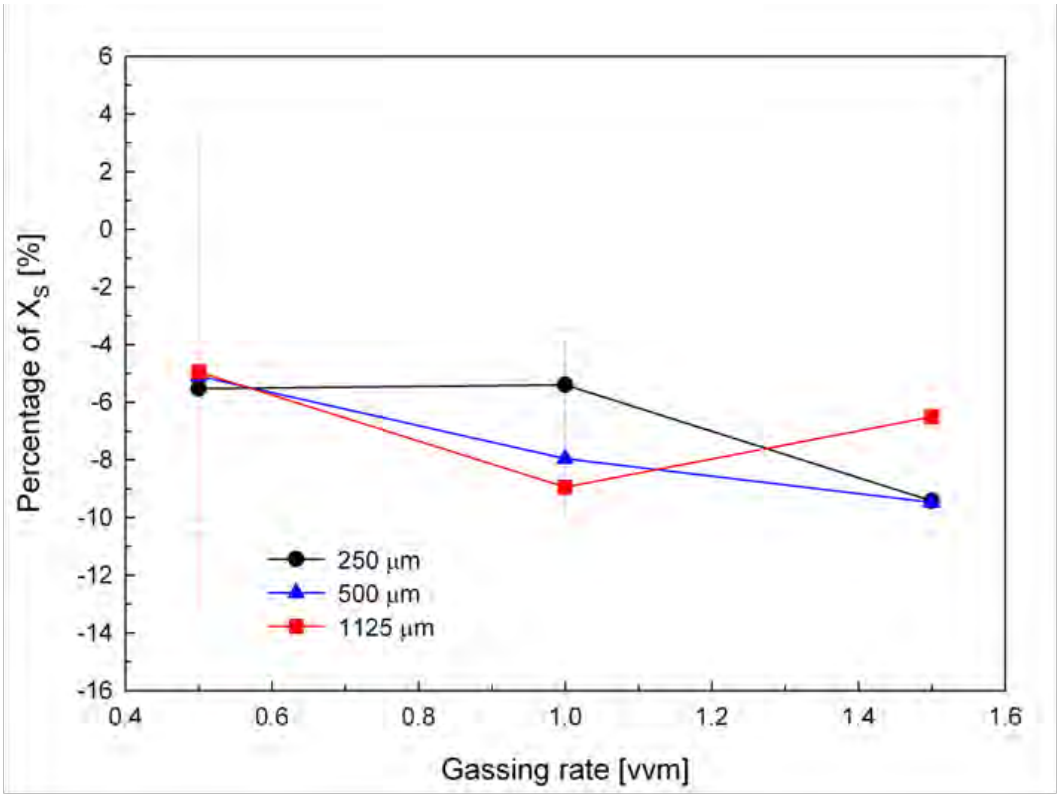

Figure 65 : Effect of particle size and sparge rate on micromixing – in percent of gas-liquid segregation index – near surface

Such micromixing measurements in 3-phase stirred tanks have not been reported in open literature before. In addition there is no information from turbulence measurements, but the consistent trend in the presented data might be discussed in the context of results found in related phenomena. For instance, a number of mass transfer studies would be available but, considering the complexity of the topic with sensitivity to particle properties, surfactants (Vazquez *et al.* 2000) and ionic strength (Zuidervaart *et al.* 2000), also such data cannot be employed. Therefore, further work on three-phase systems e.g. detailed information on particle distribution and velocity fields, for instance from PEPT, would be interesting.

7.4. Sparged cloud

In addition to sparged, dilute suspensions, also cases with higher solids concentrations were investigated. The results are summarised here.

7.4.1. Near impeller

Figure 66 shows that the results for the 1125 µm cloud are close to the single-phase reference data, but the sparged 500 µm cloud consistently gives more side-product, i.e. worse micromixing. Interestingly, both three-phase graphs show a segregation index peak at 1 vvm and then drop at 1.5 vvm. The significance of these deviations, however, cannot be discussed from this graph and comparisons as percent of single-phase, gas-liquid and solid-liquid are given in Figure 67, Figure 68 and Figure 69, respectively. Figure 67 confirms that, near the impeller, micromixing in the sparged cloud of 1125 µm particles is similar to the liquid-only behaviour, as the deviations are less than 4% of segregation index and therefore within the error expected for such experiments. In contrast, a dampening effect of the cloud of smaller particles can be seen, especially at 1 vvm with -13.5% deviation in segregation index.

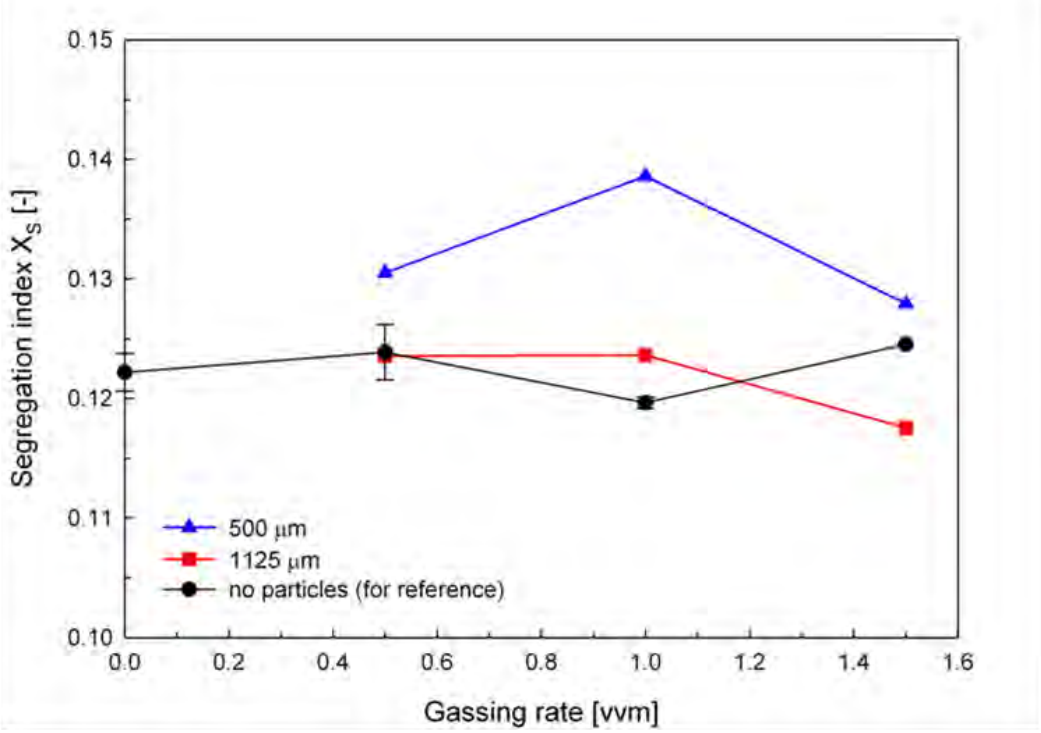

Figure 66: Segregation index as a function of gassing rate in dense suspension (11.63 wt.%) - feed near impeller

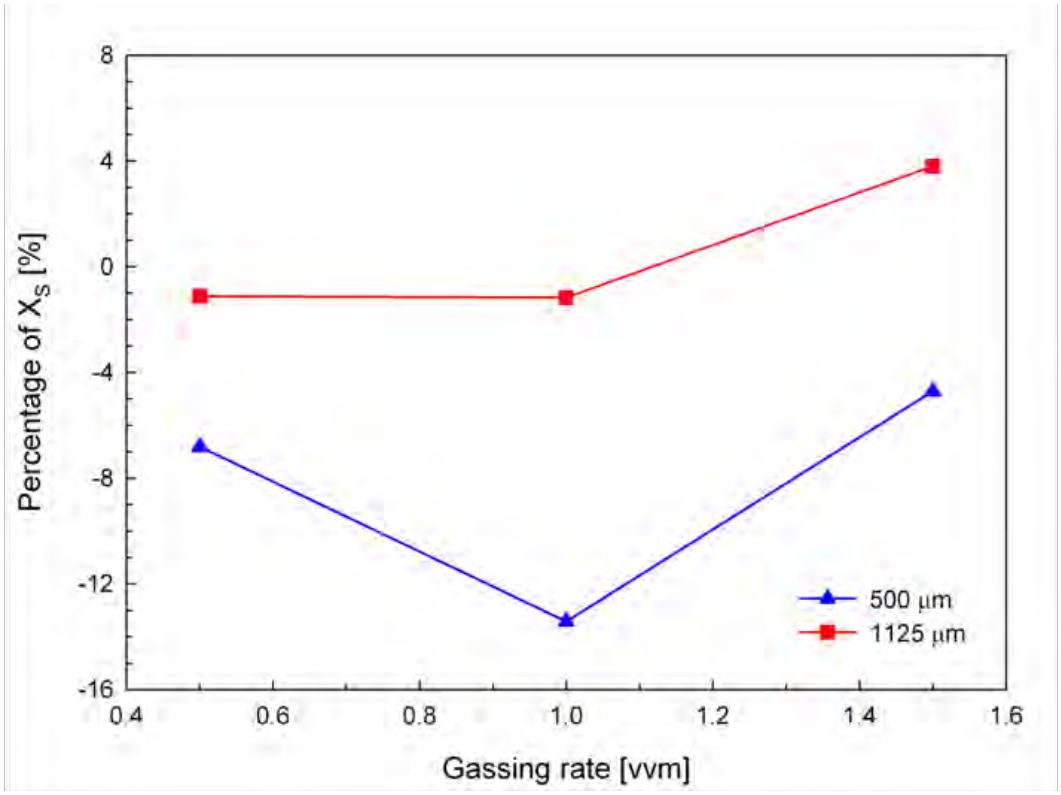

Figure 67 : Effect of particle size and sparge rate on micromixing – in percent of single-phase segregation index – near impeller

Considering that the gas sparging had no significant effect on micromixing near the impeller, it is not surprising that the trend in Figure 68 is comparable to the single-phase comparison in Figure 67. Again, the sparged cloud of larger particles leads to little deviations in micromixing efficiency, while the smaller ones do cause significant suppression. This does not reflect the dominant effect of the impeller observed in gas-liquid cases anymore, but at least for the larger particles the cloud seems to have been compensated for.

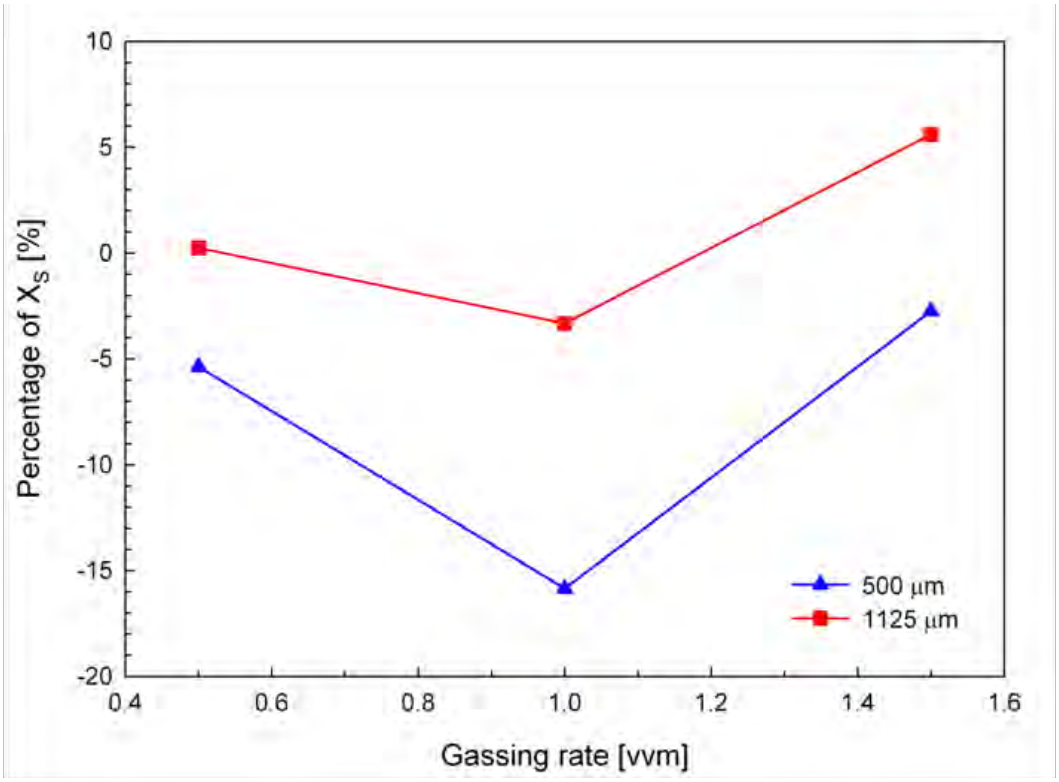

Figure 68 : Effect of particle size and sparge rate on micromixing – in percent of gas-liquid segregation index – near impeller

Figure 69 allows the comparison to the cloud and shows that a consistent improvement for the 1125 µm Ballotini occurs when sparging, but very little effect for the cloud of smaller particles. Interestingly, there is still a dip to -5% of segregation index at 1 vvm compared to the solid-liquid case which might be within experimental error, considering that the power input had to be measured too. Comparisons for a

second feed position might give a better indication of whether the deviations at 1 vvm need more attention or if they can be neglected.

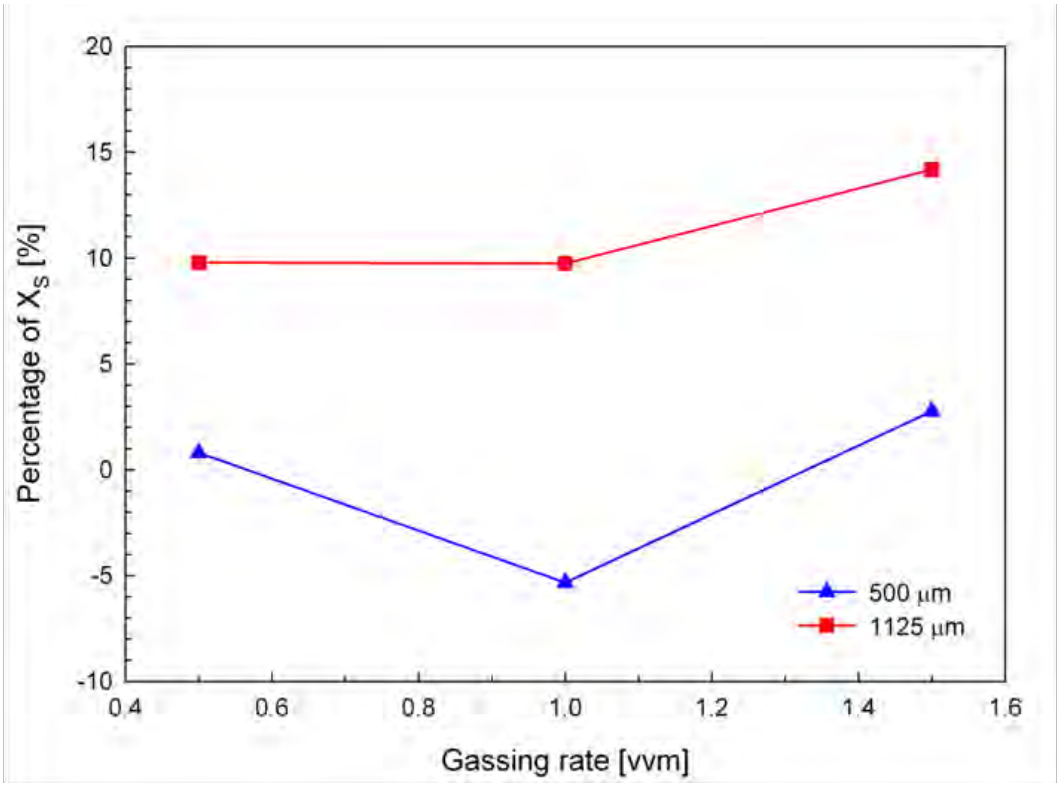

Figure 69 : Effect of particle size and sparge rate on micromixing – in percent of solid-liquid segregation index – near impeller

Overall, it is remarkable that the dampening effect of the cloud of larger particles, which resulted in a drop of 14.2% in the unsparged experiments compared to liquid-only, seems to be fully compensated for by the presence of the gas bubbles. On the other hand, the smaller particles also only gave a reduction of 7.7% compared to single-phase at this power input, but that cloud seems to be less affected by the sparging.

7.4.2. Near surface

On their own, the above results do not give a full picture of the three-phase system and similar experiments were performed for feeding near the liquid surface. A clear

layer of liquid with poor micromixing (see section 6.5.2.) would normally be found in this location above the cloud, but the gas bubbles might affect this.

Figure 70 shows the downward trend of the single-phase and gas-liquid data for reference and some fluctuating but for both particle sizes consistent behaviour. At 0.5 vvm, feeding above both sparged clouds leads to more side-product than in the equivalent sparged case. In fact, the data is close to the single-phase result at the same impeller power input. Interestingly, the segregation indices drop below the reference data at 1 vvm and then increase again slightly at 1.5 vvm. This is different from the previous consistently higher result in the more dilute suspension (see section 7.4.2.), but again shows deviations at 1 vvm, as already noted for feeding near the impeller at the same conditions. Moreover, the errors reach up to 5.5% which is relatively encouraging, considering up to 25% error reported by Barresi (1997) for high particle concentrations in 2-phase experiments.

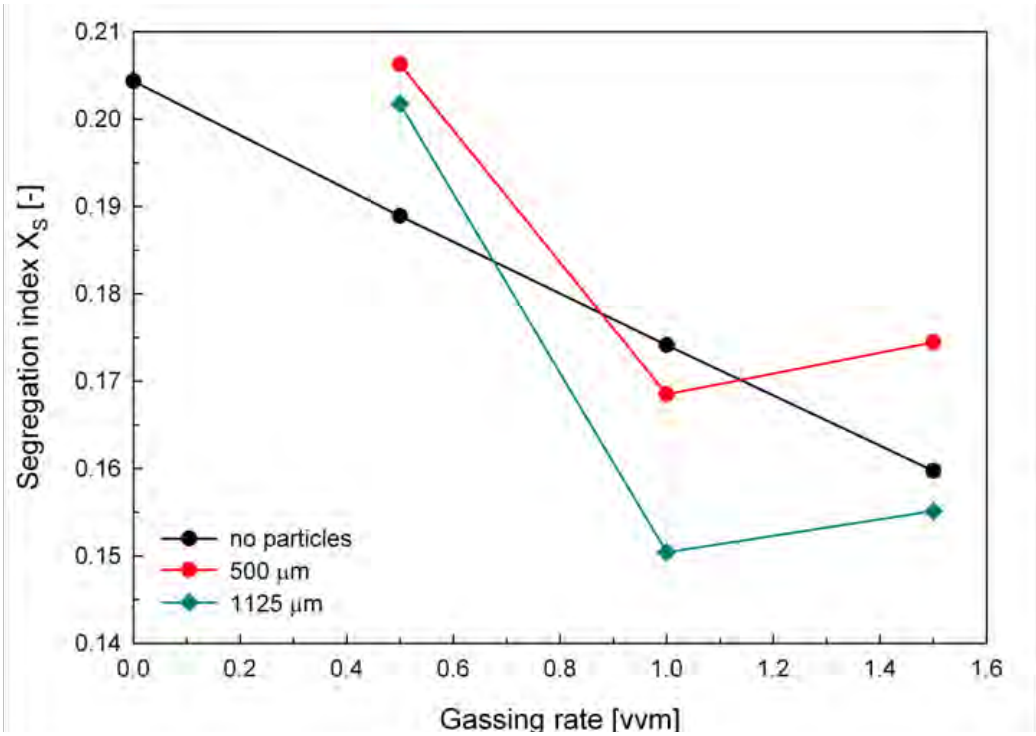

Figure 70: Segregation index as a function of gassing rate in dense suspension (11.63 wt.%) – feed near impeller

In order find an indication for the trends in Figure 70, the data is compared to the three reference options. Firstly, the percentages of single-phase data are plotted in Figure 71, which confirms that the results at 0.5 vvm are the same as in the liquid only experiments, while 1.0 and 1.5 vvm lead to significant improvements in spite of the 11.63 wt.% particles in the tank. The previously observed direct dependence on gas sparge rate is not found in this case, though it clearly improves micromixing in the higher range investigated.

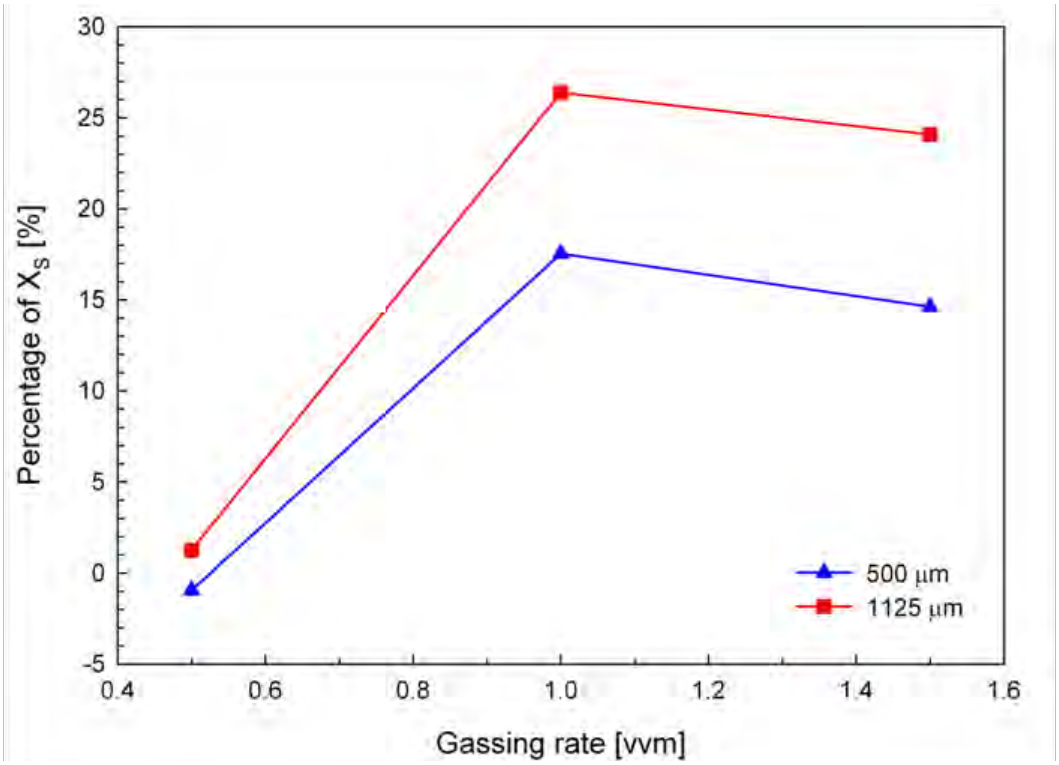

Figure 71 : Effect of particle size and sparge rate on micromixing – in percent of single-phase segregation index – near surface

Figure 72 confirms the point that the improvements are not directly related to the gas rate and the deviations at 1 vvm are especially clear in this graph. While it can be argued that in these conditions, the 500 µm solids cloud only has a negligible effect on micromixing, there is significant improvement with the larger particles, i.e. ~13.6 % deviation from the g-l result. Figure 73 emphasises that sparging the clouds

improves micromixing near the surface for all conditions – compared to the cloud equivalents, which had to be expected due to the poor results found in those reference cases. It might, however, be argued that micromixing still improved from 0.5 to 1.0 vvm and then stabilised around that value. This would put the data at 1.0 vvm more into context with the rest of the results, instead of being an unexplained fluctuation. On the other hand, these trends are consistent and the results near the impeller already showed slight deviations at 1.0 vvm as well. Unfortunately, the mixture was opaque at these conditions, so even visual observations of the flow were only possible to a limited extent and did not aid understanding of the results. New measurement methods, however, might give detailed insights into liquid and solid behaviour of such complex flows (Guida 2010) and might help interpretation.

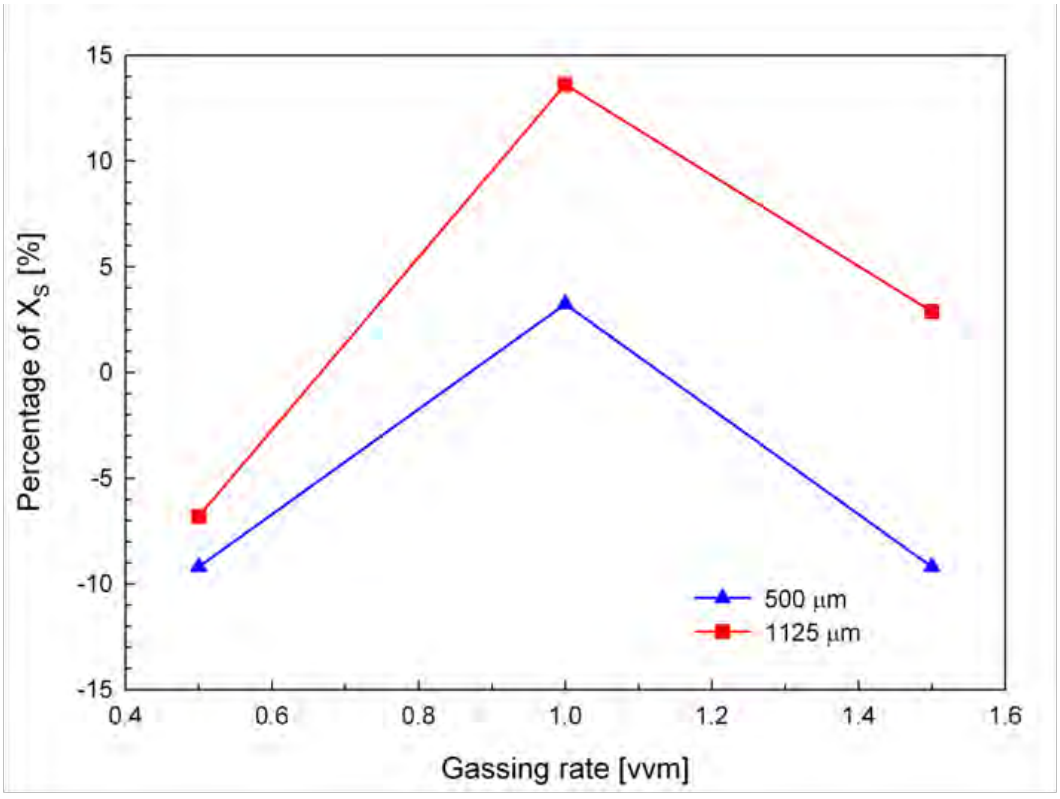

Figure 72 : Effect of particle size and sparge rate on micromixing – in percent of gas-liquid segregation index – near surface

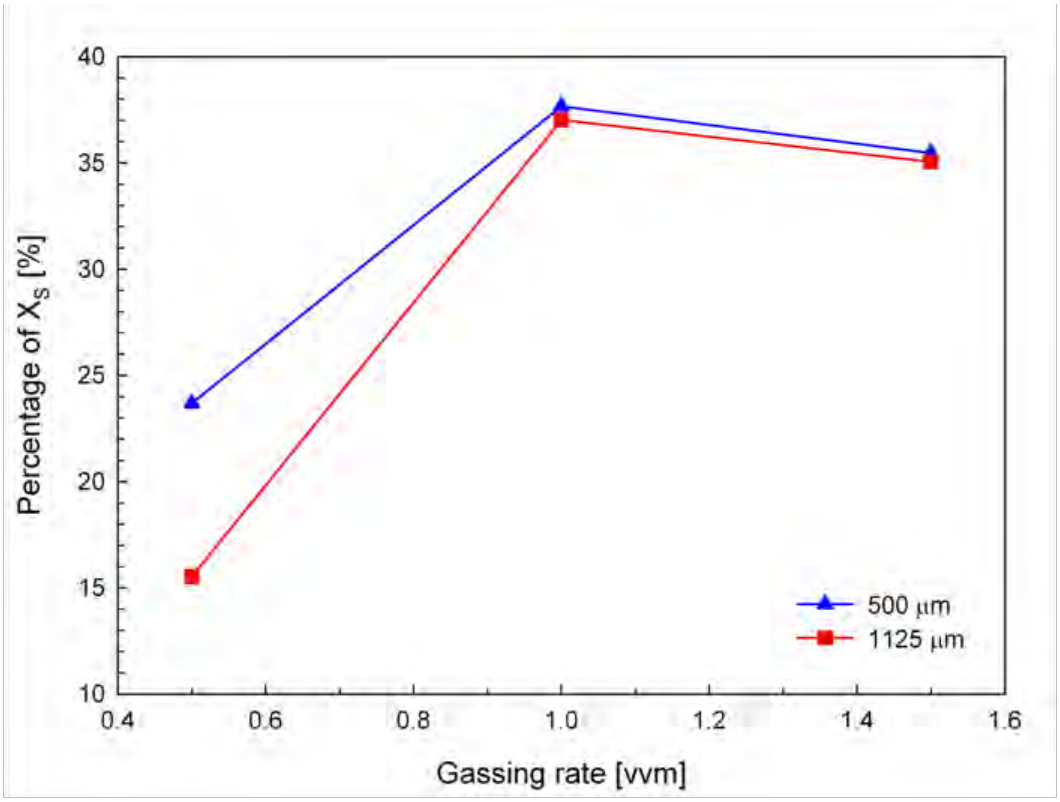

Figure 73 : Effect of particle size and sparge rate on micromixing – in percent of solid-liquid segregation index – near surface

As mentioned above, such studies in gas-solid-liquid stirred tanks have not been performed before, but other relevant factors like flow field and particle distribution in the vessel are also not as well studied as in dilute systems. However, it has been found that the significant increases in macromixing time due to cloud formation can be reduced back to near single-phase levels by gas sparging (Nienow and Bujalski 2002). This follows a similar line as the micromixing data presented here, but further investigation in particular of the flow field might be useful for feed pipe positioning.

In addition to these relatively qualitative comparisons, a more quantitative look, in particular at energy dissipation, could be useful for industry.

7.5. Interpretation with micromixing model

7.5.1. Dilute, sparged suspension

The results in section 7.3. indicate that the combination of gas and even low amounts of particles leads to changes in micromixing behaviour. Using the micromixing model variations discussed in chapter 4, the differences compared to single- and two-phase reference data will be discussed here.

Near surface – compared to single-phase

With increasing gas sparge rate there are still considerable increases, compared to liquid-only, in estimated local specific energy dissipation rates near the surface, as summarised in Table 43. However, the improvements are lower, with only around 200% for 1.5 vvm, in contrast to over 500% without added particles as shown in section 5.9.2. for the surface feed.

Table 43: Effect of sparging in dilute suspensions on ε_T – average of particle sizes compared to single-phase data – pos. 1 (near surface)

	original model	diluted + kinetics: Xie *et al.*	adapted interpolated kinetics
0.5 vvm	18.8%	24.5%	24.3%
1 vvm	70.8%	98.2%	97.0%
1.5 vvm	162.8%	243.8%	239.8%

Near surface – compared to gassed

The significant reduction in improvement of micromixing near the surface is quantified in Table 44. The changes around 30 to 40% would clearly be significant to

industrial processes. Nevertheless, the improvements shown in Table 43 still indicate major advantages of such three-phase systems over single-phase cases at equivalent mean specific power inputs. Of course, also other factors like flow stability also have to be considered for real multi-phase applications.

Table 44: Effect of sparging in dilute suspensions on ε_T – average of particle sizes compared to gas-liquid data – pos. 1 (near surface)

	original model	**diluted + kinetics: Xie *et al.***	**adapted interpolated kinetics**
0.5 vvm	-26.1%	-32.0%	-31.8%
1 vvm	-33.1%	-40.1%	-39.8%
1.5 vvm	-34.8%	-42.2%	-41.8%

Near impeller – compared to single-phase

The deviations of the segregation indices were much smaller near the impeller, in fact roughly within experimental error, and further quantification of these changes might indicate whether further studies are needed or whether the deviations can be considered negligible.

The largest changes in Table 45 are around 20% and, like those found for the most "extreme" dilute s-l case, indicate only a small, though consistent effect. For these condition there is, however, more reference data, i.e. also the s-l results, which should give similar values as found here, considering the small effect found for particles near the impeller.

Table 45: Effect of sparging in dilute suspensions on ε_T – average of particle sizes compared to single-phase data – pos. 2 (near impeller)

	original model	diluted + kinetics: Xie *et al.*	adapted interpolated kinetics
0.5 vvm	-18.4%	-22.9%	-22.6%
1 vvm	-13.1%	-16.5%	-16.2%
1.5 vvm	-4.7%	-5.9%	-5.8%

Near impeller – compared to gassed

As expected, the values in Table 46 are similar to the equivalents in Table 45 and confirm that there is an effect, which might be considered small compared to the large changes near the surface.

Table 46: Effect of sparging in dilute suspensions on ε_T – average of particle sizes compared to gas-liquid data – pos. 2 (near impeller)

	original model	diluted + kinetics: Xie *et al.*	adapted interpolated kinetics
0.5 vvm	-13.5%	-16.9%	-16.7%
1 vvm	-20.6%	-25.6%	-25.3%
1.5 vvm	3.2%	4.2%	4.1%

7.5.2. Sparged cloud

Near surface

As the patterns found for the sparged cloud did not show a clear pattern, the data will be expressed as deviation from the single-phase results using the model variations. Firstly, the effect near the surface is summarised in Table 47 and Table 48 for 500

and 1250 μm particles, respectively. At 0.5 vvm, the deviations are relatively small, around -7 to 11% of the single-phase value. The effect of the gas bubbles, however, becomes more noticeable, with improvements by several 100%, at higher gas sparge rates. This agrees with the results from the other gassed cases, but the correlation is not as clear anymore for the sparged cloud. Actually, the consistent improvements at 1 vvm stand out and comparisons for both particle sizes to the gas-liquid equivalents, in Table 49 and Table 50, emphasise this point: while the solid's negative effect is reflected in the estimated energy dissipation rates at 0.5 vvm, there are improvements for both particle sizes at 1 vvm and again worse results at 1.5 vvm.

The improvements near the surface, even compared to gas-liquid, might indicate that the particles affect the gas bubbles for instance enhancing coalescence, which might lead to more dramatic bursts at the top, or leading to some other turbulence enhancing effect. Unfortunately, the changes of behaviour cannot be explained at this point, because there is not enough information on such three-phase fluid flows.

With consideration of these changes near the surface, the feed position near the impeller needs to be addressed as well.

Table 47: Effect of sparging in dense suspensions on ε_T – 500 μm particles – compared to liquid-only data – pos. 1 (near surface)

	original model	**diluted + kinetics: Xie *et al.***	**adapted interpolated kinetics**
0.5 vvm	-6%	-7%	-7%
1 vvm	205%	316%	310%
1.5 vvm	153%	227%	223%

Table 48: Effect of sparging in dense suspensions on ε_T – 1250 μm particles – compared to liquid-only data – pos. 1 (near surface)

	original model	diluted + kinetics: Xie *et al.*	adapted interpolated kinetics
0.5 vvm	8%	11%	11%
1 vvm	445%	775%	755%
1.5 vvm	367%	619%	604%

Table 49: Effect of sparging in dense suspensions on ε_T – 500 μm particles – compared to gas-liquid data – pos. 1 (near surface)

	original model	diluted + kinetics: Xie *et al.*	adapted interpolated kinetics
0.5 vvm	-41%	-49%	-49%
1 vvm	19%	25%	25%
1.5 vvm	-37%	-45%	-45%

Table 50: Effect of sparging in dense suspensions on ε_T – 1250 μm particles – compared to gas-liquid data – pos. 1 (near surface)

	original model	diluted + kinetics: Xie *et al.*	adapted interpolated kinetics
0.5 vvm	-33%	-40%	-39%
1 vvm	113%	164%	161%
1.5 vvm	16%	21%	20%

Near impeller

Table 51 and Table 52 give the specific energy dissipation rates near the impeller for 500 and 1125 μm particles, respectively, compared to the single-phase case. In Table 53 and Table 54 this data is given relative to the gas-liquid data. As gas-

sparging did not affect micromixing near the impeller, the results in these table groups are very similar: while the 500 μm particles do still dampen turbulence in the cloud, the one with the larger solids seems to have been broken up by the gas sparging. Even though the 1125 μm glass beads had a stronger effect at this feed position without gas, the cloud was less pronounced. This might explain why with is more easily affected by changes in the flow. Interestingly, the deviation at 1 vvm can also be seen with the smaller particles in this case, but neither visual observation of the flow nor the limited knowledge of such flows aids understanding of these novel results. They do, however, give valuable information on micromixing and also feed pipe positioning in multi-phase stirred reactors.

Table 51: Effect of sparging in dense suspensions on ε_T – 500 μm particles – compared to liquid-only data – pos. 2 (near impeller)

	original model	diluted + kinetics: Xie *et al.*	adapted interpolated kinetics
0.5 vvm	-25%	-31%	-30%
1 vvm	-43%	-51%	-50%
1.5 vvm	-18%	-22%	-22%

Table 52: Effect of sparging in dense suspensions on ε_T – 1250 μm particles – compared to liquid-only data – pos. 2 (near impeller)

	original model	diluted + kinetics: Xie *et al.*	adapted interpolated kinetics
0.5 vvm	-5%	-6%	-6%
1 vvm	-5%	-7%	-7%
1.5 vvm	18%	23%	23%

Table 53: Effect of sparging in dense suspensions on ε_T – 500 μm particles – compared to gas-liquid data – pos. 2 (near impeller)

	original model	diluted + kinetics: Xie *et al.*	adapted interpolated kinetics
0.5 vvm	-20%	-25%	-25%
1 vvm	-48%	-56%	-56%
1.5 vvm	-11%	-14%	-14%

Table 54: Effect of sparging in dense suspensions on ε_T – 1250 μm particles – compared to gas-liquid data – pos. 2 (near impeller)

	original model	diluted + kinetics: Xie *et al.*	adapted interpolated kinetics
0.5 vvm	1%	1%	1%
1 vvm	-14%	-17%	-17%
1.5 vvm	27%	36%	36%

7.6. Conclusions

Micromixing in a gas-solid-liquid stirred tank was investigated using the Iodide/iodate reaction scheme, using dilute and dense suspensions for two particle sizes over a range of gas sparge rates while keeping mean specific energy input constant. Experimental conditions were chosen to give good particle suspension while still allowing reference measurements without entrainment of air from the surface.

While low concentrations of glass beads had not affected micromixing in the solid-liquid measurements, it was found that already these small amounts lower micromixing efficiency compared to just sparged conditions. In sparged clouds, the effects were consistent but less straight-forward to summarise: the gas bubbles

improved micromixing near the surface, compared to the very poor solid-liquid results and, overall, also to the single-phase ones. Near the impeller, there clearly were effects due to sparging the cloud. However, these cannot be explained at this point but seem to depend on aeration rate and particle size.

8. CONCLUSIONS AND FUTURE WORK

8.1. Conclusions – discussed by chapter

The aims set out in the introduction in section 1.1 have been addressed throughout this thesis and the conclusions are given here briefly. For clarity, they are summarised for each chapter separately.

Incorporation model: adaption and its use to interpret experimental data

In order to quantify experimental results obtained from the iodide/iodate method, employing a reliable micromixing model would be useful, but, so far, such approaches have not been very successful for this reaction scheme. This might be explained by kinetic data on the Dushman reaction used in previous studies. In addition, the sulphuric acid has been assumed to be fully dissociated which has been shown to be wrong. Therefore, the incorporation model was extended to include the ionisation of the sulphuric acid and a range of kinetic rate laws from literature were tested. It was found that such modelling is useful for comparison purposes. Moreover, the adapted version of the model employing estimated kinetic behaviour for these specific conditions gives realistic absolute values for local specific energy dissipation rates. At the moment, it has to be concluded that there is still need for information on the chemistry involved. However, some steps in this direction have been made here and, once new data becomes available, the variations of the Incorporation model as presented here can be adapted accordingly.

Micromixing in gas-liquid systems

The suitability of using air for experiments with the Iodide/Iodate reaction scheme was confirmed and three feed positions were studied. There was no effect of gas sparging for feeding near the impeller, when power from the impeller was kept constant, and also little, if any, effect below the impeller. Near the free surface, however, there were significant improvements with increasing gas sparge rate. Estimates from the micromixing model suggest increases of up to 2000% compared to the single-phase equivalents which indicates positive effects for such industrial applications, though even higher micromixing efficiencies were still found for feeding near the impeller.

Micromixing in solid-liquid systems

The use of glass beads was validated for use with the employed reaction scheme. Considering the conflicting literature, the possible effects of a range of particle sizes and concentrations were investigated for feeding near the surface, near the impeller and at ε_{max}. At low concentrations, when particle interaction was not significant, micromixing was not affected by the presence of the solids. When particle interaction became relevant, i.e. in more dense suspensions, micromixing became worse. Especially the formation of clouds leads to significant damping, in the cloud and even more in the clear liquid layer above the cloud. This clearly showed the importance of feed pipe positioning. The effects were also evaluated using the micromixing model. In literature, a small amount of information on turbulence levels above a solids cloud has been reported and good agreement with the results presented here has been found.

Micromixing in liquid-gas-solid systems

Even low amounts of solid particles have been found to negatively affect micromixing under gas-solid-liquid conditions compared to just gas-liquid, although this is not the case in solid-liquid equivalents. At higher solids concentration, i.e. when cloud formation occurs, gas sparging improved micromixing near the surface compared to feeding into the clear liquid layer without gas bubbles. Overall, complex behaviour was found at these conditions for feeding near the surface and near the impeller. Unfortunately, there is little information on fluid flow behaviour for these conditions and, therefore, explanation of the observed micromixing data is difficult.

8.2. Suggestions for future work

Although a range of questions and tasks have been tackled, further work can, of course, be done in this context. Some new results might be studied from different points of view to find explanations for the observations made here and a few other ideas or suggestions could be followed in the future.

For the reaction scheme itself, further studies on the kinetics are necessary, especially work considering the conditions of micromixing experiments in stirred tanks. This should allow adequate comparison of different reactant concentrations and ultimately give a quantitatively reliable method.
Such data could be easily applied to the presented model variations.

Although light has been shed on the effect of the presence of solid particles, it is still a conflicting topic in mixing literature and a smaller study comparing different flows,

i.e. from a Rushton turbine and pitched-blade impeller, using competing reactions and PIV would be of interest. In addition, a dished bottom might allow better solid suspension without air entrainment from the surface which would widen the range of possible experimental conditions.

There is still a lack of knowledge on details of fluid flow and particle distribution in three-phase systems. This is limiting for the interpretation of the results found here. However, newer methods like PEPT could soon give new insights into such systems.

REFERENCES

Agreda B., J. A., R. J. Field and N. J. Lyons (2000). "Kinetic Evidence for Accumulation of Stoichiometrically Significant Amounts of H2I2O3 during the Reaction of I- with IO3." The Journal of Physical Chemistry A **104**(22): 5269-5274.

Anderson, J. D. (1995). Computational fluid dynamics: the basics with applications. New York ; London, McGraw-Hill.

Argoul, F., A. Arneodo, G. Grasseau, Y. Gagne, E. J. Hopfinger and U. Frisch (1989). "Wavelet analysis of turbulence reveals the multifractal nature of the Richardson cascade." Nature **338**(6210): 51-53.

Armenante, P. M., C. Luo, C.-C. Chou, I. Fort and J. Medek (1997). "Velocity profiles in a closed, unbaffled vessel: comparison between experimental LDV data and numerical CFD predictions." Chemical Engineering Science **52**(20): 3483-3492.

Ascanio, G., B. Castro and E. Galindo (2004). "Measurement of Power Consumption in Stirred Vessels--A Review." Chemical Engineering Research and Design **82**(9): 1282-1290.

Assirelli, M. (2004). Micromixing studies in turbulent stirred baffled and unbaffled vessels agitated by a Rushton turbine: an experimental study. School of Engineering, Chemical Engineering, University of Birmingham. **PhD thesis**.

Assirelli, M., W. Bujalski, A. Eaglesham and A. W. Nienow (2002). "Study Of Micromixing in a Stirred Tank Using a Rushton Turbine: Comparison of Feed Positions and Other Mixing Devices." Chemical Engineering Research and Design **80**(8): 855-863.

Assirelli, M., W. Bujalski, A. Eaglesham and A. W. Nienow (2005). "Intensifying micromixing in a semi-batch reactor using a Rushton turbine." Chemical Engineering Science **60**(8-9): 2333-2339.

Assirelli, M., W. Bujalski, A. Eaglesham and A. W. Nienow (2008a). "Macro- and micromixing studies in an unbaffled vessel agitated by a Rushton turbine." Chemical Engineering Science **63**(1): 35-46.

Assirelli, M., S. P. Lee and A. W. Nienow (2011a). "Further Studies of Micromixing: Scale-Up, Baffling and Feed Pipe Backmixing." Journal of Chemical Engineering of Japan **44**(11): 901-907.

Assirelli, M., S. P. Lee and A. W. Nienow (2011b). "Further Studies of Micromixing: Scale-Up, Baffling and Feed Pipe Backmixing." Journal of Chemical Engineering of Japan **44**.

Assirelli, M., E. J. W. Wynn, W. Bujalski, A. Eaglesham and A. W. Nienow (2008b). "An extension to the incorporation model of micromixing and its use in estimating local specific energy dissipation rates." Industrial & Engineering Chemistry Research **47**(10): 3460-3469.

Aubin, J., M. Ferrando and V. Jiricny (2010). "Current methods for characterising mixing and flow in microchannels." Chemical Engineering Science **65**(6): 2065-2093.

Awtrey, A. D. and R. E. Connick (1951). "The Absorption Spectra of I2, I3-, I-, IO3-, S4O6= and S2O3=. Heat of the Reaction I3- = I2 + I." Journal of the American Chemical Society **73**(4): 1842-1843.

Baccar, N., R. Kieffer and C. Charcosset (2009). "Characterization of mixing in a hollow fiber membrane contactor by the iodide-iodate method: Numerical simulations and experiments." Chemical Engineering Journal **148**(2-3): 517-524.

Balachandar, S. and J. K. Eaton (2010). "Turbulent Dispersed Multiphase Flow." Annual Review of Fluid Mechanics **42**(1): 111-133.

Baldi, G., R. Conti and E. Alaria (1978). "Complete suspension of particles in mechanically agitated vessels." Chemical Engineering Science **33**(1): 21-25.

Baldi, S. and M. Yianneskis (2004). "On the quantification of energy dissipation in the impeller stream of a stirred vessel from fluctuating velocity gradient measurements." Chemical Engineering Science **59**(13): 2659-2671.

Baldyga, J. and J. R. Bourne (1984). "A fluid mechanical approach to turbulent mixing and chemical reaction part II Micromixing in the light of turbulence theory." Chemical Engineering Communications **28**(4-6): 243-258.

Baldyga, J. and J. R. Bourne (1989a). "Simplification of micromixing calculations. I. Derivation and application of new model." The Chemical Engineering Journal **42**(2): 83-92.

Baldyga, J. and J. R. Bourne (1989b). "Simplification of micromixing calculations. II. New applications." The Chemical Engineering Journal **42**(2): 93-101.

Baldyga, J. and J. R. Bourne (1990). "Comparison of the engulfment and the interaction-by-exchange-with-the-mean micromixing models." The Chemical Engineering Journal **45**(1): 25-31.

Baldyga, J. and J. R. Bourne (1992). "Interactions between mixing on various scales in stirred tank reactors." Chemical Engineering Science **47**(8): 1839-1848.

Baldyga, J. and J. R. Bourne (1999). Turbulent mixing and chemical reactions, John Wiley & Sons Inc.

Baldyga, J., J. R. Bourne and S. J. Hearn (1997). "Interaction between chemical reactions and mixing on various scales." Chemical Engineering Science **52**(4): 457-466.

Baldyga, J. and J. R. Y. Bourne, Yang (1993). "Influence of feed pipe diameter on mesomixing in stirred tank reactors." Chemical Engineering Science **48**(19): 3383-3390.

Baldyga, J., W. Podgórska and R. Pohorecki (1995). "Mixing-precipitation model with application to double feed semibatch precipitation." Chemical Engineering Science **50**(8): 1281-1300.

Baldyga, J. and R. Pohorecki (1995). "Turbulent micromixing in chemical reactors - a review." The Chemical Engineering Journal **58**(2): 183-195.

Balkovsky, E., G. Falkovich and A. Fouxon (2001). "Intermittent Distribution of Inertial Particles in Turbulent Flows." Physical Review Letters **86**(13): 2790.

Bamford, C. H. and C. F. H. Tipper (1972). Comprehensive chemical kinetics. Amsterdam, Elsevier.

Barigou, M. and M. Greaves (1992). "Bubble-size distributions in a mechanically agitated gas-liquid contactor." Chemical Engineering Science **47**(8): 2009-2025.

Barresi, A. A. (1997). "Experimental investigation of interaction between turbulent liquid flow and solid particles and its effects on fast reactions." Chemical Engineering Science **52**(5): 807-814.

Barresi, A. A. (2000). "Selectivity of mixing-sensitive reactions in slurry systems." Chemical Engineering Science **55**(10): 1929-1933.

Barton, A. F. M. and G. A. Wright (1968). "Kinetics of the iodate-iodide reaction: catalysis by carboxylate and phosphate ions." Journal of the Chemical Society A: Inorganic, Physical, Theoretical: 2096-2103.

Bennington, C. P. J. and J. R. Bourne (1990). "Effect of suspended fibres on macro-mixing and micro-mixing in a stirred tank reactor." Chemical Engineering Communications **92**(1): 183-197.

Bennington, C. P. J. and V. K. Thangavel (1993). "The use of a mixing-sensitive chemical reaction for the study of pulp fibre suspension mixing." The Canadian Journal of Chemical Engineering **71**(5): 667-675.

Best, J., S. Bennett, J. Bridge and M. Leeder (1997). "Turbulence Modulation and Particle Velocities over Flat Sand Beds at Low Transport Rates." Journal of Hydraulic Engineering **123**(12): 1118-1129.

Bhattacharya, S. and S. M. Kresta (2004). "Surface Feed with Minimum by-Product Formation for Competitive Reactions." Chemical Engineering Research and Design **82**(9): 1153-1160.

Bichsel, Y. and U. von Gunten (2000). "Hypoiodous acid: kinetics of the buffer-catalyzed disproportionation." Water Research **34**(12): 3197-3203.

Bittorf, K. J. and S. M. Kresta (2003). "Prediction of Cloud Height for Solid Suspensions in Stirred Tanks." Chemical Engineering Research and Design **81**(5): 568-577.

Boulton-Stone, J. M. and J. R. Blake (1993). "Gas bubbles bursting at a free surface." Journal of Fluid Mechanics **254**: 437-466.

Bourne, J. R. (1994). "Distribution of energy dissipation rate in an agitated gas-liquid system." Chemical Engineering & Technology **17**(5): 323-324.

Bourne, J. R. (1997). Mixing and the selectivity of fast chemical reactions. Handbook of batch process design. P. N. Sharratt. London, Blackie Academic and Professional.

Bourne, J. R. (2008). "Comments on the iodide/iodate method for characterising micromixing." Chemical Engineering Journal **140**(1-3): 638-641.

Bourne, J. R., F. Kozicki, U. Moergeli and P. Rys (1981a). "Mixing and fast chemical reaction--III : Model-experiment comparisons." Chemical Engineering Science **36**(10): 1655-1663.

Bourne, J. R., F. Kozicki and P. Rys (1981b). "Mixing and fast chemical reaction--I : Test reactions to determine segregation." Chemical Engineering Science **36**(10): 1643-1648.

Bourne, J. R. and S. A. Thoma (1991). "Shorter Communication-Some Factors Determining The Critical Feed Time of a Semi-Batch Reactor." Chemical Engineering Research and Design **69**(a): 321-323.

Bourne, J. R. and G. Tovstiga (1988). "Micromixing and Fast Chemical-Reactions in a Turbulent Tubular Reactor." Chemical Engineering Research and Design **66**(1): 26-32.

Bourne, J. R. and S. Yu (1994). "Investigation of micromixing in stirred tank reactors using parallel reactions." Industrial & Engineering Chemistry Research **33**(1): 41-55.

Brennen, C. E. (2005). Fundamentals of Multiphase Flow, Cambridge University Press.

Brilman, D. W. F., R. Antink, W. P. M. van Swaaij and G. F. Versteeg (1999). "Experimental study of the effect of bubbles, drops and particles on the product distribution for a mixing sensitive, parallel-consecutive reaction system." Chemical Engineering Science **54**(13-14): 2325-2337.

Brucato, A. and V. Brucato (1998). "Unsuspended mass of solid particles in stirred tanks." The Canadian Journal of Chemical Engineering **76**(3): 420-427.

Brucato, A., F. Grisafi and G. Montante (1998). "Particle drag coefficients in turbulent fluids." Chemical Engineering Science **53**(18): 3295-3314.

Bujalski, J. M. (2003). Computational fluid dynamic modelling of stirred reactors : power, baffle stresses, mixing times and semi-batch precipitation. School of Engineering, Department of Chemical Engineering, University of Birmingham. **PhD thesis**.

Bujalski, J. M., Z. Jaworski, W. Bujalski and A. W. Nienow (2002). "The Influence of the Addition Position of a Tracer on CFD Simulated Mixing Times in a Vessel Agitated by a Rushton Turbine." Chemical Engineering Research and Design **80**(8): 824-831.

Bujalski, W. (1986). Three phase mixing: studies of geometry, viscosity and scale. Department of Chemical Engineering. Birmingham, University of Birmingham. **PhD thesis**.

Bujalski, W., A. W. Nienow, S. Chatwin and M. Cooke (1987). "The dependency on scale of power numbers of Rushton disc turbines." Chemical Engineering Science **42**(2): 317-326.

Bujalski, W., K. Takenaka, S. Paoleni, M. Jahoda, A. Paglianti, K. Takahashi, A. W. Nienow and A. W. Etchells (1999). "Suspension and Liquid Homogenization in High Solids Concentration Stirred Chemical Reactors." Chemical Engineering Research and Design **77**(3): 241-247.

Buxton, G. V. and Q. G. Mulazzani (2007). "On the hydrolysis of iodine in alkaline solution: A radiation chemical study." Radiation Physics and Chemistry **76**(6): 932 - 940-932 - 940.

Buxton, G. V. and R. M. Sellers (1985). "Radiation-induced redox reactions of iodine species in aqueous solution. Formation and characterisation of III, IIV, IVI and IVIII, the stability of hypoiodous acid and the chemistry of the interconversion of iodide and iodate." Journal of the Chemical Society, Faraday Transactions 1: Physical Chemistry in Condensed Phases **81**(2): 449-471.

Camps Rota, M. (1998). Etude du micromelange dans des reactuers chimiques. Final Year Project Report, Institut National Polytechnique de Lorraine (ENSIC).

Chapman, C. M., M. Cooke, A. W. Nienow and J. C. Middleton (1983a). "Particle-gas-liquid mixing in stirred vessels-Part 3: three phase mixing." Chemical Engineering Research and Design **61**: 167-81.

Chapman, C. M., A. W. Nienow, M. Cooke and J. C. Middleton (1983b). "Particle-gas-liquid mixing in stirred vessels-Part I: Particle-Liquid Mixing." Chemical Engineering Research and Design **61**(a): 71-81.

Chapman, C. M., A. W. Nienow, M. Cooke and J. C. Middleton (1983c). "Particle-gas-liquid mixing in stirred vessels-Part II: Gas-Liquid Mixing." Chemical Engineering Research and Design **61**(a): 82-95.

Chiti, F. (2008). Lagrangian studies of turbulent mixing in a vessel agitated by a rushron turbine: positron emission particle tracking (PEPT) and computational fluid dynamics (CFD). , University of Birmingham. **PhD Thesis**.

Chiti, F., S. Bakalis, W. Bujalski, M. Barigou, A. Eaglesham and A. W. Nienow (2011). "Using Positron Emission Particle Tracking (PEPT) to Study the Turbulent Flow in a Baffled Vessel Agitated by a Rushton Turbine: Improving Data Treatment and Validation." Chemical Engineering Research and Design **89**(10): 1947–1960.

Ciofalo, M., A. Brucato, F. Grisafi and N. Torraca (1996). "Turbulent flow in closed and free-surface unbaffled tanks stirred by radial impellers." Chemical Engineering Science **51**(14): 3557-3573.

Clay Mathematics, I. (2011). "Clay Mathematics Institute Millennium Prize." Retrieved 15. 11. 2011, from http://www.claymath.org/millennium/Navier-Stokes_Equations/.

Cooke, M., J. C. Middleton and J. R. Bush (1988). Mixing and mass transfer in filamentous fermentations. Proceedings of the 2nd International Conference on Bioreactor Fluid Dynamics, BHRA, Cambridge, Elsevier Applied Science Publishers: Amsterdam.

Cooper, C. M., G. A. Fernstrom and S. A. Miller (1944). "Performance of agitated gas-liquid contactors." Industrial and Engineering Chemistry **36**: 504-509.

Costa, P. and C. Trevissoi (1972a). "Reactions with non-linear kinetics in partially segregated fluids." Chemical Engineering Science **27**(11): 2041-2054.

Costa, P. and C. Trevissoi (1972b). "Some kinetic and thermodynamic features of reactions between partially segregated fluids." Chemical Engineering Science **27**(4): 653-668.

Costes, J. and J. P. Couderc (1988). "Study by laser Doppler anemometry of the turbulent flow induced by a Rushton turbine in a stirred tank: Influence of the size of the units--II. Spectral analysis and scales of turbulence." Chemical Engineering Science **43**(10): 2765-2772.

Craig, V. S. J., B. W. Ninham and R. M. Pashley (1993). "The effect of electrolytes on bubble coalescence in water." The Journal of Physical Chemistry **97**(39): 10192-10197.

Crowe, C. T., T. R. Troutt and J. N. Chung (1996). "Numerical models for two-phase turbulent flows." Annual Review of Fluid Mechanics **28**(1): 11-43.

Custer, J. J. and S. Natelson (1949). "Spectrophotometric Determination of Microquantities of Iodine." Analytical Chemistry **21**(8): 1005-1009.

Cutter, L. A. (1966). "Flow and turbulence in a stirred tank." AIChE Journal **12**(1): 35-45.

Davidson, P. A. (2004). Turbulence: an introduction for scientists and engineers, Oxford University Press, USA.

Davies, J. T. (1972). Turbulence phenomena, Academic Press New York.

Deen, N. G. and B. H. Hjertager (2002). "Particle image velocimetry measurements in an aerated stirred tank." Chemical Engineering Communications **189**(9): 1208-1221.

Derksen, J. J. (2003). "Numerical simulation of solids suspension in a stirred tank." AIChE Journal **49**(11): 2700-2714.

Dong, L., S. T. Johansen and T. A. Engh (1994a). "Flow induced by an impeller in an unbaffled tank--I. Experimental." Chemical Engineering Science **49**(4): 549-560.

Dong, L., S. T. Johansen and T. A. Engh (1994b). "Flow induced by an impeller in an unbaffled tank--II. Numerical modelling." Chemical Engineering Science **49**(20): 3511-3518.

Doroodchi, E., G. M. Evans, M. P. Schwarz, G. L. Lane, N. Shah and A. Nguyen (2008). "Influence of turbulence intensity on particle drag coefficients." Chemical Engineering Journal **135**(1-2): 129-134.

Ducci, A. and M. Yianneskis (2005). "Direct determination of energy dissipation in stirred vessels with two-point LDA." AIChE Journal **51**(8): 2133-2149.

Dushman, S. (1904). "The Rate of the Reaction between Iodic and Hydriodic Acids." The Journal of Physical Chemistry **8**(7): 453-482.

Dyster, K., E. Koutsakos, Z. Jaworski and A. Nlenow (1993). "An LDA study of the Radial discharge velocities generated by a Rushton turbine." Transactions of the Institution of Chemical Engineers **71**: 11-23.

Eaton, J. K. and J. R. Fessler (1994). "Preferential concentration of particles by turbulence." International Journal of Multiphase Flow **20**(Supplement 1): 169-209.

Einsele, A. and R. K. Finn (1980). "Influence of Gas Flow Rates and Gas Holdup on Blending Efficiency in Stirred Tanks." Industrial & Engineering Chemistry Process Design and Development **19**(4): 600-603.

Elghobashi, S. (1994). "On predicting particle-laden turbulent flows." Applied Scientific Research **52**(4): 309-329.

Falk, L. and J. M. Commenge (2010). "Performance comparison of micromixers." Chemical Engineering Science **65**(1): 405-411.

Fang, J. Z. and D. J. Lee (2001). "Micromixing efficiency in static mixer." Chemical Engineering Science **56**(12): 3797-3802.

Fangary, Y. S., M. Barigou, J. P. K. Seville and D. J. Parker (2000). "Fluid trajectories in a stirred vessel of non-newtonian liquid using positron emission particle tracking." Chemical Engineering Science **55**(24): 5969-5979.

Ferrante, A. and S. Elghobashi (2003). "On the physical mechanisms of two-way coupling in particle-laden isotropic turbulence." Physics of Fluids **15**(2): 315-329.

Fessler, J. R. and J. K. Eaton (1999). "Turbulence modification by particles in a backward-facing step flow." Journal of Fluid Mechanics **394**(-1): 97-117.

Fort, I., V. Machon and P. Kadlec (1993). "Distribution of energy dissipation rate in an agitated gas-liquid system." Chemical Engineering & Technology **16**(6): 389-394.

Fournier, M. C., L. Falk and J. Villermaux (1996a). "A new parallel competing reaction system for assessing micromixing efficiency--Determination of micromixing time by a simple mixing model." Chemical Engineering Science **51**(23): 5187-5192.

Fournier, M. C., L. Falk and J. Villermaux (1996b). "A new parallel competing reaction system for assessing micromixing efficiency--Experimental approach." Chemical Engineering Science **51**(22): 5053-5064.

Fox, R. O. (1998). "On the relationship between Lagrangian micromixing models and computational fluid dynamics." Chemical Engineering and Processing **37**(6): 521-535.

Fox, R. O. and J. Villermaux (1990). "Unsteady-state IEM model: numerical simulation and multiple-scale perturbation analysis near perfect-micromixing limit." Chemical Engineering Science **45**(2): 373-386.

Frijlink, J. J., A. Bakker and J. M. Smith (1990). "Suspension of solid particles with gassed impellers." Chemical Engineering Science **45**(7): 1703-1718.

Gabriele, A., A. W. Nienow and M. J. H. Simmons (2009). "Use of angle resolved PIV to estimate local specific energy dissipation rates for up- and down-pumping pitched blade agitators in a stirred tank." Chemical Engineering Science **64**(1): 126-143.

Gabriele, A., A. N. Tsoligkas, I. N. Kings and M. J. H. Simmons (2011). "Use of PIV to measure turbulence modulation in a high throughput stirred vessel with the addition of high Stokes number particles for both up- and down-pumping configurations." Chemical Engineering Science **66**(23): 5862-5874.

Geisler, R. K. and A. B. Mersmann (1988). Local velocity distribution and power dissipation rate of suspensions in stirred vessels. Sixth European Conference on Mixing, Pavia, Italy, BHRA Cranfield, Bedford (England).

Gore, R. A. and C. T. Crowe (1989). "Effect of particle size on modulating turbulent intensity." International Journal of Multiphase Flow **15**(2): 279-285.

Gore, R. A. and C. T. Crowe (1991). "Modulation of turbulence by a dispersed phase." Journal of Fluids Engineering **113**(2): 304-307.

Guha, D., P. A. Ramachandran and M. P. Dudukovic (2007). "Flow field of suspended solids in a stirred tank reactor by Lagrangian tracking." Chemical Engineering Science **62**(22): 6143-6154.

Guichardon, P. (1996). Caracterisation chimique du micromelange par la reaction iodure-iodate. Nancy, France, Institut national polytechnique de Lorraine ENSIC. **PhD thesis**.

Guichardon, P. and L. Falk (2000). "Characterisation of micromixing efficiency by the iodide-iodate reaction system. Part I: experimental procedure." Chemical Engineering Science **55**(19): 4233-4243.

Guichardon, P., L. Falk, M. C. Fournier and J. Villermaux (1995). "Study of micromixing in a liquid-solid suspension in a stirred reactor." AIChE Symposium Series **91**(305): 123-130.

Guichardon, P., L. Falk and J. Villermaux (2000). "Characterisation of micromixing efficiency by the iodide-iodate reaction system. Part II: kinetic study." Chemical Engineering Science **55**(19): 4245-4253.

Guida, A. (2010). Positron Emission Particle Tracking Applied to Solid-Liquid Mixing in Mechanically Agitated Vessels. School of Chemical Engineering. Birmingham, University of Birmingham. **PhD thesis**.

Guida, A., A. W. Nienow and M. Barigou (2010). "PEPT measurements of solid-liquid flow field and spatial phase distribution in concentrated monodisperse stirred suspensions." Chemical Engineering Science **65**(6): 1905-1914.

Guiraud, P., J. Costes and J. Bertrand (1997). "Local measurements of fluid and particle velocities in a stirred suspension." Chemical Engineering Journal **68**(2-3): 75-86.

Harada, M., K. Arima, W. Eguchi and S. Nagata (1962). "Micro-mixing in a continuous flow reactor (coalescence and redispersion models)." The Memoirs of the Faculty of Engineering, Kyoto University **24**: 431–446.

Harnby, N., M. F. Edwards and A. W. Nienow (1997). Mixing in the Process Industries. Oxford, Butterworth-Heinemann.

Harris, D. C. (1995). Quantitative Chemical Analysis. New York, WH Freeman and Company.

Herbo, C. and J. Sigalla (1957). "Principes de l'iodimétrie absorptiométrique." Analytica Chimica Acta **17**: 199-207.

Hetsroni, G. (1989). "Particles-turbulence interaction." International Journal of Multiphase Flow **15**(5): 735-746.

Hiby, J. W. (1979). "Definition und Messung der Mischgüte in flüssigen Gemischen." Chemie Ingenieur Technik **51**(7): 704-709.

Hicks, M. T., K. J. Myers and A. Bakker (1997). "Cloud height in solids suspension agitation." Chemical Engineering Communications **160**(1): 137-155.

Hilber, C. P. (1987). Untersuchungen zur Mikrovermischung in der flüssigen Phase eines begasten Rührkessels, ETH Zuerich. **PhD thesis**.

Hinze, J. O. (1975). Turbulence. New York, McGraw-Hill.

Hofinger, J., R. W. Sharpe, W. Bujalski, S. Bakalis, M. Assirelli, A. Eaglesham and A. W. Nienow (2011). "Micromixing in two-phase (G-L and S-L) systems in a stirred vessel." The Canadian Journal of Chemical Engineering **89**(5): 1029-1039.

Hutchinson, P., G. F. Hewitt and A. E. Dukler (1971). "Deposition of liquid or solid dispersions from turbulent gas streams: a stochastic model." Chemical Engineering Science **26**(3): 419-439.

Joshi, J. B., A. B. Pandit and M. M. Sharma (1982). "Mechanically agitated gas-liquid reactors." Chemical Engineering Science **37**(6): 813-844.

Kasat, G. R. and A. B. Pandit (2005). "Review on Mixing Characteristics in Solid-Liquid and Solid-Liquid-Gas Reactor Vessels." The Canadian Journal of Chemical Engineering **83**(4): 618-643.

Khopkar, A. R., J. Aubin, C. Xuereb, N. Le Sauze, J. Bertrand and V. V. Ranade (2003). "Gas-Liquid Flow Generated by a Pitched-Blade Turbine: Particle Image Velocimetry Measurements and Computational Fluid Dynamics Simulations." Industrial & Engineering Chemistry Research **42**(21): 5318-5332.

Khopkar, A. R., A. R. Rammohan, V. V. Ranade and M. P. Dudukovic (2005). "Gas-liquid flow generated by a Rushton turbine in stirred vessel: CARPT/CT measurements and CFD simulations." Chemical Engineering Science **60**(8-9): 2215-2229.

Kölbl, A. (2008). "Further comments on the Iodide Iodate Reaction Method for characterising micromixing." Chemical Engineering Journal **145**(1): 176-177.

Kölbl, A., V. Desplantes, L. Grundemann and S. Scholl (2011). Investigation of the Dushman Reaction at Concentrations relevant to Mixing Studies in Stirred Tank Reactors. AIChE Annual Meeting, Minneapolis.

Kölbl, A. and K. Hecht (2012). Personal communication on pH-measurements and equilibrium calculations. Karlsruhe.

Kölbl, A., M. Kraut and K. Schubert (2008). "The iodide iodate method to characterize microstructured mixing devices." AIChE Journal **54**(3): 639-645.

Kölbl, A. and S. Schmidt-Lehr (2010). "The iodide iodate reaction method: The choice of the acid." Chemical Engineering Science **65**(5): 1897-1901.

Kolmogorov, A. (1941). The local structure of turbulence in incompressible viscous fluid for very large Reynolds' numbers. Doklady Akademiia Nauk SSSR. **30:** 301-305.

Kowalski, A. J., M. Cooke and S. Hall (2011). "Expression for turbulent power draw of an in-line Silverson high shear mixer." Chemical Engineering Science **66**(3): 241-249.

Kraume, M. (1992). "Mixing times in stirred suspensions." Chemical Engineering & Technology **15**(5): 313-318.

Kresta, S. (1998). "Turbulence in stirred tanks: Anisotropic, approximate, and applied." The Canadian Journal of Chemical Engineering **76**(3): 563-576.

Kresta, S. M. and P. E. Wood (1993). "The flow field produced by a pitched blade turbine: Characterization of the turbulence and estimation of the dissipation rate." Chemical Engineering Science **48**(10): 1761-1774.

Lane, G. L., M. P. Schwarz and G. M. Evans (2004). "Numerical modelling of gas-liquid flow in stirred tanks." Chemical Engineering Science **60**(8-9): 2203-2214.

Langheinrich, C. and A. W. Nienow (1999). "Control of pH in large-scale, free suspension animal cell bioreactors: Alkali addition and pH excursions." Biotechnology and Bioengineering **66**(3): 171-179.

Laufhütte, H. D. and A. Mersmann (1987). "Local energy dissipation in agitated turbulent fluids and its significance for the design of stirring equipment." Chemical Engineering & Technology **10**(1): 56-63.

Lee, K. C. and M. Yianneskis (1998). "Turbulence properties of the impeller stream of a Rushton turbine." AIChE Journal **44**(1): 13-24.

Lee, S. P., M. Assirelli and A. W. Nienow (2007). Effects Of Feed Pipe Backmixing on Micromixing: An Experimental Study. Mixing XXI. Park City, Utah.

Leenson, I. A. (2004). "Sulfuric Acid and Water: Paradoxes of Dilution." Journal of Chemical Education **81**(7): 991-994.

Lessard, R. R. and S. A. Zieminski (1971). "Bubble Coalescence and Gas Transfer in Aqueous Electrolytic Solutions." Industrial & Engineering Chemistry Fundamentals **10**(2): 260-269.

Levins, D. M. and J. R. Glastonbury (1972). "Particle-Liquid Hydrodynamics and Mass Transfer in a Stirred Vessel-Part II-Mass Transfer." Chemical Engineering Research and Design **50**(a): 132-146.

Li, Y.-f., H.-q. Ye, X.-d. He, K. Han and H. Liu (2012). "Synthesis of Ce-doped yttrium aluminum garnet phosphor by impinging streams co-precipitation." Journal of Central South University of Technology **19**(2): 324-330.

Liebhafsky, H. A. and G. M. Roe (1979). "The detailed mechanism of the Dushman reaction explored by computer." International Journal of Chemical Kinetics **11**(7): 693-703.

Lin, W. W. and D. J. Lee (1997). "Micromixing effects in aerated stirred tank." Chemical Engineering Science **52**(21): 3837-3842.

Lohse, D. (2008). "Particles go with the flow." Physics **1**: 18.

Lu, W.-M. and S.-J. Ju (1987). "Local gas holdup, mean liquid velocity and turbulence in an aerated stirred tank using hot-film anemometry." The Chemical Engineering Journal **35**(1): 9-17.

Marchisio, D. L. and A. A. Barresi (2003). "CFD simulation of mixing and reaction: the relevance of the micro-mixing model." Chemical Engineering Science **58**(16): 3579-3587.

Mavros, P. (2001). "Flow Visualization in Stirred Vessels: A Review of Experimental Techniques." Chemical Engineering Research and Design **79**(2): 113-127.

Maxey, M. R. (1987). "The gravitational settling of aerosol particles in homogeneous turbulence and random flow fields." Journal of Fluid Mechanics **174**: 441-465.

Melling, A. (1997). "Tracer particles and seeding for particle image velocimetry." Measurement Science and Technology **8**(12): 1406.

Micale, G., G. Montante, F. Grisafi, A. Brucato and J. Godfrey (2000). "CFD Simulation of Particle Distribution in Stirred Vessels." Chemical Engineering Research and Design **78**(3): 435-444.

Michaelides, E. (2006). Particles, bubbles & drops: their motion, heat and mass transfer, World Scientific Pub Pte Inc.

Michel, B. J. and S. A. Miller (1962). "Power requirements of gas-liquid agitated systems." AIChE Journal **8**(2): 262-266.

Micheletti, M., S. Baldi, S. L. Yeoh, A. Ducci, G. Papadakis, K. C. Lee and M. Yianneskis (2004). "On Spatial and Temporal Variations and Estimates of Energy Dissipation in Stirred Reactors." Chemical Engineering Research and Design **82**(9): 1188-1198.

Micheletti, M. and M. Yianneskis (2004). "Study of fluid velocity characteristics in stirred solid-liquid suspensions with a refractive index matching technique." Proceedings of the Institution of Mechanical Engineers, Part E: Journal of Process Mechanical Engineering **218**(4): 191-204.

Mmbaga, J. P. and C. P. J. Bennington (1998). "The use of mixing-sensitive chemical reactions to study mixing in dispersed fibre systems: Adsorption of reactants and product dyes on the dispersed phase." The Canadian Journal of Chemical Engineering **76**: 670-679.

Montante, G., D. Horn and A. Paglianti (2008). "Gas-liquid flow and bubble size distribution in stirred tanks." Chemical Engineering Science **63**(8): 2107-2118.

Montante, G., G. Micale, F. Magelli and A. Brucato (2001). "Experiments and CFD Predictions of Solid Particle Distribution in a Vessel Agitated with Four Pitched Blade Turbines." Chemical Engineering Research and Design **79**(8): 1005-1010.

Montante, G., M. H. Occulti, F. Magelli and A. Paglianti (2010). PIV measurements of mean flow and turbulence modulation in dilute solid-liquid stirred tanks. 15th Int Symp on Applications of Laser Techniques to Fluid Mechanics. Lisbon, Portugal.

Morud, K. E. and B. H. Hjertager (1996). "LDA measurements and CFD modelling of gas-liquid flow in a stirred vessel." Chemical Engineering Science **51**(2): 233-249.

Nagata, S. (1975). Mixing: principles and applications, John Wiley & Sons Inc.

Ng, D. J. W. and M. Assirelli (2007). "Mixing study in batch stirred vessels using a fibre-optic UV-VIS monitoring technique: A novel method." Chemical Engineering Research and Design **85**(A10): 1348-1354.

Nienow, A. W. (1968). "Suspension of solid particles in turbine agitated baffled vessels." Chemical Engineering Science **23**(12): 1453-1459.

Nienow, A. W. (1996). "Gas-liquid mixing studies: a comparison of Rushton turbines with some modern impellers." Chemical Engineering Research and Design **74**(a): 417-423.

Nienow, A. W. (1997). "On impeller circulation and mixing effectiveness in the turbulent flow regime." Chemical Engineering Science **52**(15): 2557-2565.

Nienow, A. W. (1998). "Hydrodynamics of Stirred Bioreactors." Applied Mechanics Reviews **51**(1): 3-32.

Nienow, A. W. and R. Bartlett (1974). The measurement and prediction of particle-fluid slip velocities in agitated vessels. Proceedings of the first European conference on mixing and centrifugal separation Cambridge, BHRA Fluid Engineering, Cranfield.

Nienow, A. W. and W. Bujalski (2002). "Recent Studies on Agitated Three-Phase (Gas-Solid-Liquid) Systems in the Turbulent Regime." Chemical Engineering Research and Design **80**(8): 832-838.

Nienow, A. W. and R. Conti (1978). "Particle abrasion at high solids concentration in stirred vessels." Chemical Engineering Science **33**(8): 1077-1086.

Nienow, A. W., G. Hunt and B. C. Buckland (1994). "A fluid dynamic study of the retrofitting of large agitated bioreactors: Turbulent flow." Biotechnology and Bioengineering **44**(10): 1177-1185.

Nienow, A. W., M. Konno and W. Bujalski (1986). "Studies on three-phase mixing: a review and recent results." Chemical Engineering Research and Design **64**(a): 35-42.

Nienow, A. W. and D. Miles (1969). "A Dynamometer for Accurate Measurement of Mixing Torque." Journal of Physics E-Scientific Instruments **2**(11): 994-&.

Nienow, A. W., M. M. C. G. Warmoeskerken, J. M. Smith and M. Konno (1985). On the flooding/loading transition and the complete dispersal condition in aerated vessels agitated by a Rushton-turbine. 5th European Conference on Mixing, Wurzburg.

Nienow, A. W. and D. J. Wisdom (1974). "Flow over disc turbine blades." Chemical Engineering Science **29**(9): 1994-1997.

Nouri, J. M. and J. H. Whitelaw (1992). "Particle velocity characteristics of dilute to moderately dense suspension flows in stirred reactors." International Journal of Multiphase Flow **18**(1): 21-33.

Ochieng, A. and M. S. Onyango (2008). "Drag models, solids concentration and velocity distribution in a stirred tank." Powder Technology **181**(1): 1-8.

Owen, P. R. (1969). "Pneumatic transport." Journal of Fluid Mechanics **39**: 407-432.

Palmer, D. A. and L. J. Lyons (1988). Kinetics of iodine hydrolysis in unbuffered solutions.

Patterson, G. K., J. L. Zakin and J. M. Rodriguez (1969). "DRAG REDUCTION - Polymer Solutions, Soap Solutions, and Solid Particle Suspensions in Pipe Flow." Industrial & Engineering Chemistry **61**(1): 22-30.

Paul, E. L., V. A. Atiemo-Obeng and S. M. Kresta (2004). Handbook of industrial mixing: science and practice. Hoboken, USA, John Wiley & Sons.

Pianko-Oprych, P., A. W. Nienow and M. Barigou (2009). "Positron emission particle tracking (PEPT) compared to particle image velocimetry (PIV) for studying the flow generated by a pitched-blade turbine in single phase and multi-phase systems." Chemical Engineering Science **64**(23): 4955-4968.

Poelma, C. and G. Ooms (2006). "Particle-turbulence interaction in a homogeneous, isotropic turbulent suspension." Applied Mechanics Reviews **59**: 78.

Post, S. (2010). Applied and Computational Fluid Mechanics. Sudbury, MA Jones and Bartlett Publishers LLC.

Quraishi, A. Q., R. A. Mashelkar and J. Ulbrecht (1976). "Torque suppression in mechanically stirred liquids and multiphase liquid systems." Journal of Non-Newtonian Fluid Mechanics **1**(3): 223-245.

Rao, A. M. and R. S. Brodkey (1972). "Continuous flow stirred tank turbulence parameters in the impeller stream." Chemical Engineering Science **27**(1): 137-156.

Rewatkar, V. B., K. S. Rao, M. S. Raghava and J. B. Joshi (1991). "Critical impeller speed for solid suspension in mechanically agitated three-phase reactors. 1. Experimental part." Industrial & Engineering Chemistry Research **30**(8): 1770-1784.

Reynolds, O. (1883). "An Experimental Investigation of the Circumstances Which Determine Whether the Motion of Water Shall Be Direct or Sinuous, and of the Law of Resistance in Parallel Channels." Philosophical Transactions of the Royal Society of London **174**: 935-982.

Rhodes, M. (2008). Introduction to Particle Technology, John Wiley & Sons, Ltd.

Rice, R. W. and R. E. Baud (1990). "The role of micromixing in the scale-up of geometrically similar batch reactors." AIChE Journal **36**(2): 293-298.

Richardson, L. F. (1922). Weather Prediction by Numerical Process, Cambridge Univ. Press.

Roman, R. V. and R. Z. Tudose (1997). "Studies on transfer processes in mixing vessels: effect of particles on gas-liquid hydrodynamics using modified Rushton turbine agitators." Bioprocess and Biosystems Engineering **16**(3): 135-144.

Rousseaux, J.-M., L. Falk, H. Muhr and E. Plasari (1999). "Micromixing efficiency of a novel sliding-surface mixing device." AIChE Journal **45**(10): 2203-2213.

Saffman, P. G. (1962). "On the stability of laminar flow of a dusty gas." Journal of Fluid Mechanics **13**(01): 120-128.

Saito, F., A. W. Nienow, S. Chatwin and I. P. T. Moore (1992). "Power, gas dispersion and homogenisation characteristics of Scaba SRGT and Rushton turbine impellers." Journal of Chemical Engineering of Japan **25**(3): 281-287.

Salazar, J. P. L. C., J. De Jong, L. Cao, S. H. Woodward, H. U. I. Meng and L. R. Collins (2008). "Experimental and numerical investigation of inertial particle clustering in isotropic turbulence." Journal of Fluid Mechanics **600**: 245-256.

Saric, W. S., H. L. Reed and E. J. Kerschen (2002). "Boundary-Layer Receptivity to Freestream Disturbances." Annual Review of Fluid Mechanics **34**(1): 291-319.

Schaer, E., P. Guichardon, L. Falk and E. Plasari (1999). "Determination of local energy dissipation rates in impinging jets by a chemical reaction method." Chemical Engineering Journal **72**(2): 125-138.

Schäfer, M. (2001). Charakterisierung, Auslegung und Verbesserung des Makro- und Mirkomischens in geruehrten Behaeltern, Universitaet Erlangen-Nuernberg. **PhD Thesis**.

Schetz, J. A. and A. E. Fuhs (1996). Handbook of fluid dynamics and fluid machinery. New York, Wiley.

Schmitz, G. (1999). "Kinetics and mechanism of the iodate-iodide reaction and other related reactions." Physical Chemistry Chemical Physics **1**(8): 1909-1914.

Schmitz, G. (2000). "Kinetics of the Dushman reaction at low I–concentrations." Physical Chemistry Chemical Physics **2**(18): 4041-4044.

Schmitz, G. (2008). "Inorganic reactions of iodine(III) in acidic solutions and free energy of iodous acid formation." International Journal of Chemical Kinetics **40**(10): 647-652.

Schwartzberg, H. G. and R. E. Treybal (1968). "Fluid and Particle Motion in Turbulent Stirred Tanks. Particle Motion." Industrial & Engineering Chemistry Fundamentals **7**(1): 6-12.

Sebodblack-Nagy, K. and T. Körtvélyesi (2004). "Kinetics and mechanism of the hydrolytic disproportionation of iodine." International Journal of Chemical Kinetics **36**(11): 596-602.

Sharp, K. V. and R. J. Adrian (2001). "PIV study of small-scale flow structure around a Rushton turbine." AIChE Journal **47**(4): 766-778.

Siddiqui, S. W. (2009). Use of the Confined Impinging Jet Reactor for Production of Nanoscale Iron Oxide Particles. Department of Chemical and Materials Engineering, University of Alberta. **PhD thesis**.

Sommerfeld, M. (2001). "Validation of a stochastic Lagrangian modelling approach for inter-particle collisions in homogeneous isotropic turbulence." International Journal of Multiphase Flow **27**(10): 1829-1858.

Sommerfeld, M. and S. Decker (2004). "State of the Art and Future Trends in CFD Simulation of Stirred Vessel Hydrodynamics." Chemical Engineering & Technology **27**(3): 215-224.

Squires, K. D. and J. K. Eaton (1991). "Preferential concentration of particles by turbulence." Physics of Fluids A: Fluid Dynamics **3**(5): 1169-1178.

Ståhl, M. and Å. C. Rasmuson (2009). "Towards predictive simulation of single feed semibatch reaction crystallization." Chemical Engineering Science **64**(7): 1559-1576.

Stoots, C. M. and R. V. Calabrese (1995). "Mean velocity field relative to a Rushton turbine blade." AIChE Journal **41**(1): 1-11.

Su, Y., G. Chen and Q. Yuan (2011). "Ideal micromixing performance in packed microchannels." Chemical Engineering Science **66**(13): 2912–2919.

Sundaram, S. and L. R. Collins (1997). "Collision statistics in an isotropic particle-laden turbulent suspension. Part 1. Direct numerical simulations." Journal of Fluid Mechanics **335**: 75-109.

Tanaka, T. and J. K. Eaton (2008). "Classification of Turbulence Modification by Dispersed Spheres Using a Novel Dimensionless Number." Physical Review Letters **101**(11): 114502.

Tennekes, H. and J. L. Lumley (1972). First Course in Turbulence. Cambridge, MIT Press.

Thoma, S., V. V. Ranada and J. R. Bourne (1991). "Interaction between micro- and macro-mixing during reactions in agitated tanks." The Canadian Journal of Chemical Engineering **69**(5): 1135-1141.

Thomas, T. R., D. T. Pence and R. A. Hasty (1980). "The disproportionation of hypoiodous acid." Journal of Inorganic and Nuclear Chemistry **42**(2): 183-186.

Truesdale, V. W. (1995). "Effect of iodide concentration upon the kinetics of disproportionation of hypoiodous acid in borate buffer." Journal of the Chemical Society, Faraday Transactions **91**(5).

Truesdale, V. W. (1997). "Kinetics of disproportionation of hypoiodous acid at high pH, with an extrapolation to rainwater." Journal of the Chemical Society, Faraday Transactions **93**(10): 1909-1914.

Truesdale, V. W., G. W. Luther and J. E. Greenwood (2003). "The kinetics of iodine disproportionation: a system of parallel second-order reactions sustained by a multi-species pre-equilibrium." Physical Chemistry Chemical Physics **5**(16).

Unadkat, H. (2009). Investigation of turbulence modulation in solid-liquid suspensions using FPIV and micromixing experiments. Department of Chemical Engineering, Loughborough University. **PhD thesis**.

Unadkat, H., C. Rielly and Z. Nagy (2009a). Application of Fluorescent PIV and digital image analysis to measure turbulence properties of solid-liquid stirred suspensions. 13th European Conference on Mixing. King's College, London.

Unadkat, H., C. D. Rielly, G. K. Hargrave and Z. K. Nagy (2009b). "Application of fluorescent PIV and digital image analysis to measure turbulence properties of solid–liquid stirred suspensions." Chemical Engineering Research and Design **87**(4): 573-586.

Urbansky, E. T., B. T. Cooper and D. W. Margerum (1997). "Disproportionation Kinetics of Hypoiodous Acid As Catalyzed and Suppressed by Acetic Acidâˆ'Acetate Buffer." Inorganic Chemistry **36**(7): 1338-1344.

Vaillancourt, P. A. and M. K. Yau (2000). "Review of Particle-Turbulence Interactions and Consequences for Cloud Physics." Bulletin of the American Meteorological Society **81**(2): 285-298.

Van't Riet, K. (1979). "Review of Measuring Methods and Results in Nonviscous Gas-Liquid Mass Transfer in Stirred Vessels." Industrial & Engineering Chemistry Process Design and Development **18**(3): 357-364.

Van't Riet, K. and J. M. Smith (1975). "The trailing vortex system produced by Rushton turbine agitators." Chemical Engineering Science **30**(9): 1093-1105.

Vazquez, G., M. A. Cancela, C. Riverol, E. Alvarez and J. M. Navaza (2000). "Application of the Danckwerts method in a bubble column: Effects of surfactants on mass transfer coefficient and interfacial area." Chemical Engineering Journal **78**(1): 13-19.

Versteeg, H. K. and W. Malalasekera (2007). An Introduction to Computional Fluid Dynamics: The Finite Volume Method, Pearson Education.

Vicum, L. (2005). Investigation of the influence of turbulent mixing on precipitation processes carried out in stirred tank reactors. Zürich, Eidgenössische Technische Hochschule ETH Zürich. **PhD thesis**.

Vicum, L. and M. Mazzotti (2007). "Multi-scale modeling of a mixing-precipitation process in a semibatch stirred tank." Chemical Engineering Science **62**(13): 3513-3527.

Villermaux, J. (1990). Micromixing and chemical reaction semi-quantitative criteria based on comparison of characteristic time constants. A.I.Ch.E. Meeting, Chicago.

Villermaux, J. and R. David (1983). "Recent advances in the understanding of micromixing phenomena in stirred reactors." Chemical Engineering Communications **21**(1-3): 105-122.

Villermaux, J. and J. C. Devillon (1972). Representation de la coalescence et de la redispersion des domaines de segregation dans un fluide par un modele interaction phenomenologique. Proceed, 2nd Inc. Symp. Chem. React. Engng., Amesterdam.

Villermaux, J. and L. Falk (1994). "A generalized mixing model for initial contacting of reactive fluids." Chemical Engineering Science **49**(24): 5127-5140.

Villermaux, J., L. Falk and M. C. Fournier (1994). "Potential use of a new parallel reaction system to characterize micromixing in stirred reactors." AIChE Symposium Series **90**(299): 50-54.

Villermaux, J., L. Falk, M. C. Fournier and C. Detrez (1992). "Use of parallel competing reactions to characterize micromixing efficiency." Process mixing: chemical and biochemical applications: 6.

Virdung, T. and A. Rasmuson (2007). "Measurements of Continuous Phase Velocities in Solid-Liquid Flow at Elevated Concentrations in a Stirred Vessel Using LDV." Chemical Engineering Research and Design **85**(2): 193-200.

Virdung, T. and A. Rasmuson (2008). "Solid-liquid flow at dilute concentrations in an axially stirred vessel investigated using particle image velocimetry." Chemical Engineering Communications **195**(1): 18-34.

Wang, L. P. and A. S. Wexler (2000). "Statistical mechanical description and modelling of turbulent collision of inertial particles." Journal of Fluid Mechanics **415**: 117-153.

Warmoeskerken, M., M. C. Van Houwelingen, J. J. Frijlink and J. M. Smith (1984). "Role of cavity formation in stirred gas-liquid-solid reactors." Chemical Engineering Research and Design **62**(3): 197-200.

White, C. M. and M. G. Mungal (2008). "Mechanics and Prediction of Turbulent Drag Reduction with Polymer Additives." Annual Review of Fluid Mechanics **40**(1): 235-256.

Wu, H. and G. K. Patterson (1989). "Laser-Doppler measurements of turbulent-flow parameters in a stirred mixer." Chemical Engineering Science **44**(10): 2207-2221.

Wygnanski, I. and H. Fiedler (1969). "Some measurements in the self-preserving jet." Journal of Fluid Mechanics **38**(03): 577-612.

Xie, Y., M. R. McDonald and D. W. Margerum (1999). "Mechanism of the Reaction between Iodate and Iodide Ions in Acid Solutions (Dushman Reaction)." Inorganic Chemistry **38**(17): 3938-3940.

Yeoh, G. H. and J. Tu (2010). Gas-Particle Flows. Computational Techniques for Multiphase Flows. Oxford, Butterworth-Heinemann.

Zhou, G. and S. M. Kresta (1996). "Impact of tank geometry on the maximum turbulence energy dissipation rate for impellers." AIChE Journal **42**(9): 2476-2490.

Zuidervaart, E., M. A. Reuter, R. H. Heerema, R. G. J. M. Van Der Lans and J. J. Derksen (2000). "Effect of dissolved metal sulphates on gas-liquid oxygen transfer in agitated quartz and pyrite slurries." Minerals Engineering **13**(14-15): 1555-1564.

Zwietering, T. N. (1958). "Suspending of solid particles in liquid by agitators." Chemical Engineering Science **8**(3-4): 244-253.

Zwietering, T. N. (1984). "A backmixing model describing micromixing in single-phase continuous-flow systems." Chemical Engineering Science **39**(12): 1765-1778.

APPENDICES

A. CALIBRATION OF TRIIODIDE MEASUREMENT

Guichardon and Falk (2000) showed that the extinction coefficients for triiodide reported in literature vary. Their own measurements gave slightly deviating results when using two different spectrophotometers and the authors suggest that the diversity of apparatus might be an explanation.

Therefore, the extinction coefficient was measured to calibrate the method using the available spectrophotometer, a Cecil CE 1020. To measure the absorbance at varied triiodide concentrations the procedure described by Assirelli (2004) was followed and the resulting graph is shown in Appendix figure 1.

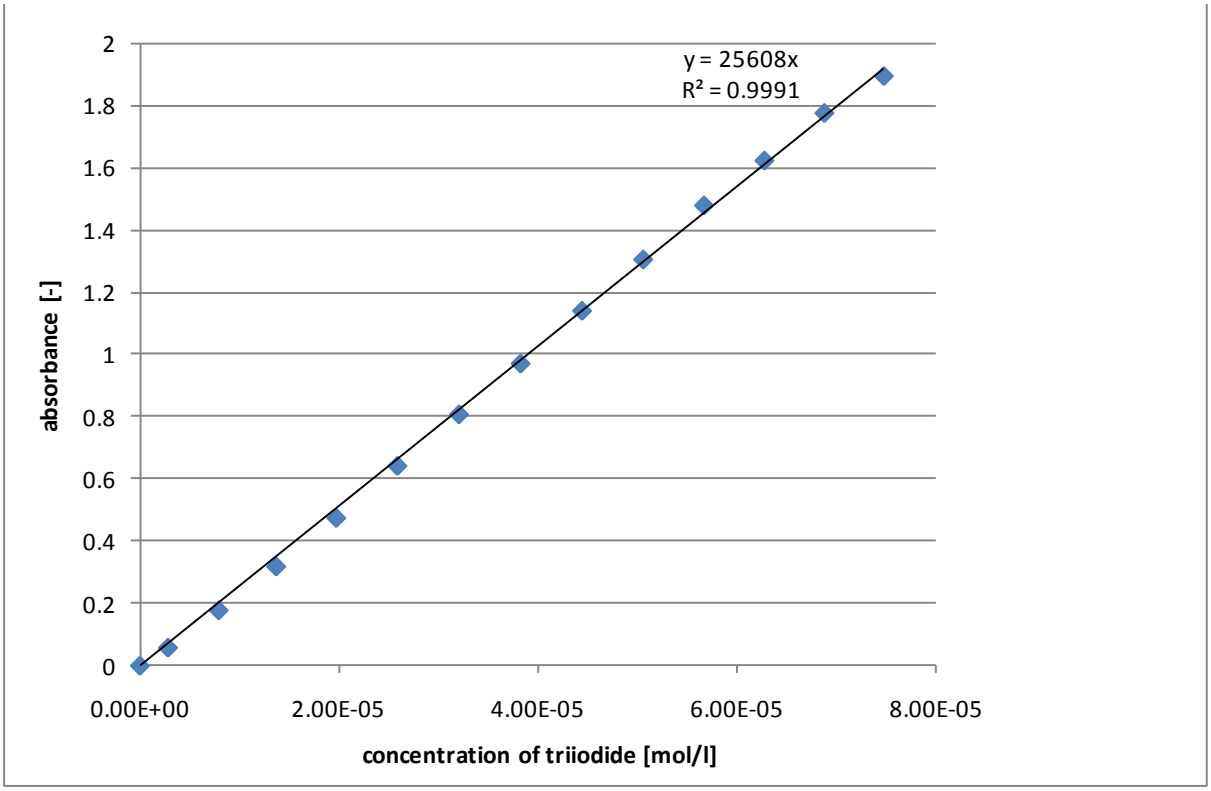

Appendix figure 1: Calibration curve for extinction coefficient of triiodide

The obtained extinction coefficient, 2560.8 m^2/mol at 353 nm, falls well into the range of reported values in literature, as is illustrated in Appendix table 1.

Appendix table 1: Some reported values for the extinction coefficient of triiodide [extended and amended from Guichardon and Falk (2000)]

Abbreviations: **SB = single beam**
DB = double beam

Reference	Wavelength [nm]	Extinction coefficient [m^2/mol]
Custer and Natelson (1949)	352	2590
Awtrey and Connick (1951)	353	2640
Herbo and Sigalla (1957)	350	2510
Thomas *et al.* (1980)	353	2580
Palmer *et al.* (1984)	350	2575
Guichardon and Falk (2000)(SB)	353	2395.9
Guichardon and Falk (2000)(DB)	353	2606
Assirelli (2004)(DB)	353	2541.2
Baccar *et al.* (2009)	353	2127
Siddiqui (2009)	352	1914.8
Unadkat (2009)	353	2686
Su *et al.* (2011)	353	2254
This work (SB)	353	2560.8

B. PROGRAMME FOR SOLUTION OF MICROMIXING MODEL – FURTHER DETAILS

As stated in chapter 4, the approach was similar to what previous workers (Fournier *et al.* 1996a; Assirelli 2004) have reported. Therefore, it is not necessary to discuss or even print the entire code here – only the differences are emphasised here for clarity.

Regarding the second dissociation of sulphuric acid, the equilibrium was solved, as would be done in the manual equivalent. For that calculation step, the dimensionless variables for the species were converted back to actual concentrations and then, after solving the equilibrium, converted back again. This expression was easily included for the changes in H^+, HSO_4^- and SO_4^{2-} which would then be returned to the Runge-Kutta-algorithm. The main issue in this case is that the change directly depends on the time step size and that this change was always calculated for the step ahead. Therefore, a constant step size had to be used. Clearly, this was far from ideal in terms of computational efficiency and led to relatively time-consuming runs. This was, nevertheless, the most suitable solution overall, as it gave flexibility with making changes to the code. In addition, it was ensured that all results are time step independent.

The adaptations for testing the different kinetic rate laws were relatively straightforward. Only the fact that the calculations use dimensionless values had to be considered and consistent use of the respective variables is crucial.

C. UNBAFFLED STIRRED TANKS - CFD

Introduction and background

Experiments as described in this thesis have also been conducted in liquid-only unbaffled vessels and the comparison of baffled and unbaffled agitated vessels has lead to a surprising result: the segregation index measured in the bulk of unbaffled tanks tends to be lower than in equivalent baffled configurations, i.e. micromixing is more efficient – at same mean specific power input and at same impeller speeds (Rice and Baud 1990; Assirelli *et al.* 2008a). Assirelli *et al.* (2008a) reported that similar micromixing results were obtained near the impeller and when feeding onto the surface for baffled and unbaffled cases at same impeller speed. Moreover, there was a dramatic improvement in the unbaffled case when submerging the feed pipe into the liquid in contrast to dropping the reactant onto the surface, while feeding onto or submerged into the liquid surface did not lead to such improvements in the baffled case. These results were not expected by the authors (Assirelli *et al.* 2008a), but might be explained by different flow patterns near the feed pipe.

In general, unbaffled vessels have not been investigated as much as baffled ones, but some experimental and computational studies of the flow field and local energy dissipation levels have been reported. For instance, mean and RMS velocities from LDA measurements have been reported by Dong *et al.* (1994a) for two impeller clearances and relatively modest Reynolds numbers, i.e. 3273 and 4908, using an eight-blade, flat-paddle impeller. It was found that turbulence is relatively homogenous and lower than average in the bulk with much higher intensities, as in baffled cases, near the impeller and also increased levels near the shaft. In addition,

they reported damped turbulence levels near the liquid-gas interface. This data has also been used to validate results from CFD simulations (Dong *et al.* 1994b; Ciofalo *et al.* 1996). Other workers, for instance Armenante *et al.* (1997), used lids to maintain a flat surface for experimental studies, which also simplifies the approach in CFD as it is not necessary to account for the changing shape of the free surface. Regarding local energy dissipation levels, Armenante *et al.* (1997) also found that these are higher near the impeller than in other parts of the vessel. Unfortunately, it has not been shown whether the flat surface would affect turbulence levels or micromixing efficiency.

Explanations for the unexpectedly good micromixing in unbaffled vessels could consequently not be found in literature and further investigation is necessary. This aspect will be briefly discussed here.

Method and set-up

Computational fluid dynamics (CFD) allows investigating fluid flows in great detail and, therefore, seems suitable for giving a better idea of the unexpectedly good micromixing results in unbaffled tanks. This method has been used for a range of studies on fluid flow in stirred vessels and a brief overview will be given. First, however, the approach for CFD, particularly in this context, is presented.

General approach in CFD

CFD consists of having a defined geometry for the fluid domain, for instance a CAD drawing of an agitated tank. This is then meshed first, i.e. discretisised spatially into a number of mesh cells. During pre-processing the fluid properties, the boundaries

and any other for the simulation relevant information are defined. Then the actual calculations take place: the solver tries to numerically find solutions for the equations of interest. Once a specified convergence has been reached, the simulation is finished and the data can be used and for instance plotted in graphs or vector images. This final step is called post-processing.

There are good introductions available which explain the fundamentals of fluid dynamics and also CFD in detail. For brevity, only the approach chosen in this work is presented in the next section and the reader is referred to literature for further explanation of the models and the equations solved in the simulations, e.g. Anderson (1995) and Post (2010).

Software

Initially, the simulations were performed locally using Ansys CFX 11.0 and Workbench, which included CFX-Mesh for generating tetrahedral meshing. Moreover, ICEM 11.0 was used for more complicated and structured meshing, e.g. for producing hexahedral grids. During this project, the software was updated to versions 12 and then 13. In addition, there was the option to run larger calculations on the university's computer cluster, BlueBEAR, which allowed realising more demanding simulations. Again, different software versions became available on the cluster over the course of the project.

Modelling and meshes

The comparison of a baffled and an unbaffled case has already been mentioned as the main purpose of these simulations. In addition, some smaller tests were planned,

for instance: a slight difference between the power inputs at different liquid heights could be observed experimentally, which is also going to be simulated – however, covering a wider range of Reynolds numbers than in the experiments.

Different approaches might be employed for these different objectives: to get useful information regarding micromixing, detailed information about the flow around the feed is necessary and the meshing of this region should take this into account accordingly. Therefore, the tank was split into sections which allowed producing finer structured meshes near the feed pipe. The split geometry is shown in Figure C-1. An example of the mesh is given in Figure C-2, which shows the region directly in front of the feed pipe tip (here half of the pipe).

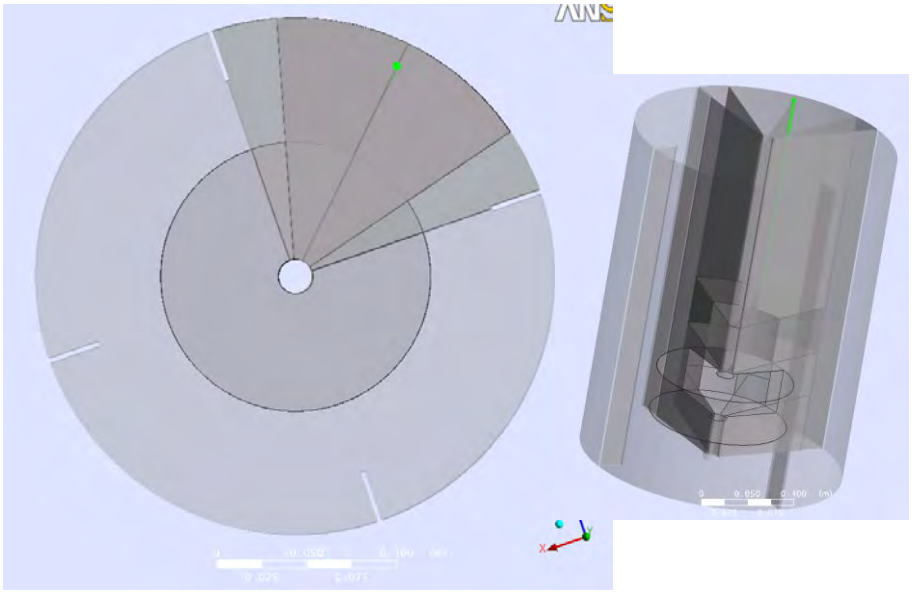

Appendix figure 2: Segments of geometry for detailed structured meshing

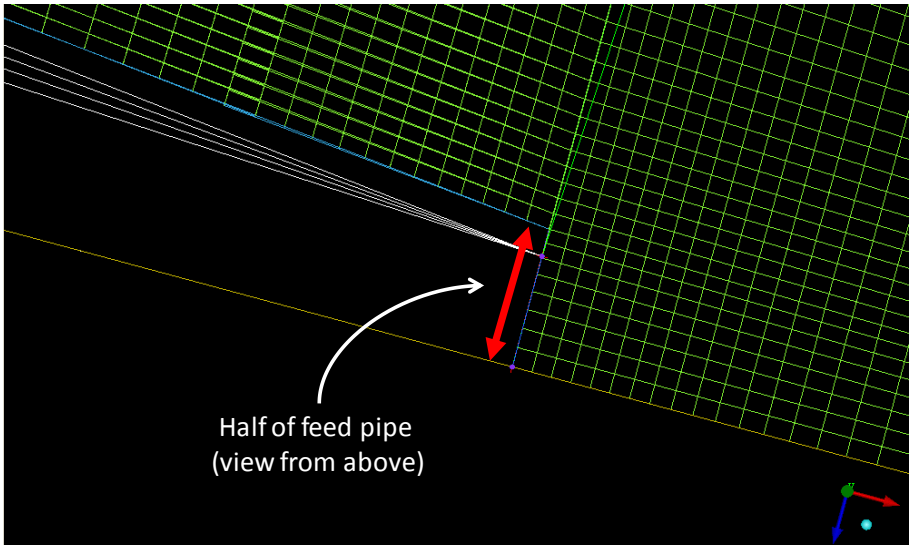

Appendix figure 3: Details of structured mesh – showing half of feed pipe

On the other hand, for the simulations of the power inputs, it was sufficient to use a less sophisticated mesh which captures the general flow and the pressure field around the boundaries, like a tetrahedral mesh with appropriate use of inflation layers.

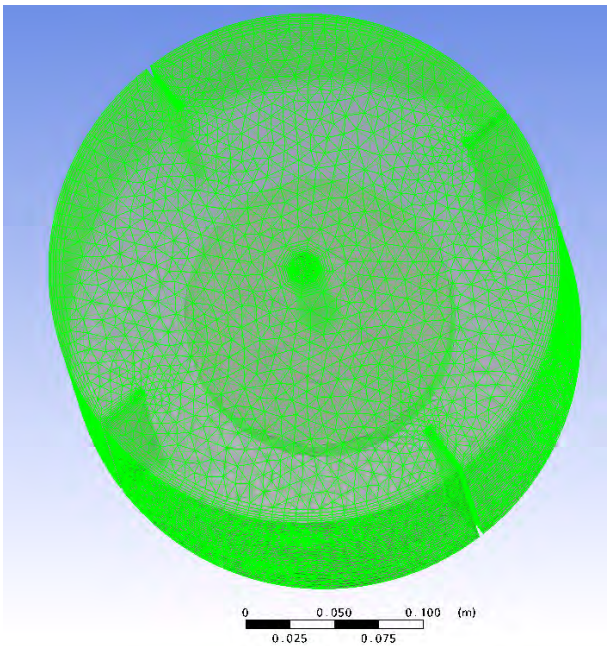

Appendix figure 4: Simpler mesh using tetrahedral elements and inflation layers around the boundaries, for general simulations

Usually the standard k-ε-model was used, but also other turbulence models were employed for initial tests. The fluid was water and most simulations were in steady-state. Therefore, the impeller rotation was usually described using moving frames of reference. A few cases were solved transient, also including the time-dependent impeller effects using a sliding mesh.

For the unbaffled cases, the shape of the free surface was included by different approaches:

- Volume-of-Fluid model: adding an additional fluid domain at the top of the tank and directly calculating the shape of the gas-liquid interface.
- Estimate from literature (Nagata 1975): an equation suggested by Nagata allowed to estimate the shape of the free surface, which was then given an a free-slip wall boundary.
- Estimate from pressure field around surface: this approach is similar to a more automated one in literature (Ciofalo *et al.* 1996). Starting from a flat surface, the simulation is solved, the obtained pressure field indicates where the surface needs to be altered in shape. The geometry is adapted manually, a new mesh is created and then after the next simulation improved again and so on. This iterative approach was another option for approximating the shape of the free surface.

Results and discussion

This section summarises the results for the initial test on the baffled tank and then gives an overview of the unbaffled cases.

Initial validation and general results – baffled tank

The power number of Rushton turbines is well studied and, consequently, the first validation was to calculate Po for a range of Reynolds numbers. Po could be obtained from the torque on the impeller and the shaft (primary Po), the walls and the baffles (secondary) or by integrating the turbulent energy dissipation rates (Bujalski 2003). The results for the primary power number are given in Appendix figure 5 for different turbulence models, which do not seem to affect Po significantly in the turbulent region. Even without turbulence model the power input is calculated correctly. In the laminar regime, there are deviations between the k-ε model and the laminar approach. The results for SST look as expected as it should behave like the laminar approach in this flow regime.

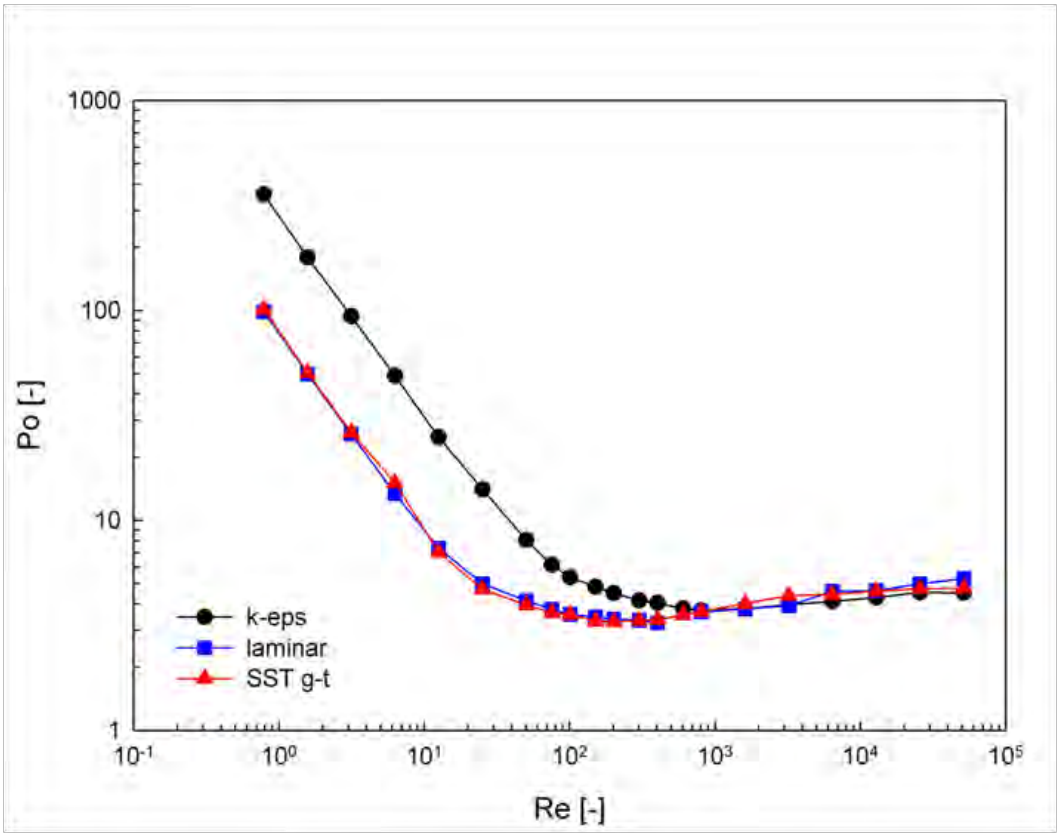

Appendix figure 5: Power number as function of Re – CFD results for k-ε and SST turbulence models and without turbulence model (laminar)

One part on the power input calculations was to check if the small influence of the liquid height which was seen in the experiments can also be observed in the simulations and Appendix table 2 shows that this is the case. Also the quantitative prediction is quite good as the experimental difference was ~3.6% while the simulations give ~5%.

Appendix table 2: Power input for different liquid fill levels – calculated from torque on impeller or walls and baffles or integrated ε_T

H/T [-]	Power number [-]		
	primary	secondary	dissip.
1	4.57	4.57	0.77
1.3	4.81	4.82	0.73

The calculated flow field could also be validated by checking that the characteristic flow is developed, as shown in Appendix figure 6.

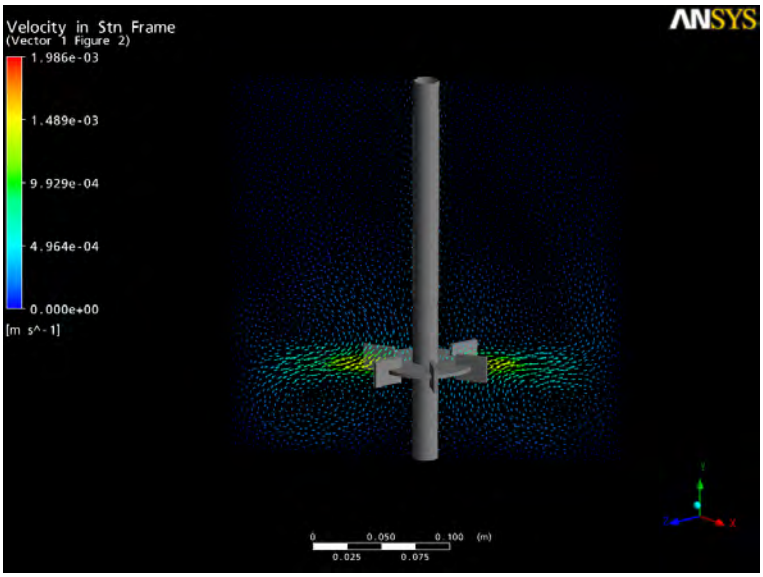

Appendix figure 6: Flow field in turbulent regime – turbulence model: SST gamma-theta

To compare a range of Re, the flow number is plotted in Appendix figure 7. The results from all models, overall, agree with literature (Chiti 2008) though there again

is a difference between laminar and k-ε-model in the laminar regime (for which it is not intended to be used).

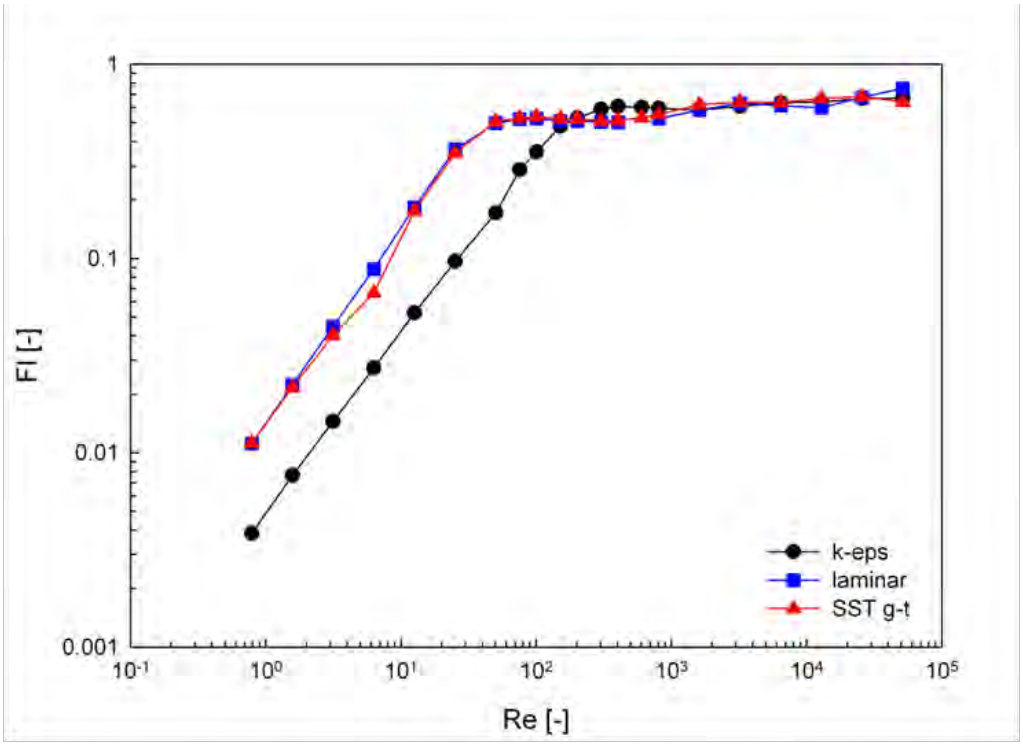

Appendix figure 7: Fl as function of Re – CFD results

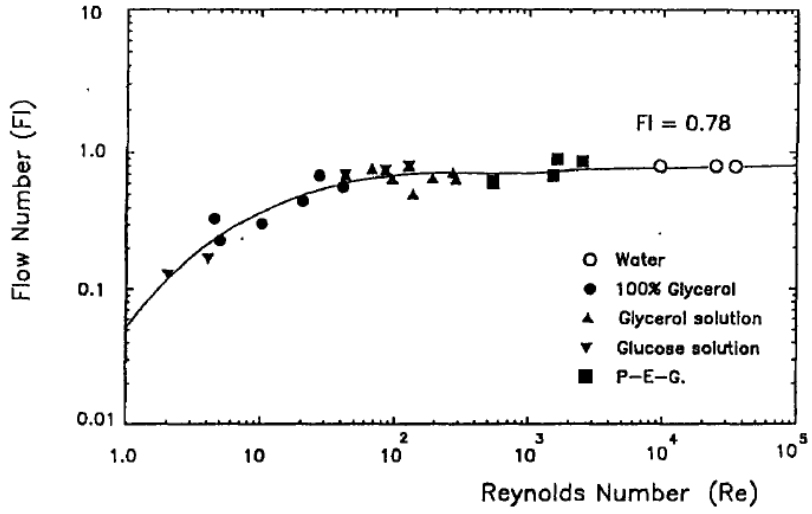

Appendix figure 8: Fl as function of Re – experimental data from literature (Dyster et al. 1993)

A comparison of the results for Fl from CFD to experimental, i.e. LDA, data from literature (Dyster *et al.* 1993) shows very good agreement.

Initial validation and general results – unbaffled tank

For the unbaffled tank, the correct development of the free surface and the overall flow field were of interest. From the various options mentioned in the method section, the Volume of Fluid approach was the computationally most demanding. Unfortunately, the flow also switched between single- and double-loop which also did not aid convergence or quick calculations of realistic surface shapes. Therefore, an estimate from the literature equation (Nagata 1975) was made. An example of these shapes is illustrated in Appendix figure 9 for 300 rpm. The videos of the experiments by Assirelli (2004) would indicate a stronger vortex at these conditions and also the flow field in these simulation cases resembled a single-loop flow – although a double-loop would be expected from the experiment videos by observing bubbles entrained in the liquid.

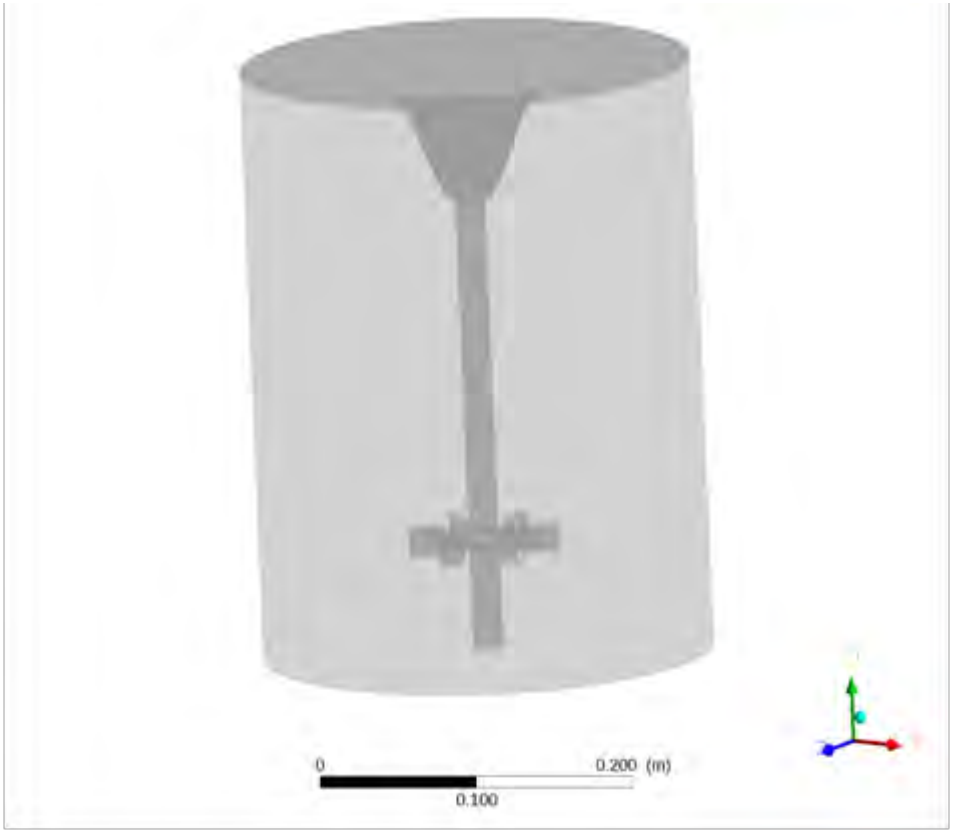

Appendix figure 9: Surface shape from Nagata equation for 5 rps

The third option was calculating the shape from the pressure field near the surface. An example of a not yet fully developed surface is given in Appendix figure 10. The challenges with this method were keeping the vessel volume constant and deciding on when the surface shape was developed. The first point could be checked in the software. The question of surface "convergence" was settled by continuing until the changes in for the surface shape did not lead to improvements regarding the pressure anymore but started to settle around the same values. In these cases, the flow field was usually the expected double-loop, but single-loops were found in some early cases as well.

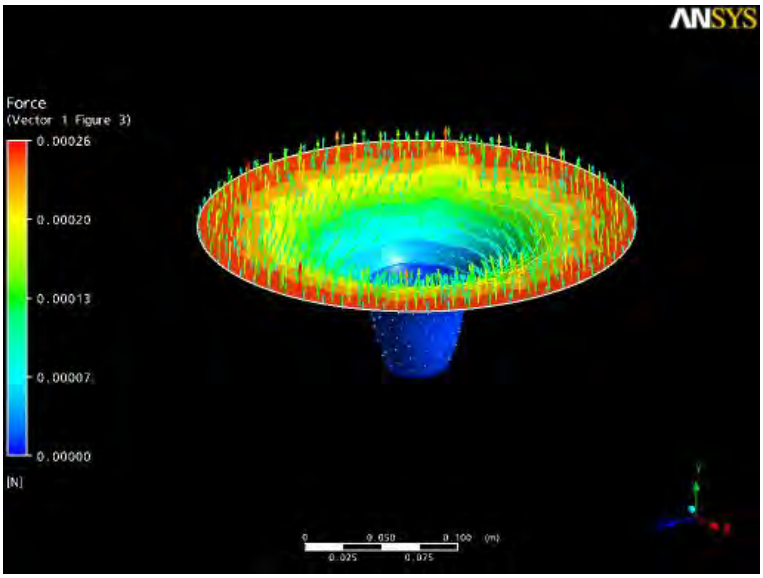

Appendix figure 10: Development of surface shape with pressure field – contours: pressure; vectors: force

Comparisons of baffled and unbaffled tanks

Micromixing depends on the local conditions near the tip of the feed pipe, i.e. the conditions experienced by the reactant. Therefore, particle tracking might indicate why micromixing was unexpectedly efficient in the unbaffled experiments. Such simulations were conducted in steady-state and time-dependent cases – of course,

as in the experiments, at H=1.3T. Such a comparison can be seen in Appendix figure 11 – the different perspectives were chosen to show each case possibly clearly. While the baffled flow goes more towards the wall, the unbaffled particles seem to be following the "rotation" of the flow. Unfortunately, such simple simulations using RANS models do not give reliable quantitative information on turbulence values like local specific energy dissipation rates. Therefore, the colours of the particle tracks and comparisons of such values are not found reliable enough for explaining the experimental results.

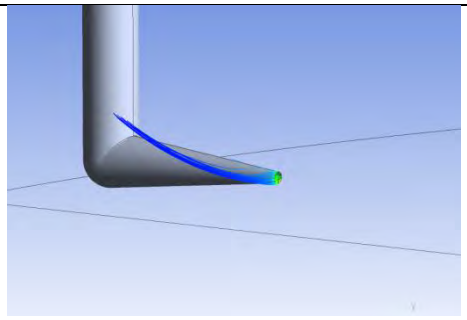	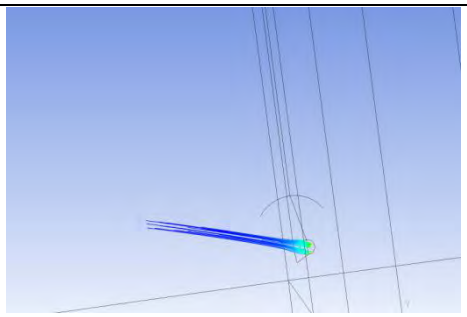
baffled	unbaffled

Appendix figure 11: Comparison of particle tracks

There is, however, another option which would deserve further attention in future work: there might be formation of vortices or eddies behind the feed pipes which could lead to significant effects on micromixing efficiency.

Conclusion and future work

The results presented here only reflect part of the data produced as also the chemical reactions were included in some of the simulations. This work did give some insight into the fluid flows and might be a starting point for future attempts. However, the results summarised here did not lead to better understanding of the

unbaffled data found in literature. In order to explain these unexpected experimental values for micromixing efficiency (Rice and Baud 1990; Assirelli *et al.* 2008a) a more targeted approach is needed. This might also involve more computationally demanding transient cases, fine meshes and possibly realistic treatment of turbulence.